

| | | |
|--|--|---------------------------------------|
| 1. REPORT NUMBER CA16-2265 | 2. GOVERNMENT ASSOCIATION NUMBER | 3. RECIPIENT'S CATALOG NUMBER |
| 4. TITLE AND SUBTITLE Seismic Performance of Precast Girder-to-Cap Connections for Accelerated Bridge Construction of Integral Bridges | 5. REPORT DATE July 2015 | |
| | 6. PERFORMING ORGANIZATION CODE | |
| 7. AUTHOR Justin Vander Werff, Robert Pegg, Zhao Cheng, and Sri Sritharan | 8. PERFORMING ORGANIZATION REPORT NO. | |
| 9. PERFORMING ORGANIZATION NAME AND ADDRESS Department of Civil, Construction and Environmental Engineering Iowa State University | 10. WORK UNIT NUMBER | |
| | 11. CONTRACT OR GRANT NUMBER 65A0411 | |
| | 12. SPONSORING AGENCY AND ADDRESS California Department of Transportation Division of Engineering Services 1801 30th Street, MS #9-2/5i Sacramento, CA 95816 | |
| 13. TYPE OF REPORT AND PERIOD COVERED Final Report January 2011-July 2015 | | 14. SPONSORING AGENCY CODE 913 |
| 15. SUPPLEMENTARY NOTES Prepared in cooperation with the State of California Department of Transportation | | |
| 16. ABSTRACT This report presents the research conducted as part of an investigation for the California Department of Transportation (Caltrans) regarding the seismic response and overall moment capacity of precast concrete girder-to-cap connections that are well-suited for accelerated bridge construction (ABC) for bridges with integral superstructures in high seismic regions. The investigation included connections for dapped-end I-shaped precast girders with end blocks to inverted-tee cap beams and connections for precast bulb tee girders to cap beams. Current design practice, as outlined by Caltrans' Seismic Design Criteria, assumes that precast girder-to-cap connections may degrade in severe seismic events and should be designed as a pinned connection, decreasing the appeal of using precast girders on many projects. One 50% scale test unit and two 40% scale test units of the cap beam and girder connection region were designed to experimentally investigate six different girder-to-cap connection details. Two of the details were designed for connections between dapped-end I-shaped girders with end blocks and precast inverted-tee cap beams (50% scale test unit), and four of the details were designed for connections between bulb tee girders with no end blocks and rectangular cast-in-place cap beams (40% scale test units). The test units were designed to simulate shear and moment in the girder-cap connection region due to both horizontal and vertical seismic excitation. The primary consideration in the experimental investigation was the capability of the connections to provide resistance to vertical shear along with both positive and negative moment demands. The experimental results verify that the proposed connection details are sufficient to provide essentially elastic superstructure behavior well beyond the overstrength moment in the column due to horizontal seismic forces. Further, the results confirm that connections are sufficient to maintain shear and moment stability for significant vertical acceleration demands. (The project test videos and other additional information may be found at: http://sri.cce.iastate.edu/abc-seismic/) Design recommendations have been developed for the connection details to assist in sizing the strand and reinforcement elements in the connection related to expected moment demands. These recommendations can be used for similar connection details. The girder-to-cap connection details investigated in this work are structurally sufficient and simple to construct. They provide a viable | | |
| 17. KEY WORDS Seismic; bridge; precast; concrete; connections; superstructure; experimental; testing; accelerated bridge construction | 18. DISTRIBUTION STATEMENT No restriction. This document is available to the public through the National Technical Information Service, Springfield, Virginia 22161 | |
| 19. SECURITY CLASSIFICATION (of this report) Unclassified | 20. NUMBER OF PAGES 241 | 21. COST OF REPORT CHARGED |

DISCLAIMER STATEMENT

This document is disseminated in the interest of information exchange. The contents of this report reflect the views of the authors who are responsible for the facts and accuracy of the data presented herein. The contents do not necessarily reflect the official views or policies of the State of California or the Federal Highway Administration. This publication does not constitute a standard, specification or regulation. This report does not constitute an endorsement by the Department of any product described herein.

For individuals with sensory disabilities, this document is available in alternate formats. For information, call (916) 654-8899, TTY 711, or write to California Department of Transportation, Division of Research, Innovation and System Information, MS-83, P.O. Box 942873, Sacramento, CA 94273-0001.

*J. Vander Werff, R. Peggarr,
Z. Cheng, S. Sritharan*

**Seismic Performance of
Precast Girder-to-Cap Connections for
Accelerated Bridge Construction
of Integral Bridges**

Submitted to the
California Department of Transportation
Caltrans Project: 65A0411
Report No.: CA15-2265

JULY 2015

Final

REPORT

IOWA STATE UNIVERSITY
OF SCIENCE AND TECHNOLOGY

**Department of Civil, Construction
and Environmental Engineering**

Seismic Performance of Precast Girder-to-Cap Connections for Accelerated Bridge Construction of Integral Bridges

by

Justin Vander Werff
Assistant Professor of Engineering, Dordt College

Robert Pegg
Graduate Research Assistant, Iowa State University

Zhao Cheng
Graduate Research Assistant, Iowa State University

Sri Sritharan
Wilson Engineering Professor, Iowa State University

Caltrans Project: 65A0411

Report No.: CA15-2265

Final Report to the California Department of Transportation

**Department of Civil, Construction and Environmental Engineering
Iowa State University
Ames, IA 50011**

July 2015

ACKNOWLEDGMENTS

The research team thanks the following individuals for their support and assistance in the completion of the research presented in this report. Without their help and kindness, much of this research would not have been possible:

- Caltrans for sponsoring this research project and Dr. Charles Sikorsky for serving as the project manager for this research contract.
- The following members of Caltrans for serving on the project advisory panel and providing advice and assistance: Ron Bromeschenkel, Sonny Ferreira, Steve Harvey, Steve Jaques, Michael Keever, Craig Knapp, Mary Kopsa, Roberto Lacalle, Say-Gunn Low, Jim Ma, Ric Maggenti, Mark Mahan, Karla Meier, Dorie Mellon, Tom Ostrom, and Talal Sadek;
- Rick Snyder, Jay Holombo and Zach Thiemann for their work on Caltrans project 05-0160, which laid the groundwork for this portion of the work; and
- Owen Steffens and Doug Wood in the ISU Structures Laboratory, for all of their hard work, assistance, and expertise in the construction and testing of the test unit.

This work was funded by California Department of Transportation under Agreement #65A0411.

ABSTRACT

This report presents the research conducted as part of an investigation for the California Department of Transportation (Caltrans) regarding the seismic response and overall moment capacity of precast concrete girder-to-cap connections that are well-suited for accelerated bridge construction (ABC) for bridges with integral superstructures in high seismic regions. The investigation included connections for dapped-end I-shaped precast girders with end blocks to inverted-tee cap beams and connections for precast bulb tee girders to cap beams. Current design practice, as outlined by Caltrans' Seismic Design Criteria, assumes that precast girder-to-cap connections will degrade in a seismic event and consequently need to be designed as a pinned connection, decreasing the appeal of using precast girders in seismic regions. One 50% scale test unit and two 40% scale test units of the cap beam and girder connection region were designed to experimentally investigate six different girder-to-cap connection details. Two of the details were designed for connections between dapped-end I-shaped girders with end blocks and precast inverted-tee cap beams (50% scale test unit), and four of the details were designed for connections between bulb tee girders with no end blocks and rectangular cast-in-place cap beams (40% scale test units).

The test units were designed to simulate shear and moment in the girder-cap connection region due to both horizontal and vertical seismic excitation. The primary consideration in the experimental investigation was the capability of the connections to provide resistance to vertical shear along with both positive and negative moment demands. The experimental results verify that the proposed connection details are sufficient to provide elastic superstructure behavior well beyond the overstrength moment in the column due to horizontal seismic forces. Further, the results confirm that connections are sufficient to maintain shear and moment stability for significant vertical acceleration demands. (The project test videos and other additional information may be found at: <http://sri.cce.iastate.edu/abc-seismic/>)

Design recommendations have been developed for the connection details to assist in sizing the strand and reinforcement elements in the connection related to expected moment demands. These recommendations can be used for similar connection details. The girder-to-cap connection details investigated in this work are structurally sufficient and simply constructible. They provide a viable opportunity for the implementation of ABC methods in high seismic regions.

TABLE OF CONTENTS

| | |
|--|-----------|
| Title page | i |
| Technical Report Documentation Page | ii |
| Disclaimer | iii |
| Acknowledgements | iv |
| Abstract | v |
| Table of Contents | vi |
| | |
| CHAPTER 1. INTRODUCTION | 1 |
| | |
| 1.1 Background | 1 |
| 1.1.1 Limitations of precast concrete in seismic regions | 1 |
| 1.1.2 Accelerated Bridge Construction | 2 |
| | |
| 1.2 Inverted-tee system | 5 |
| | |
| 1.3 System test | 8 |
| | |
| 1.4 Vertical acceleration effects | 13 |
| | |
| 1.5 Literature review | 14 |
| 1.5.1 Previous review | 14 |
| 1.5.2 Updated review of ABC in seismic regions | 14 |
| 1.5.3 Connections for Segmental Construction in Seismic Regions | 17 |
| 1.5.4 Seismic Vertical Acceleration | 18 |
| | |
| CHAPTER 2. CONNECTION TEST SETUP AND DESIGN FOR PRECAST I-GIRDERS | 25 |
| | |
| 2.1 Evaluation of system test | 25 |
| 2.1.1 Comparison of as-built and improved connections | 25 |
| 2.1.2 Limitations of system test | 26 |

| | | |
|---|--|---------------|
| 2.2 | Experimental configuration | 27 |
| 2.2.1 | Cap beam and column design | 28 |
| 2.2.2 | Girder, diaphragm, and deck design | 31 |
| 2.3 | Load protocol | 31 |
| 2.3.1 | Target shear and moment values | 33 |
| 2.3.2 | Proposed load sequence | 34 |
| CHAPTER 3. CONNECTIONS FOR I-GIRDERS AND CAP BEAM UTILIZING UNSTRESSED STRANDS | | 36 |
| 3.1 | Connection details for dapped end I-shaped girders and inverted tee cap beams | 36 |
| 3.1.1 | GUSC detail | 36 |
| 3.1.2 | LUSC detail | 37 |
| 3.2 | Construction of GUSC/LUSC test unit | 39 |
| 3.2.1 | Construction | 39 |
| 3.2.2 | Instrumentation | 42 |
| 3.3 | Experimental results | 52 |
| 3.3.1 | Overall connection behavior | 52 |
| 3.3.2 | Failure mechanisms | 54 |
| 3.3.3 | Behavior of the connection interface | 56 |
| 3.3.4 | Performance of the GUSC detail | 57 |
| 3.3.5 | Performance of the LUSC detail | 60 |
| CHAPTER 4. ESBF AND ESSP CAP BEAM CONNECTIONS FOR BULB TEE GIRDERS | | 69 |
| 4.1 | Prototype Design | 69 |
| 4.1.1 | Column Design | 70 |
| 4.1.2 | Bent Cap Design | 70 |

| | | |
|---|--|----------------|
| 4.1.3 | Girder and Deck Design | 71 |
| 4.1.4 | Connection Design | 71 |
| 4.2 | Test Unit Design | 77 |
| 4.2.1 | Girder Design | 78 |
| 4.2.2 | Connection Design | 79 |
| 4.2.3 | Footing and Column Design | 80 |
| 4.3 | Test Unit Construction | 86 |
| 4.3.1 | Construction sequence | 86 |
| 4.4 | Instrumentation | 90 |
| 4.4.1 | General | 90 |
| 4.4.2 | Internal Instrumentation | 90 |
| 4.4.3 | External Instrumentation | 94 |
| 4.5 | Loading Protocol | 97 |
| 4.5.1 | General | 97 |
| 4.5.2 | Gravity Load | 97 |
| 4.5.3 | Horizontal Ground Motion | 100 |
| 4.5.4 | Vertical Ground Motion | 100 |
| 4.5.5 | Combination of Forces for the Loading Protocol | 101 |
| 4.6 | Experimental Testing and Results | 105 |
| 4.6.1 | General | 105 |
| 4.6.2 | ESBF Connection | 107 |
| 4.6.3 | ESSP Connection | 115 |
| CHAPTER 5. ESMS AND ESLS CAP BEAM CONNECTIONS FOR BULB TEE GIRDERS | | 121 |
| 5.1 | Prototype Design | 121 |
| 5.1.1 | Connection Design | 121 |

| | | |
|--|---|------------|
| 5.2 | ESMS/ESLS Test Unit Design | 123 |
| 5.3 | ESMS/ESLS Test Unit Construction | 124 |
| 5.3.1 | Construction Sequence | 124 |
| 5.3.2 | Construction Challenges | 128 |
| 5.4 | Instrumentation | 129 |
| 5.4.1 | Bent Cap | 129 |
| 5.4.2 | Precast Bulb-Tee Girder | 131 |
| 5.4.3 | Precast Bulb-Tee Girder to Bent Cap Connections | 132 |
| 5.5 | Load Protocol | 137 |
| 5.6 | Experimental Observations and Results | 138 |
| 5.6.1 | ESMS Connection | 138 |
| 5.6.2 | ESLS Connection | 148 |
| CHAPTER 6. DESIGN RECOMMENDATIONS | | 157 |
| 6.1 | Negative Moment Resistance | 157 |
| 6.2 | Positive Moment Resistance | 162 |
| 6.2.1 | Shear Friction | 163 |
| 6.2.2 | Extended Girder Strands | 168 |
| 6.2.3 | Modified approach for dapped end I-girders | 172 |
| 6.2.4 | Modified approach for dowel bar confinement from looped strands | 173 |
| 6.3 | Recommended Connection Design Approach | 174 |
| 6.3.1 | Positive Moment Resistance | 174 |
| 6.3.2 | Selection of Connection Details | 177 |
| 6.3.3 | Design Procedure | 180 |
| 6.3.4 | Detailing Requirements | 181 |

| | |
|--|-----|
| CHAPTER 7. CONCLUSIONS AND BENEFITS | 184 |
| 7.1 Overview | 184 |
| 7.2 Summary of Connection Test Results | 186 |
| 7.2.1 I-Girder and Inverted-Tee Cap Beam | 186 |
| 7.2.2 Bulb-Tee Girder and Cast-in-Place Cap Beam | 190 |
| 7.3 Conclusions | 195 |
| 7.4 Benefits of Research Results | 198 |
| REFERENCES | 199 |
| APPENDIX A: I-GIRDER TEST UNIT | 206 |
| APPENDIX B: EQUATIONS AND CALCULATIONS | 211 |
| APPENDIX C: BULB-TEE TEST UNIT | 214 |
| APPENDIX D: BULB-TEE TEST UNIT LOADING PROTOCOL | 220 |
| APPENDIX E: DESIGN EXAMPLE | 225 |

Chapter 1. Introduction

1.1 Background

The ever-growing population and always-expanding transportation infrastructure in the state of California require continuing innovation in the state's bridges. In 2010 the state had over 24,500 highway bridges, with an average age of 44.4 years and more than 8300 bridges over 50 years old (Shoup, 2011). In addition to the number and age of bridges in California, the threat of earthquakes is also a significant factor. As research continues to advance seismic design approaches, the seismic vulnerability of the current bridge inventory is constantly being reviewed by the California Department of Transportation (Caltrans). In addition, Caltrans has undertaken an ambitious retrofit program, which is largely complete for the state highway system. According to Caltrans' data, over 98% of the state-maintained bridges have undergone seismic safety retrofit work, as have about 45% of local agency bridges in the state (Caltrans, 2014). While some retrofit work remains, perhaps of even more importance is the replacement of bridges nearing the end of their life span. Therefore, practical and easily-constructible methods for new construction of bridges that are seismic-sufficient must continue to be developed. Given California's propensity for earthquakes, Caltrans has been at the forefront of the development of seismic solutions for earthquake loading for decades, both for retrofits and new construction.

Many states around the country have similar infrastructure concerns as California. Consequently, new methods to quickly construct bridges are increasingly being developed and promoted. Approaches that seek to minimize field construction time are typically referred to as Accelerated Bridge Construction (ABC) methods. ABC methods continue to be advanced around the country, as evidenced by events such as the 2014 National ABC Conference which was co-sponsored by 26 state departments of transportation along with several other national and regional organizations (Florida International University, 2014).

1.1.1 Limitations of precast concrete in seismic regions

One of the most common ways to incorporate ABC techniques is to use prefabricated elements, especially precast concrete elements. However, precast concrete has historically performed poorly when subjected to earthquake loading, primarily due to connection failures. Consequently, the incorporation of such techniques in moderate-to-high seismic regions has been

limited. The reluctance to incorporate precast concrete is seen in the current bridge data from Caltrans, which shows that cast-in-place concrete accounts for over 70 percent of the bridges while precast concrete accounts for about 5 percent (Hida, 2012). The vulnerability of precast structures has been largely due to the inadequate performance of connections and failing to ensure satisfactory load paths. Precast concrete structures were observed to experience connection failures (especially in buildings) in past seismic events including the Loma Prieta earthquake in 1989 (Housner & Thiel, 1990) and the Northridge earthquake in 1994 (Seismology Committee, July, 2010), (Priestley et al., 1994). For Caltrans to utilize the benefits of ABC methods in seismic regions, new connection details for precast concrete members must be developed that ensure the seismic performance of a structure built with precast elements will be similar to a cast-in-place structure.

1.1.2 Accelerated Bridge Construction

Accelerated Bridge Construction (ABC) methods are increasingly desired to be implemented because of the many advantages such methods offer. ABC methods allow the total field construction time to be significantly reduced when compared to traditional field construction techniques. The primary underlying technique to a variety of ABC approaches is to use prefabricated components, thus diverting construction time from the field and into the controlled shop environment. Precast concrete members, in particular, are used heavily in ABC projects. If precast concrete members are utilized, components can simply be pieced together in the field, rather than all of the formwork, concrete placement, and curing time that is required with traditional cast-in-place concrete techniques. One example of the time-savings that can occur with the implementation of ABC methods is the U.S. 6 Keg Creek Bridge as shown in a construction photograph in Figure 1.1. This ABC project was under the oversight of the Iowa Department of Transportation. According to AASHTO, the construction time on this project was cut from approximately six months using normal field construction methods to a total time of only two weeks (AASHTO, US 6 Keg Creek Bridge, 2011). While this project, conducted in rural Iowa, certainly has different constraints and aspects than a project in urban California, the project clearly demonstrated how ABC methods offer the opportunity to construct ordinary bridges much faster than with traditional techniques. Given the multitude of ordinary bridges in California that need replacement, ABC methods suitable for seismic regions are clearly advantageous.



Figure 1.1: Keg Creek Bridge constructed using ABC methods (AASHTO, US 6 Keg Creek Bridge, 2011)

Such reduction in construction time brings many tangential benefits. First, traffic diversion during construction is significantly decreased, and consequently traffic and jobsite safety is increased (International Federation of Structural Concrete, 2007). Reduced time in the field also serves to minimize the environmental impact of such projects. In addition, because ABC methods incorporate prefabricated components, further benefits are realized by moving much of the construction process into controlled shop environments. Some of the benefits of such prefabrication that have been observed and cited by the Federal Highway Administration (FHWA) over the years include improved constructability, increased quality, and lower life cycle costs (Federal Highway Administration, 2006).

A topic that is still being explored is the cost of implementing ABC methods versus conventional bridge construction. Since field labor tends to be more costly than shop work, the FHWA notes that ABC methods can at times reduce overall cost by decreasing field time (Federal Highway Administration, 2010). However, since the use of ABC often implements new technology and introduces new challenges, the construction cost of ABC projects can be higher than construction cost with conventional methods. For example, the construction cost of the Keg Creek Bridge project, mentioned above, was about 30 percent higher than the expected cost of a

similar bridge built using conventional construction techniques (Iowa Department of Transportation, 2012). The FHWA has done some work in comparing costs of completed ABC projects to costs of comparable conventional construction methods (Federal Highway Administration, 2012). This investigation has shown that some completed ABC projects have cost more than would be expected using conventional methods, and some have cost less. However, the FHWA has concluded that the implementation of ABC is very cost-competitive when considering total cost of projects, including lost income due to diversion of traffic and costs related to environmental impact during construction. In addition, as ABC continues to be promoted and becomes more standard practice, the cost of ABC will continue to be reduced because of multiple-use benefits and increasing familiarity with the technology.

As a result of the many benefits associated with ABC techniques, states around the country are pursuing a variety of ways to incorporate such methods. While brief searches related to almost any one of the many state departments of transportation around the country will yield some mention of and interest in ABC methods, states that the FHWA specifically cites as having undertaken significant ABC work include Utah, Florida, New York, Virginia, Iowa, Washington State, Louisiana, Texas, and South Carolina (Federal Highway Administration, 2009) (Federal Highway Administration, 2010). Figure 1.2 shows a photograph of Utah's Lambs Canyon Bridge constructed using ABC methods.



Figure 1.2: Lambs Canyon Bridge constructed using ABC methods (FHWA, 2010)

1.2 Inverted-tee system

A common design implemented by Caltrans utilizes cast-in-place box-girders integrally connected to a cast-in-place concrete cap beam (Caltrans, 2011). Cast-in-place designs are often still preferred because of the belief that such designs are more reliable in seismic events, tend to have lower construction costs, and can be better suited for longer spans. However, a different detail that utilizes an inverted-tee bent cap integrally connected to precast girders has been occasionally implemented for decades for bridges with shorter spans. This detail is increasingly desirable since its configuration tends to allow quick installation of girders and thus works well in projects where ABC methods are needed or desired (Thiemann, 2010). It is typically implemented by using a cast-in-place column with an inverted-tee cap beam that can be either cast-in-place or precast and set in place. Once the cap beam is positioned, the ledge, or corbel, on each side of the cap beam stem works well to support the dapped end of precast girders which can then be attached to the cap beam by the use of a cast-in-place diaphragm. The dapped-end-girder to inverted-tee concept is shown in Figure 1.3. (Note that this figure provides the concept only; specific details such as girder block ends, diaphragms, etc. that were incorporated into this research are shown in the details provide later in the report.) Finally, the bridge deck can be cast-in-place over the completed superstructure. Such a configuration has recently been used in projects where existing structures are widened, to allow for relatively quick construction time and reduced field work.

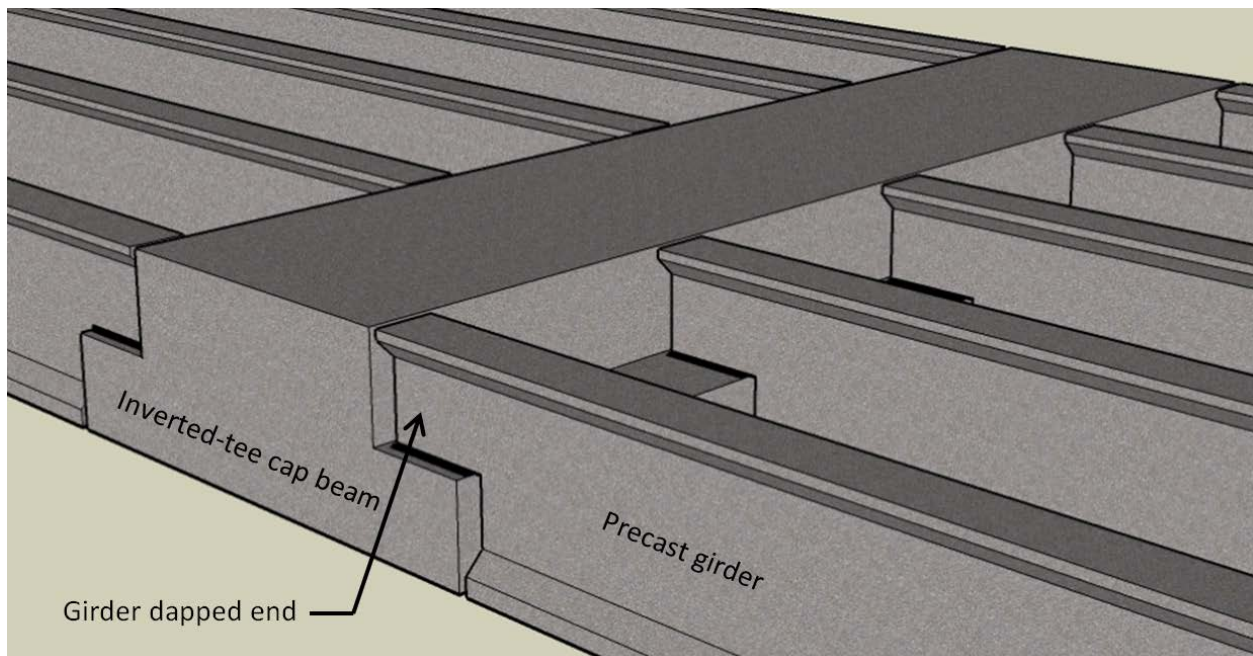


Figure 1.3: Inverted-tee and girder dapped end connection

The inverted-tee bent cap system can be used for single or multi-column bent configurations. The structure is made continuous for live load by pouring the concrete deck over the length and width of the structure, in addition to pouring a diaphragm around the girders and cap. Hooked reinforcement is typically placed between the cap and diaphragm to establish a connection between the diaphragm and inverted-tee bent cap. Additionally, dowel bars are often placed within the girders, which extend into the diaphragm in order to further establish a connection between the embedded ends of the girders and the diaphragm.

Use of the inverted-tee bent cap system has a number of significant advantages, when compared to traditional cast-in-place systems, as well as other precast methods including spliced girders made continuous. First, inverted-tee bent caps allow for the use of precast girders, which can be cast in a controlled environment off site and shipped to the site for placement. Not only does this result in a higher quality girder than would be produced in the field, but it also allows for substantial economic savings as it lends itself to accelerated bridge construction practices. Construction time is typically reduced when precast components are employed as they may be cast ahead of schedule. Additionally, once they arrive at the job site, they are typically easier and quicker to place; this reduces the amount of congestion created due to stopping or delaying traffic during construction. Also, environmental benefits may be observed, such as a reduction in noise and air pollution. Second, the use of the inverted-tee system decreases the required depth of the superstructure when compared to more traditional types of bent caps; this is especially noticed when using girders with dapped ends. Finally, compared to the method of spliced girders made continuous, the inverted-tee system requires less supporting falsework, as it would only be required when casting the inverted-tee bent cap. The girders may then be placed directly on the bent cap without any direct support from falsework. This advantage will also result in economic, time, and environmental savings.

Unfortunately, precast components are still not frequently used for bridges in areas of seismic activity, which is mainly due to lack of a definite design methodology and research validation confirming adequate seismic performance of the connections involving the precast members. However, if a design methodology were developed and proven to be reliable, it is very likely that the use of precast construction would become widely accepted in seismic areas. The advantages of this practice would be numerable, as previously discussed, and the use of precast components would contribute significantly to the accelerated bridge construction methods, which has become

a significant interest in today's industry due to the significant time and cost savings that it provides. Furthermore, if the connection between the precast I-girders and the inverted-tee bent cap were improved and tested successfully, the system could be used in future bridges as a very viable precast system, which would easily lend itself to accelerate bridge construction.

Currently, when designing bridges incorporating the inverted-tee bent cap detail, Caltrans design engineers assume that the connection has little if any positive moment resistance. In other words, the top of the column is assumed to be a pinned connection for any transverse or longitudinal loading conditions. This is done in accordance with California DOT's Seismic Design Criteria, which assumes, based on the previous seismic behavior of precast girders, that the moment connection between the girders and cap beam would likely degrade to a pinned connection (Caltrans, 2006), (Hastak et al., 2003). Therefore, the columns are designed with only one plastic hinge, located at the base of the column. However, it is likely that a significant amount of negative moment resistance would be provided given the reinforcement in the deck over the bent cap. Furthermore, given the reinforcement extending from the cap and into the diaphragm, as well as the dowel bars extending from the girders into the diaphragm, it is possible that the connection could support enough moment to develop a hinge at the top of the column as well. If that were the case, it would be possible to reduce the size of both the columns and the footings, as each hinge would experience a reduced moment demand. As a result, significant cost savings could be achieved. Additionally, the use of two plastic hinges provides additional redundancy to the system, reduces the displacement at the top of the column and therefore the likelihood of unseating of the girders, and allows for the use of a pinned-base if desired. Conversely, if the connection does have a significant moment capacity, then the inverted-tee bridges that are currently in place must be inspected as the connection could potentially pose serious consequences in the event of an earthquake. It is possible that the existing connection would not have been detailed with an adequate shear or moment capacity or an inappropriate amount of anchorage of the reinforcement that is entering column. More importantly, an unstable mechanism of inelastic response could occur at the top of the column, possibly resulting in a failure of the column. Damage to various parts of the structure, including the column and the superstructure, may also be likely if they were not designed under the capacity protection design philosophy, which ensures a suitable strength margin in order to prevent undesirable inelastic action from occurring in areas outside the specified plastic hinge regions. Finally, it has been identified that, given the potential for large rotations

between the superstructure and the cap, the potential for damage of the girders and surrounding superstructure exists. This damage could be further compounded by the fact that a relatively small contact area between the girders and inverted-tee cap is available to transfer shear forces into the joint, which could potentially further damage the concrete within the joint area. Therefore, it is likely that simply fixing the column to avoid failure would not solve all of the potential problems that could be encountered by the structure. These consequences must be addressed, as a serious possibility for large economic and human losses would exist.

1.3 System test

A joint study was completed in 2010, hereafter referred to as the “system test”, to further investigate the potential use of the inverted tee bridge system in seismic regions (see Snyder et al., 2011). This study was conducted to verify the seismic performance of the overall inverted tee bridge system. In addition, the study was used to quantify the seismic performance of an as-built girder-to-cap connection detail and also to establish an improved connection detail better equipped to handle seismic demands efficiently.

The system test utilized a 50%-scale test unit to simulate the region around the center bent of the prototype bridge shown in Figure 1.4, following a similar approach as Holombo et al. (1998). The test unit, shown in Figure 1.5, incorporated five girders approximately 28 ft long on each side of the inverted tee cap beam, along with a single-column bent, to model the portions of the center span of the prototype between the approximate horizontal seismic inflection points. The cap beam region of the test unit, shown in cross-section in Figure 1.6, was designed to incorporate the as-built connection detail along with an improved connection detail. The as-built connection incorporated three dowel bars that were encased in the cast-in-place concrete diaphragm following girder placement. However, for the improved connection detail, unstressed prestressing strands were run through ducts in the bottom flange of the girder and the bottom of the cap beam. These strands provided tension continuity for positive moment in the girder-to-cap connection, thus supplementing the negative moment tension continuity provided by the deck reinforcement.

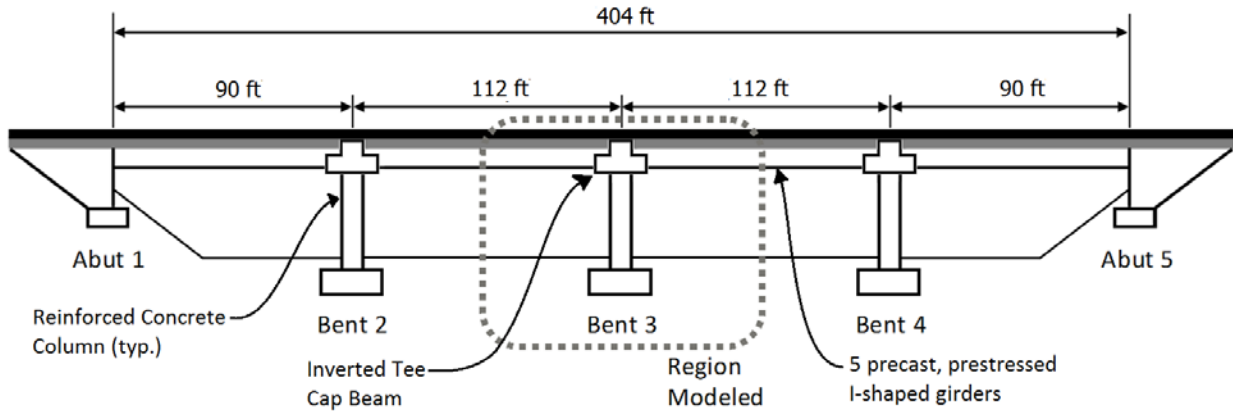


Figure 1.4: Prototype bridge utilizing the inverted tee system

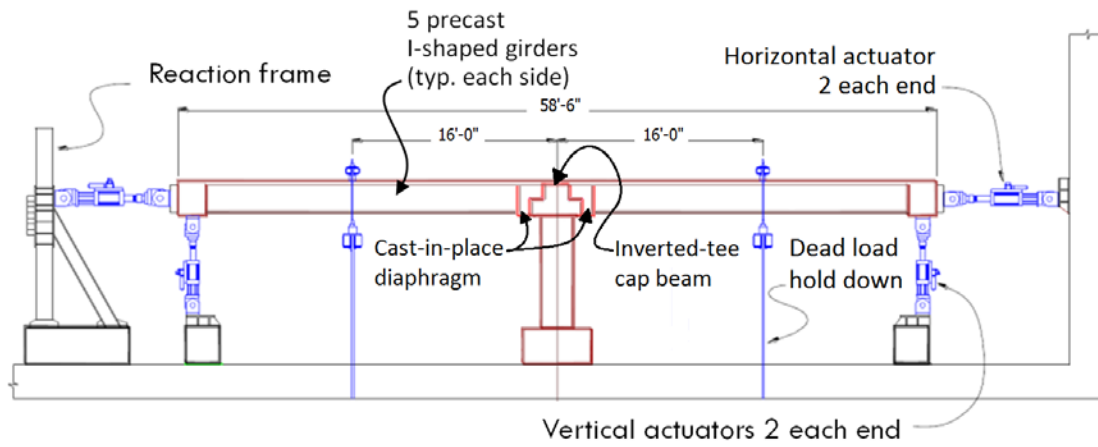


Figure 1.5: System test unit configuration

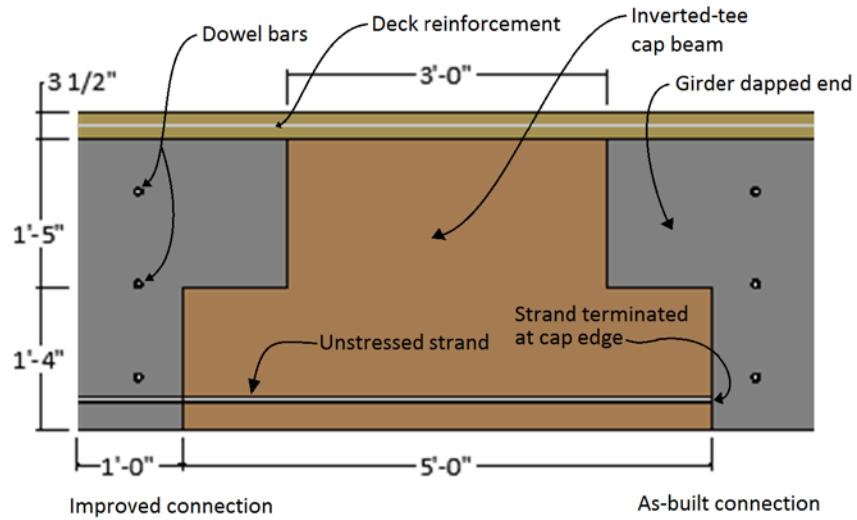


Figure 1.6: Improved girder-to-cap connection detail utilized in the system test

In Phase I of the system test, the test unit superstructure was subjected to cyclic horizontal loads and displacements in the longitudinal direction to simulate horizontal seismic action. Expectations from the test, based on analytical predictions including finite element and grillage analyses, included: (1) good overall system seismic performance, (2) similar negative moment capacity for both the as-built and improved connections, (3) positive moment capacity and vertical shear capacity for the as-built connection that would be sufficient to develop the initial column overstrength moment, and (4) increased positive moment capacity for the improved connection. The horizontal force-displacement response envelopes from this phase of testing, for both the push and pull directions, is provided in Figure 1.7. As the figure shows, the system maintained strength up to high ductility levels. Plastic hinges were successfully formed in both the top and bottom of the column. Also, although the different connection details employed on the two sides of the cap beam meant that connection flexural stiffnesses would vary for the push and pull directions, the figure shows that both connections produced very similar system performance for this phase of testing. Overall, the test clearly demonstrated the suitability of the system for high seismic regions.

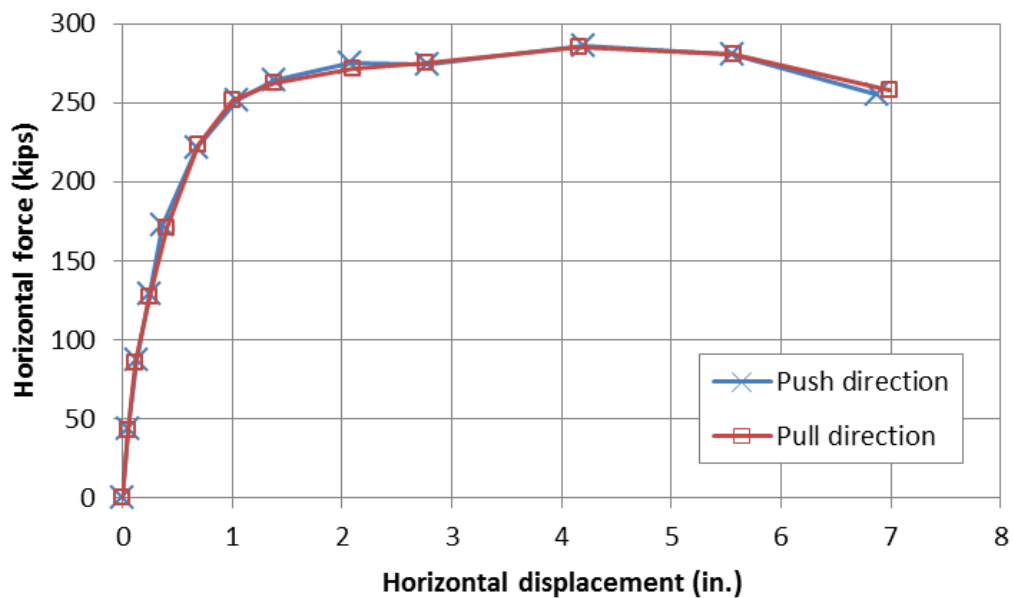
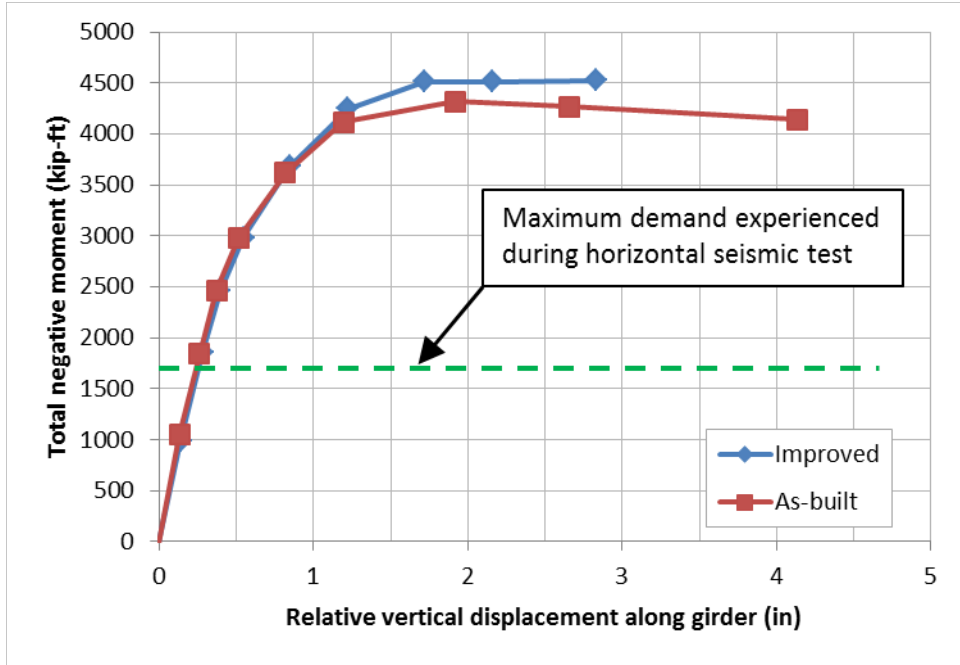


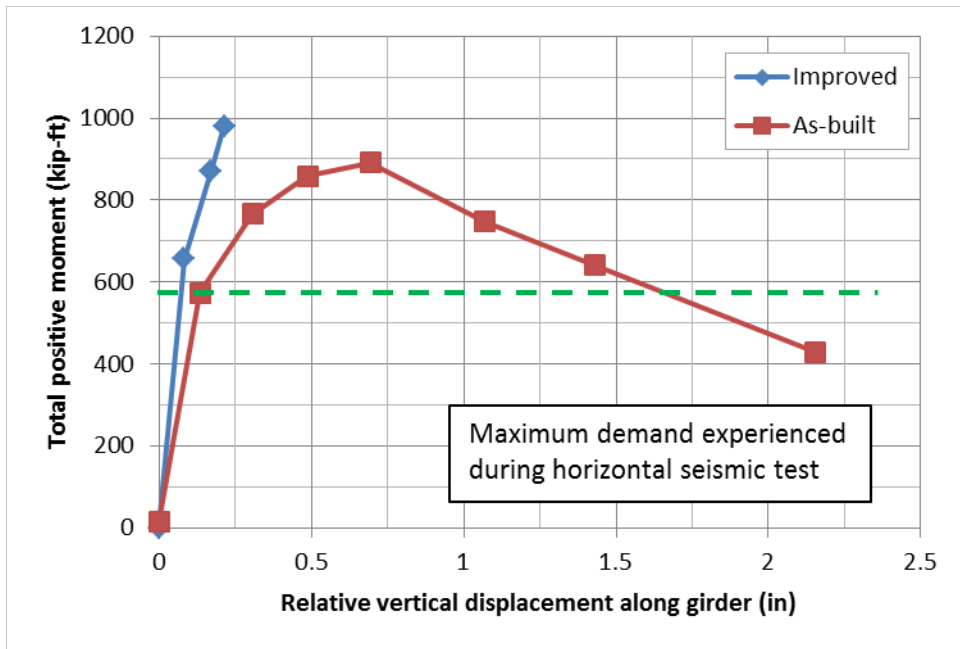
Figure 1.7: Horizontal force-displacement response envelope from system test Phase I

Phase II of the system test was designed to fully exercise the as-built and improved connection details. In this phase of testing, the horizontal actuators were used only to provide stability. The vertical actuators were moved to the hold-down locations 4.9 m (16 ft) from the

column centerline and were used to subject the superstructure to large vertical forces and displacements, also subjecting the girder-to-cap connections to large shear and moment demands. Figure 1.8 provides the peak moment values for both the improved and as-built details in both the positive and negative moment directions. In the negative moment direction, the performance of both the as-built and improved connections was similar, with slightly more strength exhibited by the improved connection. This similarity was not surprising, since the deck reinforcement provided the tension transfer mechanism for both connections. In the positive moment direction, however, the as-built connection performed noticeably poorer than the improved connection. In fact, deterioration of the as-built connection ended up dictating the end of the experimental test; once the positive moment continuity of the as-built connection was lost, the test unit configuration prevented the development of larger moments in the improved connection. Despite the loss in stiffness in the as-built connection, Figure 1.8b shows that its positive moment strength was considerably higher than the maximum demand during the seismic test, thus indicating its sufficiency in providing an integral connection and allowing plastic hinge formation in the column.



a. Negative moment in girder-to-cap connection



b. Positive moment in girder-to-cap connection

Figure 1.8: Moment-displacement behavior of system test unit due to peak vertical loads

1.4 Vertical acceleration effects

The influence of vertical ground motion during an earthquake event is an important factor of consideration for the girder-to-cap connection detail in the inverted tee system. Typical pseudostatic seismic simulations on bridge test units that have been conducted over the past couple decades have focused on the plastic hinge behavior in the column. These simulations commonly use horizontal force and displacement-controlled testing to determine shear and moment behavior in the column hinge regions. Vertical accelerations resulting from earthquake ground motion will either increase or decrease the axial load in the hinge regions but will not affect the shear and moment in these regions. Consequently, the vertical acceleration effects are often neglected in typical experimental studies of bridge specimens.

However, in the girder-to-cap connection region, vertical acceleration effects must be accounted for, because forces arising from vertical acceleration could contribute significantly to the shear and moment in the connections. In order to demonstrate the sufficiency of the inverted tee system for seismic regions, the girder-to-cap connections must be shown to be suitable for vertical acceleration effects along with demands from horizontal ground motion.

Recognizing the possible vulnerability of superstructure connection to vertical acceleration effects, Caltrans' *Seismic Design Criteria (SDC)* specifies specific vertical acceleration requirements for superstructure connections. Caltrans *SDC* stipulates, in Section 2.1.3, "For Ordinary Standard bridges where the site peak ground acceleration is 0.6g or greater, an equivalent static vertical load shall be applied to the superstructure to estimate the effects of vertical acceleration" (Caltrans, 2013). The *SDC* in Section 7.2.2 requires that this vertical load is to be 25% of the dead load, applied upward and downward. In addition, *SDC* Section 7.2.2 also stipulates that, if vertical acceleration must be considered, longitudinal side mild reinforcement in the girders must be capable by means of shear friction of resisting 125% of the dead load shear at the interface with the cap beam. This requirement exists to protect against potential shear failures should the bottom of the girder attempt to open in a seismic event; however, it has been disadvantageous with respect to the inverted-tee and precast girder system because of the need to include mild reinforcement running continuously between the girder and the cap beam. Thus, one of the objectives of the research detailed in this report was to illustrate that extending unstressed strands from the girder to the bent cap, as was incorporated in the system test improved connection, provides sufficient shear resistance in the connection with adequate capacity to resist vertical

acceleration effects. Such work will verify that the inverted-tee and precast girder system is a robust and economically advantageous option for implementing accelerated construction.

1.5 Literature review

1.5.1 Previous review

An in-depth literature review was included as part of the final report for Caltrans Project 05-0160 (Snyder et al. 2011) which detailed the system test work. This review investigated girder-to-cap superstructure connections and benefits of positive moment connections in superstructures. A number of connection types were compiled, including details that employ bent bars, bent strands, embedded girder ends, additional stirrups, through web reinforcement, and partial diaphragms. Some concerns from past work related to positive moment connections were also reviewed. In addition to design details, the literature review also considered experimental research conducted related to superstructure positive moment connections. A detailed review of grillage finite element analysis methods was also included as part of this review. This review considered analysis limitations, model construction, nonlinear behavior, hysteretic behavior (including the Takeda Model and the Pivot Model, Takeda et al., 1970), torsional behavior of concrete, strain penetration, and bond-slip behavior of strands in concrete. Knowledge gained from this literature review was instrumental in the conduction of the system test as well as the development of the improved connection detail.

1.5.2 Updated review of ABC in seismic regions

1.5.2.1 Background

Accelerated bridge construction (ABC) is being increasingly promoted and pursued by departments of transportation all across the country. Increased transportation demand related to economic and population growth is fueling the desire for rapid construction of bridge projects. Also, the need for improvements to the aging transportation infrastructure throughout the United States has increased the urgency for fast and efficient construction techniques. While brief searches related to almost any of the state departments of transportation across the country will yield some references to ABC methods, states that the FHWA specifically cites as having undertaken

significant ABC work include Utah, Florida, New York, Virginia, Iowa, Washington State, Louisiana, Texas, and South Carolina (FHWA, 2009 and 2010).

In the few years since the FHWA study mentioned above, interest and work related to ABC implementation has continued to increase. ABC's current relevance in bridge engineering is evident in the *Bridge Engineering Handbook, Second Edition: Construction and Maintenance* (Chen and Duan, 2014). An entire chapter in this updated handbook is devoted to ABC. This reference states that ABC "using streamlined engineering processes and prefabricated elements and systems (PBES) demonstrated its worth through several pilot projects and is being accepted as an innovative practice in today's construction environment" (Chen and Duan, 2014).

1.5.2.2 Use of ABC in Seismic Regions

While much information has been published related to the use of accelerated bridge construction, the main focus of this study is its implementation in seismic regions. Although the use of ABC techniques in seismic regions has been limited, considerable research work in the past several years has been devoted to adapting ABC methods to meet the structural requirements for seismic regions.

The Transportation Research Board has put forth a concerted effort to promote the use of ABC techniques in seismic regions. NCHRP Report 698 (Marsh et al., 2011), the culmination of a 2011 study, provides a literature review of the connections and systems that are currently in use or being studied for use in ABC. The review focused on connections for particular locations (pile to pile cap connections, connections between column segments, substructure to superstructure connections, for example) as well as connections for particular force transfer mechanisms (grouted ducts, integral connections, hybrid connections, etc.) The study rated the various connections using several different categories, including readiness for implementation, potential time savings, potential performance, construction risk, seismic performance, inspectability, and durability. Suggested research from this study includes work related to integral connections that form part of the load path for longitudinal seismic loading. Examples of particular areas of research include looking at flush-soffit cap beam type bridges where longitudinal post-tensioning may or may not be used and innovative connecting approaches beyond those currently in use for cap beams.

Ou et al. (2007) conducted an analytical study investigating the use of segmental columns for seismic regions. This study focused on a column detail that, at the time, had been primarily implemented in regions of low seismicity such as Florida, Texas, North Carolina, Virginia, and

New Jersey. Using first a simplified analytical model incorporating a static pushover approach followed by a detailed three-dimensional finite-element model and associated parametric study, this work investigated the appropriateness of a similar detail for high seismic regions such as California. Notable conclusions from this work included: (1) the simplified model for static pushover analysis provided a simple tool for the seismic design of segmental precast unbonded posttensioned columns, and (2) the 3D FE model was capable of predicting the experimental cyclic behavior of segmental columns with good accuracy. This work was continued when Ou et al. (2010) conducted an experimental study. The test setup utilized vertical actuators for gravity load and a horizontal actuator for lateral load as shown in Figure 1.9 to test four large-scale specimens. The study showed that the proposed columns performed well seismically, having significant ductility and good hysteretic behavior. Joint opening between the segments was found to contribute significantly in the drift and thus necessary to consider in design of similar systems for seismic regions.

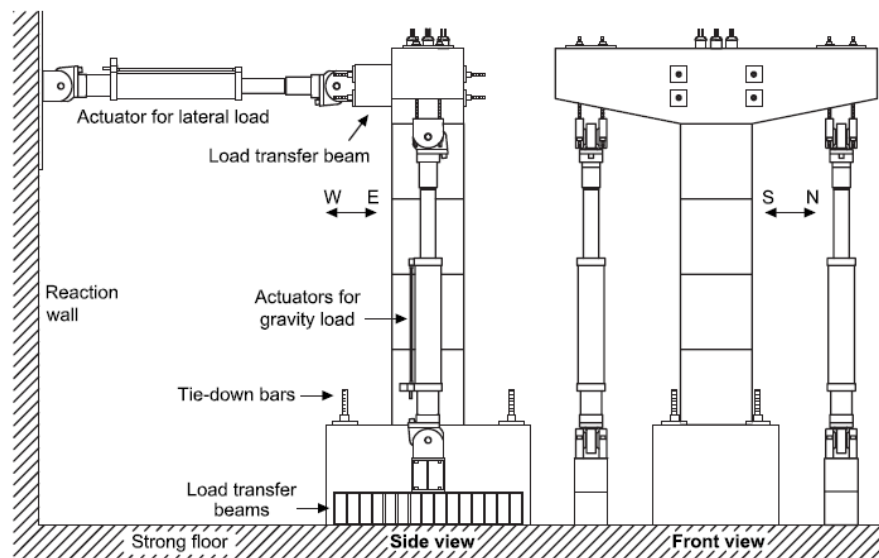


Figure 1.9. Segmental column test setup (Ou et al., 2010)

The Washington State Department of Transportation (WSDOT) is actively working to increase implementation of ABC in seismic regions. A 2010 TRB article explains WSDOT's effort to develop practice and implementation of ABC (Kyaleghi, 2010).

1.5.3 Connections for Segmental Construction in Seismic Regions

Already in the early 2000's, NCHRP was conducting studies on connections between segmental elements to encourage the implementation of ABC techniques. NCHRP 519 (Miller et al., 2004) recommends details and specifications for the design of continuity connections for precast concrete girders, including examples illustrating the design of four precast girder types made continuous for live load. The intent of the study was to recommend connections that would achieve structural continuity and thus provide integral (moment and shear resistant) connections since traditional approaches to segmental construction often conservatively approximate segmental connections to be pins (i.e. simply supported). This study proposed several revisions to the *AASHTO LRFD Bridge Design Specifications* (AASHTO, 2003) related to the following: (1) the definition of continuous precast/prestressed concrete bridges, (2) time-dependent material properties and analysis methods for continuous precast/prestressed concrete bridges, (3) effect of girder age on the connection continuity, (4) more realistic treatment of cracking effects in connection continuity, (5) design limits for service and strength limit states, (6) clarification of negative moment connection specifications, (7) possibilities for positive moment continuity connections, and (8) detailing requirements.

“Modeling of Jointed Connections in Segmental Bridges” (Veletzos and Restrepo, 2011) presents a segment joint modeling approach as a first step toward accurately estimating the seismic response of the superstructure joints due to input ground motions. The approach combines complex continuum mechanics with a simplified model utilizing rotational springs, including nonlinear tendon-grout slip response. As part of the study's approach, bond slip friction between tendons and grout or tendon ducts and concrete was investigated. The study included validation from large-scale experiments.

Related to the study mentioned above, “Equivalent Unbonded Length for Modeling of Multistrand Tendons in Precast Segmental Construction” (Veletzos, 2014) presents results and conclusions from a large-scale experimental research program that investigated the debonding characteristics of multistrand tendons. This study concluded that tendon slip relative to grout is small in comparison with the slip between the duct and the surrounding concrete. The study also developed an equation to evaluate the equivalent unbonded length of multistrand tendons, intended to be directly applied to nonlinear modeling of the segment joint response.

1.5.4 Seismic Vertical Acceleration

1.5.4.1 Background

Research and development related to structural behavior due to seismic acceleration has been extensive in the last 20 to 30 years. However, the vast majority of this work has focused on horizontal seismic acceleration. This focus makes sense, since the horizontal motion from earthquake events is largely responsible for much of the structural damage. Also, horizontal effects introduce an entirely new direction of action to a traditionally-designed structure, whereas vertical effects occur in the same direction as gravity and live load effects that have traditionally been the primary focus in structural design. Furthermore, maximum vertical effects typically occur very early during an earthquake event, whereas maximum horizontal effects tend to come a bit later in the event; therefore, maximum vertical and horizontal effects do not typically occur simultaneously.

Despite reasonable justification for focusing on horizontal effects, interest in vertical seismic acceleration effects has increased in recent years. This interest has been generated in part by the simple observation that vertical effects have not been studied that much and therefore are not understood that well. This lack of understanding can lead to overly conservative approaches. For example, in certain Caltrans details, reinforcement is added to provide an additional safety factor in preventing possible failure due to vertical effects, without specific justification for including it. The reinforcement is included simply as a precaution, in case vertical effects might cause a problem in the detail. Many designers realize that current approaches may be conservative, so they desire to have a better understanding of the vertical acceleration effects to design more efficiently.

In addition, many engineers and scientists involved with structural seismic behavior became more interested in vertical seismic effects as a result of the 2011 earthquake in Christchurch, New Zealand. This earthquake produced amazingly high vertical accelerations, even though its moment magnitude was only moderate. The vertical accelerations were to be contributing factors in some of the structural failures that produced large amounts of destruction and some loss of life.

1.5.4.2 Models that approximate geological (seismologic) observations

Many recent studies have investigated vertical peak ground acceleration (PGA) and have compared magnitudes of peak vertical accelerations with peak horizontal accelerations. In 2012, Tezcan and Cheng presented a nonparametric approach to characterize vertical seismic effects.

This approach was compared with a current empirical model for varying magnitude, distance, and local soil conditions. This reference states that it is common practice to set the ratio of vertical to horizontal spectrum (V/H) to 2/3, but it is currently recognized that this practice is not always conservative. The analytical approach presented in this reference used magnitude, source-to-site distance, and shear wave velocity in the top 30 m of the soil profile. It then employs a support vector machines algorithm to analytically develop V/H estimates; in short, as per the authors, this “algorithm learns the nonlinear relationship between a set of predictive variables and the V/H ratio directly from ground motion data.”

In 2011, a study by Bommer et al. developed a model for the prediction of V/H ratios based on similar input as incorporated in Tezcan and Cheng’s study. This model was developed from strong-motion accelerograms from the Middle East and Europe. Bommer et al. (2011) cite four current models for the prediction of V/H ratios based on magnitude, distance, and site class: Ambraseys et al. (1996), Kalkan and Gulkan (2004), Ambraseys and Douglas (2003), and Gulerce and Abrahamson (2011). Bommer et al. (2011) cite major limitations to the first three models and developed their model using a similar approach to Gulerce and Abrahamson (2011). The model uses functional forms and regression analysis to estimate V/H ratios for PGA and 5%-damped spectral accelerations up to a period of 3.0 s. This study concluded that this approach provides a reasonable method to estimate the distribution of V/H ratios of ground motions generated by shallow crustal earthquakes in the regions considered for the study. The approach is very similar to the method developed by Gulerce and Abrahamson (2011) for North American regions.

A Yang and Lee (2007) study documented the characteristics of vertical and horizontal ground motion during the earthquake in Niigata-ken Chuetsu, Japan, in 2004. This study showed that, for this data set, the ratio of peak vertical to horizontal acceleration was typically less than or equal to 2/3, but for a few sites the ratio was higher than 2/3 or even 1. The study also concluded that the ratio between peak velocity and peak acceleration depends on site-to-source distance and site condition, with ratios increasing as the epicentral distance increased or the soil stiffness decreased. Another finding was that the vertical response spectra tend to display low frequency contents at distant sites and high frequency contents at hard sites, whereas the effects of site condition and distance seemed to be less significant for horizontal response spectra. The study also showed that the peak value of the average vertical response spectra was lower and occurred at a period of about

one half the horizontal spectra. Finally, the study concluded that the V/H ratio was strongly dependent on spectra frequency, site-to-source distance, and site condition, being significantly higher than 2/3 at short periods and in the near-field region, and also exceeding 2/3 at very long periods (greater than 5 s).

The studies presented thus far focus on the V/H ratio, where V is the magnitude of vertical PGA and H is the magnitude of horizontal PGA. However, very few of these investigations have compared the simultaneous magnitude of vertical and horizontal accelerations. One of the only studies that considered vertical accelerations and horizontal accelerations at the same time was a study by Ambraseys and Douglas (2000), along with a follow-up study in 2003. In fact, these studies mentioned the limitation of omitting consideration of simultaneous behavior, saying: “A major draw-back of the acceleration ratio ... for practical purposes is that in an earthquake the maximum ground or response accelerations in the vertical and horizontal direction occur at different times.” In this study, extensive ground acceleration records from seismic events were used to develop an absolute vertical-to-horizontal spectral ratio, $q_s = (SA_v/SA_h)_{\max}$. Here, SA_v and SA_h are peak values of vertical and horizontal acceleration, adjusted for distance and site effects. This is comparable to the common V/H ratio. However, the study also developed a simultaneous vertical to horizontal spectral ratio, $q_i = u_{tt,v}(t_{\max})/SA_h$, where $u_{tt,v}$ is the vertical response acceleration at time t_{\max} , and t_{\max} is the time at which the peak horizontal acceleration occurs. Figure 1.10 is a reproduction from the study which compares the absolute ratio (top set of curves) with the simultaneous ratio (bottom set of curves). For each set of curves, the solid line is for all earthquakes, the dashed line is for normal motion, the dashed line is for thrust motion, and the dash-dot line is for strike-slip motion. While the predicted absolute ratio for all earthquakes is between 0.3 and 0.4 for periods higher than 0.3 s, the predicted simultaneous ratio for all earthquakes is close to 0.1 for the same range, significantly lower. This difference indicates the unlikelihood of vertical and horizontal peaks occurring simultaneously. Also, in the 2003 follow-up study, Ambraseys and Douglas mention that “the spectral response of the vertical acceleration and the attenuation of its spectral ordinates with magnitude and distance differ in amplitude and shape from those of the horizontal.”

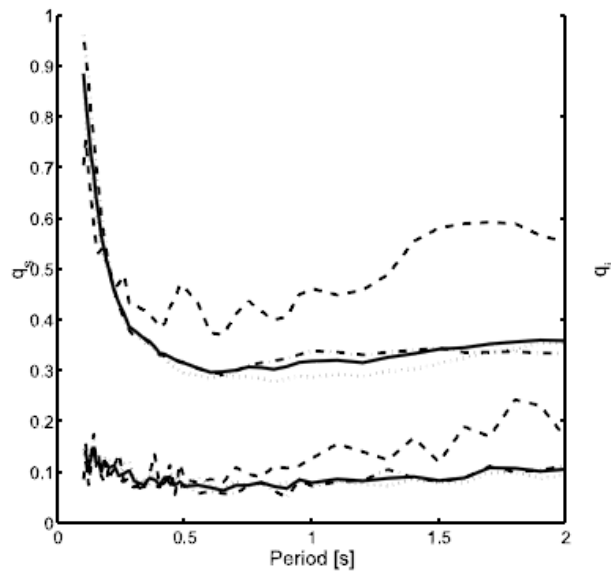


Figure 1.10 Comparison of q_s and q_i

However, especially for locations in close proximity to the fault, the peak vertical acceleration can occur almost simultaneously with the peak horizontal acceleration. Consider Figure 1.11, for example, taken from Abrahamson and Silva (1997). This figure shows acceleration time histories recorded for the 1994 Northridge earthquake (on top, at the Pacoima Dam-downstream site), and for the 1989 Loma Prieta earthquake (on bottom, at the Corralitos site). Both of these locations were within 8 km of the fault responsible for the event, and the figures show that the vertical acceleration peaks (shown as the middle record for both) occurs almost simultaneously with the horizontal peaks; in fact, the horizontal and vertical components are very similarly shaped throughout each record. Of significance related to this behavior is that both sites were rock sites. It seems that for rock sites that are close to faults, horizontal and vertical demands may be expected to similar and simultaneous. This behavior for the rock sites is seen to contrast with acceleration data from two close (9 km or less distance from fault) soil sites from the Northridge event in Figure 1.11 (see next page), also from Silva. Both of these soil sites show short-period motion significantly affecting the vertical acceleration prior to the large horizontal motions; thus, the highest V/H ratios occur prior to the peak horizontal acceleration.

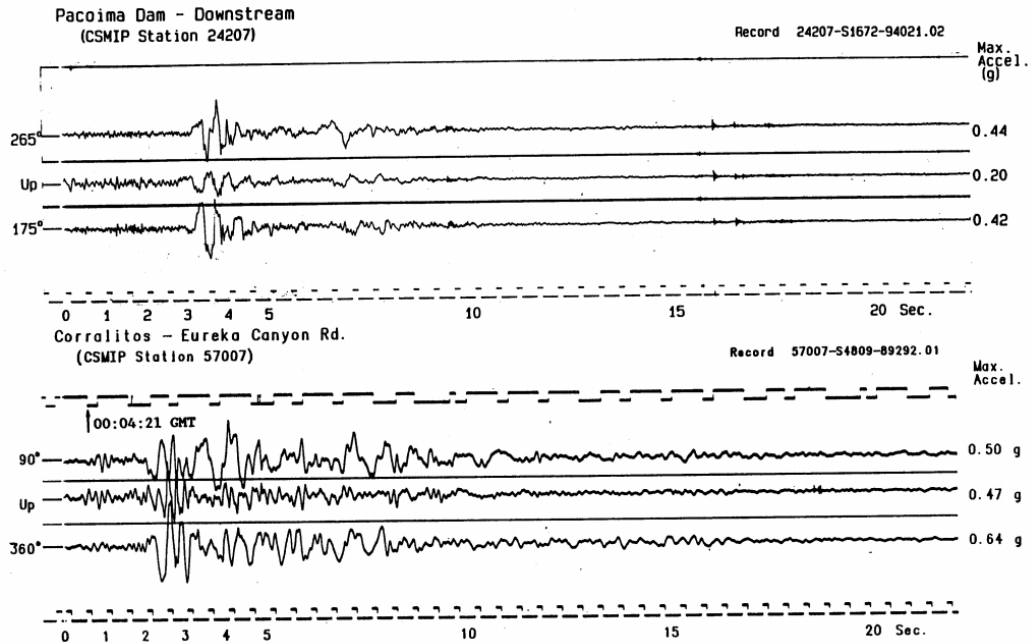


Figure 1.11. Horizontal and vertical component acceleration time histories on rock sites for the 1994 Northridge earthquake (top) and the 1989 Loma Prieta earthquake (bottom)

While not reproduced here, additional investigation by Abrahamson and Silva (1997) from the Northridge and Loma Prieta events showed that, at greater distances from the fault, both rock and soil sites behave more like the short-distance soil sites, exhibiting maximum vertical motions (and, consequently, large V/H ratios) related to short-period behavior prior to the occurrence of the peak horizontal ground motions.

In conclusion, regarding the simultaneous nature of peak vertical and horizontal motions, it appears that, for sites close to faults, relation of vertical and horizontal motion depends largely on soil type and the consequent propagation of the seismic waves through the various types of soil mediums, whereas for sites at greater distances, vertical peak behavior tends to occur prior to horizontal behavior, for both rock and soil sites. Further research on this topic would be beneficial.

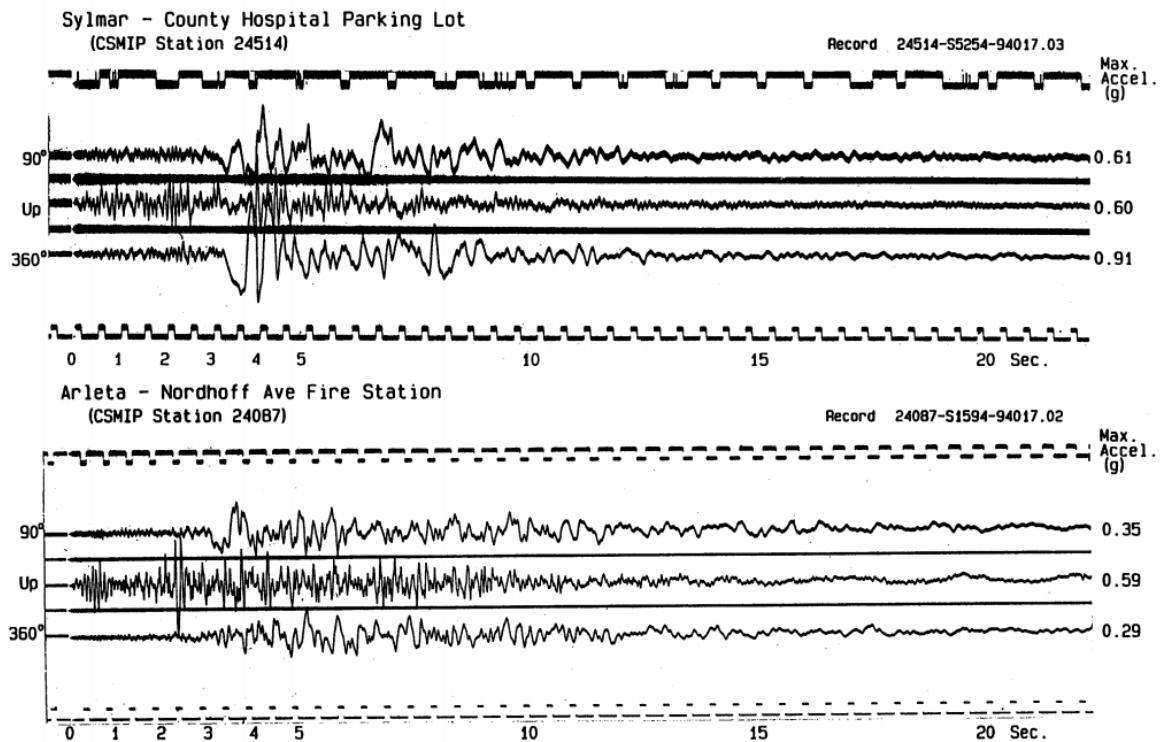


Figure 1.12. Horizontal and vertical component acceleration time histories recorded during the Northridge earthquake

The oft-cited number for the V/H ratio (note that this ratio is commonly reported as V/H, which is the inverse of the ratio mentioned in the question) is $2/3$, is mentioned in the following recently accessed sources: Tezcan and Cheng, 2012; Bommer et al., 2011; Yang and Lee, 2007; Ambraseys and Douglas, 2003; and Ambraseys and Douglas, 2000. The 2003 Ambraseys and Douglas study, which replicates the figure provided above from their 2000 study, reports that the mean ratios for strike-slip and normal events are 0.73 and 0.61, respectively, and hence are quite close to the commonly accepted ratio of $2/3$.

Papazoglou and Elnashai (1996) provide an interesting compilation of data from a few notable events related to vertical acceleration that occurred prior to the time of the study. These events include the Northridge, California quake on January 17, 1994, where a vertical acceleration of 1.18g and V/H ratio of 1.79 were observed; and the Kobe, Japan quake on January 17, 1995, where observations included a vertical acceleration of 0.33g and V/H ratio of 1.21. [Also note that one of the vertical acceleration data points reported by Ambraseys and Douglas (2000) for the Kobe quake was 0.57g.] It does not appear that there are any documented vertical accelerations higher

than the acceleration of 2.2g that was recorded during the Christchurch, New Zealand quake (Kam and Pampanin, 2011).

A sizeable amount of data is available for the two recent mega-quakes, Chile in 2010 with a magnitude of 8.8 (Boroschek et al., 2010) and Japan in 2011 with a magnitude of 9.1 (Kalkan and Sevilgen, 2011). For the Chile event, one reporting station recorded a peak vertical acceleration of 0.702g with a peak horizontal acceleration of 0.564g, for a V/H ratio of 1.24. One other station from the Chile event recorded a vertical acceleration of 0.398g and a peak horizontal acceleration of 0.402g (V/H = 0.99), but most of the stations reported V/H ratios well below 1. For the Japan event, accessing data from 273 reporting stations and comparing recorded vertical and horizontal accelerations, one station recorded 0.406g vertical PGA with 0.374g horizontal PGA (note that this is the resultant of the peaks in the two horizontal directions), for a V/H ratio of 1.09. The average V/H ratio for the reporting stations from the Japan event was 0.41. A final note on the Japan data is that the maximum horizontal PGA reported from these stations was 2.699g, and the vertical PGA recorded at that station was 1.88, for a V/H ratio of 0.70 at the location of largest recorded acceleration.

In summary, it appears that from this limited data, it is not that uncommon for vertical PGA values to exceed horizontal PGA values in large seismic events, as it occurred during about half of the large-scale events that had data available. However, it should also be noted that these occurrences seem to be at only a small fraction of the stations that are affected by a particular seismic event; in other words, even in earthquakes that have reported V/H values higher than 1, it usually only happens in a very small portion of the area affected by the overall quake. It is well-documented that the larger V/H ratios tend to occur at short periods in the near-source distance range (see, for example Silva, 1997).

Chapter 2. Connection Test Setup and Design for Precast I-Girders

2.1 Evaluation of system test

As briefly introduced in Chapter 1, the system test confirmed the inverted-tee cap beam and dapped-end girder concept as a bridge system that provides the opportunity to incorporate precast girders while providing sufficient seismic performance. A brief summary of the pertinent details from the system test that led to the connection test is provided here; for a detailed report on the system test refer to Snyder et al. (2011).

2.1.1 Comparison of as-built and improved connections

The as-built girder-to-cap connection in the system test was successful in behaving as a rigid connection during the Phase I testing, simulating gravity and full horizontal seismic conditions. It remained elastic for the duration of the Phase I test while allowing plastic hinges to fully develop at the columns ends, although its relative displacements at the girder-to-cap interface were larger than for the improved connection. The as-built detail also successfully transferred shear forces and did not allow vertical unseating or collapse of the superstructure. During Phase II testing, it successfully resisted positive moment demand equivalent to the gravity, full horizontal seismic, and 1.0g constant vertical acceleration condition. However, it exhibited nonlinear response in both the positive and negative moment directions under these large vertical load/displacement conditions. In addition, a large gap opening developed at the girder-cap interface under positive moment loading during the Phase II test.

The improved girder-to-cap connection in the system test, which incorporated grouted unstressed strands for positive moment continuity, provided excellent performance in both the Phase I and II portions of the test. It remained elastic under positive moment loading throughout the testing and successfully transferred shear forces and did not allow vertical unseating or collapse of the superstructure. During the Phase II test, which produced maximum shear and moment conditions that were approximately double the expected maximum demand from the gravity and full horizontal seismic condition, the improved connection remained essentially elastic and produced an interface gap opening that was only 6% of the corresponding opening in the as-built condition. The elastic performance of the improved connection under positive moment loading was verified at moment demands well in excess of the gravity, full horizontal seismic, and 1.0g constant vertical acceleration simulated load condition.

2.1.2 Limitations of system test

The system test verified the inverted-tee cap beam and dapped-end girder concept as providing a viable system for incorporating precast girders and accelerated bridge construction techniques in seismic regions. The as-built and improved connection details provided sufficient resistance in both the positive and negative moment loading directions, along with sufficient vertical shear capacity, to develop a plastic hinge in the column and maintain full superstructure stability under maximum horizontal seismic load conditions. However, when the girders in the system test unit were subjected to large vertical displacements (beyond the full horizontal seismic condition), the as-built connections exhibited considerably more deterioration under positive moment loading than the improved connections. Figure 2.1 shows the large opening that developed at the underside of the girder-cap interface.

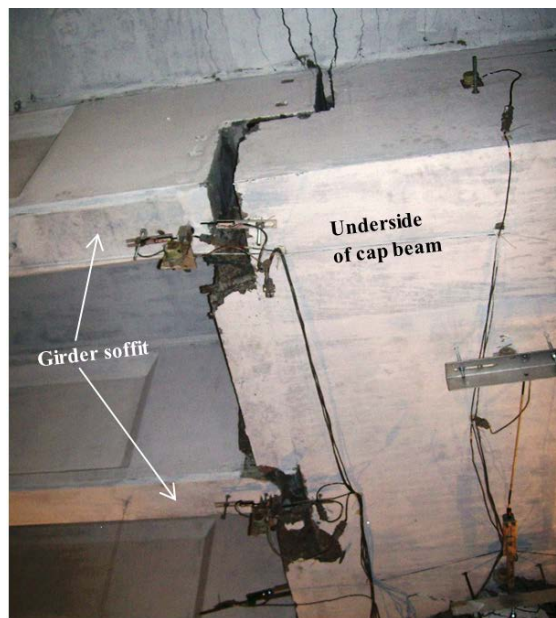


Figure 2.1: Opening of as-built connection under large positive-moment load

The loss of tension resistance for the positive moment direction resulted in the superstructure behaving essentially as if the as-built connection region was a pin, with limited rotational resistance when subjected to large positive moments. This type of behavior is schematically illustrated in Figure 2.2. The deterioration of the rotational resistance in the as-built connection in the positive-moment direction resulted in diminished ability to generate large positive moment action in the improved connection, since additional vertical displacement at the girder ends would

simply produce larger rotations in the pin-like mechanism in the as-built connection and column plastic hinge region. Consequently, the system test unit did not allow full quantification of the improved connection detail.

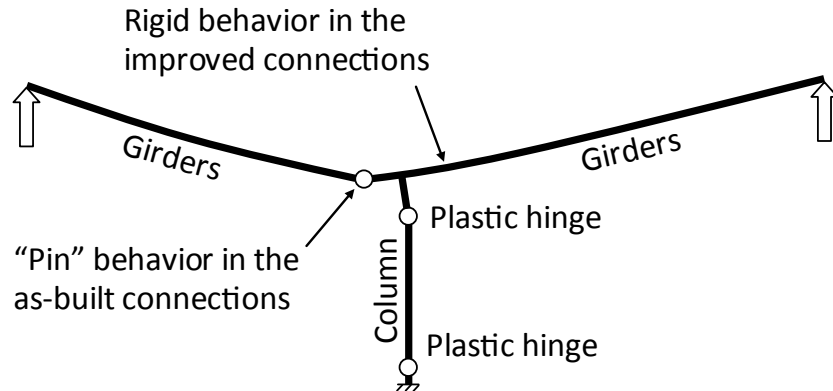


Figure 2.2: Schematic of system test superstructure behavior with girders subjected to large upward vertical displacements

2.2 Experimental configuration

To fully quantify the behavior of the improved connection from the system test, a 50%-scale component test of the connection region was devised to experimentally verify the connection detail without re-creating the whole bridge system. Figure 2.3 provides a three-dimensional representation of the connection test configuration. The test unit, which was designed to provide the opportunity to fully exercise two different girder-to-cap connection details independently from each other, consisted of a single column, footing, and cap beam, along with two I-girders. To appropriately model the composite girder section behavior, a bridge deck was included in the test unit. However, the deck was split between the two girders as shown in the figure to allow the two connection details to be tested separately.

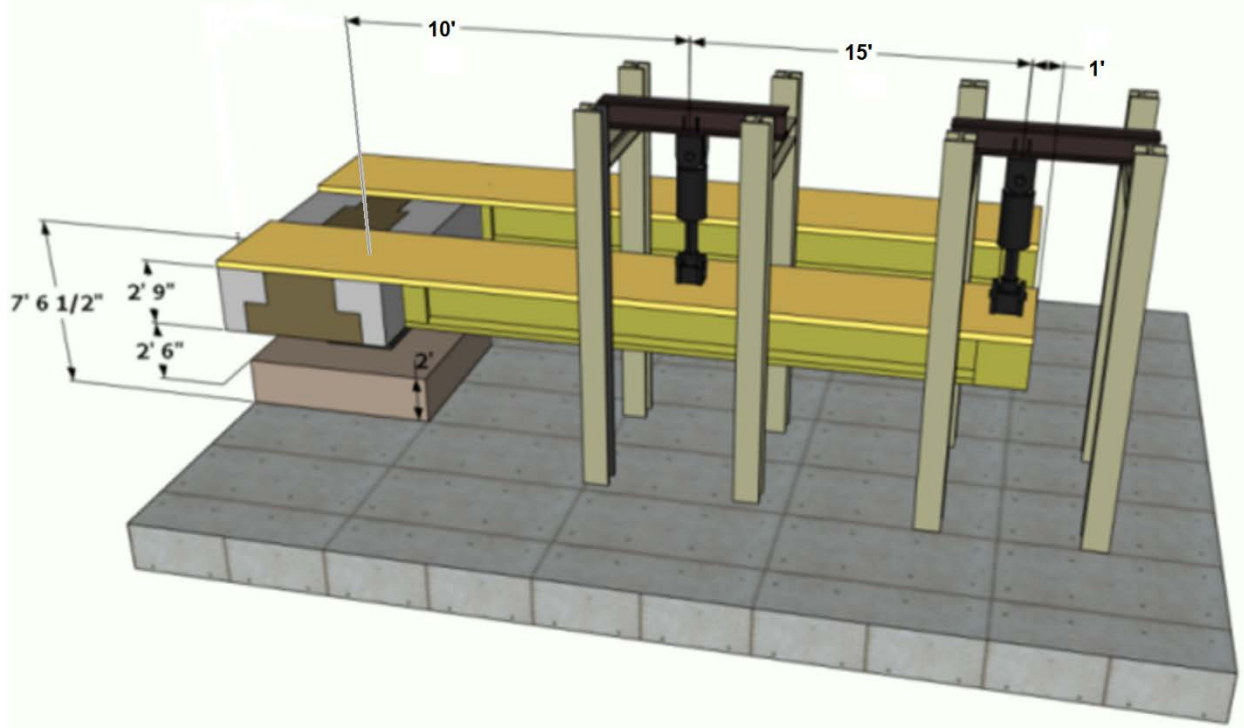
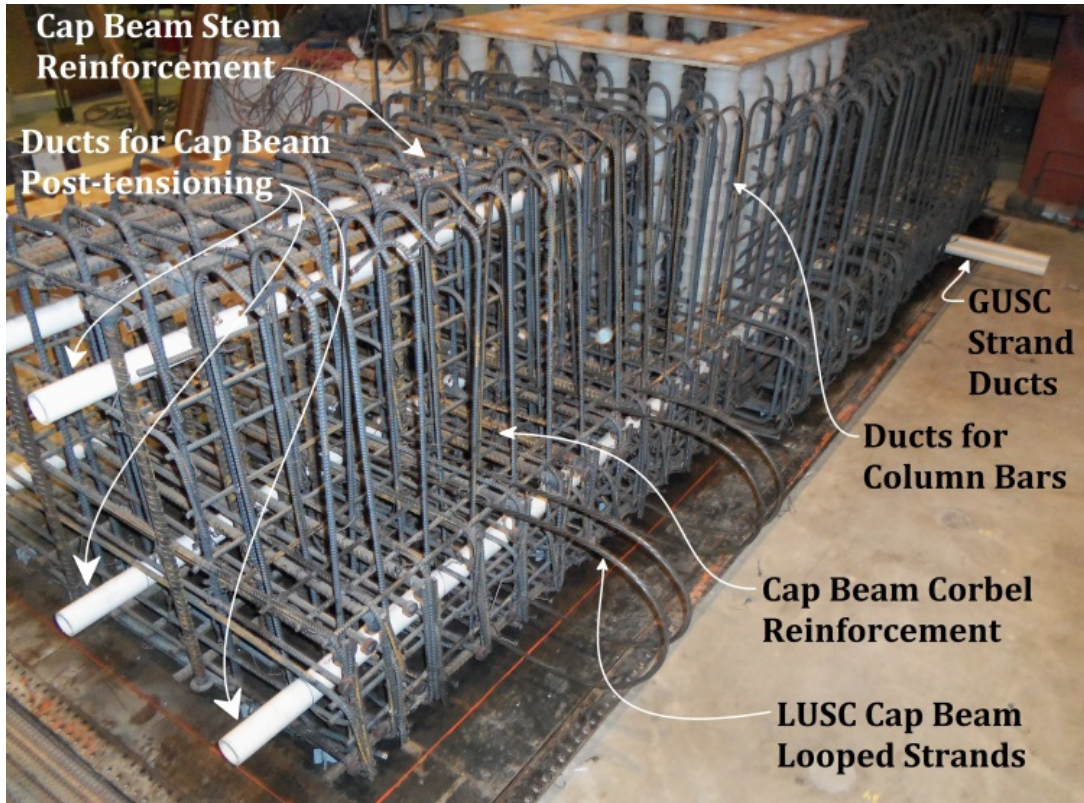


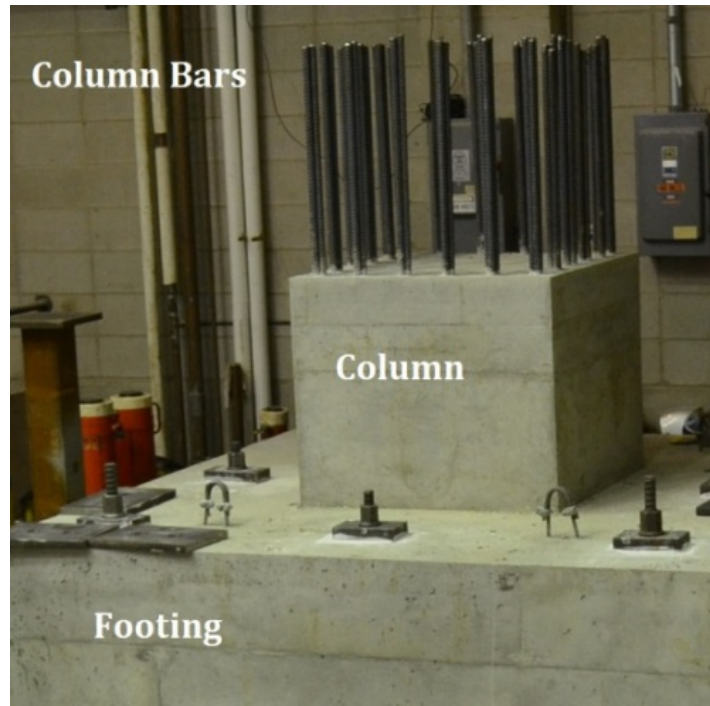
Figure 2.3: Connection test configuration concept (not to scale)

2.2.1 Cap beam and column design

A secondary objective of the connection test was to offer proof of concept for implementing a precast cap beam. The field implementation of such a concept could decrease onsite construction time and be well-suited for ABC methods. To be used as a precast element, the cap beam was designed with ducts in the column region as shown in Figure 2.4. These ducts were designed to align with the column longitudinal bars; thus, after the cap beam was precast, it was simply set in place on top of the column, with the column longitudinal bars (shown in Figure 2.4b) extending up into the cap beam ducts. The ducts were then filled with high-strength grout [$f'_c = 6700$ psi (46 MPa) at 7 days] to securely anchor the cap beam to the column.



a. Cap beam prior to casting concrete



b. Column and footing prior to cap beam placement

Figure 2.4: Connection test construction photographs

In a prototype structure, the girder-to-cap connection would be expected to remain essentially elastic, even when subjected to the highest seismic demands, since elastic superstructure behavior is critical for successful performance following capacity design principles that localize inelastic deformations in the column plastic hinge regions. In this test setup, however, the intent was to fully exercise and quantify the girder-to-cap connections well beyond their elastic limit. Therefore, the test unit cap beam was expected to be subjected to torsional loads well beyond those that would be experienced by a cap beam in a prototype structure. To account for the additional torsion, longitudinal ducts were added to the cap beam as shown in Figure 2.4a to provide the opportunity to add torsional capacity during the latter stages of testing by introducing post-tensioning. Additional steel was also added in the non-connection side of the cast-in-place diaphragm to further increase the cap's torsional resistance.

Since the girder-to-cap connection negative moment capacity was significantly higher than the positive moment capacity, the design cap beam torsion was related to the predicted negative moment connection performance. To determine this design torsion, the maximum expected negative girder-to-connection moment was estimated assuming yielding of the deck steel as the failure mechanism. The tributary area of deck steel contributing to the connection behavior was estimated as 5160 mm² (8.0 in.²), and the moment arm was conservatively estimated as 813 mm (32.0 in), based on the distance from the center of the deck steel to the top of the girder lower flange. Therefore, the expected moment was calculated as:

$$M_{\text{exp}} = A_s f_y j = (8.0 \text{ in.}^2)(60 \text{ ksi})(32 \text{ in.}) = 1280 \text{ kip-ft (1737 kN-m)} \quad (\text{Eq. 4.1})$$

This moment was increased by 10% to determine the design torsional load in the cap beam to be 1408 kip-ft (1910 kN-m). The torsional capacity of the cap beam without post-tensioning was determined using the approach from Priestley et al. (1996) to be 348 kip-ft (472 kN-m); this calculation was verified by comparing it with the ACI (2011) approach which yielded very similar results. Priestley's approach was then used to determine the additional torsional capacity of the cap beam utilizing post-tensioning and incorporating the contribution of the mild reinforcement. Post-tensioning was accomplished using six DYWIDAG bars capable of carrying 80 kips (356 kN) each, and the mild steel provided an additional clamping force of 377 kips (1677 kN). Continuing with Priestley's approach, the combined clamping force of 857 kips (3812 kN) was calculated to increase the torsional capacity of the cap to 1564 kip-ft (2120 kN-m), sufficiently larger than the predicted design torsional load.

For configuration simplicity, the test column was designed to be square, since the column itself was not part of the test specimen and was not intended to represent a prototype bridge structure. The column was designed to remain elastic up to the ultimate capacity of the girder-to-cap beam connection. A design moment value of 1408 kip-ft (1910 kN-m) was established for the column. This design value was based on the same predicted performance of the connection in the negative moment direction that was used in the cap beam design above. The predicted axial load in the column was determined to be 52 kips (231 kN), based on the girder, cap beam, and column weight and the expected actuator test loads. Using the ACI (2011) interaction approach, the required area of steel for the column was determined to be 29.8 in² (19230 mm²). To accommodate the precast cap beam connection, sixty #7 (#22M) bars were chosen to provide a total steel area of 36.0 in² (23230 mm²). These bars were arranged in bundles of three around the perimeter the column so they could easily be inserted into the ducts of the precast cap beam.

2.2.2 Girder, diaphragm, and deck design

The girders were designed to model the largest standard California I-girder and coincided with the girders that had been previously used in the system test. Modifications were made to the girder ends according to each connection detail, which will be introduced in Chapter 3.

The diaphragm was designed to duplicate the system test configuration, representative of the diaphragm that would be utilized in a prototype structure utilizing this system. However, on the side of the diaphragm opposite the girders, additional mild reinforcement was included in the cap beam longitudinal direction to increase the cap beam torsional capacity, described in detail earlier.

The bridge deck was split into two separate portions with a gap between the two girders so that each girder and connection could be exercised independently. The width of the bridge deck above each girder was 4'-8 1/2" (1435 mm), based on AASHTO's recommended tributary width (AASHTO, 2012). The reinforcement incorporated in the deck was a duplication of the reinforcement utilized in the system test, which was representative of the deck reinforcement in the prototype bridge.

2.3 Load protocol

The main objective in loading the test unit was to simulate the prototype shear and moment in the girder-to-cap connection region for conditions simulating gravity and horizontal seismic loading along with consideration for vertical acceleration effects. Since both connection details are

intended for use in a bridge configuration similar to the system test unit, analytical predictions (for example Snyder, 2010 and Thiemann, 2010) and experimental results from the system test provided helpful data in determining a suitable load protocol. The system test study was used to establish test-scale magnitudes of 32 kips (142 kN) and 84 kip-ft (115 kN-m) for the gravity-only shear and negative moment, respectively, as shown in Table 2.1. The system test results were also used to establish the column overstrength moment due to horizontal seismic loading that the bridge superstructure would be required to resist. Lateral load distribution results from the system test as well as other similar large-scale experimental studies (for example: Sritharan et al., 2005, and Holombo et al., 1998) were used to determine comparable shear and moment magnitudes that would be experienced in the individual girder connections. A detailed explanation of this lateral load distribution work is found in Vander Werff and Sritharan (2015). Resulting shear and moment values, in both the positive and negative directions, are shown in the second row of Table 2.1 for the load scenario that includes gravity load and full horizontal seismic load in either longitudinal direction.

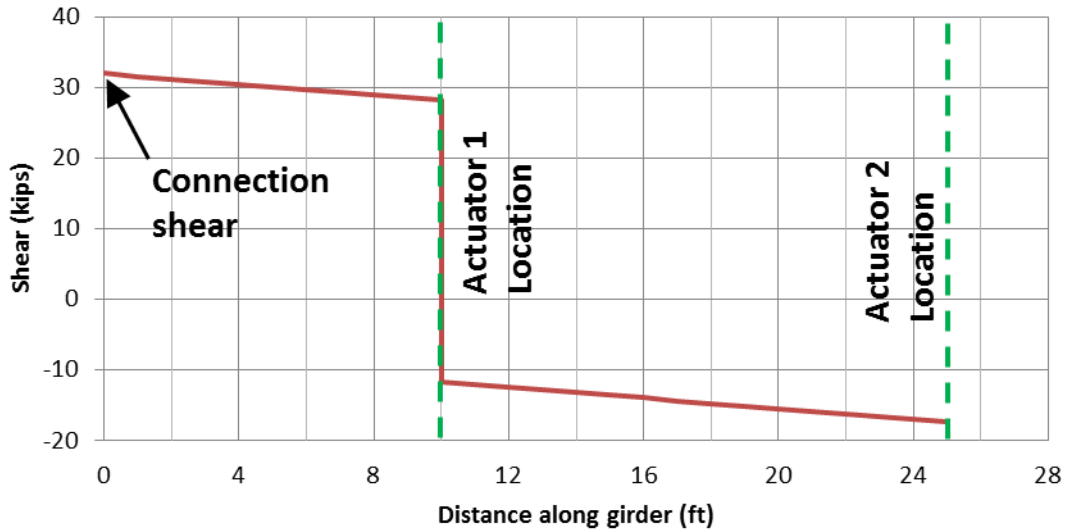
The other aspect of seismic loading that the connection test was designed to investigate was vertical ground motion. The Caltrans SDC mild side reinforcement requirement for vertical acceleration shear mentioned in Section 4.2 is a major impediment to implementation of the inverted-tee cap and dapped-end girder system, because there is no room on the bottom flange of the girder to include this additional steel. In addition, recent earthquakes (especially the 2011 Christchurch, New Zealand, event) raised awareness of the susceptibility of structures to vertical acceleration effects (Kam and Pampanin, 2011). Observations during the system test had indicated that the improved connection detail likely had sufficient shear capacity to meet the vertical acceleration demands without including additional reinforcement. A main goal of the connection test was to verify this indication from the system test by subjecting the connection details to simulated vertical acceleration load to demonstrate that the connections could be implemented without including the additional reinforcement required by the current Caltrans SDC (2013). To accomplish this objective, the load protocol as shown in Table 2.1 was developed to include simulated vertical acceleration effects in the connection region in addition to the expected shear and moment demand from gravity and horizontal seismic loading.

Table 2.1: Proposed connection test load protocol

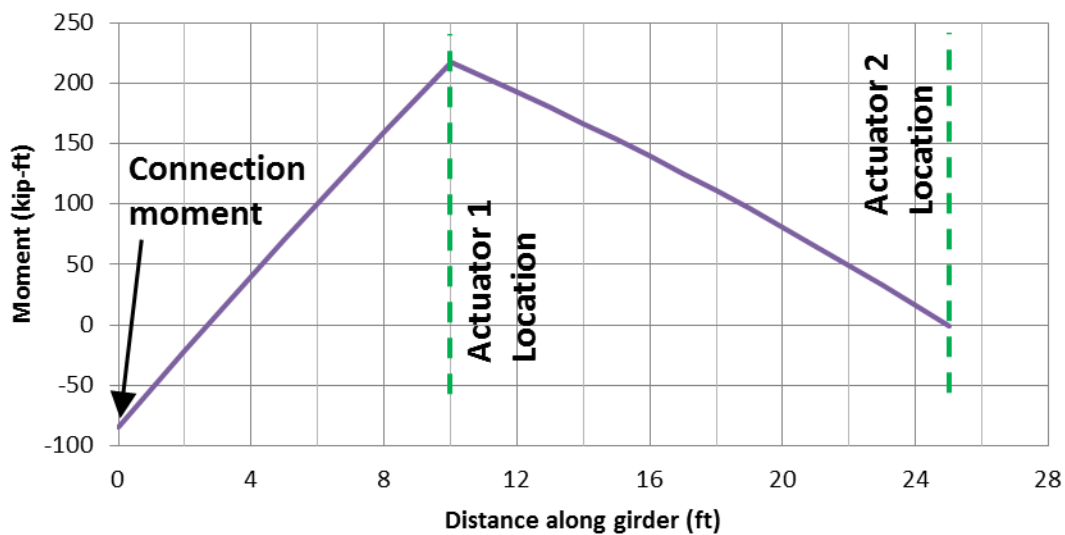
| LOADING PROTOCOL | Negative Shear and Moment | | Positive Shear and Moment | |
|--|---------------------------|-----------------------|---------------------------|-----------------------|
| | Shear, kips (kN) | Moment, kip-ft (kN-m) | Shear, kips (kN) | Moment, kip-ft (kN-m) |
| Gravity Only | 32 (142) | 84 (114) | 0 | 0 |
| Gravity + 100% Seismic No vertical acceleration | 36 (160) | 323 (438) | 21 (93) | 170 (230) |
| Gravity + 100% Seismic + 0.25 g Vertical Acceleration | 43 (191) | 350 (475) | 24 (107) | 176 (239) |
| Percentage increase from gravity/horizontal | 19% | 8% | 14% | 4% |
| Gravity + 100% Seismic + 0.5 g Vertical Acceleration | 50 (222) | 376 (510) | 27 (120) | 183 (248) |
| Percentage increase from gravity/horizontal | 39% | 16% | 29% | 8% |
| Gravity + 100% Seismic + 1.0 g Vertical Acceleration | 64 (285) | 429 (582) | 33 (147) | 217 (294) |
| Percentage increase from gravity/horizontal | 78% | 33% | 57% | 28% |

2.3.1 Target shear and moment values

Since the performance of the girder-to-cap connection was the primary focus of the test, the goal of the load protocol was to properly simulate the shear and moment in the connection region rather than duplicate the shear and moment along the entire length of the girders. Therefore, with the test setup introduced earlier in Figure 2.3, the two actuators [one located 10 ft (3.05 m) from the connection and a second located 25 ft (7.6 m) from the connection] could be used to vary the connection region shear and moment appropriately. To illustrate this approach, Figure 2.5 provides the shear and moment diagrams for the gravity-only simulated condition shown in row 1 of Table 2.1. While the shear and moment values along the length of the girder vary due to the concentrated loads introduced by the actuators, the connection shear and moment values are properly simulated. By varying both actuator loads in both directions as needed, any desired shear and moment values could be developed in the connection of the test unit.



a. Shear diagram



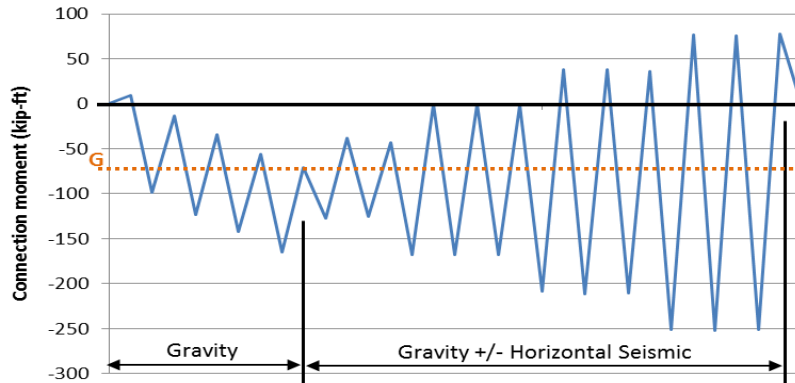
b. Moment diagram

Figure 2.5: Test unit shear and moment diagrams

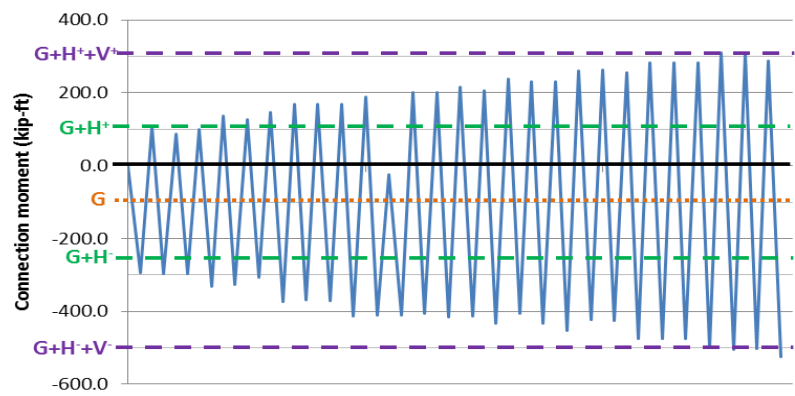
2.3.2 Proposed load sequence

Once the target values were established, a cyclic load protocol was developed to incrementally reach the target peaks. The protocol was divided into three phases. Phase I incorporated cyclic loading to reach the full gravity-plus-horizontal-seismic load condition. Phase II included gravity and horizontal seismic but also added the effects of increasing magnitudes of vertical acceleration, applied as pseudostatic loads based on the scaled prototype mass. Finally, Phase III utilized large

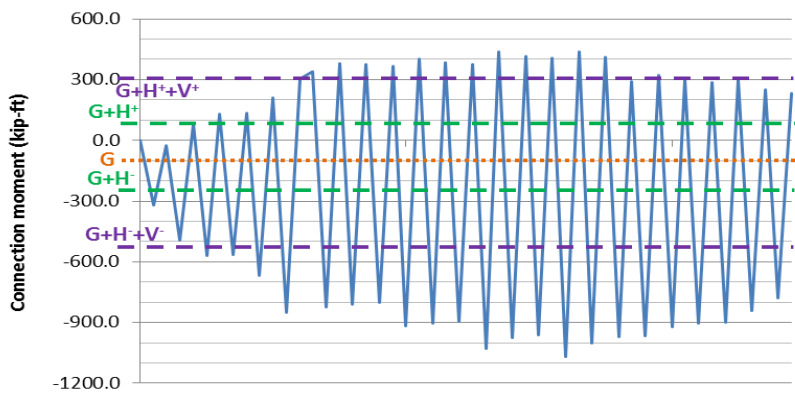
forces and displacements to fully exercise the girder connections. Figure 2.6 shows the connection moment for the load sequence in each of the three phases. Note that these figures have been adjusted to represent the actual loads used during testing, rather than the planned loads prior to testing. The corresponding connection shear followed a very similar pattern to the connection moment, so the shear load sequence figures are omitted for brevity.



a. Phase I (Gravity and horizontal seismic load)



b. Phase II (Gravity, horizontal seismic, and vertical acceleration load)



c. Phase III (Displacement control)

Figure 2.6: Load protocol for connection test of GUSC detail

Chapter 3. Connections for I-Girders and Cap Beam Utilizing Unstressed Strands

3.1 Connection details for dapped end I-shaped girders and inverted tee cap beams

3.1.1 GUSC detail

One of the girder-to-cap connection details implemented in the connection test was a duplicate of the improved connection in the previous system test. Since this connection concept incorporated unstressed strands positioned in the girder bottom flange and the lower region of the cap beam and then grouted in place, it was referred to as the Grouted Unstressed Strand Connection (GUSC). The GUSC configuration is provided in Figure 3.1. The GUSC detail duplicated the improved connection from the system test, including the dowel bars from the as-built connection but relying primarily on the deck reinforcement for negative moment tension continuity and the unstressed strands for positive moment continuity (see Figure 3.2a). For the unstressed strands in the GUSC detail and all other connections investigated in this work, Grade 270 seven-wire uncoated strands were utilized. In the system test, the unstressed strand was run through ducts extending through the girder bottom flange for the entire longitudinal girder length, as shown in Figure 3.2b. However, strand testing after the system test indicated that terminating the strand a certain distance from the connection region would provide sufficient anchorage to develop the full tension capacity of the strand. Thus, for the GUSC detail in the connection test, the strand ducts were fluted out from the girder bottom flange 3.0 m from the girder-cap interface at the test unit scale, as shown in Figure 3.2c.

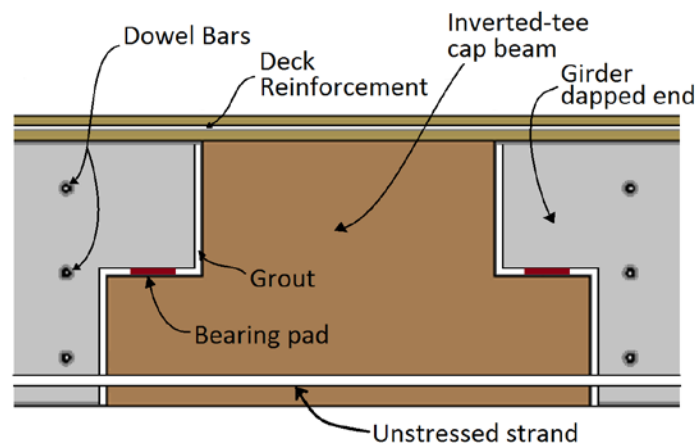
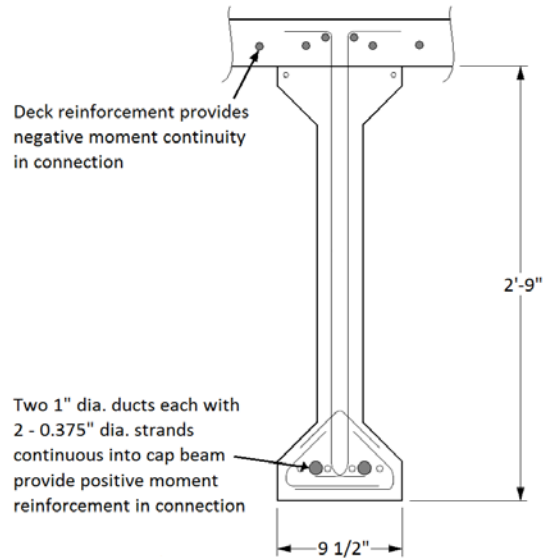
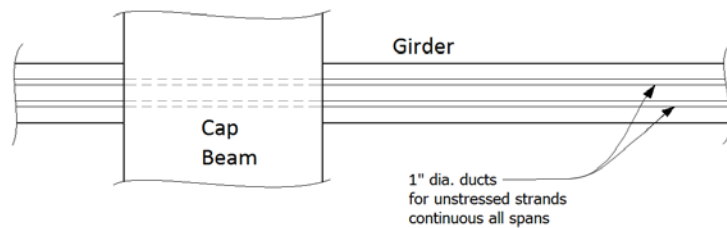


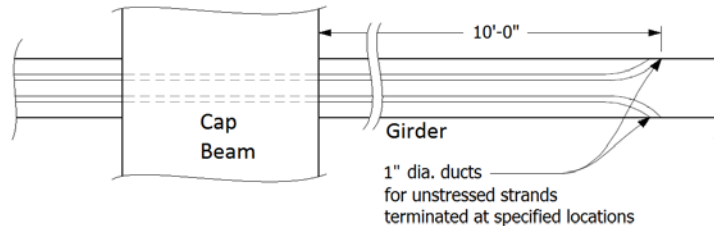
Figure 3.1: Grouted unstressed strand connection (GUSC) detail



a. Location of connection reinforcement



b. Continuous strands in girder bottom flange



c. Anchorage of strands beyond connection region

Figure 3.2. Reinforcement in grouted unstressed strand connection (GUSC) (test unit scale)

3.1.2 LUSC detail

A schematic view of the second girder-to-cap connection detail investigated in the connection test is shown in Figure 3.3. This detail, provided by Caltrans, was referred to as the Looped Unstressed Strand Connection (LUSC). Moment continuity in this connection was accomplished by enlarging and relocating the dowel bars to the lower portion of the girder and extending them through continuous looped unstressed strands that extended out from the cap beam

ledge. The desired tension load path at the bottom of the girder was completed by additional unstressed strand cast into the girder. These additional girder strands were intended to provide confinement of the dowel bars passing through the girder by looping around the dowel bar blockouts. The blockouts were filled with grout to ensure bond between the girder and dowels. The entire region was again encased by a cast-in-place concrete diaphragm, similar to the GUSC detail. The positive moment continuity in the LUSC detail was different from the GUSC detail in that the LUSC detail utilized an offset path of continuous longitudinal steel between the girder bottom flange and the cap beam. While this load path may have been slightly less straightforward than the tension continuity provided in the GUSC detail, the LUSC had the advantage of not requiring precise alignment of strand ducts during field assembly like the GUSC specimen. Looped strands that protrude from the cap beam ledge on either side of the girder provided ample clearance as they wrapped around the T-headed dowel bars that ran through the girder and formed a link with added strand in the girder. A shear friction mechanism between the dowel bars and the looped strands was expected to be the primary path for positive moment tension load transfer. As for negative moment continuity, there was little difference in the LUSC and GUSC concepts, since the deck reinforcement provided the principle negative moment tension continuity for both details. Additional information on the design concepts for both the GUSC and LUSC details is provided in Sritharan et al. (2013).

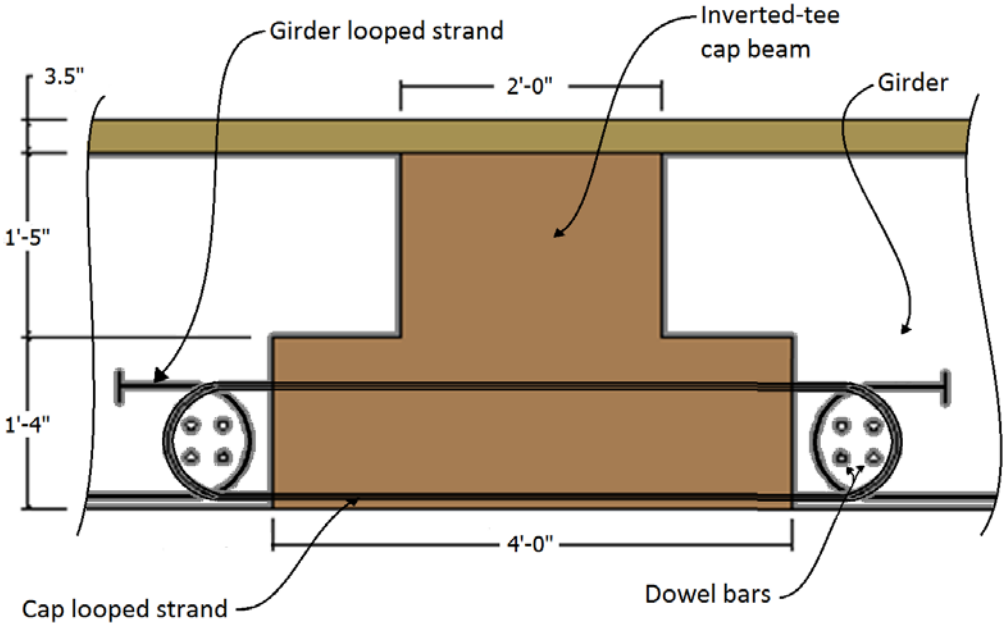


Figure 3.3: Looped unstressed strand connection (LUSC) detail

3.2 Construction of GUSC/LUSC test unit

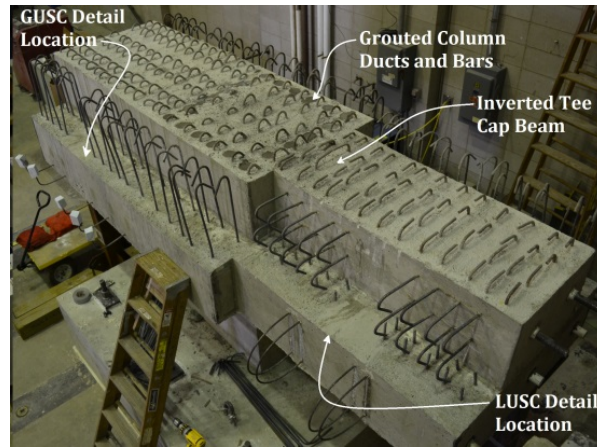
3.2.1 Construction

Construction of the test unit was completed in the structural laboratory of Iowa State University (ISU). Traditional cast-in-place concrete methods were used for the footing and column. The cap beam was also constructed as a separate unit at ISU to demonstrate the viability of using precast cap beams as part of ABC. Figure 3.4 provides photographs of the cap beam prior to concrete placement and the column/footing assembly prior to cap beam placement. For the column-to-cap connection, the sixty #7 (#22M) column longitudinal bars (in bundles of 3) were extended to approximately the top of the cap beam, but the column concrete was cast only to the bottom surface of the cap beam. In the cap beam, corrugated ducts were positioned to match the column longitudinal bar locations. This detail allowed the cap beam to be easily set in place and positioned by lining it up with the column bars and sliding it down. Once positioned, the cap-to-column interface was filled using high-strength fiber-reinforced grout [$f'_c = 8900$ psi (61 MPa) at 7 days] and the ducts were filled with high-strength grout without fibers [$f'_c = 6700$ psi (46 MPa) at 7 days] to complete the connection. Steel fibers with 0.75 in. (19 mm) length were included in the cap-to-column interface grout, using a volumetric fiber-to-grout ratio of 0.015, because of the cyclic tension and compression load that the interface would experience, but they were excluded from the ducts for ease of grout placement. The specific fibers and quantities used were based on results from previous successful tests. The completed column-cap assembly is shown in Figure 3.4a.

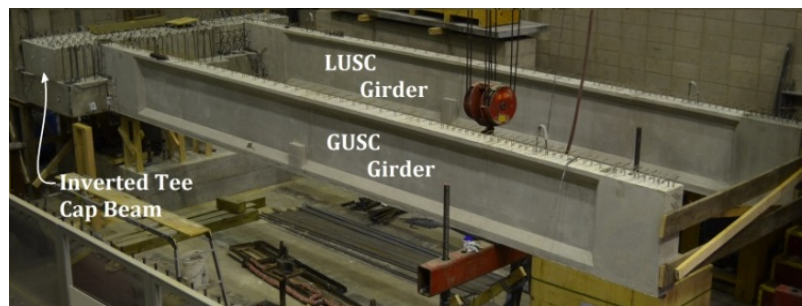
The precast girders were constructed by Andrews Prestressed Concrete in Clear Lake, Iowa, and shipped to ISU. The girders were positioned on the cap beam and supported at the free end by temporary steel formwork as shown in Figure 3.4b. Dowel bars were placed through the girders and into the diaphragm region according to each connection detail. For the GUSC, the four unstressed strands were run through the girder and cap beam by simply aligning the girder and cap beam and sliding the strands through. The quantity of strands was chosen by designing them to resist the tension produced by the positive moment that would be expected to develop in the connection under full seismic conditions. The strands were then grouted in place, after which they were anchored against the back side of the cap beam using standard anchorage chucks. Although previous component testing had indicated that the grout alone would provide sufficient strand anchorage, the chucks were included as a precaution to allow continuation of the test in the event

of bond anchorage failure. The load at one of the anchorage points was monitored during the test to determine whether the grout alone was sufficient to anchor the strand.

High-strength grout [$f'_c = 12.7$ ksi (88 MPa) at 7 days] was used to complete the interface between the girders and cap beam. Because of the cyclic nature of the connection load under seismic conditions, steel fibers were incorporated into the grout mix in the same manner as for the column-to-cap interface. Once the girder-cap interface was established, the formwork for the diaphragms on the front and back sides of the cap beam was erected. In addition, the formwork for the two split decks was erected by using temporary girder brackets on each side of the two girders; this formwork is shown in Figure 3.4c. After placement of the diaphragm and deck concrete and removal of the formwork, the test actuator frames were positioned over the GUSC girder and the two actuators were attached as shown in Figure 3.4d. After testing the GUSC detail, the frames and actuators were repositioned over the LUSC girder for testing of that connection detail. Concrete strengths for the girders, cap beam, and diaphragm are provided in Table 3.1 and a complete set of test unit drawings is included in Appendix A.



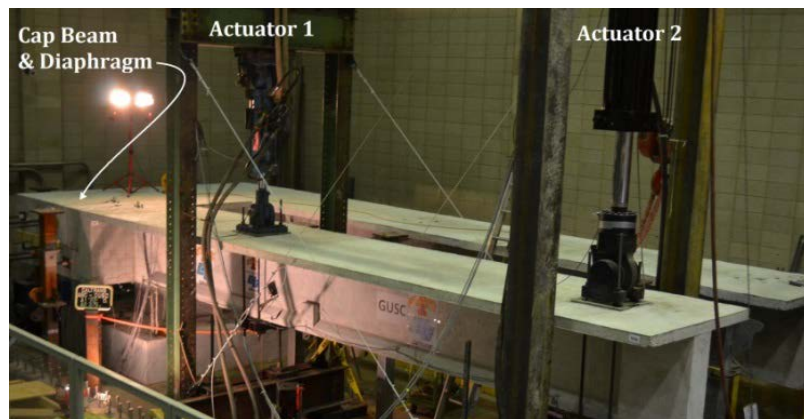
a. Cap beam prior to girder, diaphragm and deck placement



b. Girders prior to diaphragm and deck placement



c. Deck formwork and reinforcement



d. Completed test unit and load frames

Figure 3.4: Construction and test configuration photographs

Table 3.1: Test unit concrete strengths

| Component | 7-day strength, psi (MPa) | 28-day strength, psi (MPa) | Test day strength, psi (MPa) |
|------------------|---------------------------|----------------------------|------------------------------|
| Cap beam corbel | 4750 (33) | 5918 (41) | 7005 (48) |
| Cap beam stem | 3653 (25) | 4704 (32) | 5618 (39) |
| Girder | Not recorded | 10,200 (70) | Not recorded |
| Deck & Diaphragm | 4319 (30) | Not recorded | 5460 (38) |

3.2.2 Instrumentation

Approximately 100 strain gages were installed on the reinforcement in the test unit. These strain gages were positioned to investigate the cap beam, girder, deck, diaphragm, and column performance, with a focus on the behavior of the connection region. In addition, approximately 30 external displacement transducers were utilized during each of the connection tests to record the test unit movement and deformation.

Figure 3.5 shows the locations of the strain gages on the column longitudinal bars. The column was designed to remain elastic throughout the connection test, acting as a fixture in the test unit and not as prototype-modeling component. Therefore, the strain gages were included on the column reinforcement simply to monitor the column condition and ensure that it was not being overstressed during the connection tests. Gages were located on the corner bars to monitor strains from moment about either axis, and bars nearer the neutral axis were gaged to monitor strains related to axial loading.

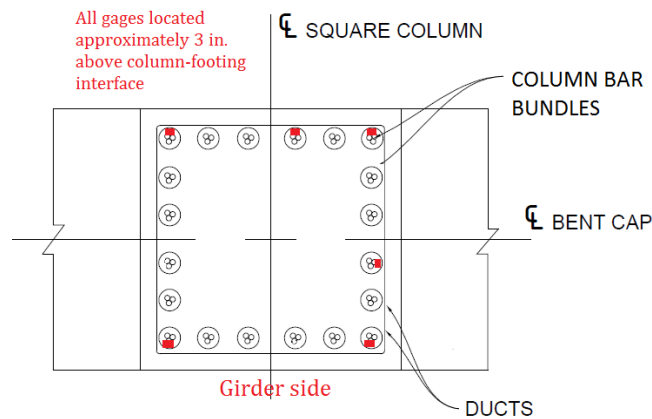
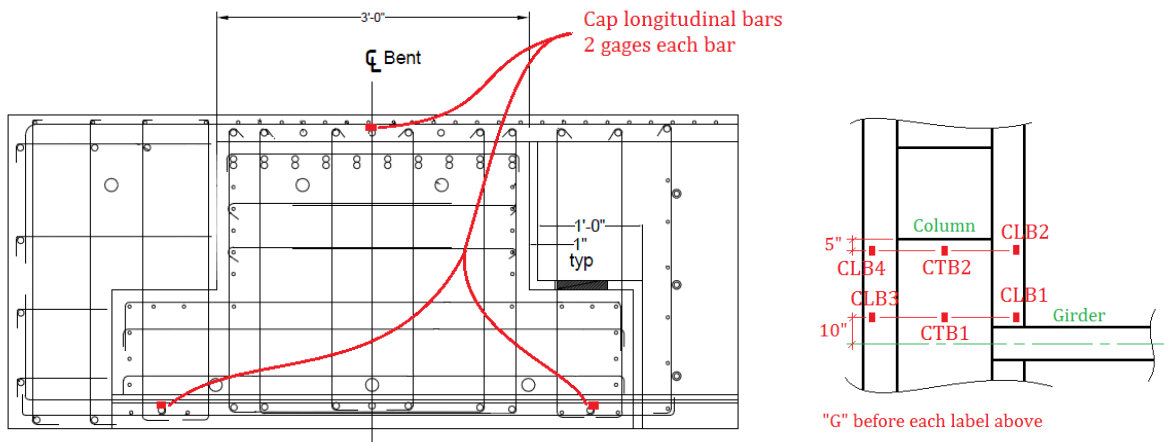


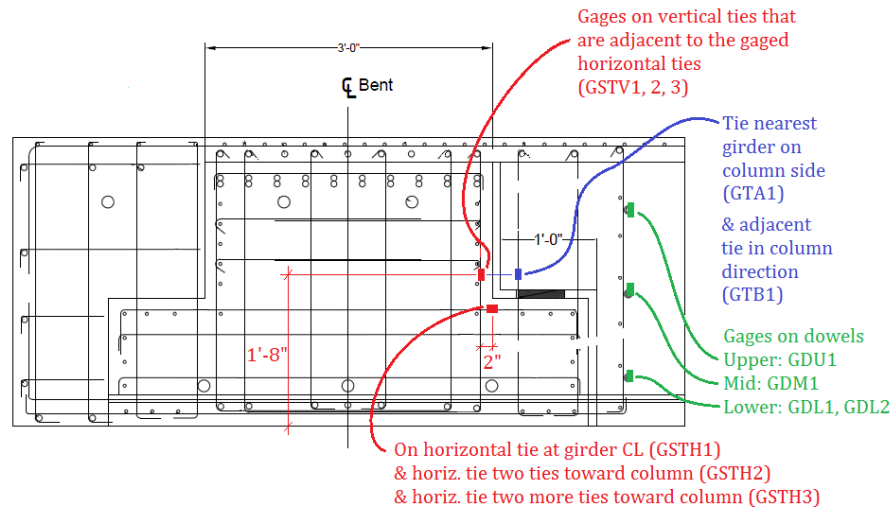
Figure 3.5: Column strain gages

Figure 3.6 provides the location of strain gages on the cap beam and diaphragm reinforcement in the GUSC region. The gages on the cap beam longitudinal reinforcement were located to monitor the flexural behavior of the cap beam during the test. Gages were included on both upper and lower bars to measure tension behavior due to both positive and negative moment action. The gages were located longitudinally near the girder to measure cap behavior near the connection. A second set of gages were located near the column to measure cap behavior in the maximum moment region.



a. Section near GUSC showing cap longitudinal gages

b. Plan of cap longitudinal gages near GUSC



c. Section near GUSC showing gages on ties and dowels

Figure 3.6: Strain gages on cap beam reinforcement near GUSC detail

Figure 3.7 shows the location of strain gages on the cap beam longitudinal reinforcement near the LUSC detail. These locations were very similar to the locations near the GUSC detail shown in Figure 3.6a,b; the gages were located to monitor flexural behavior on the LUSC side of the cap beam. Figure 3.8 provides the location of strain gages on the headed bars that were utilized for shear reinforcement in the cap beam and diaphragm near the LUSC detail. These gages were included to compare the effectiveness of the headed bars in the LUSC detail to the ties in the GUSC detail.

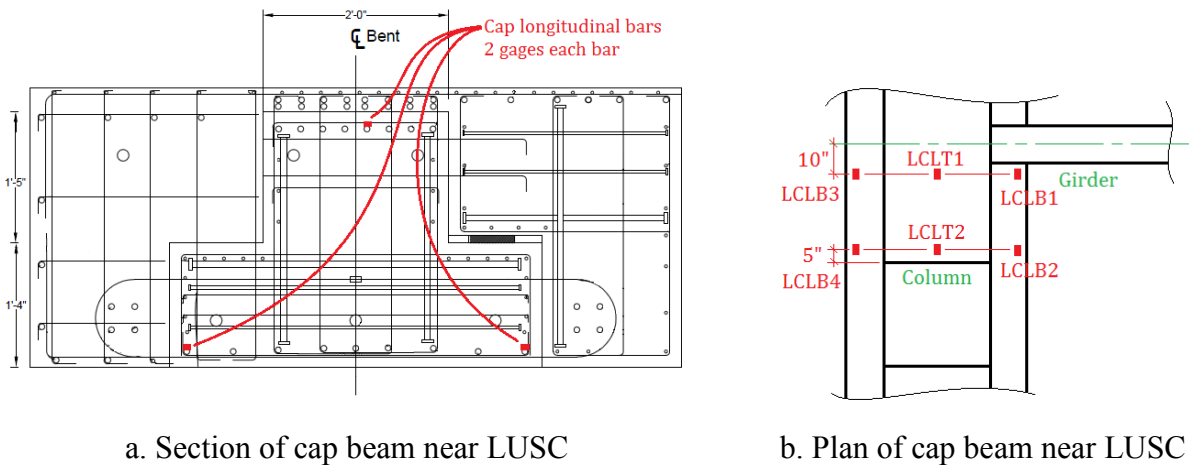


Figure 3.7: Strain gages on longitudinal cap reinforcement near LUSC detail

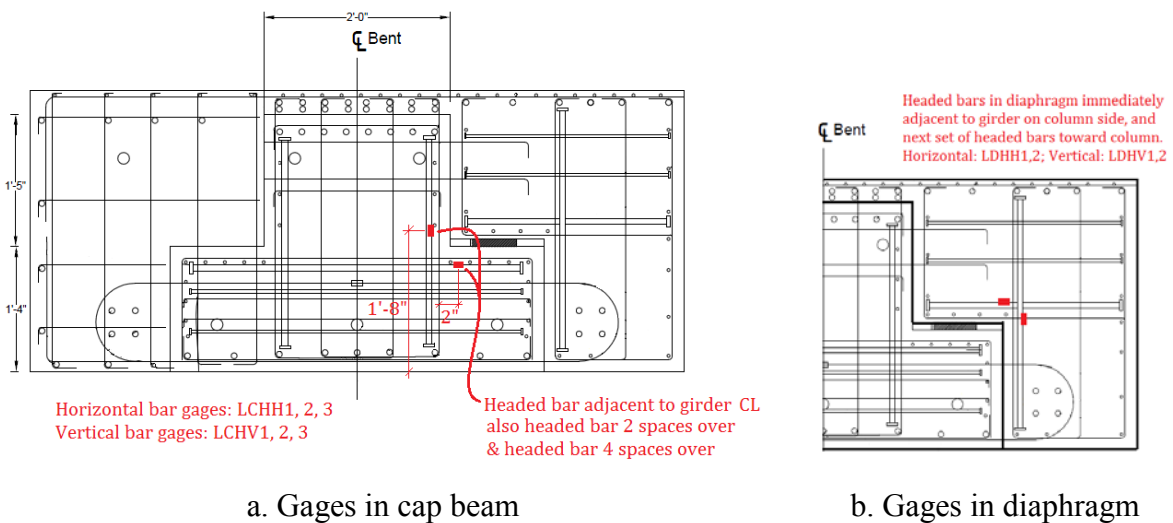


Figure 3.8: Strain gages on headed bars in the LUSC region

Many of the strain gages utilized in the GUSC/LUSC test unit were located to investigate the girder-to-cap connection behavior, specifically the transfer of shear and moment load from the girders into the cap beam. In the GUSC detail, the primary tension load transfer mechanism for positive-moment loading was expected to be the set of grouted unstressed strands running through the lower flange of the girder into the cap beam. As Figure 3.9 shows, gages were located on each of the strand pairs at the girder-to-cap interface, gages were located on a single pair 30 in. in either direction from the interface, and a final gage was located 60 in. from the interface into the girder. These gages were positioned to investigate the force transfer at the interface and also the adequacy of anchorage of the strands into the cap beam and girder.

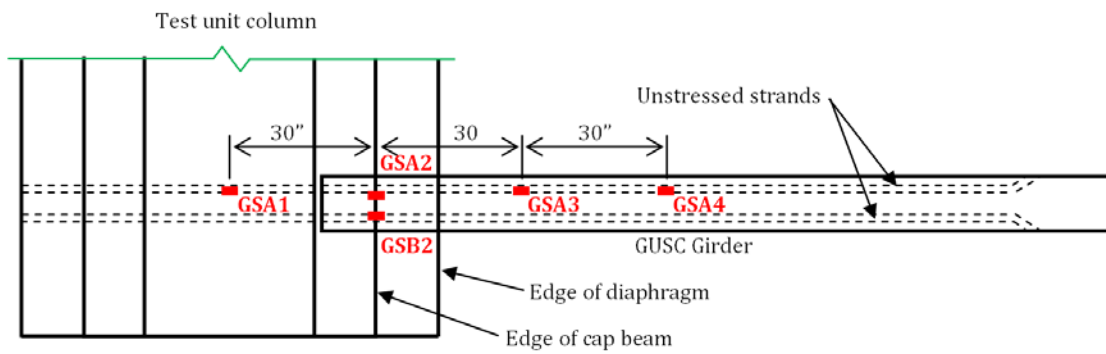


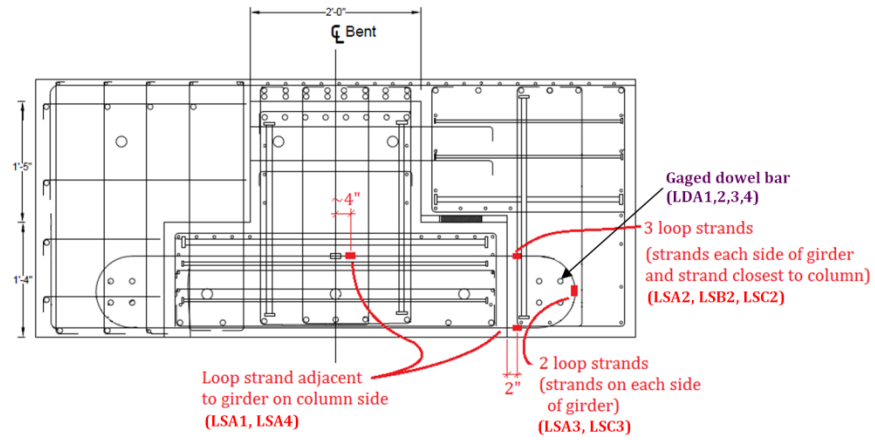
Figure 3.9: Strain gages on unstressed strand in GUSC detail

Figure 3.10 provides locations of the strain gages utilized on the looped strand and dowel bars in the LUSC detail. Since the LUSC detail did not have a similar direct-tension-transfer mechanism such as the strand provided in the GUSC detail, more strain gages were utilized to monitor the connection behavior. These gages were intended to provide the opportunity to quantify the load transfer mechanism in the LUSC detail, specifically with respect to the tension continuity of the lower portions of the girder and cap beam under positive moment loading in the connection region. The preliminary concept for this detail was that the dowel bars would transfer load from the girder to the diaphragm by a shear friction mechanism, with the looped strands providing confinement and facilitating load transfer from the girder to the dowel bars and from the dowel bars into the diaphragm and cap beam. Thus, strain gages were included on the dowel bars and also on the looped strands in both the girder and the diaphragm and cap beam.

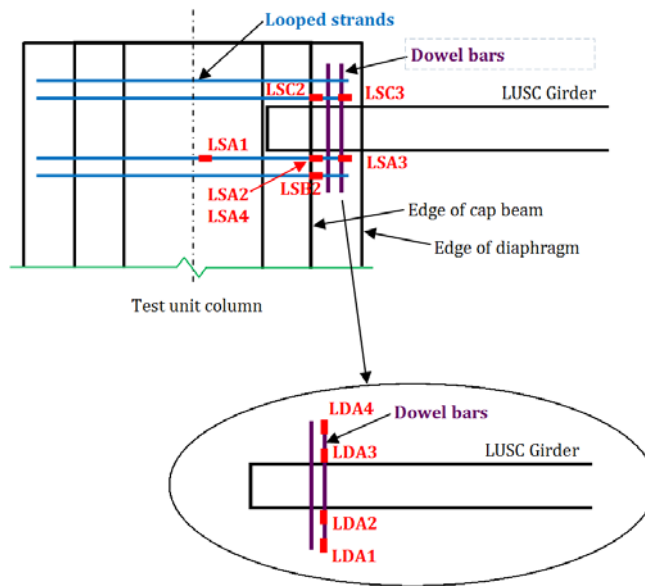
Figure 3.11 shows strain gage locations on the reinforcement of the girders used for both the GUSC and LUSC details. Gages were included on one of the harped strands in each girder to

monitor the overall flexural behavior of the girders during testing. Gages were also included on the stirrups in the block portion of each of the girders near the cap connection to monitor the shear performance of the connection region. In addition, gages were included on the dapped end ties as shown in Figure 3.11b. These ties were designed based on a strut-and-tie model of the dapped end load transfer, so the gages were included to investigate the appropriateness of using such a model for these connection details.

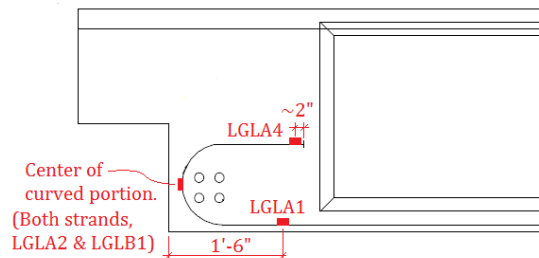
Strain gages were also included on several of the longitudinal reinforcing bars in the deck segments above each of the connection details, as shown in Figure 3.12. These gages were primarily intended to investigate the negative moment behavior of the connection details, since the deck reinforcement is the primary tension transfer mechanism for connection negative moment loading. The gages located towards the far end of the deck segments (near the right edge as shown in the figure) were located primarily to monitor the deck action near the far actuator location and secondarily to investigate the dissipation of the connection load in the deck along the length of the girder.



a. Elevation of looped strands in cap beam and diaphragm

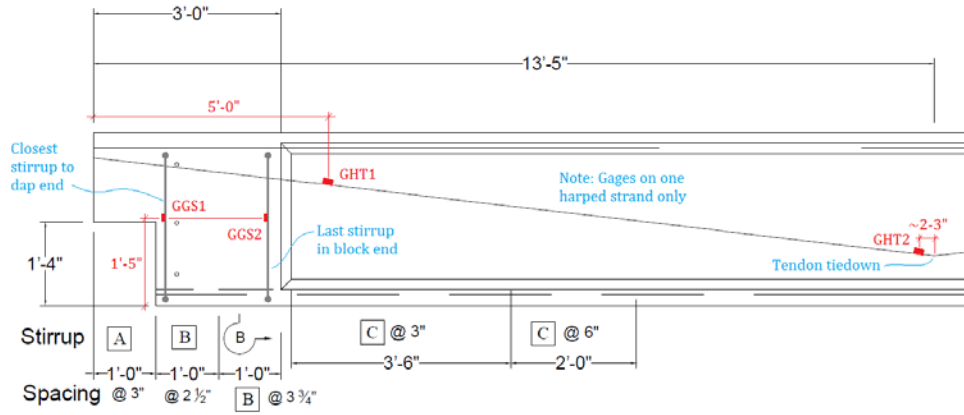


b. Plan and detail of looped strand and dowel bars in cap beam and diaphragm



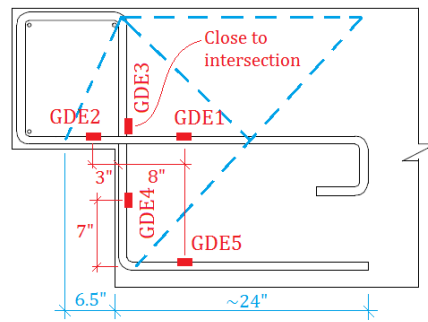
c. Elevation of looped strand in girder

Figure 3.10: Strain gages on strand and dowel bars in LUSC detail



a. Gages on stirrups in blocked end and harped strand

Gages on middle dapped end bar only (both GUSC & LUSC)



b. Gages on dapped end reinforcement

Figure 3.11: Strain gages on reinforcement in girders for GUSC and LUSC details

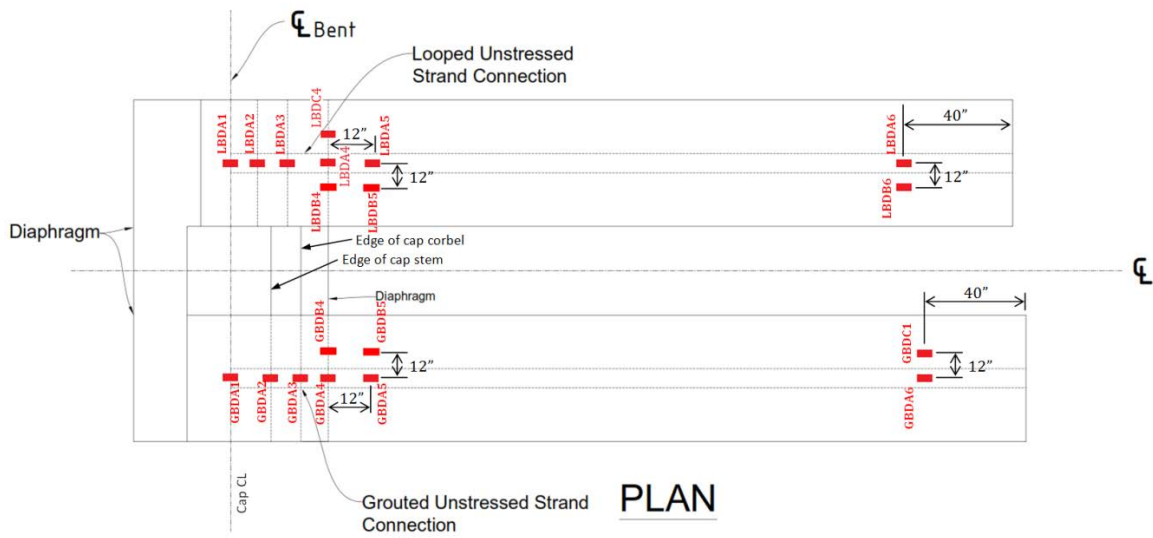


Figure 3.12: Strain gages on deck reinforcement

External instrumentation was also implemented on both the GUSC and LUSC portions of the test unit. Displacement transducers were used to ensure the stability of the footing, as shown in Figure 3.13a. Displacement transducers were also used to monitor the vertical and horizontal position and movement of the cap beam, as shown in Figure 3.13b.

To investigate the connection behavior, displacement transducers were located on both the GUSC and LUSC details as shown in Figure 3.14. These transducers were located to investigate the relative displacement of the cap beam and diaphragm and the diaphragm and girder at both the top and bottom of the connection region. The location of these transducers was especially intended to identify gap openings developing at any of these interfaces.

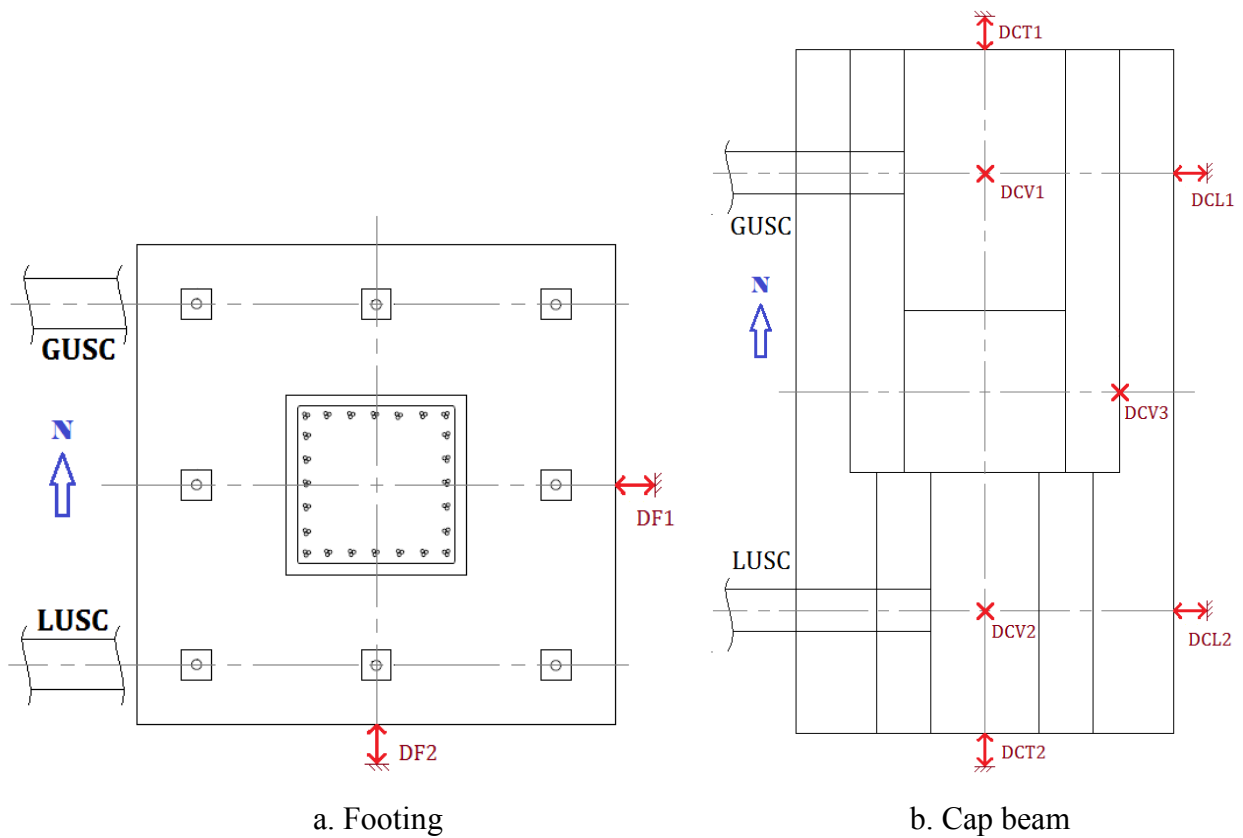


Figure 3.13: Plan of displacement transducers on footing and cap beam

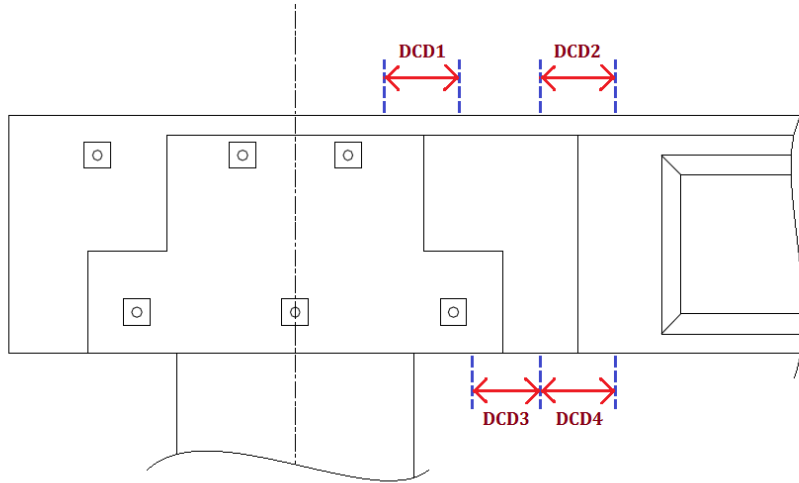


Figure 3.14: Displacement transducers in GUSC and LUSC connection regions (section)

Displacement transducers were also incorporated along the girders for both the GUSC and LUSC details, as shown in Figure 3.15. The “DGV” transducers were used at the actuator locations to measure the girder vertical displacement, which was the primary load and displacement direction used throughout both the GUSC and LUSC tests. The “DGT” transducers were used to monitor the lateral stability of the girders during the tests. However, at high displacements, these transducers were removed because of the large vertical travel that was being applied in the direction transverse to these transducers. The “DSR” displacement transducers shown in Figure 3.15 were attached between the girders and the protruding ends of the unstressed strand in the GUSC detail. These transducers were located to detect any slip that developed between the strand and the girder due to bond and anchorage issues.

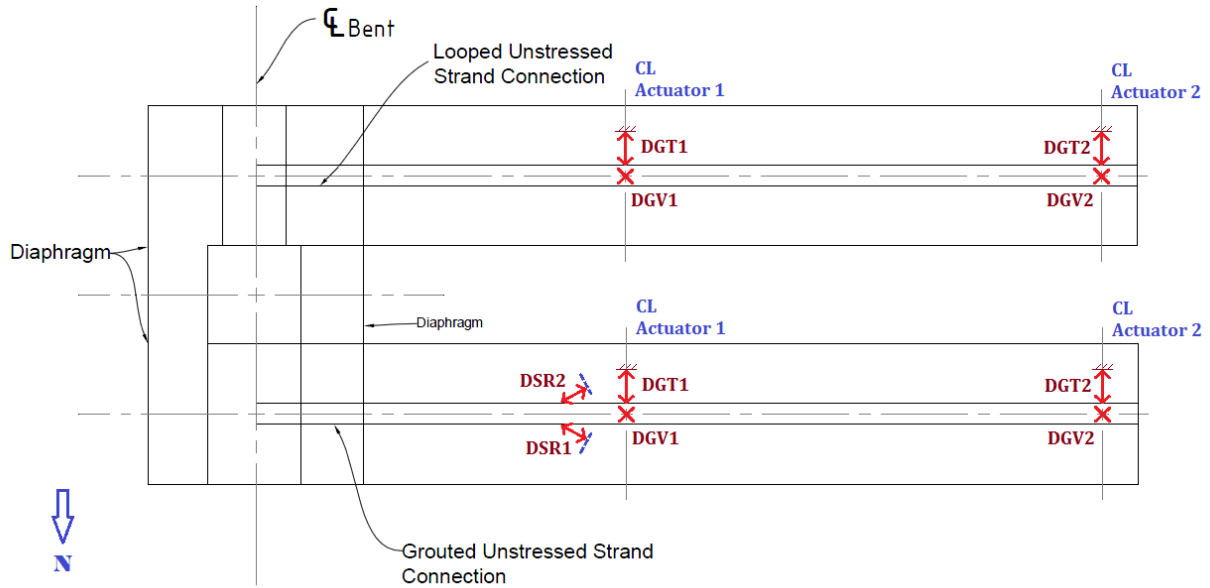


Figure 3.15: Displacement transducers on girders for GUSC and LUSC details (plan)

Both the GUSC and LUSC details were instrumented with LED position indicators, as shown in Figure 3.16. The data from these indicators enabled the determination of the relative displacement of the girder compared to the face of the diaphragm. Since positive moment performance in particular was of interest, the LED data was used to look at the relative movement of the girder bottom flange and thus provide an indication of how much slip was occurring between the girder and the cap beam. The LED data was also useful in monitoring the overall behavior of the exterior surface of the connection regions, identifying any movement-related signs of distress around the connections during the test.



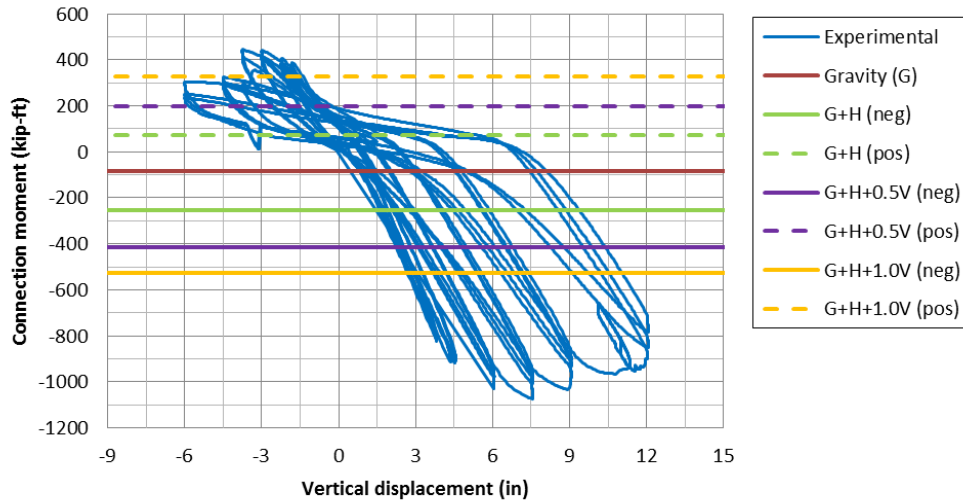
Figure 3.16: LED indicators to record position during experimental testing

3.3 Experimental results

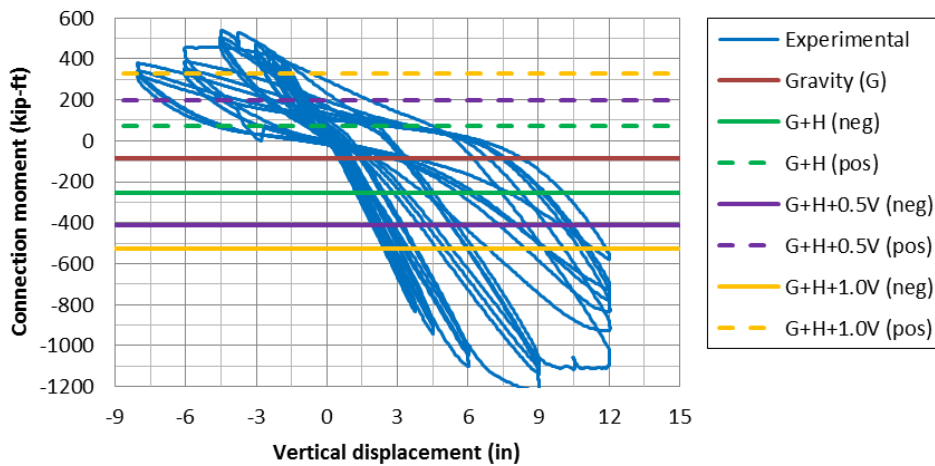
3.3.1 Overall connection behavior

Both the GUSC and LUSC details performed very well during the experimental testing. Both exhibited elastic behavior for positive moment magnitudes considerably higher than the expected demand at the full horizontal seismic condition. In fact, for both details the elastic behavior continued to magnitudes approximately 1.25 times higher than the demand expected at full horizontal seismic load plus 1.0-g vertical acceleration. Figure 3.17 shows the connection moment history for both tests plotted as functions of vertical displacement at the Actuator 2 location (see Figure 3.4c). In these plots, “H” signifies the maximum expected horizontal seismic demand based on the column overstrength moment and “V” signifies the demand expected from 1.0-g magnitude vertical acceleration. These plots are helpful in identifying the magnitude of moment demand generated during the tests. Both connections demonstrated elastic behavior up to positive connection moment magnitudes near 400 kip-ft, almost 2.4 times higher than the expected full horizontal seismic positive moment of 170 kip-ft, and almost double the full horizontal plus 1.0-g vertical condition of 215 kip-ft. The plots also clearly demonstrate elastic moment behavior in both

connections up to magnitudes considerably higher than expected seismic demands, including both horizontal and vertical effects. In addition, the plots show that both connections exhibited considerable ductility for both positive and negative moment response.



a. GUSC test



b. LUSC test

Figure 3.17: Recorded connection moment as a function of vertical displacement at the far actuator

Figure 3.18 shows the connection shear at the first load/displacement peaks during the GUSC test (a very similar pattern was used for the LUSC test) plotted as a function of connection moment. The initial portion of the boxed pattern shows the load incrementally advancing to the full gravity condition. Then the remainder of the boxed pattern extending to higher shear values and larger negative moment values shows the negative shear and moment conditions advancing

through horizontal seismic and into large vertical acceleration simulations. The diamond patterns show the conditions associated with positive moment during the horizontal seismic simulation initially and concluding with the larger vertical acceleration simulations. The “x” and triangle patterns show the large force/displacement conditions that were not simulations of any specific prototype conditions but rather were intended to fully exercise and quantify the connection behavior.

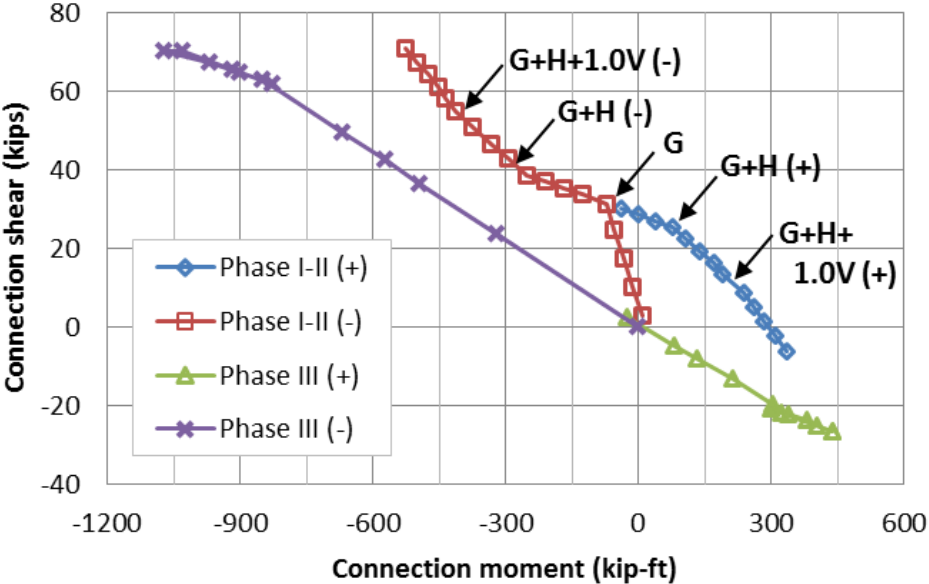


Figure 3.18: Connection shear resistance in GUSC

3.3.2 Failure mechanisms

The concrete in the connection region of the GUSC detail remained largely intact for the duration of testing. The primary failure mechanism of the connection was the fracture of one of the connection strands. Figure 3.19 provides a view looking straight up into the connection region at the girder-to-cap interface under the maximum positive moment displacement. The strand on the right in the photograph is seen to have remained intact, while the strand on the left fractured. The photograph also shows that, even at this extreme stage of the test, the grout pad between the girder vertical face and the cap beam girder face remained in place, held by the unstressed strand.

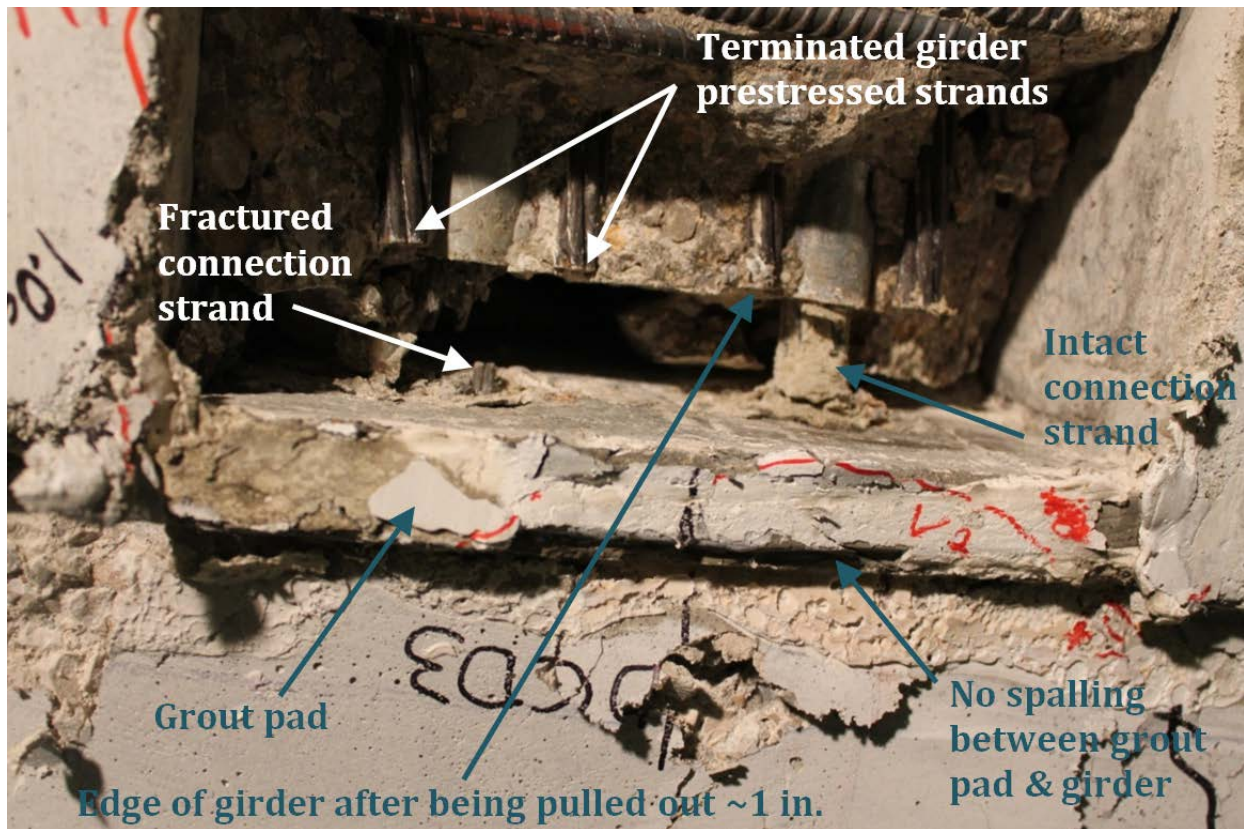


Figure 3.19: GUSC girder-cap interface during peak positive-moment displacement (looking up)

Fracture of the strand as the primary failure mechanism is significant for a couple of reasons. First, its fracture indicated that the grout on both sides of the interface (in the cap beam as well as in the girder bottom flange) provided sufficient anchorage to fully develop the strength of the strand. As mentioned earlier, a load cell was used to monitor the behavior of the strand at the back side of the cap beam. This monitoring revealed that, for the duration of the test, no load was transferred at the strand's anchorage point; thus, the grout/strand bond in the cap beam was sufficient to completely anchor the strand. Second, the fracture of the strand under positive moment loading indicated that the strand played a significant frictional role in providing positive moment connection capacity, as per the design intent.

The positive moment failure mechanism in the LUSC detail was not as straightforward as the GUSC detail. Observations at the conclusion of the LUSC test indicated that the failure of the connection under positive moment loading was related to the interaction of the diaphragm concrete, the looped strands, and the dowel bars. At the highest displacement cycles of Phase III loading, a clearly defined crack and separation of the diaphragm around the dowel bars was observed, as shown in Figure 3.20.

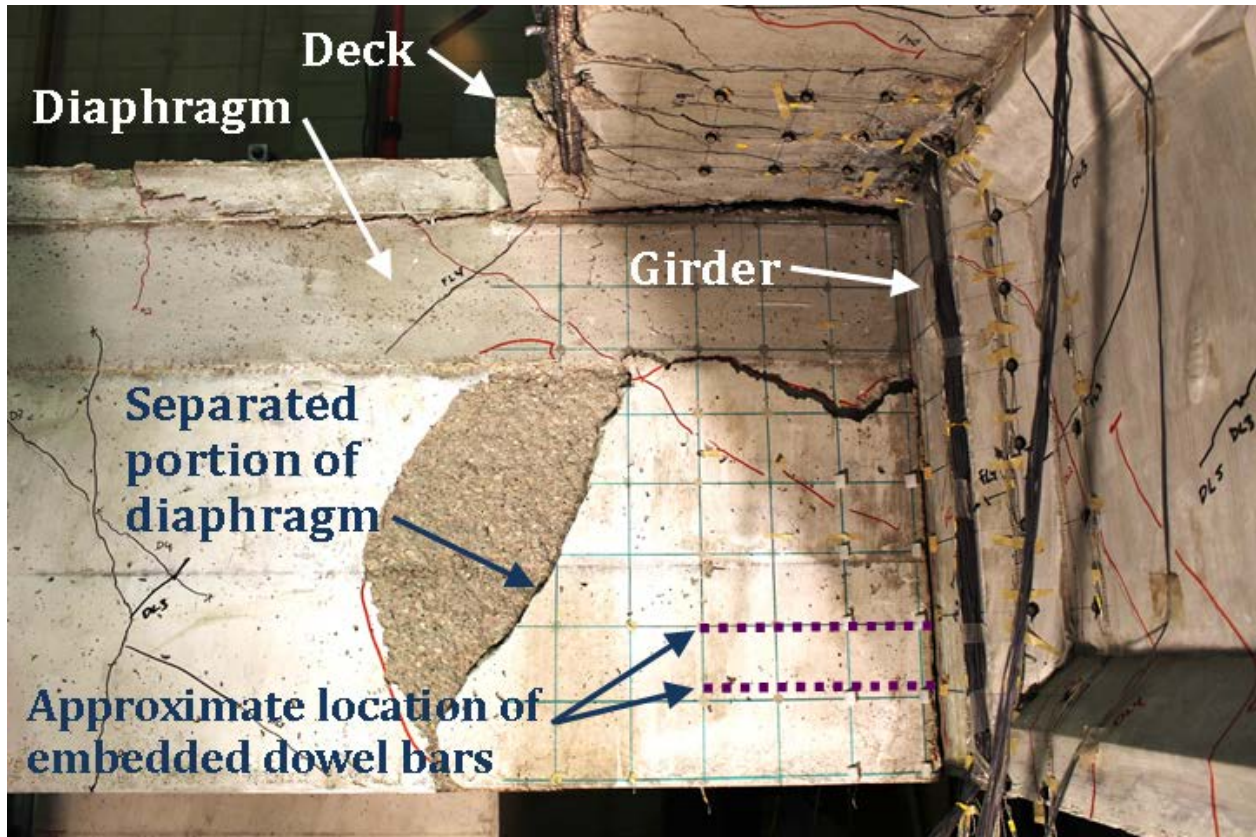
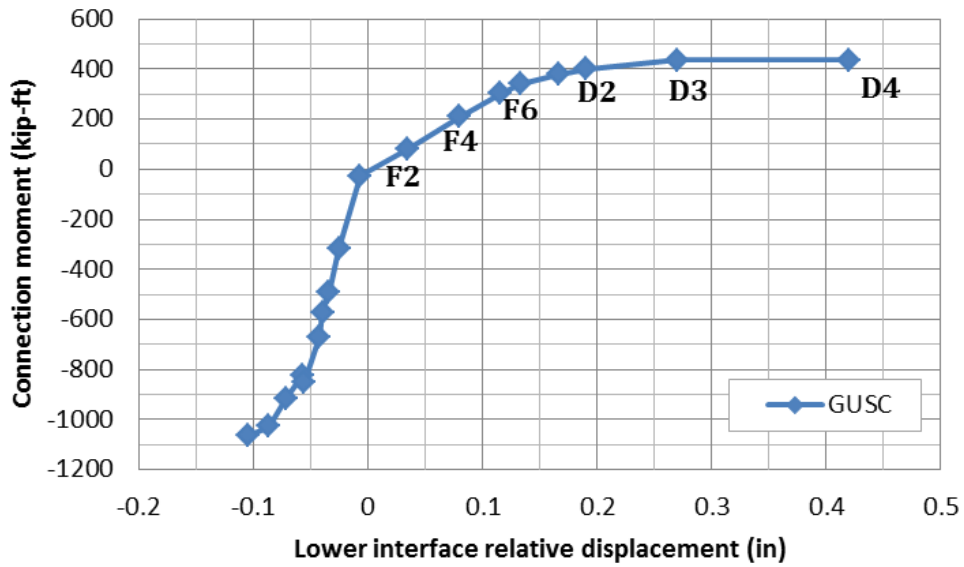


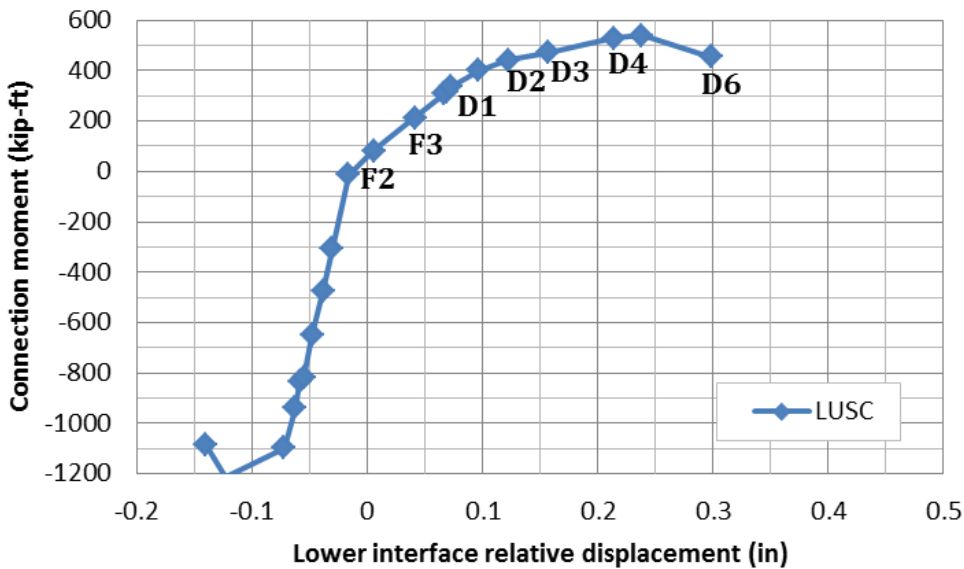
Figure 3.20: Condition of the diaphragm of LUSC detail at peak positive (upward) girder displacement of 4.5 in. at Actuator 2

3.3.3 Behavior of the connection interface

The LED indicators introduced in Section 3.2.2 were used to investigate the relative displacement between the girder and diaphragm at their interface. Figure 3.21 uses this data to quantify the connection moment behavior in both details compared to the relative interface displacement. Both details exhibited similar relative displacement tendencies. The relative displacements in the GUSC are slightly higher than for the LUSC. The slightly lower stiffness of the GUSC connection in the positive moment direction can be attributed to the positive moment tension mechanism. In the GUSC, the unstressed strand is primarily responsible for tension transfer, so as it elongates elastic it allows slight movement at the girder-to-cap interface. In the LUSC detail, on the other hand, the tension continuity is provided by the interaction of the dowel bars, strands, and concrete, thus resulting in less elastic movement prior to reaching the connection ultimate capacity.



a. GUSC detail



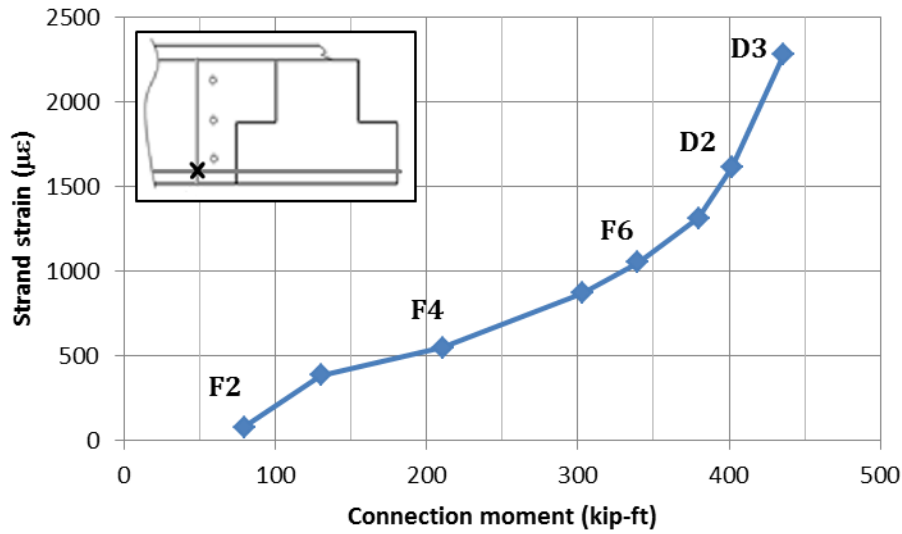
b. LUSC detail

Figure 3.21: Relative displacement of lower interface between girder and diaphragm

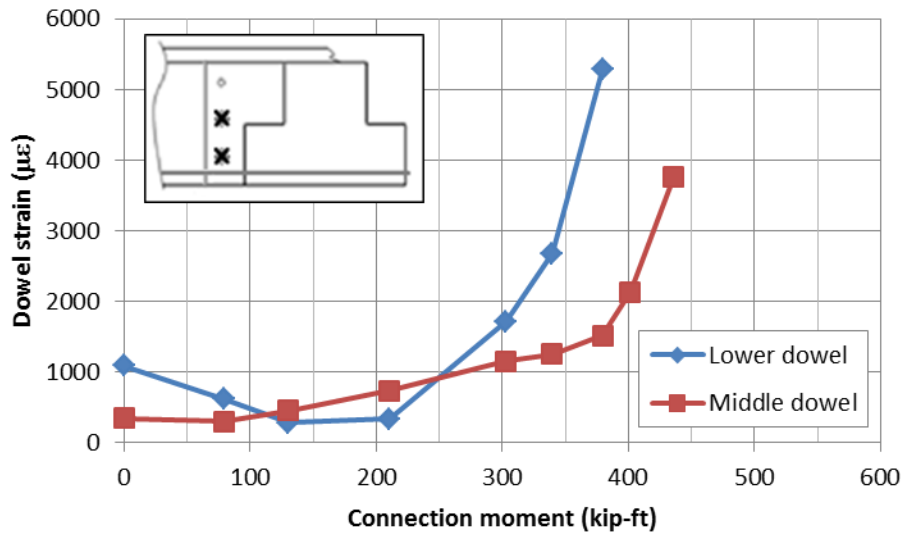
3.3.4 Performance of the GUSC detail

Strain gages were used to monitor the strain in the unstressed strands throughout the GUSC test. Figure 3.22a provides strain values from near the connection interface in one of the strands for the positive moment peak conditions for most of the Phase III portion of the test. The dowel

bars that were duplicated from the as-built connection also contributed to the connection performance; Figure 3.22b provides these strain values for the same peak conditions as in Figure 3.22a. The labels by the points on each curve indicate the corresponding load/displacement peak; the points labeled as “F” were the peaks from the force-control portion of Phase III, whereas the points labeled as “D” were the peaks from the displacement-control portion.



a. Unstressed strand strain for positive moment peaks



b. Dowel bar strain for positive moment peaks

Figure 3.22: Performance of unstressed strand and dowel bars in GUSC detail

The increase in slope in Figure 3.22a at high moments shows that the strands carried a greater portion of the load when the connection was subjected to large moments and displacements. Therefore, it can be inferred that another positive moment transfer mechanism was contributing significantly in the lower load portions of the test, but as the moment increased the strand was required to contribute more to resist the required demand. The other primary mechanisms in the GUSC detail that could contribute to resisting positive moment tension were shear friction between the diaphragm concrete and the general confinement and restraint provided by the diaphragm concrete. Figure 3.22b offers insight into the dowel bar and diaphragm mechanism. These plots show the measured strains in the lower and middle dowel bars at peak displacements producing positive moment in the connection. The dowel bar strains here exhibit a similar trend to the strand strain presented above. The data indicates that the dowel bars and unstressed strand act in concert to resist positive moment tension, and this combined mechanism picks up more load under high displacements as the ability of the concrete to provide confinement and anchorage lessens.

Figure 3.24 presents the strand strain as a function of the relative displacement measured at the lower interface of the girder and diaphragm. The linear behavior of the strand strain here indicates two important behaviors. First, the strand strain is directly related to the gap opening (relative interface displacement); thus, the strand is a primary contributor in the performance of the connection. The strand provides a successful tension load path to significantly improve the positive moment performance of the connection detail and maintain a linear tendency in the separation of the girder from the cap beam and diaphragm. Second, these data confirm the successful anchorage of the strand in the girder and cap beam, since the relative displacement of the connection shows no indication of irregularity in the relationship between the strand strain and location. Any slipping occurring in the anchorage regions of the strands would affect the relationship at the interface, so these data match the strand load cell data mentioned earlier in confirming the successful anchorage of the strand.

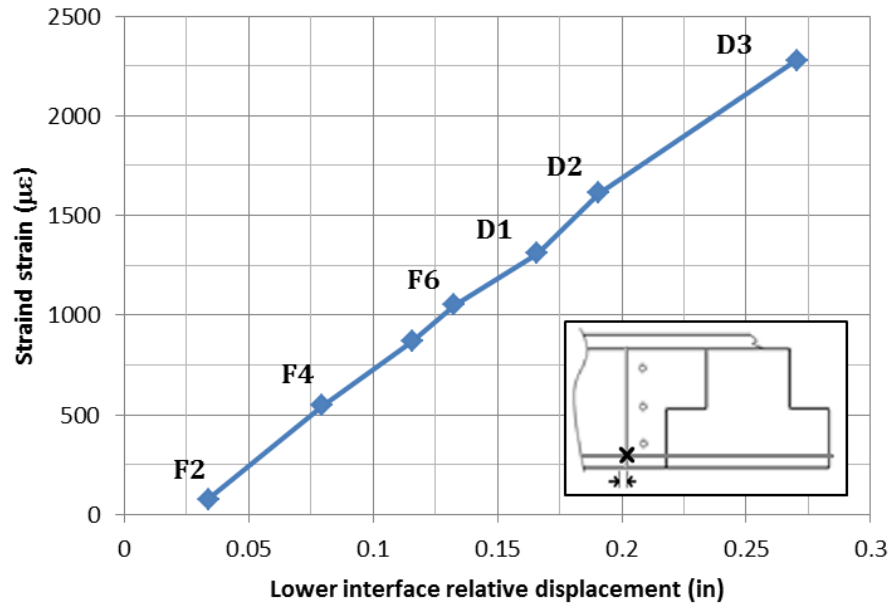


Figure 3.23: Strand strain related to relative interface displacement

3.3.5 Performance of the LUSC detail

Because of the complexity of the positive moment tension transfer mechanism in the LUSC detail, data from the dowel bars, diaphragm looped strands, and girder looped strands were investigated and compared to quantify the connection performance. Figure 3.24 shows measured strain in one of the four dowel bars near the girder web plotted as a function of the relative displacement of the girder lower flange and the diaphragm. The positive relative displacements correspond with positive moment loading and are of primary interest. These data reveal a regular and linear trend throughout the Phase III test. The uniformity of this relationship suggests that the dowel bars are indeed a primary contributor in the positive moment performance of the LUSC detail. Another notable observation is that the maximum strain of 1783 $\mu\epsilon$ measured in the dowel bars was noticeably lower than the approximate yield strain of 2300 $\mu\epsilon$. The relatively low strain demand indicates that the dowel bar size (#6 bars in the test unit) could be reduced without affecting the connection performance; however, additional investigation would be helpful prior to developing a specific design recommendation.

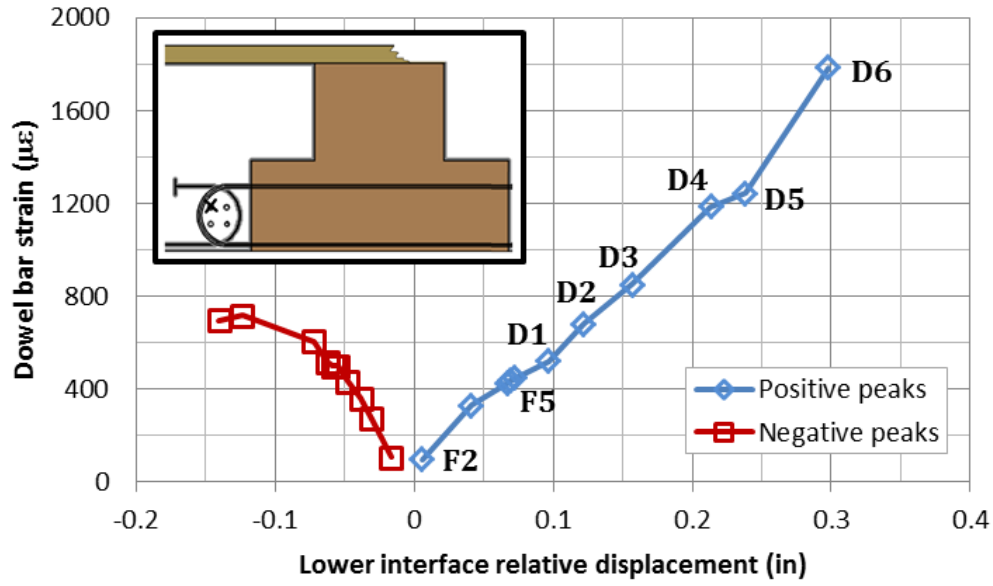
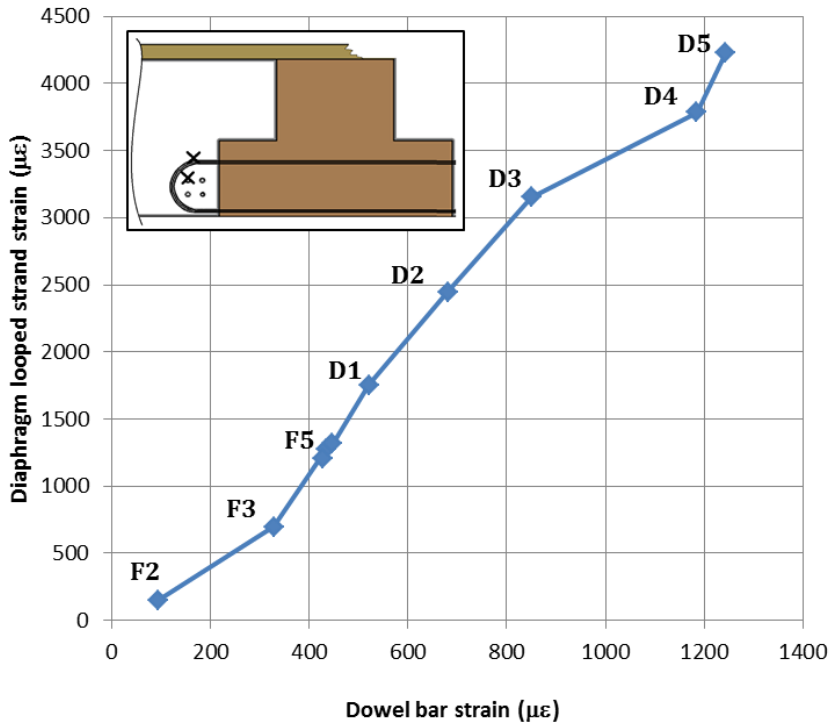
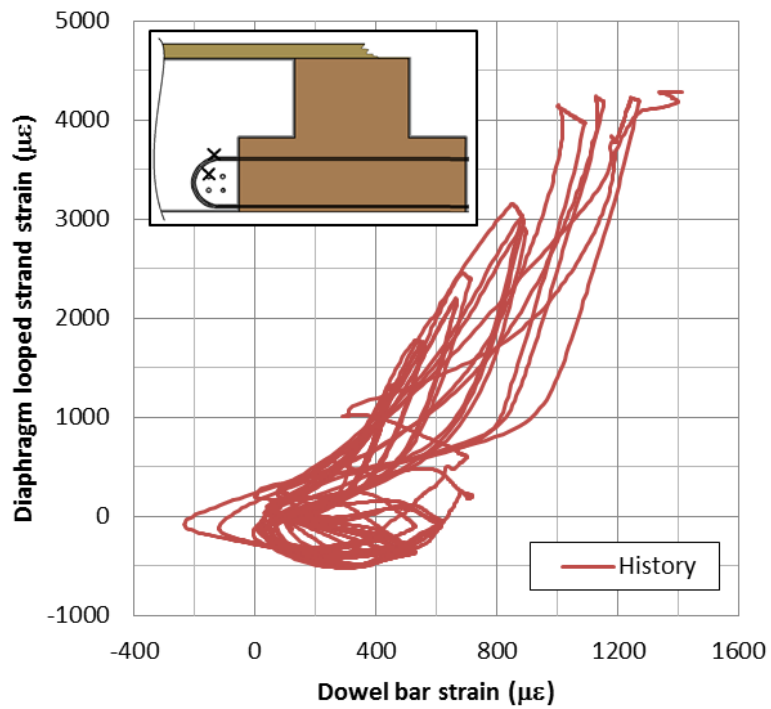


Figure 3.24: LUSC dowel bar strain as a function of interface relative displacement

Confinement for the dowel bars was expected to be provided by the looped strands in the diaphragm and girder. Figure 3.25a shows how this mechanism performed in the diaphragm; this figure presents the diaphragm looped strand strain at peak displacements as a function of the dowel bar strain. This relationship is again relatively linear throughout the test. The regularity of this relationship suggests that the diaphragm loops were an important component in the successful positive moment behavior of the connection detail. The strain history of the relationship between the looped strand strain and dowel bar strain throughout the test, plotted in Figure 3.25b, also confirms the regular relationship between the two. While there is relaxation in the strain as the load reverses, the pattern is quite uniform throughout the test and indicates regular interaction between the looped strands and the dowel bars.



a. Peak positive moment displacements

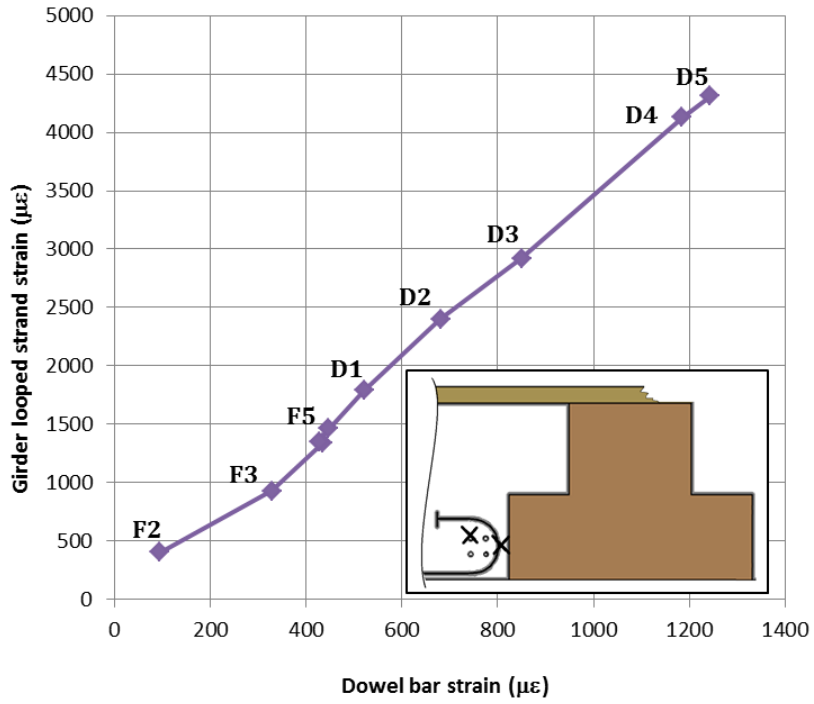


b. Strain history

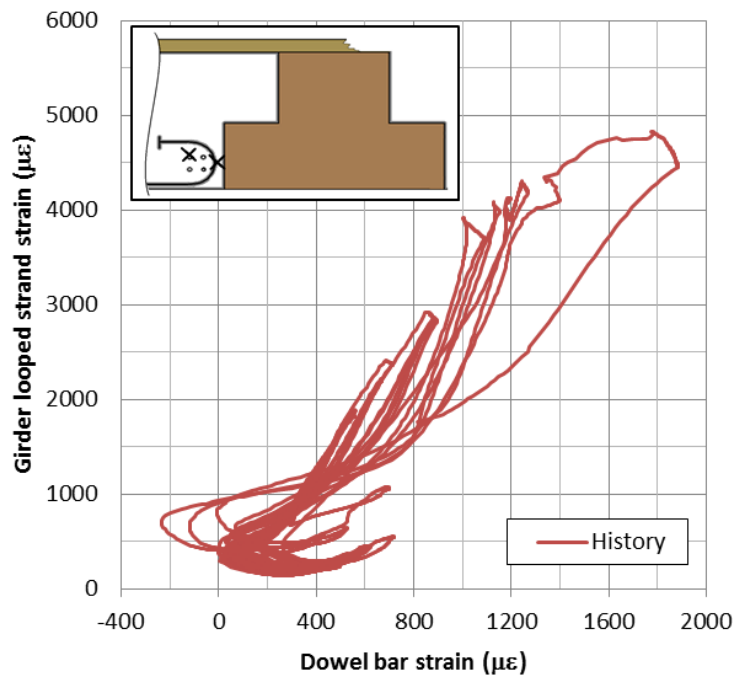
Figure 3.25: LUSC looped strand strain as a function of dowel bar strain

One more observation from Figure 3.25 is that the maximum diaphragm looped strand strain was around $4300 \mu\epsilon$, significantly lower than the strand yield strain of $7900 \mu\epsilon$. In a detail based on this design concept, the looped strand could likely be reduced without compromising the connection performance.

The interaction of the dowel bars with the girder looped strands was also crucial to successful positive moment connection performance. Figure 3.26a shows the strain at peak displacements in the girder looped strand plotted as a function of dowel bar strain. This figure is strikingly similar to Figure 3.25a, indicating the girder strands were similarly engaged in the force transfer and also similarly equipped to perform as intended. Likewise, Figure 3.26b is very similar to Figure 3.25a, verifying a regular relationship between the girder looped strand and the dowel bar strain. The final similarity of the girder loops to the diaphragm loops was the strain magnitudes, as the maximum girder strand strain is noticeably lower than the yield strain. Similar to the diaphragm loops, these loop strands could likely be reduced without significantly altering the performance of the connection.



a. Peak positive moment displacements



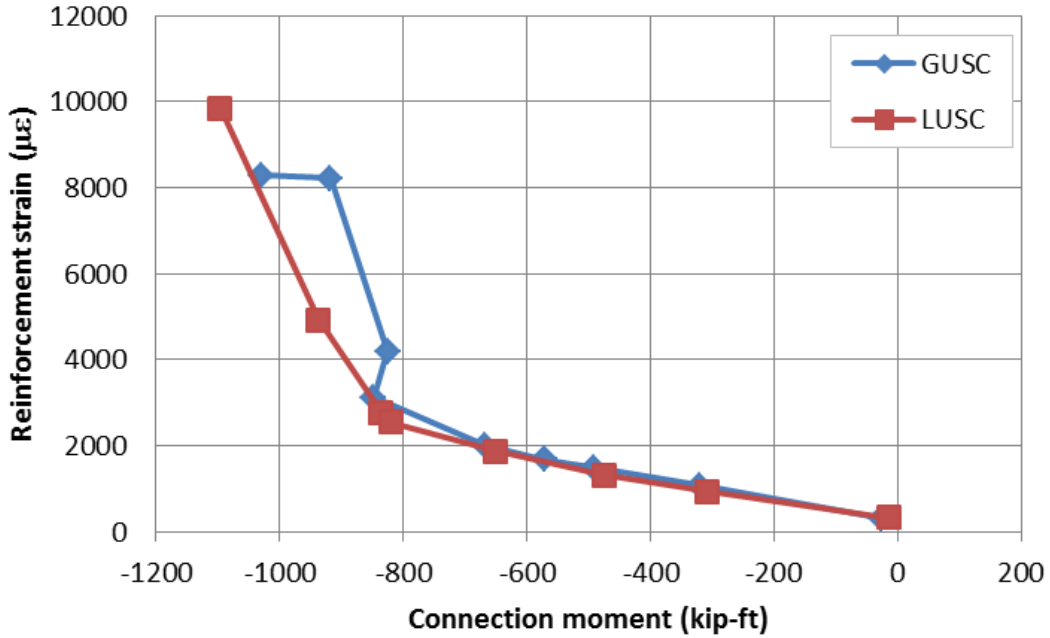
b. Strain history

Figure 3.26: LUSC girder looped strand as a function of dowel bar strain

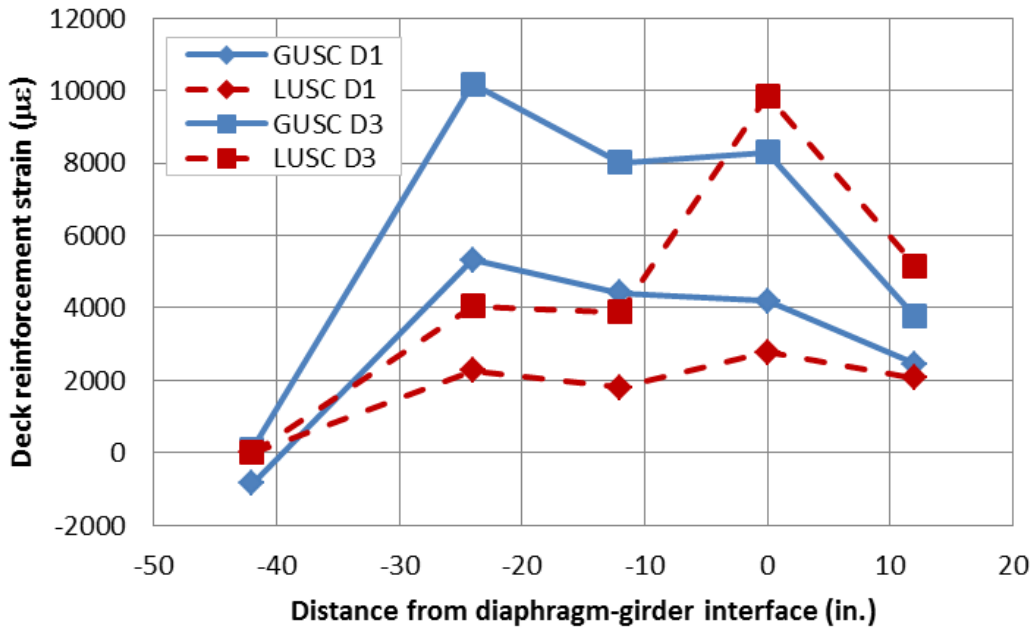
Figure 3.27 provides the measured strains in the deck reinforcement above the GUSC and LUSC cap-girder interfaces. Since the deck reinforcement is the primary tension transfer mechanism across the connection for negative moment action, these strains provide an indicator of the negative moment connection performance of the GUSC and LUSC details.

In Figure 3.27a, the deck strains are shown as a function of connection moment at peak loads and displacements producing negative moment throughout the Phase III test. This figure shows that the negative moment connection behavior was very similar for both the GUSC and LUSC details. The behavior is elastic and almost identical up to a negative moment of approximately 850 kip-ft. At higher negative moments, the GUSC and LUSC deck strains exhibit bilinear behavior, picking up higher deck strains for lower increases in connection moment; however, at these high moments the GUSC data is slightly more irregular. The bilinear behavior indicates that as the connection begins to deteriorate due to high positive and negative moment cycles, more load is transferred to the deck reinforcement in order to transfer the negative moment through the connection region.

Figure 3.27b provides the strain profiles from the deck reinforcement above the girders for both the GUSC and LUSC details. In this figure, the negative distance indicates positions on the cap beam side of the interface, while positive distance indicates positions on the girder side of the interface. Two different negative moment peak displacements during the Phase III test are shown, D1 and D3. The profiles for both details at the D1 peak displacement are relatively similar, but considerably higher strains were measured along the GUSC connection. At the higher D3 peak displacement, the deck strain in the LUSC girder is seen to increase noticeably directly above the cap-girder interface, whereas the GUSC deck strains increase more uniformly from the interface back into the cap. This data indicates a couple behaviors of the connections. First, during negative moment elastic behavior, the LUSC looped strand and dowel bar mechanism provides a partial alternate negative moment tension path, resulting in lower deck reinforcement tension during negative moment loading. Second, this alternate load path produces slightly more irregular strain behavior in the LUSC detail at high displacements near failure, whereas the GUSC detail shows relatively regular tension transfer in the deck reinforcement even when subjected to very high negative moment action.



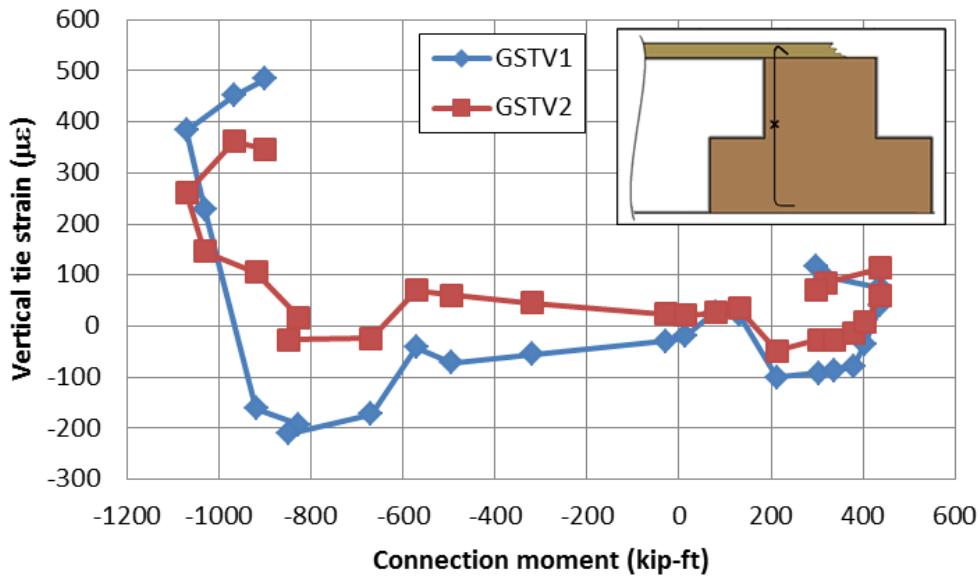
a. Negative moment peak values above girder-cap interface



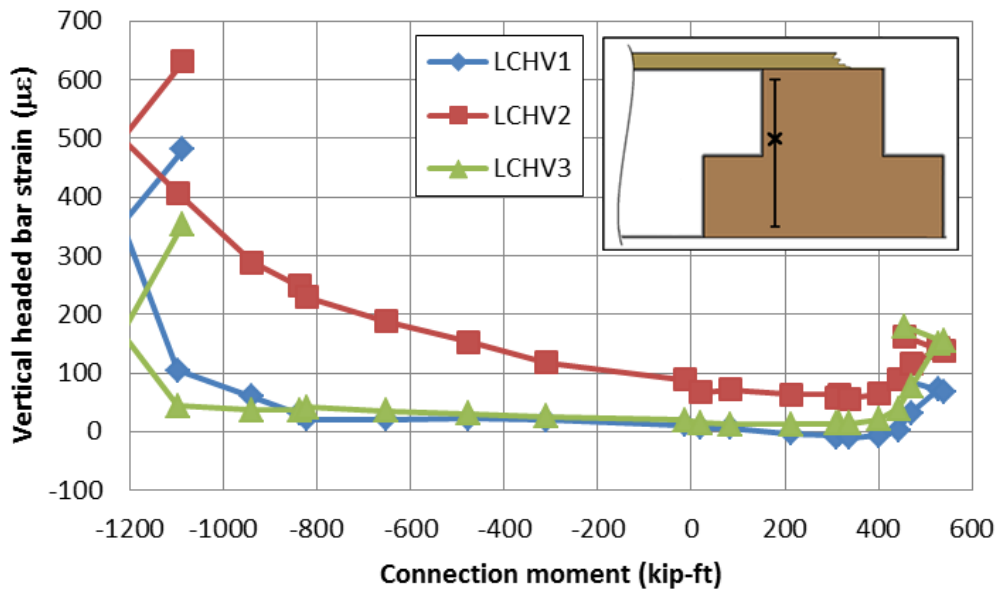
b. Profiles at negative moment peaks D1 and D3

Figure 3.27: Strains in deck reinforcement for GUSC and LUSC details

The shear reinforcement utilized in the cap beam for the LUSC detail consisted of horizontal and vertical headed bars, rather than the hooked ties that were used for the GUSC detail and in the earlier system test. Observation of the cap beam during the GUSC and LUSC tests revealed no noticeable difference in behavior between the two details. To more closely investigate the effectiveness of the headed bars, Figure 3.28 shows the strains measured on the ties and headed bars in the two details for the peak loads/displacements throughout the Phase III portion of the tests. Figure 3.28a provides measured strains on the vertical ties in the GUSC detail, while Figure 3.28b shows the measured strains on the vertical headed bars in the LUSC detail. The biggest observation of note here is that the strains are very low for both details, with strain magnitudes never going above $630 \mu\epsilon$ for the ties or headed bars in either of the details. A second observation is that the strain behavior of the headed bars is slightly more uniform than the strain behavior in the vertical ties. Overall, both the ties and the headed bars appear to be sufficient to accomplish satisfactory cap beam performance.



a. Vertical tie reinforcement in GUSC detail



b. Vertical headed bars in LUSC detail

Figure 3.28: Strains on vertical tie reinforcement and vertical headed bars

Chapter 4. ESBF and ESSP Cap Beam Connections for Bulb Tee Girders

4.1 Prototype Design

Following the completion of the first connection test, the possibility of using ABC details to bridges with longer span lengths and precast bulb-tee girders was examined. The 112 ft prototype span length of the first connection test unit was actually longer than the preferred span length for I-girders which Caltrans specifies to be 95 ft (Caltans, 2012). However, use of the 112 ft span ensured that the connections would work well for any I-girder bridge. Bridges using bulb-tee or wide-flange girders with span lengths of up to 150 ft are not uncommon in California. Therefore it was decided to use bulb-tee girders for the second connection test with a 150 ft prototype span length in order to accurately investigate the connection behavior for longer bridge spans.

The 150 ft span length required use of California Bulb-Tee 85 girders (CA-BT85) which are the largest bulb-tee girders currently used in the state of California (Caltans, 2012). To replicate the system test, a single column bent was used for the bulb-tee prototype along with the maximum superstructure width which corresponded to five girders. The maximum girder size and span length generated the maximum moment possible at the girder to cap connection region for a single column bent, bulb-tee girder bridge. Since the system test provided a fully designed prototype structure, the design of the bulb-tee prototype followed the system test design. In order to adequately design the bulb-tee prototype, the scale factors listed in Table 4.1 were formulated to appropriately increase the dimensions of the system test prototype. The scale factors provided very close approximation for superstructure length and depth as well as the appropriate section areas.

Table 4.1: Scale factors for bulb-tee prototype

| Parameter | Scale Factor |
|-----------|--------------|
| Length | 1.34 |
| Area | 1.8 |
| Stress | 1 |
| Force | 1.8 |
| Moment | 2.41 |

Using details from the system test, along with the appropriate scale factors shown above, the bulb-tee prototype structure was developed as shown in Figure 4.1. Specific design considerations for sections of the bridge including the column, girders and deck, bent cap, and connection regions are discussed in the following sections.

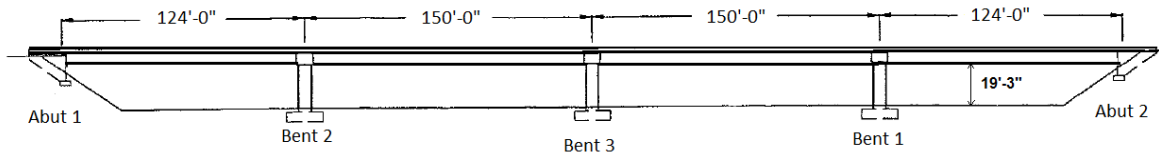


Figure 4.1: Bulb-tee prototype structure

4.1.1 Column Design

In the system test, a circular column was designed with plastic hinge locations at both the top and bottom of the column with a corresponding column overstrength moment of 17,662 k-ft (Thiemann, 2010). The scale factors listed in Table 4.1 and the overstrength moment from the system test were used to determine the overstrength moment for the bulb-tee prototype. The overstrength moment was found to be 42565 k-ft. It was not necessary to scale the column height from the system test; therefore the bulb-tee prototype had a clearance height of 19 ft 3 in. Scaling of the column section area resulted in a possible column diameter ranging from 6-8 ft depending on the reinforcement detail and plastic hinge design method. A specific column detail was not necessary for the connection tests since the column overstrength moment and clearance height would be sufficient to adequately design the test unit and connection details.

4.1.2 Bent Cap Design

The prototype for the first connection test (GUSC and LUSC connections) utilized a precast inverted-tee bent cap which provided a bearing surface for dapped end I-girders. To better understand how the bearing surface affected the cap connection and to further evaluate the use of the inverted-tee, the bulb-tee prototype was designed with a cast-in-place, square bent cap and girders without dapped ends or end blocks. The square bent cap eliminated the bearing surface provided by the inverted-tee, while the lack of girder end blocks provided an opportunity to investigate girder to cap connections with differing girder details. Due to the cast-in-place cap beam, a set of reference drawings was provided by Caltrans and were used to supplement the system test reinforcement details. The drawings contained details for a proposed widening project

of interstate I-215/I-10 in California. The widening project used a square cap that would be added to an existing multi-column bent. By scaling the system test cap beam and referencing the provided Caltrans drawings, the dimensions and details of the cap beam were determined. The depth of the cap was 7 ft 0-5/8 in. to correspond with the CA-BT85 girders, and the cap length was set to 34 ft 5 in. to accommodate five girders with 8 ft center-to-center spacing. The ends of the bulb-tee girders were extended into the cap beam a length of 1 ft 4 in.

4.1.3 Girder and Deck Design

The CA-BT85 girders were designed according to dimensions specified in Caltrans Bridge Design Aids (BDA) (Caltrans, 2012). The details of the girder reinforcement were slightly different than the system test due to the change from an I-girder to the bulb-tee. The reference drawings provided by Caltrans included details of bulb-tee girder reinforcement for CA-BT73 girders and were able to be used in combination with the system test drawings to correctly detail reinforcement for the CA-BT85 girders. The deck dimensions from the system test were not scaled since a typical 8 in. thick deck was used for both the I-girder and bulb-tee prototypes according to current Caltrans design standards.

4.1.4 Connection Design

4.1.4.1 General Design

The design of the bulb-tee connections was completed based on a combination of current field practices and research results. Each connection would be subject to both positive and negative moments and needed to be designed accordingly. The magnitudes of the positive and negative design moments are normally calculated based on the distribution of moment generated by horizontal seismic forces at the connection region. In the report by Snyder et. al. (2011), percentages of the column overstrength moment were used with 45% corresponding to the positive moment and 55% to the negative moment. These percentages however, do not account for the effects of vertical seismic acceleration. Results from the first connection test were examined and it was found through a force based approach that the percentages changed to 30% for positive moment and 70% for negative moment if vertical acceleration was considered. The shift in percentage of moment can be attributed to the vertical acceleration in the positive moment direction being counteracted by the mass of the structure. However, it is important to note that the column overstrength design moment increases if vertical acceleration is considered. The increase

in the column overstrength design moment results in the 30% moment due to vertical acceleration being higher than the 45% moment due to only horizontal forces. Equations 4.1 and 4.2 were used to calculate the positive and negative design moments of the bulb-tee prototype.

$$M_{pos} = pos\% * M_o \quad (4.1)$$

$$M_{neg} = neg\% * M_o \quad (4.2)$$

M_{pos} = positive design moment

M_{neg} = negative design moment

M_o = column overstrength moment

pos% = percentage of overstrength moment applied in positive direction

neg% = percentage of overstrength moment applied in negative direction

Applied percentages:

$$M_{pos} = 0.30 * 42565 = 12770 \text{ k-ft}$$

$$M_{neg} = 0.70 * 42565 = 29796 \text{ k-ft}$$

The connection negative moment would be resisted by the deck reinforcement. To obtain the negative moment for a single girder, the total negative design moment was multiplied by a distribution factor of 0.24. The distribution factor is a result of previous research (Vander Werff and Sritharan, 2015), and resulted in a single girder negative design moment of 7150 k-ft. An equivalent stress block approach was then used to calculate an appropriate steel area and compression block depth. The girder and deck act as a composite section and therefore are assumed to be similar to a T-beam. Equations 4.3 and 4.4 were both solved for the area of steel and then set equal to each other to determine the appropriate area of steel and compression block depth. A more detailed calculation is presented in Appendix B.

$$M_{neg} = A_s f_y \left(d - \frac{a}{2} \right) \quad (4.3)$$

$$A_s f_y = 0.85 f'_c a b_f \quad (4.4)$$

M_{neg} = Negative design moment

A_s = Area of steel

f_y = yield strength of steel

d = depth from center of deck steel to bottom of girder

a = depth of compressive block

$f'c$ = compressive strength of concrete

b_f = width of lower flange

Solving Equations 4.3 and 4.4 resulted in a steel area of 15.56 in.² per girder and an equivalent compression block depth of 10.24 in. The total area of deck steel compares well to the system test which was not designed for vertical acceleration and had a total deck reinforcement area of 12.7 in.² per girder.

To resist positive moment, both 0.6 in. diameter strands extending through the connection interface and dowel bars placed transversely through the web of each girder were implemented. The combination of strand and dowel bars had been used in both the system test's improved connection and in the GUSC connection test. Results from these tests showed that the dowel bars provided significant positive moment capacity and therefore would reduce the required number of extended strands needed in the connection. For this reason, the same size dowel bars as the system test were included in the bulb-tee connections. By examining data from the system test and GUSC connection test, it was determined that the dowel bars would provide a moment resistance of 1280 k-ft per girder. While this assumption was considered sufficient for the design of the test unit, additional guidelines are provided for quantifying the dowel contribution under design recommendations based on the findings from all connection tests. The positive moment requirement for a single girder in the test unit was calculated by multiplying the previously calculated positive design moment (M_{pos}) by the distribution factor of 0.24 and was found to be 3065 k-ft. Equations 4.5 and 4.6 were then formulated using an equivalent stress block approach with the assumptions that the girder and deck would again act as a composite section and that the compressive area of the section would occur within the deck slab. Equations 4.5 and 4.6 were then set equal to each other and solved to provide the total number of strands required for each girder. Derivation and detailed calculations are again included in Appendix B.

$$N_s = (M_{pos} - M_{DA}) / (f_{ys} * A_{strand} * (d_s - \frac{a}{2})) \quad (4.5)$$

$$N_s = \frac{0.85 f'c b_d * a}{A_{strand} * f_{ys}} \quad (4.6)$$

N_s = number of strands

M_{DA} = dowel action moment resistance

f_{ys} = yield strength of strand

A_{strand} = area of single prestressing strand

d_s = depth from top of deck to centroid of strands

a = depth of compression block

b_d = effective width of bridge deck for a single girder

Solving Equations 4.5 and 4.6 resulted in the use of five 0.6 in. diameter strands per girder with a compressive block depth of 0.71 inches.

4.1.4.2 ESBF Connection

The first bulb-tee connection design was labeled as the Extended Strand Bent with Free end (ESBF) connection, and is shown in Figure 4.2. The connection utilizes extended strands bent at 90 degrees, three grouted bars placed through the girder web, and crossies which connect the dowel bars on each side of the cap beam.

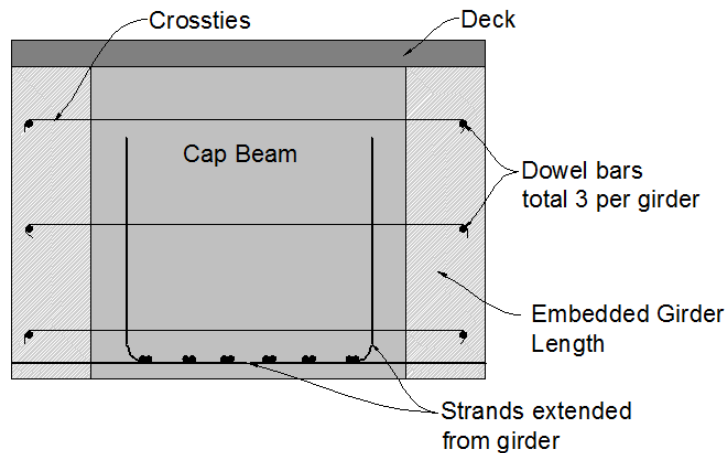


Figure 4.2: ESBF connection schematic

Precast girder connections with extended strands bent at 90 degrees have been designed and tested to resist positive moments resulting from volume changes caused by creep, temperature shrinkage, and loading in spans away from the supports. The bent strand connection performed well in these tests (Miller et al., 2004); however, the concept had not yet been tested for seismic loading. The goal of the ESBF connection design was to extend the bent strand detail to seismic applications and determine the bent strand performance under larger loads caused by seismic action. Dowel bars were also included in the design of the connection in order to decrease the

number of extended strands required for positive moment resistance and thereby reduce congestion at the connection region.

The extended strands in the ESBF connection rely on development length for anchorage in the bent cap. Development length of an extended strand is the length required for proper anchorage based on the bond strength between the strands and concrete. The 90 degree bend in the strand allows for a longer development length within the cap beam and also provides tension continuity in the superstructure as the strands from girders on opposite sides of the bent cap overlap.

Current research conducted at ISU provided recommended development lengths for different sizes and configurations of strands. The recommendations were based on a series of pull-out tests performed on strands. For the 0.6 in. diameter strands used in the prototype, the recommended development length of a curved strand was 70 in. (including the curved portion of the strand). While extensive testing of different proportions of curved and straight portions of the developed strand was not conducted, it is suggested to use a bend radius that is not more than one third the embedment length. The initial placement of the strands was designed to be under the longitudinal reinforcement bars in the cap beam so that the strands could be bent around the longitudinal bars as shown in Figure 4.2. For placing the bent extended strands, strands can be bent at 90 degrees and set in place prior to assembling the cap reinforcement or the strands can also be threaded through the completed cap reinforcement.

4.1.4.3 ESSP Connection

The second connection, known as the Extended Strand with Splice and end Plate (ESSP) connection, is shown in Figure 4.3. The extended strands and addition of strand ties in this connection were designed according to details used by the Washington Department of Transportation (WSDOT) (Khaleghi, 2012).

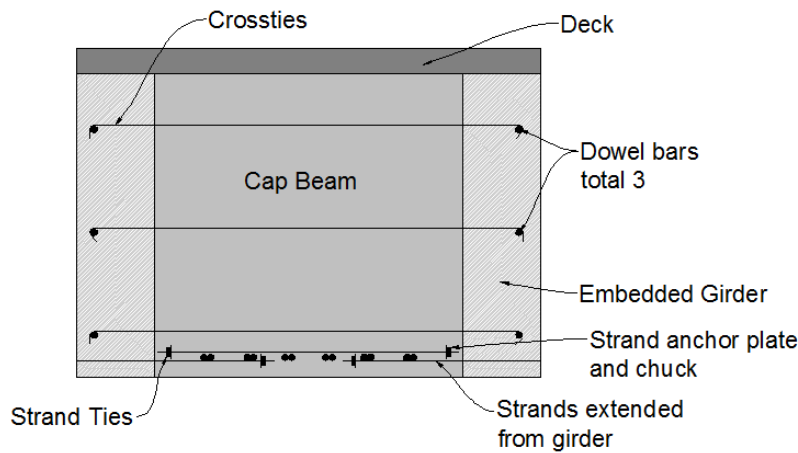


Figure 4.3: ESSP connection schematic

For the ESSP connection which can also be used where girders are on curved alignment, WSDOT has provided design recommendations, but the connection detail has not been experimentally verified. The detail is beneficial to bridges where congestion of cap beam reinforcement makes it difficult to extend strands further into the cap beam to provide tension continuity. Experimental verification of the capacity of the connection will validate the design guidelines specified by WSDOT and also provide a better understanding of how force transfers through the connection.

In the ESSP connection, the prestressed strands from the girders extend a short distance into each side of the cap beam and are anchored with plates and strand chucks. Strand ties are placed to overlap the extended strands on both sides of the cap and create tension continuity along the bottom of the cap beam as shown in Figure 4.3. The strand ties are also anchored on both ends with a plate and anchor chuck. The WSDOT design does not include dowel bars, but based on the system test each girder contains three dowel bars connected with crossties in order to reduce the required number of extended strands.

The spliced strand concept relies on the idea that the tension force developed in the strand under positive moment will transfer from the extended girder strand into the strand tie through a manner similar to a strut-and-tie model as shown in Figure 4.4. The plate and anchor chuck on each end of the strand tie provide anchorage and resist the tension force generated by positive moment. WSDOT guidelines state that there must be at least 8 in. of overlap between the extended strands and the strand tie. It is not clear if the 8 in. includes the plate and chuck anchorage, so it is

assumed that there must be 8 in. between the anchor plates of the extended strand and strand tie. The strand ties allow for flexibility in the placement of the strands if the connection region is congested or if the girder strands cannot extend straight into the cap. In these cases, the strand ties can be moved as long as the ends remain reasonably close to the strands extending from the girder. It is likely that placement of the strands and strand ties would need to be completed prior to the completion of the cap reinforcement due to space required to place the anchor plates and chucks.

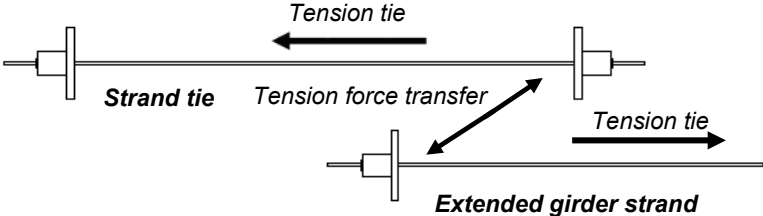


Figure 4.4: Strut and tie model

4.2 Test Unit Design

The second set of the connection tests was performed to test the capacity of the bulb-tee ESBF and ESSP connections. Based on the prototype bridge dimensions presented in Figure 4.1, a 40% scale test unit was designed. The design was based on the region of the prototype where moments in the girder to cap connection would be the highest during seismic activity. This region was determined to be located at Bent 3 as indicated in Figure 4.5.

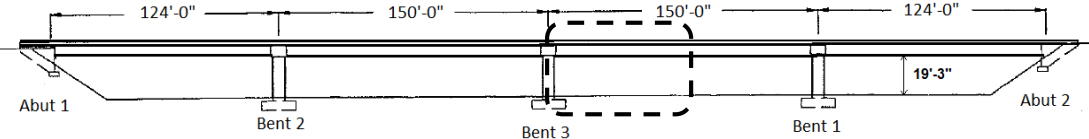


Figure 4.5: Region of highest moment during seismic activity

In designing the test unit, consideration was given to positioning girders on both sides of the cap beam or only on a single side. It was decided to place girders on only one side of the cap beam in order to simplify testing because placing girders on both sides of the cap would require simultaneous testing of opposing girders. Therefore the test unit was designed with two girders placed on one side of the cap beam. One girder would test the ESBF connection, and the other the

ESSP connection. Each girder was designed with an individual deck to prevent interaction between connections. The factors shown in Table 4.2 were used to design the test unit by appropriately scaling the prototype structure. Details regarding the design of the girders, test unit connections, column and footing, and cap beam are discussed in the following sections. A complete set of drawings for the test unit are attached in Appendix C.

Table 4.2: Test unit scale factors

| Parameter | Scale Factor |
|--------------|--------------|
| Length | 0.4 |
| Area | 0.16 |
| Stress | 1 |
| Force | 0.16 |
| Moment | 0.064 |
| Uniform Load | 0.4 |
| Displacement | 0.4 |

4.2.1 Girder Design

The first members of the test unit to be designed were the precast girders. The scale factors listed in Table 4.2 were used to scale the girder dimensions which resulted in the scaled girder cross-section shown in Figure 4.6.

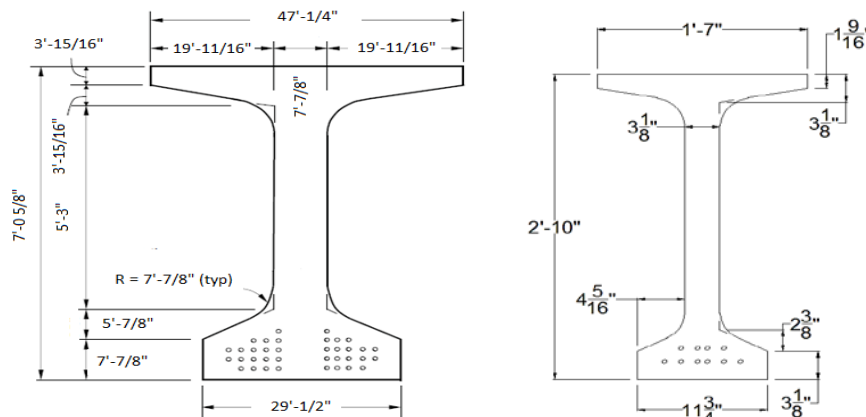


Figure 4.6: Cross-sections of prototype girder (left) and scaled test unit girder

Half of the 150 ft prototype span was scaled for design of the test unit since, due to symmetry, the moment behavior of the girder could be accurately represented without considering the entire

span length. Scaling half the 150 ft span length resulted in a 30 ft test unit girder, but also required the design of the prestressed strands in the girder to be adjusted due to the shorter girder length. The prestressing force from the prototype girder was scaled for the test unit and 3/8 in. strands were selected to provide the appropriate strand area. Next, the permissible stresses at transfer were checked and it was found that the extreme fiber stresses in tension were too high. To solve this problem, the number of strands in the girder was reduced until the stresses fell within the required range. The final design of the girder resulted in the use of ten 3/8 in. strands instead of thirteen strands in the bottom flange of the girder. The reduction in strands resulted in a decrease of approximately 18% in the overall girder moment capacity. The negative cracking moment of the girder at the connection interface was calculated to be 287 k-ft with a positive cracking moment of 158 k-ft. Scaling of the girder reinforcement resulted in the use of wire mesh since standard rebar sizes were too large. Wire mesh was previously used in the system test girders as well as the girders for the first connection test without encountering any problems. At one end of each girder, 1 in. diameter holes were placed to allow for the insertion of dowel bars.

4.2.2 Connection Design

Both the ESSP and ESBF connections were designed based on the scaled prototype positive and negative design moments using Equations 4.7-4.8. The test unit column overstrength moment was calculated using Equation 4.7.

$$M_o^t = M_o * sf * df * n \quad (4.7)$$

M_o^t = test unit column overstrength moment

sf = prototype to test unit scale factor

df = load distribution factor

n = number of girders

$$M_o^t = 42565 * 0.064 * 0.24 * 2 = 1308 \text{ k-ft}$$

Positive and negative design moments were then calculated:

$$M_{pos} = 0.30 * 1308 = 393 \text{ k-ft}$$

$$M_{neg} = 0.70 * 1308 = 916 \text{ k-ft}$$

For the design negative moment the required amount of deck steel was calculated in the same manner as the prototype structure. The amount of deck steel that coincided to the negative design

moment and allowed for even distribution across the width of the deck was calculated to be 5.26 in.², which results in a negative moment capacity of 940 k-ft.

Design of the connection for positive moment also followed the prototype design process using 3/8 in. strands. The moment resistance from dowel action needed to be calculated at the test unit scale and was found to be 160 k-ft for a single girder based on data from the system test and the test for the GUSC connection. The number of strands per connection was then calculated in the same manner as the prototype structure and five 3/8" strands were found to be required for each girder.

The embedment length of the curved strands for the ESBF connection was also based on current research at ISU and set at the recommended length of 60 inches. For the ESSP connection, the minimum overlap length of the strand ties and extended strands at the prototype level was specified by WSDOT as 8 in. For the test unit the overlap length was not scaled but instead was kept at the minimum prototype length of 8 in. to ensure integrity of the connection and facilitate force transfer from the extended strands to the strand ties.

After determining the amount of deck steel and the number of strands, the embedment length of the girder into the cap beam was scaled to 6.4 in. The embedment length of the girder has a direct impact on the amount dowel action developed for positive moments. One of the ways in which positive moment connections can be better designed is to gain an improved understanding of dowel action. Data from the GUSC connection in the first connection test provided useful information regarding dowel action behavior, however, the GUSC connection had a larger embedment length of 12 in. In order to generate dowel action behavior comparable to the GUSC connection, the embedment length was increased to 9 in. The embedment length could have been increased to 12 in. for direct comparison. However, this would have created an unnecessarily large cap width at the prototype level. While the 9 in. embedment length corresponds to an increased prototype cap width, the increase was more reasonable and allowed for adequate comparison of dowel action behavior.

4.2.3 Footing and Column Design

4.2.3.1 General

Since the testing focused on the connections, the column was designed to remain elastic throughout the test and the footing was then designed to resist the overstrength moment of the column. As the test unit was being designed, planning was underway for the design of a third

connection test for the ESMS and ESLS connection. With this in mind, the footing and column of the test unit were designed to be reused after completion of the ESBF and ESSP connection tests. A cast-in-place square column and footing were chosen and post-tensioning ducts were inserted in the column and footing for placement of 2 in. diameter, 150 ksi post-tensioning bars. As shown in Figure 4.7, the post-tensioning bars would be anchored in a pocket underneath the footing, run through the column, and be extended through the top of ducts. The bars would be post-tensioned to secure the cap to the column and also provide column moment resistance. At the completion of the test, the tension in the bars would be released, the cap beam removed, and the footing and the column reused.

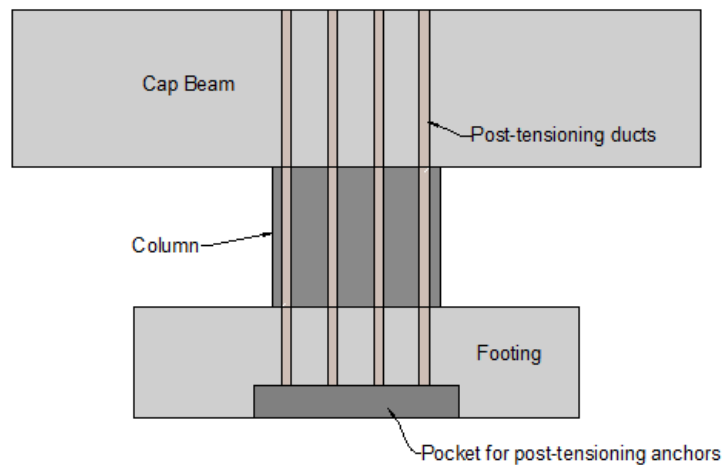


Figure 4.7: Post-tensioning bar schematic

4.2.3.2 Column Design

The column was designed based on the expected connection positive and negative moments. The negative design moment would produce the largest force at the column cross-section and was calculated to be 940 k-ft. Inelastic behavior of the connection could cause a large negative moment with a maximum value of 1410 k-ft assuming all the deck steel reaches an ultimate stress of 99 ksi. Therefore, the column design moment was taken to be 1410 k-ft.

A 3 ft x 3 ft square column section was chosen and twelve round 2.37 in. ducts were placed in the column as shown in Figure 4.8. A check was performed for the post-tensioning force required in the bars to meet the design moment of 1410 k-ft by using stress calculations and setting Equations 4.8 and 4.9 equal to each other.

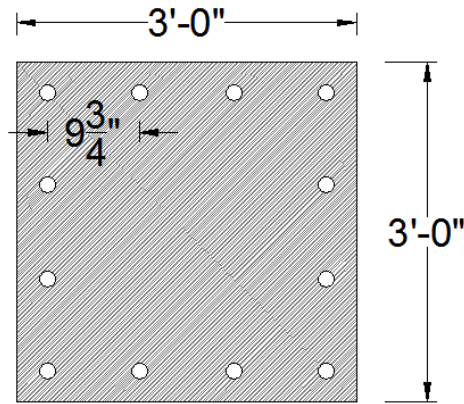


Figure 4.8: Column cross-section

Equation 4.8 assumes that the moment is applied diagonally from one corner of the column due to the girders being tested individually:

$$\sigma = (M_o^t * y) / I \quad (4.8)$$

σ = bending stress

y = distance from centroid to point of bending (measured diagonally)

I = moment of inertia of column section

$$\sigma = (1410 * 12 \text{ in./ft} * 25.45 \text{ in.}) / 139986 \text{ in.}^4 = 3.07 \text{ ksi}$$

Equation 4.9 was used to check the required force in prestressing bars:

$$P = (A * \sigma) / n_b \quad (4.9)$$

P = force in bars

A = area of column section

n_b = number of bars

$$P = \frac{1296 \text{ in.}^2 * 3.07 \text{ ksi}}{12 \text{ bars}} = 332 \text{ kips}$$

A single 2 in. diameter, 150 ksi post-tensioning bar yields at a force of 308 kips. Therefore the post-tensioning bars would not be able to resist the design moment of 1410 k-ft. A lower force in the bars of 275 kips corresponded to a column moment resistance of 1170 k-ft. This moment resistance was above the negative design moment of 940 k-ft and also allowed for some inelastic behavior in the negative direction. It was decided that the moment of 1170 k-ft would be acceptable

for the test in order to prevent yielding of the post-tensioning bars or increasing the column dimensions. Stirrups were then added to the design at 3” on center spacing.

4.2.3.3 Footing Design

The design of the footing was based on column design moment of 1410 k-ft in order to be conservative. The layout of the ISU laboratory strong floor, which has tie down locations spaced every 3 ft, was also considered in the design. The footing was designed as an 8 ft x 8 ft x 2 ft square and the reinforcement details were calculated using Equations 4.10-4.13.

Force developed at tie down locations:

$$F_c = M_o^t / s \quad (4.10)$$

F_c = Force couple developed at tie down locations

s = largest spacing between tie downs

$$F_c = \frac{1410}{6 \text{ ft}} = 235 \text{ kips}$$

Calculation of moment at column face:

$$M_{cf} = F_c * h \quad (4.11)$$

M_{cf} = Moment at column face due to tie down force

h = height of footing

$$M_{cf} = 235 \text{ kips} * 24 \text{ inches} = 5640 \text{ k-in.}$$

Equivalent stress block equations were used for calculating moment capacity:

$$a = \frac{A_s f_y}{0.85 * f'_c * b} \quad (4.12)$$

$$M_{cf} = A_s f_y \left(d - \frac{a}{2} \right) \quad (4.13)$$

a = depth of equivalent stress block

A_s = area of steel

f_y = yield stress of steel

f'_c = concrete strength

b = effective width of footing (distance between tie down locations)

d = depth from top of footing to location of tension steel

The following values were used for each variable:

$$M_{cf} = 5640 \text{ k-in}$$

$$f_y = 60 \text{ ksi}$$

$$f'_c = 4 \text{ ksi}$$

$$b = 72 \text{ inches}$$

$$d = 21 \text{ inches (assuming 3 in. was used for clear cover and stirrups)}$$

Iteration of A_s was performed to reach a solution:

$$A_s = 4.5 \text{ in.}^2$$

$$a = 1.21 \text{ inches}$$

The area of steel (A_s) was then divided by the effective width (b) to provide a required amount of 0.75 in.^2 of steel per foot. Two #6 bars spaced at 6 inches meets this requirement. Although #6 bars were specified, a miscalculation caused #7 bars to be used. This did not adversely affect the design or construction of the footing, but did provide the footing with additional moment capacity. Stirrups were added to the footing according to current Caltrans design details. A 44 in. x 44 in. x 7 in. block out was left underneath the footing to anchor the column post-tensioning bars as shown in Figure 4.9.

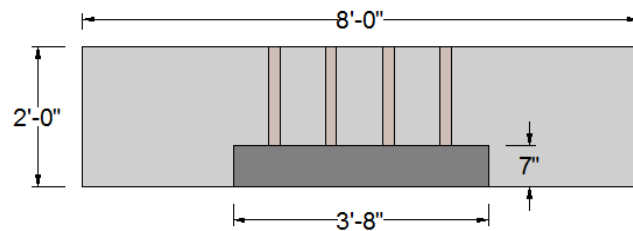


Figure 4.9: Footing block out detail

4.2.3.4 Cap Beam Design

The cap beam for the test unit was also scaled from the prototype structure. Post-tensioning ducts were placed at the center of the beam to allow connection to the column. The cap reinforcement was detailed to accommodate the two girders which were attached 4 feet on either side of the column centerline to allow construction of each girder with its own deck. The cap had a design width of 54 in., height of 37.25 in., and length of 12 ft 4 inches.

Design for torsional forces within the cap was required since girders were only attached to one side of the cap beam and each girder would reach full flexural capacity as a girder-deck composite member. The torsional resistance of the cap needed to be greater or equal to the design moment of the column since the moment at the connection would be roughly equivalent to the cap beam torsion. The Priestley method, based on plastic shear friction, was used to approximate the

torsional capacity by dividing the cap beam into triangular quadrants as shown in Figure 4.10 (Priestley S. C., 1996).

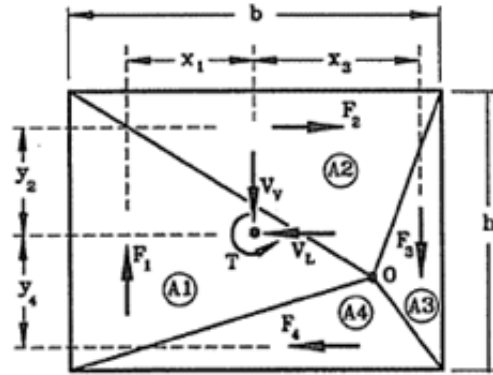


Figure 4.10: Cap beam section with triangular quadrants

Torsional resistance of the cap beam was then calculated using the following equations:

$$T = F_1x_1 + F_2y_2 + F_3x_3 + F_4y_4 \quad (4.14)$$

T = torsional capacity

F_i = force component of triangular area (Figure 4.10)

x_i, y_i = distance from section centroid to triangle centroid

Equation 4.14 can also be rewritten as:

$$T = \frac{\mu P}{A} (A_1x_1 + A_2y_2 + A_3x_3 + A_4y_4) \quad (4.14a)$$

P = clamping force

μ = coefficient of friction of cap interface

A_i = triangular area of cap beam

$$P = F + V_T + 0.0006E_sA_{st} \quad (4.15)$$

F = cap beam prestressing force

V_T = column transverse shear force

E_s = modulus of elasticity of steel

A_{st} = total area of cap beam longitudinal reinforcement

Since no prestressing force is applied to the cap and the column transverse shear is assumed to be zero:

$$P = 0.0006E_sA_{st}$$

$$P = 0.0006(29000 \text{ ksi})(22.88 \text{ in.}^2) = 398 \text{ kips}$$

Two more equations were then used to solve for torsion:

$$V_v = F_1 - F_3 = \frac{\mu P}{A}(A_1 - A_3) \quad (4.16)$$

$$V_L = F_2 - F_4 = \frac{\mu P}{A}(A_2 - A_4) \quad (4.17)$$

V_v = vertical shear

V_L = lateral shear

No lateral shear would be experienced by the cap beam, therefore F_2 is equal to F_4 and A_2 is equal to A_4 . Equations 4.14a, 4.16, and 4.17 were then used along with the following values and iterated to calculate a cap torsional capacity of 670 k-ft.

$$\mu = 1.4 \text{ (Priestley S. C., 1996)}$$

$$A = 2012 \text{ in.}^2$$

$$V_v = 110 \text{ kips}$$

$$x_i, y_i = \text{calculated based on areas } A_1\text{-}A_4$$

Since the torsional capacity of the cap was lower than the column design moment, longitudinal post-tensioning ducts were added to the design. The ducts were designed for six 1-3/8 in. diameter Diwidag bars that would be post-tensioned to 80 kips each. The post-tensioning added 480 kips to the clamping force (P) and increased the torsional capacity of the cap beam to 1537 k-ft, which was greater than the required value of the column design moment. It was determined that the post-tensioning of the Diwidag bars would not need to take place until loads higher than the combination of gravity, horizontal seismic, and 0.5g vertical acceleration were applied to the test unit.

4.3 Test Unit Construction

4.3.1 Construction sequence

Construction of the test unit took place in the ISU structures laboratory. The reinforcement cage for the footing and column were tied as a single piece and a wood insert was placed at the bottom of the footing to form a 7" pocket for the post-tensioning anchorage. Steel plates with holes at the post-tensioning bar locations were placed on top of the wood insert (Figure 4.11). The plates would be cast into the footing and provide a bearing surface for the post-tensioning anchors.

Twelve 59 mm post-tensioning ducts were tied to the column stirrups and PVC tubes were inserted in the footing reinforcement to allow the footing to be secured to the strong floor of the laboratory. The column post-tensioning bars were then set in the ducts to ensure that the ducts stayed straight during the both the footing and column concrete pours.

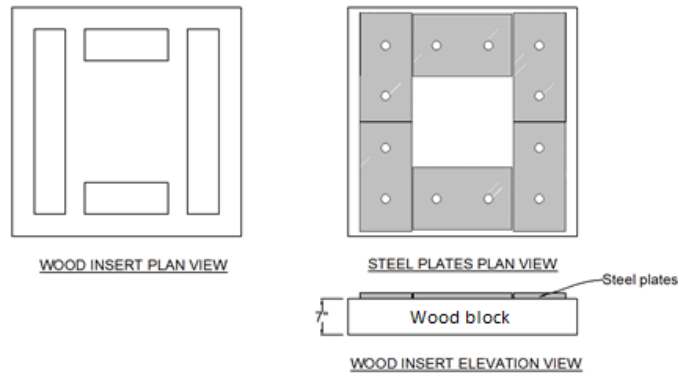


Figure 4.11: Wood insert details

The footing was poured first and a second pour was done a week later for the column (Figure 4.12). Once the concrete had cured and the formwork was removed, the footing was moved to the test location within the laboratory. The footing was lifted so that nuts and washers could be attached to anchor the post-tensioning bars inside the 7 in. pocket. The footing was then set in place, a layer of hydrostone was poured underneath to ensure a level bearing surface, and the footing was secured to the laboratory strong floor.

The cap beam was constructed following the completion of the footing. Most of the reinforcement cage was tied on the floor (Figure 4.12) with ducts set in place for both the column and longitudinal post-tensioning. A platform was constructed around the cap beam and the cap was then lifted and lowered into place over the column post-tensioning bars (Figure 4.12). Strain gages were attached at specific locations on the cap and a portion of the cap steel was left unfinished until the girders were set in place.



Figure 4.12: Footing and column pour (left); cap beam reinforcement cage (center); cap beam on platform (right)

The precast girders were cast at Cretex Concrete Products in Iowa Falls, Iowa and shipped to the ISU structures lab. A visit was made to the precast plant before pouring of the girders to attach instrumentation and ensure correct placement of rebar (Figure 4.13).



Figure 4.13: Girder strand layout and rebar cage

The girders arrived at the ISU laboratory with six of the ten strands extending 8 feet from each girder. Since six strands were extended but only five were needed for the connection, the strand in the upper row that would be located furthest away from the test unit column was cut. The girders were then placed on temporary formwork and the five remaining strands were instrumented and extended into the cap beam according to each connection detail. The bent strands from the ESBF connection were curved and threaded through the cap reinforcement (Figure 4.14). For the ESSP connection (Figure 4.14) strand chucks were welded to anchor plates and then attached to

the strand ties and extended strands. Two additional strands were also added on the back side of the cap for the ESSP connection in order to simulate strands from an opposite girder as shown in Figure 4.15. The added strands were instrumented to see if any force would be transferred from the ESSP connection to the opposite side of the cap beam. If force is transferred all the way through the cap, it could result in force interaction between girders on each side of the cap beam and result in a decreased connection moment capacity.



Figure 4.14: ESBF connection (left) prior to cutting one strand and inserting strands into cap beam; ESSP connection (right) prior to cutting one strand and attaching anchor plates and chucks

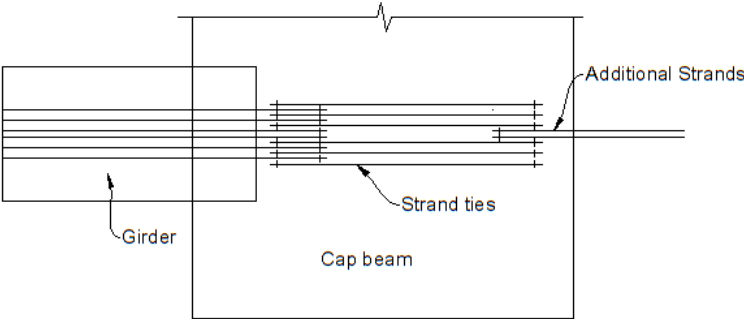


Figure 4.15: Additional strands on backside of cap beam for ESSP connection

Before the remainder of the cap reinforcement was added, the dowel bars were instrumented, inserted through the web of the girders, and grouted in place. The rest of the cap reinforcement was then added and the cap formwork was fabricated and set into place. The longitudinal cap post-

tensioning bars were also inserted to make sure that the ducts remained straight during the concrete pour. The deck formwork was constructed with bridge hangars, brackets, and plywood. Deck reinforcement was placed over the girders and tied both along the girder and into the cap beam (Figure 4.16). The reinforcement was instrumented and plastic inserts were placed in the formwork to allow actuators to be attached to each girder. The cap and deck concrete were then placed in one continuous pour and allowed to cure (Figure 4.16).



Figure 4.16: Individual bridge decks before (left) and after (right) concrete pour

4.4 Instrumentation

4.4.1 General

To capture the behavior of the girder to cap beam connections in the test unit, instrumentation was attached both internally and externally. The internal instrumentation consisted of strain gages placed on rebar, extended strands, and dowel bars. The external instrumentation included DCDT's, string pots, and an Optotrak camera system.

4.4.2 Internal Instrumentation

Strain gages were placed in specific locations to capture the response of the cap beam. On the cap longitudinal reinforcement, gages were placed to capture the torsional behavior as shown in Figure 4.17. Gage labels are shown with CTL corresponding to gages placed on the cap top longitudinal reinforcement and CBL corresponding to the cap bottom longitudinal reinforcement. At girder connection regions, gages were placed at and around the girder interface on the cap transverse reinforcement to monitor the effects of the girder movement as shown in Figure 4.18. The gage labels indicate either the spliced strand (CTSS) or curved strand (CTCS) connection.

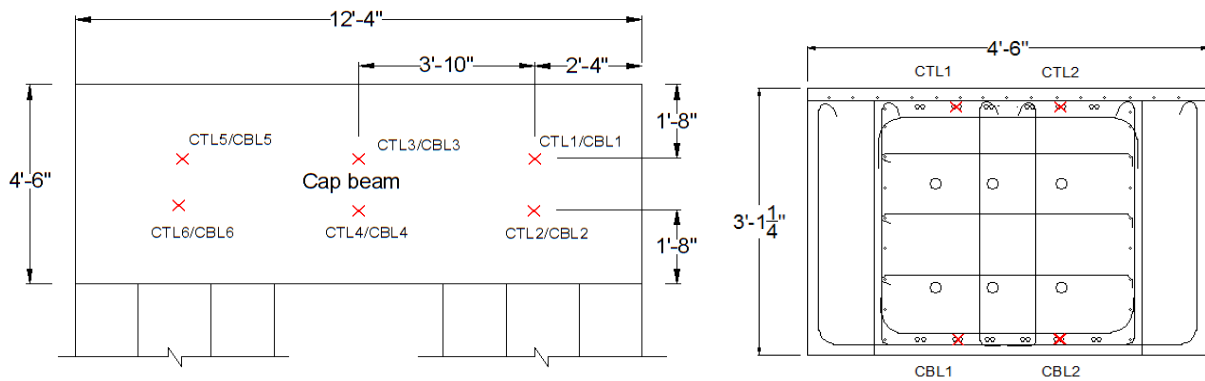


Figure 4.17: Cap longitudinal gages

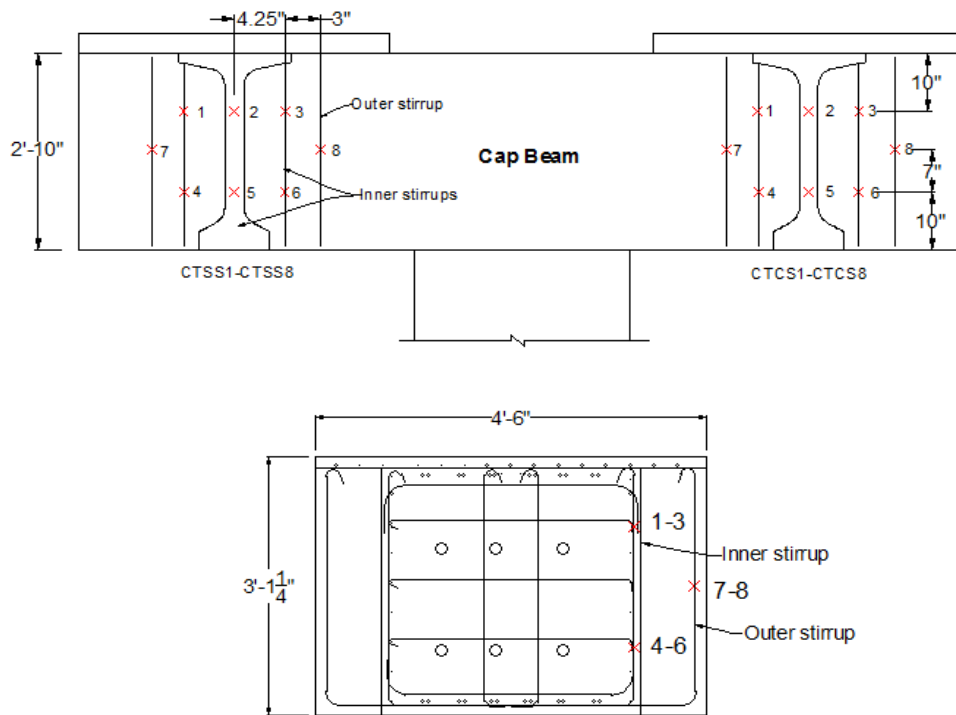


Figure 4.18: Cap stirrup gages

For the ESBF connection, the two middle girder extended strands in the bottom row were instrumented. Gages were placed at the connection interface between the girder and cap and also

15 inches on either side of the bend as shown in Figure 4.19. The gage labels CS1-CS3 correspond to the middle strand closest to the column. For the ESSP connection, instrumentation was placed on the same strands as the ESBF connection. Gages were placed at the connection interface, at plate and chuck locations, and also at two additional points on the stand ties to monitor the transfer of tension force as shown in Figure 4.20. Gage labels SS1-SS2 and SS5-SS8 were located on the strand furthest from the test unit column.

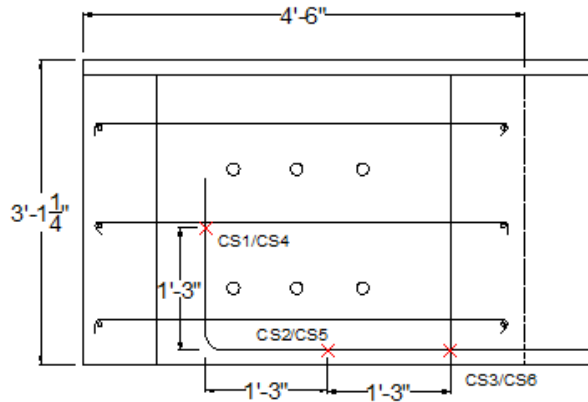


Figure 4.19: ESBF extended strand gages

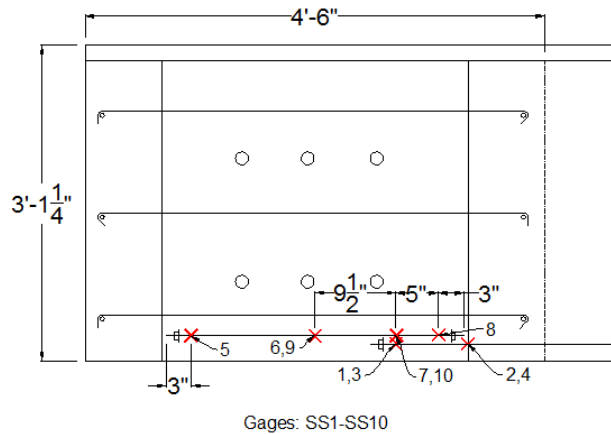


Figure 4.20: ESSP strand gages

For both connections gages were also placed on the dowel bars and crossties as shown Figure 4.21. Gage labels are only shown for the ESBF connection (indicated by “CS” in label name) but gages were placed in the same locations for the ESSP connection. Three crosstie gages (CSC1-CSC3) were added with CSC1 and CSC3 placed on the column side of the connection and CSC2 placed on the lowest crosstie at the outside of the connection. A larger number of gages were placed on the lower dowel bars to better quantify the dowel resistance for positive moments.

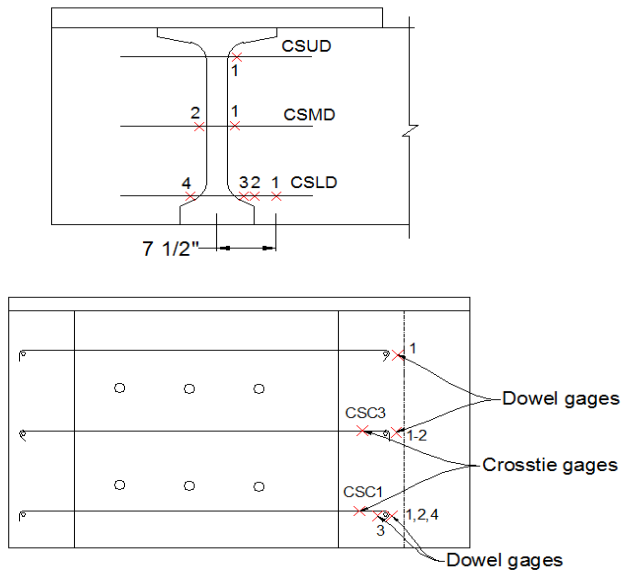


Figure 4.21: Dowel and crosstie gages

Gages were also placed on the prestressing strands inside the girders as shown in Figure 4.22. The gages were attached after the strands were pulled to the proper prestressing force but before the girder concrete was cast. Strands were placed 1, 2, 4, and 15 feet from end of the girder and were located on the center strand noted in Figure 4.23. These gages would monitor the length of strain penetration into the girder caused by tension forces under positive moments. Gages were also placed on the top layer of deck steel to monitor the deck reinforcement strains under negative moments as shown in Figure 4.24.

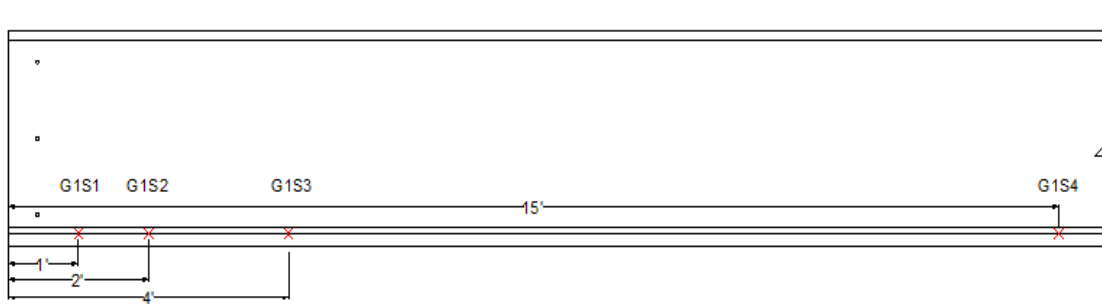


Figure 4.22: Girder strand gages

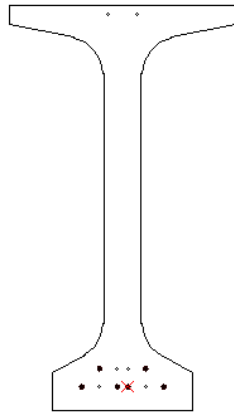


Figure 4.23: Girder cross section

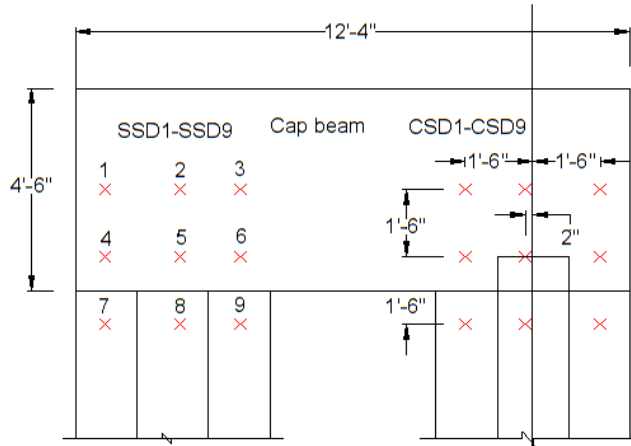


Figure 4.24: Deck steel gages

4.4.3 External Instrumentation

To record movement of the girder at the girder to cap interface, three DCDT linear displacement transducers were used. One was located underneath the girder to cap connection as shown in Figure 4.25, another of at the top of the girder to cap connection, and a third was located on top of the deck at the edge of the cap beam (Figure 4.25). DCDT's were also placed at the column to cap connection to monitor the movement of the cap beam and ensure that the column post-tensioning bars were not overloaded. For the ESSP connection, a DCDT was placed on one of the additional strands at the backside of the cap beam and a load cell was placed on the second in order to monitor possible load transfer from the connection region through the strand ties.



Figure 4.25: DCDT's on underside (left) and top of girder (right)

String pots were used to measure displacement at various points on the test unit and along the girders. Four string pots were placed horizontally on the sides of the cap beam along with two vertical string pots under the cap to monitor rotation. Two additional string pots were also placed horizontally at the actuator locations to monitor out-of-plane movement of the girders. Lastly, a string pot was placed vertically under the girder at each actuator location to record vertical displacements (Figure 4.26 and Figure 4.27).

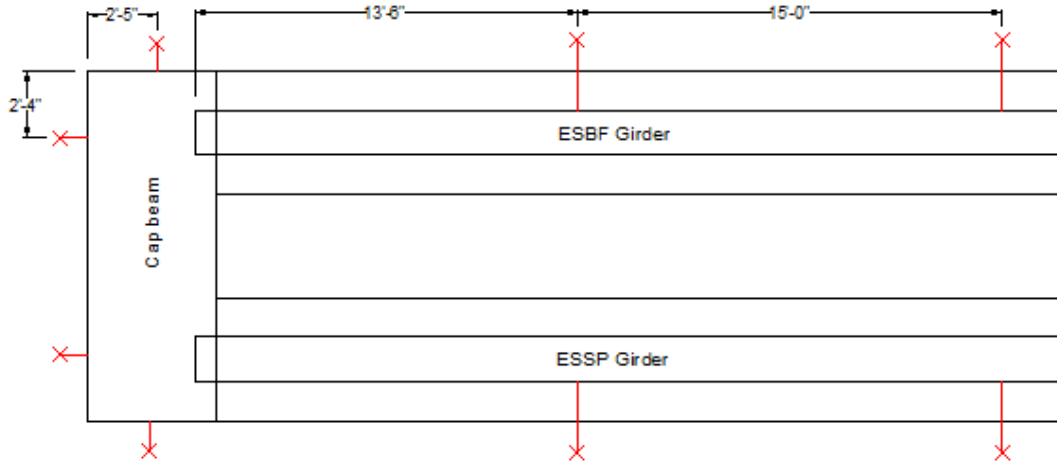


Figure 4.26: Locations of horizontal string pots

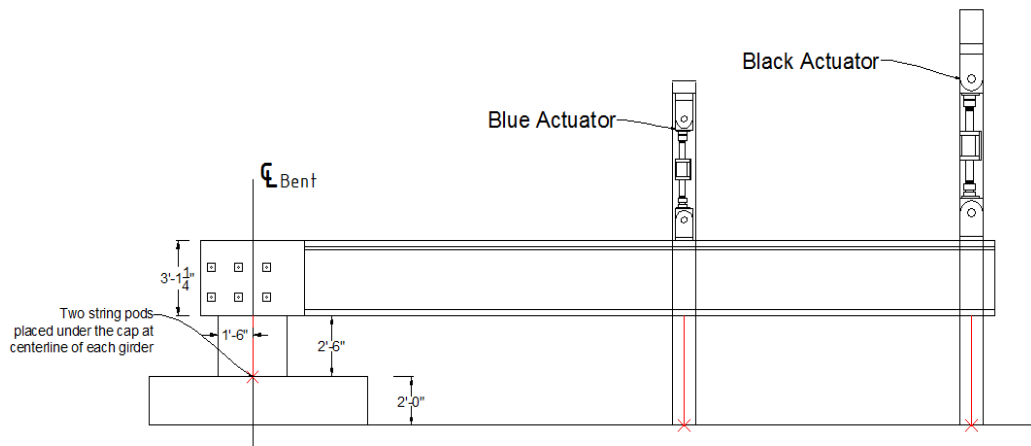


Figure 4.27: Location of vertical string pots

An Optotrak camera system was used to record 3-dimensional movement on the surface of the connection region. LED sensors were glued to the inside region of each connection as shown in Figure 4.28. During the testing of each connection, the Optotrak camera recorded the movement of the LED's which would allow surface displacements and cracking to be measured.



Figure 4.28: LED configuration at connection region

4.5 Loading Protocol

4.5.1 General

To test the capacity of the connections, each girder would be individually tested by pushing and pulling a pair of actuators pseudo-statically in a manner similar to the GUSC and LUSC connection tests as shown in Figure 4.29. The actuator forces applied to the test unit corresponded to target shear and moment values determined by the loading protocol. Prototype loads resulting from gravity, horizontal ground acceleration, and vertical ground acceleration forces were calculated and then properly scaled. Each type of load will be discussed in the following sections.

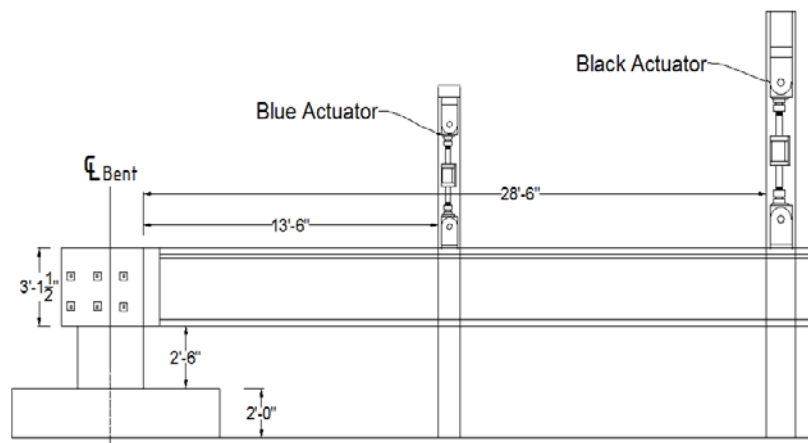


Figure 4.29: Test unit setup

4.5.2 Gravity Load

The gravity moment values for a precast girder to cap connection is dependent on the type of bent cap used in construction. A precast bent cap such as the one used for the GUSC and LUSC connections causes different loads to occur at the connection region than those produced by use of a cast-in-place cap. To understand the difference in loads, the construction loading process for the precast cap will be explained first, followed by the differences initiated by a cast-in-place bent.

For a precast cap beam, the cap is attached to the bridge column and then precast girders are set in place. The ends of the girders rest on the cap and eliminate the need for falsework to support the girder end. In this condition, the end of the girder is simply supported and no moment is generated at the connection region. Formwork is then set in place for the bridge diaphragm and deck. During the pouring of the diaphragm and deck, the liquid weight of the deck can cause a slight rotation at the end of the girder. However, since the diaphragm is also liquid, the girder is allowed to rotate and no moment is generated at the connection region. Upon hardening of the

deck and diaphragm, the girder to cap connection becomes fixed, but no moment is generated by the girder or deck because the girder was allowed to rotate before the concrete hardened. Following complete hardening of the deck, the bridge wearing surface is applied along with traffic barriers. The maximum possible future load including weight of the wearing surface and barriers produces a moment at the fixed girder to cap connection which is referred to as the gravity or self-weight moment.

The construction process for a cast-in-place cap is similar to that of the precast girder with the exception that falsework is used at the bent cap location to support the girder throughout the construction process as shown in Figure 4.30.

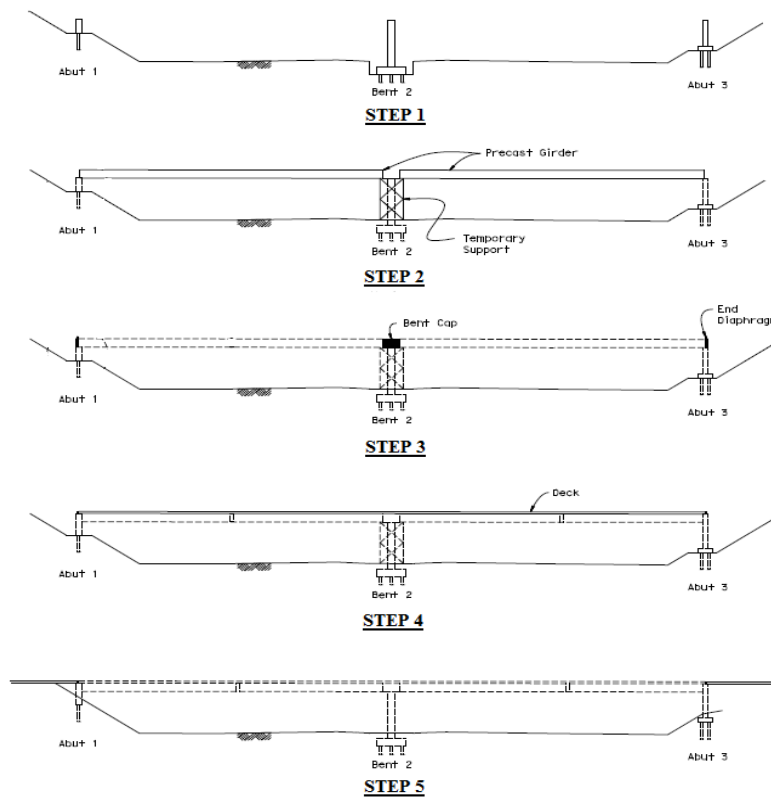


Figure 4.30: Construction sequence (Caltrans, 2013)

The cast-in-place cap eliminates the need for the diaphragm and the cap can be poured prior to or simultaneously with the deck. The girder is simply supported by the falsework throughout the construction process until the cap beam and deck are poured. After hardening of the cap and deck

concrete, the falsework is removed and the weight of the deck and girder produces a moment at the fixed girder to cap the connection. The wearing surface and barriers are also added so that the combined gravity moment is a result of the self-weight of the girder, deck, wearing surface, and barriers.

The gravity moment generated by the two types of cap are different, however, it is important to note that for both bent caps the shear at the connection is the same due to an equal shear transfer in both cap types. A test unit moment diagram showing the difference in gravity moment for the two bent caps is shown in Figure 4.31 with the girder to cap connection occurring at 30 ft.

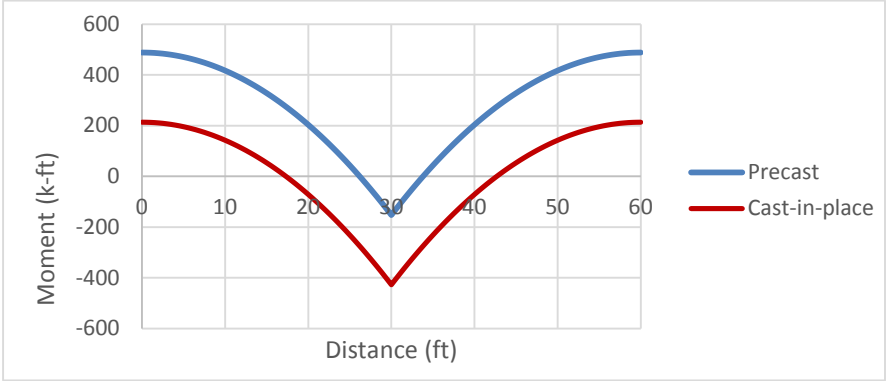


Figure 4.31: Moment difference between precast and cast-in-place cap beam

Due to the difference in gravity load, the effects of seismic forces on the girder to cap connection are also different. Horizontal and vertical ground acceleration due to seismic activity cause both positive and negative moments, these moments are added to the gravity moment of the structure with negative moments acting in the same direction as the gravity moment and positive moments acting in the opposite direction. The addition of positive and negative moments to a precast cap results in the connection being subject to higher positive moments and lower negative moments than the cast-in-place cap as shown in Figure 4.32. The difference in the connection moment stems from the larger gravity moment of the cast-in-place cap which must be overcome for the connection to experience a net positive moment.

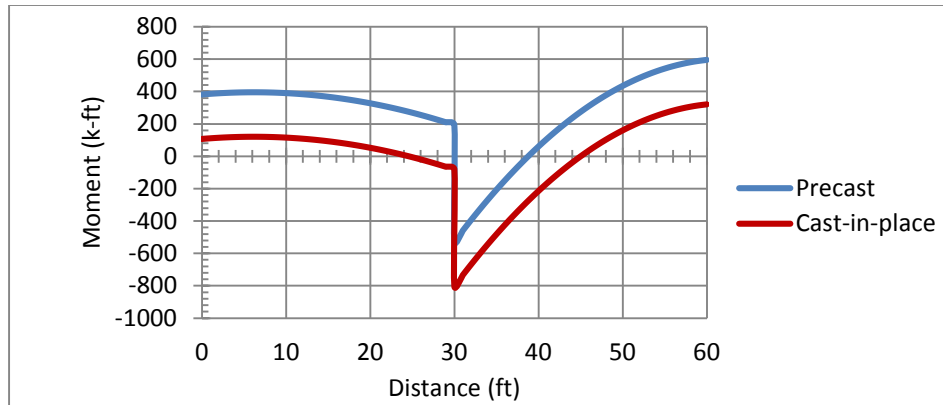


Figure 4.32: Moment difference at gravity + horizontal seismic + 0.5gV

One of the goals of the connection tests is to quantify the positive moment capacity of each connection. The maximum positive moment generated at a connection would occur for a precast cap beam since there is less gravity moment to overcome during horizontal and vertical ground acceleration. For this reason a precast cap beam was chosen, as a worst case scenario, to formulate the test unit loading protocol. Therefore the self-weight of the wearing surface and barrier were used to produce the gravity moment and shear values for the loading protocol.

4.5.3 Horizontal Ground Motion

The previously mentioned system test was used to calculate forces caused by horizontal ground motion acting longitudinal to the bridge girders. Results of the system test gave the largest horizontal force experienced by a single girder in the system test prototype. This force was then multiplied by the appropriate scale factor to convert the force to the current prototype. The scaled force was converted to the connection moment value by multiplying by half the height of the prototype column since it was assumed that a plastic hinge would form at each end of the column. The resulting moment was then multiplied by the factor of 0.45 for the positive direction and 0.55 for the negative direction (see Snyder, 2010) in order to distribute the horizontal seismic forces and then scaled for application to the test unit.

4.5.4 Vertical Ground Motion

The vertical ground acceleration forces were calculated based on the mass of the prototype structure. Target values for vertical acceleration were 0.5g and 1.0g. Since weight is mass multiplied by acceleration, the entire self-weight of the prototype girder and slab was multiplied by 1.5 and 2.0 respectively to reach the target values. The multiplied self-weights were then used

to calculated moment and shear values for the connection region assuming that connection behaved as a fixed connection.

4.5.5 Combination of Forces for the Loading Protocol

Upon determining the gravity, horizontal seismic, and vertical seismic target moment and shear values, a loading protocol was developed by combining each load. Figure 4.33-Figure 4.35 show the progression of adding horizontal and vertical seismic forces to the gravity load at the connection region. The graphs are formulated to show two 30 ft girders which meet at the connection region (distance equals zero on graph). The graphs do not show forces in the cap beam, instead zero is taken to represent the end of each girder at the connection region. It is important to note that the loads applied by the actuators only matched the prototype loads in the connection region in order to simplify the testing.

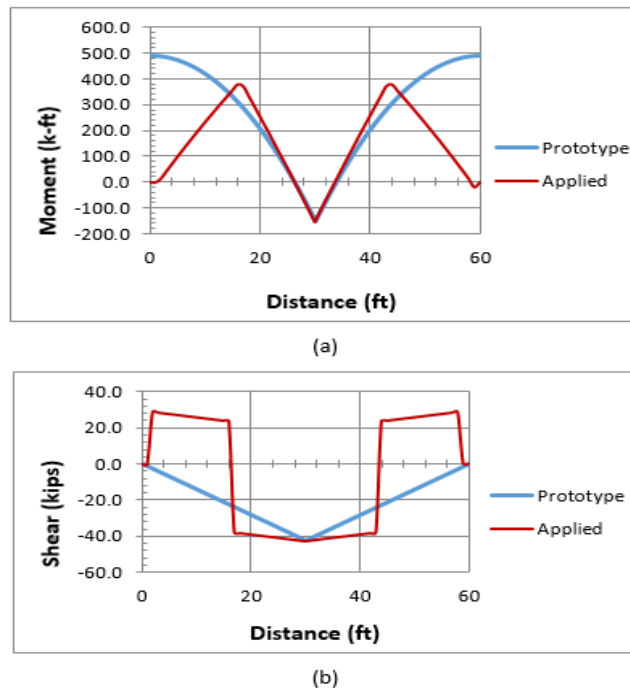
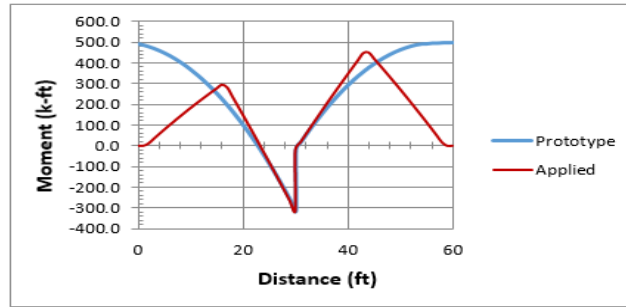
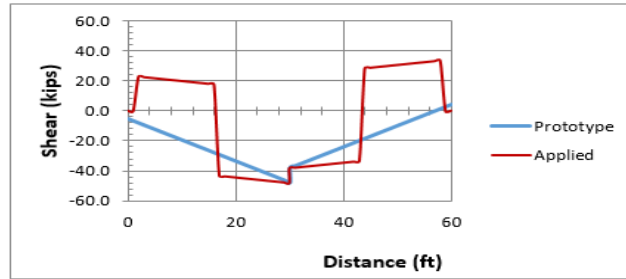


Figure 4.33: Gravity load moment (a) and shear (b) diagrams

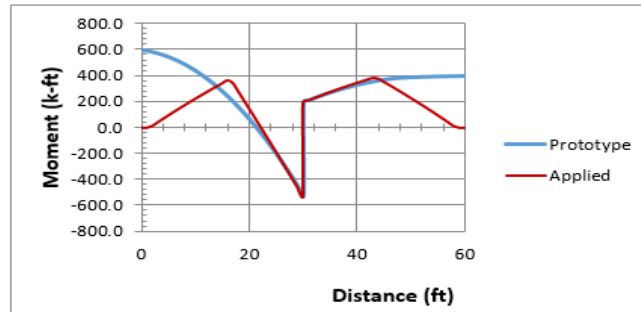


(a)

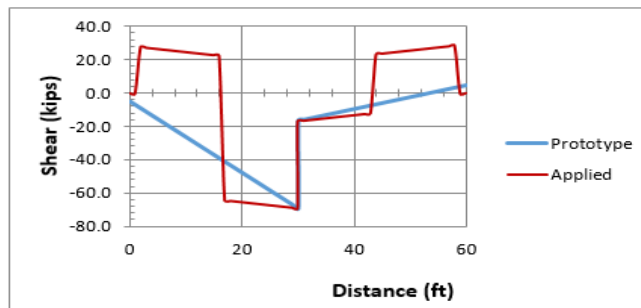


(b)

Figure 4.34: Gravity + horizontal seismic moment (a) and shear (b) diagrams



(a)



(b)

Figure 4.35: Gravity + horizontal seismic + vertical seismic moment (a) and shear (b) diagrams

For the test unit, each girder was attached to two actuators and cantilevered from the bent cap. The actuators had the option of being controlled by either force or displacement input values.

Force values were used to match the shear and moments applied to the test unit with scaled loads calculated from the prototype. Four target moment and shear values are shown in Table 4.3 which represent a gradual increase in force and the target levels of girder performance. The target values, with the exception of the gravity load, each contained values for positive moment, positive shear, negative moment and negative shear in order to accurately simulate the reversal of forces that the prototype structure would experience.

Table 4.3: Target Moment and Shear Values

| Target Values | Positive Moment (k-ft) | Positive Shear (k) | Negative Moment (k-ft) | Negative Shear (k) |
|---------------------------------------|------------------------|--------------------|------------------------|--------------------|
| Gravity (G) | - | - | -152.4 | -27.5 |
| G + Horizontal Seismic (H) | -20.4 | -23.1 | -313.7 | -32.8 |
| G + H + 0.5g Vertical Seismic (0.5gV) | 177 | -9.3 | -511.1 | -46.6 |
| G + H + 1.0g Vertical Seismic (1.0gV) | 374.4 | 4.4 | -708.5 | -60.3 |

After applying the gravity load, a series of four load steps were exercised as the load was increased to the next target value. Each load step contained both a positive and negative moment value which the girder was cycled between three times. The cycling of actuators was performed in order to simulate seismic activity and fully exercise the connection. The actuators are labeled by color and located along the length of the girder. The blue actuator was located 13.5 ft from the connection interface while the black actuator was located 28.5 ft from the interface. The connection interface was assumed to be located at the end of the girder embedded in the cap beam. An example of the four load steps between gravity and the horizontal seismic target values (G+H) is shown in Table 4.4. For the actuator forces a positive value indicated that the actuator would push down while negative indicated that the actuator would pull up. An extra load step was added between 0.5g and 1.0g vertical acceleration in order to provide more details regarding the connection performance beyond the target value of 0.5g. The force loading protocol for the entire testing sequence is included in Appendix D, however a graphical representation is provided in Figure 4.36. In order to fully quantify each connection detail, the actuators would be switched to displacement control when the connections exhibited inelastic behavior. Each connection would then be exercised to failure. A loading sequence for the displacement cycles is shown in Figure

4.37. Negative displacements correspond to an upward displacement of the girder which generated a positive moment.

Table 4.4: Sample loading protocol from gravity (G) to G + horizontal seismic (H)

| | Blue Actuator (kips) | Black Actuator (kips) | Moment (k-ft) | Shear (kips) |
|-------------|----------------------|-----------------------|---------------|--------------|
| Gravity (G) | 7.9 | -8.2 | -37.7 | 10.7 |
| | 25.7 | -15.3 | -75.7 | 21.4 |
| | 43.3 | -22.3 | -113.8 | 32 |
| | 61.1 | -29.4 | -151.7 | 42.7 |
| G±0.25H | 60.9 | -27.9 | -191.8 | 44 |
| | 61.2 | -30.6 | -118.9 | 41.6 |
| | 60.9 | -27.9 | -191.8 | 44 |
| | 61.2 | -30.6 | -118.9 | 41.6 |
| | 60.9 | -27.9 | -191.8 | 44 |
| | 61.2 | -30.6 | -118.9 | 41.6 |

| | Blue Actuator (kips) | Black Actuator (kips) | Moment (k-ft) | Shear (kips) |
|----------------------------|----------------------|-----------------------|---------------|--------------|
| G±0.5H | 60.8 | -26.4 | -233.2 | 45.4 |
| | 61.3 | -31.8 | -86 | 40.5 |
| | 60.8 | -26.4 | -233.2 | 45.4 |
| | 61.3 | -31.8 | -86 | 40.5 |
| | 60.8 | -26.4 | -233.2 | 45.4 |
| | 61.3 | -31.8 | -86 | 40.5 |
| G±0.75H | 60.6 | -24.9 | -273.2 | 46.7 |
| | 61.4 | -33 | -53.2 | 39.4 |
| | 60.6 | -24.9 | -273.2 | 46.7 |
| | 61.4 | -33 | -53.2 | 39.4 |
| | 60.6 | -24.9 | -273.2 | 46.7 |
| | 61.4 | -33 | -53.2 | 39.4 |
| G ± Horizontal Seismic (H) | 60.6 | -23.5 | -313.1 | 48.1 |
| | 61.5 | -34.2 | -20.3 | 38.3 |
| | 60.6 | -23.5 | -313.1 | 48.1 |
| | 61.5 | -34.2 | -20.3 | 38.3 |
| | 60.6 | -23.5 | -313.1 | 48.1 |
| | 61.5 | -34.2 | -20.3 | 38.3 |

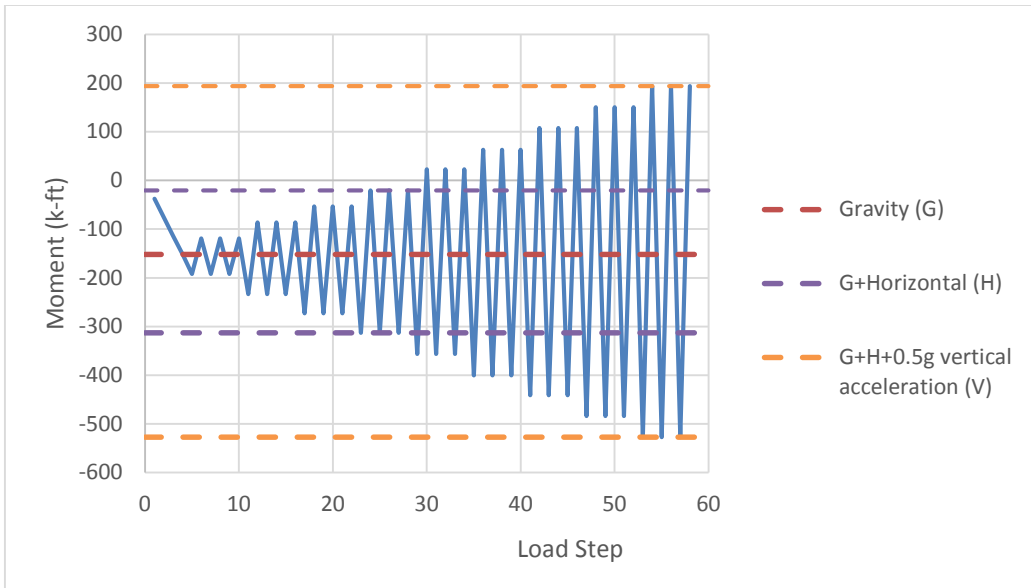


Figure 4.36: Force control loading sequence

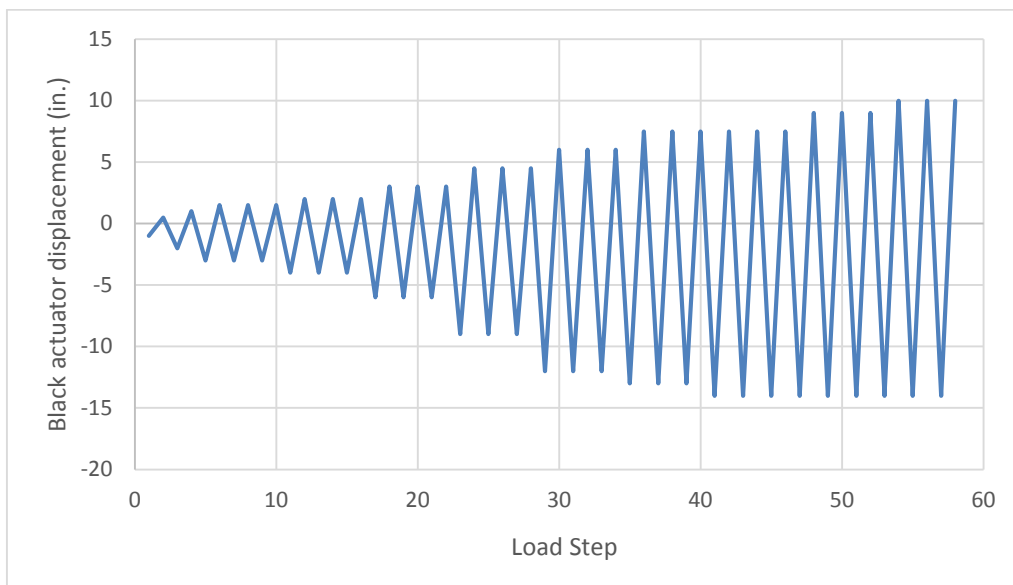


Figure 4.37: Displacement control loading sequence

4.6 Experimental Testing and Results

4.6.1 General

Following the completion of the test unit construction, the two loading actuators were attached to frames and secured to the strong floor of the ISU laboratory. The actuators were attached to a single girder and lateral braces were placed between the load frames as shown in Figure 4.38 to prevent out of plane movement. Instrumentation was then connected to external

data acquisition systems and a post-tensioning force of 200 kips was applied to each of the twelve column bars in a series of four steps as shown in Table 4.5. The column moment capacity after post-tensioning was 850 k-ft which would be sufficient for testing until displacement cycles were reached.

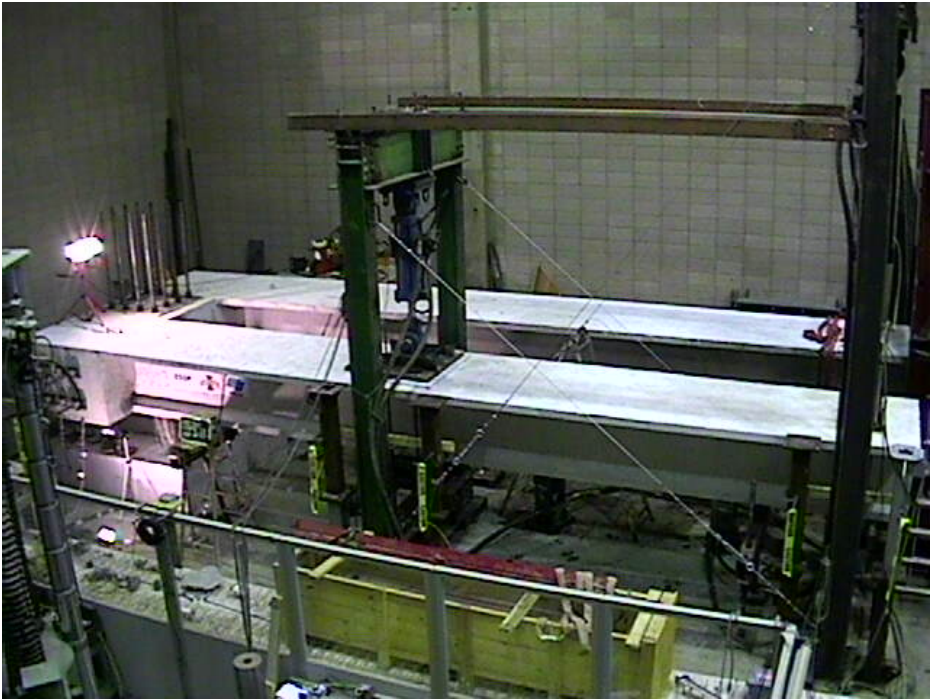


Figure 4.38: Test setup

Table 4.5: Post-tensioning sequence

| Step | Post-tensioning force (kips) |
|------|------------------------------|
| 1 | 25 |
| 2 | 75 |
| 3 | 120 |
| 4 | 200 |

4.6.2 ESBF Connection

4.6.2.1 Overall Performance

The ESBF connection was loaded following the previously outlined loading protocol. Damage was limited to small cracks on the deck for load steps up to the gravity (G) + horizontal seismic load (H). The girder was then loaded to (G)+(H)+0.5g vertical acceleration (0.5gV). Girder cracking began to occur near the connection region due to application of negative moment at the load G+H+0.1gV. At G+H+0.5gV multiple cracks were present in the deck and girder as shown in Figure 4.39. Under positive moment, a 1/16 in. gap opened between the bottom of the girder and the cap beam at G+H+0.5gV. There was also a small amount of cracking on the side of the cap beam near the girder interface as shown in Figure 4.40. After reaching 0.5gV, the cap was post-tensioned to provide higher torsional capacity before increasing the loads to G+H+1.0gV. More damage occurred in the connection region as loading increased above 0.5gV. Under negative moment cracking continued to increase on the bridge deck and girder. The gap between the girder and cap beam due to positive moment widened throughout the loading cycle reaching a maximum opening of 3/32 in at G+H+1.0gV.



Figure 4.39: Girder cracking due to negative moment



Figure 4.40: Cracking on side of cap next to girder interface

After the load of $G+G+1.0gV$ was reached, the test unit actuators were placed in displacement control since the connection was beginning to exhibit inelastic behavior. Controlling the actuators by displacement allowed the capacity of the connection to be fully quantified. The connection was cycled through a series of load steps for the displacement cycle as outlined in the loading protocol (Figure 4.37). Positive values of displacement corresponded to downward movement of the girder and negative moments while negative values of displacement corresponded to upward movement of the girder and positive moments. The blue actuator was held at a constant force value in each loading direction in order to apply a consistent shear at the connection interface. For the displacement cycles, the values of girder displacement measured at the black actuator location began at +2 in./-1 in. and were gradually increased until the ultimate displacements of +15 in./-7.5 in. were reached. As the displacement cycles were increased, cracking continued in the deck and girder due to negative moments. The girder also began to pull away from the deck as damage to the cap beam increased. A large amount of cap cover concrete began to spall due to the rotation of the dowel bars under positive and negative moments as shown in Figure 4.41. Concrete also began to spall at the bottom of the girder to cap connection as shown in Figure 4.41. Under positive moment the gap between the girder and cap widened and exposed the extended strands (Figure 4.41). During the displacement cycles the DCDT's at the column to cap connection were monitored to prevent decompression of the column post-tensioning bars. No movement was observed at the column to cap interface.

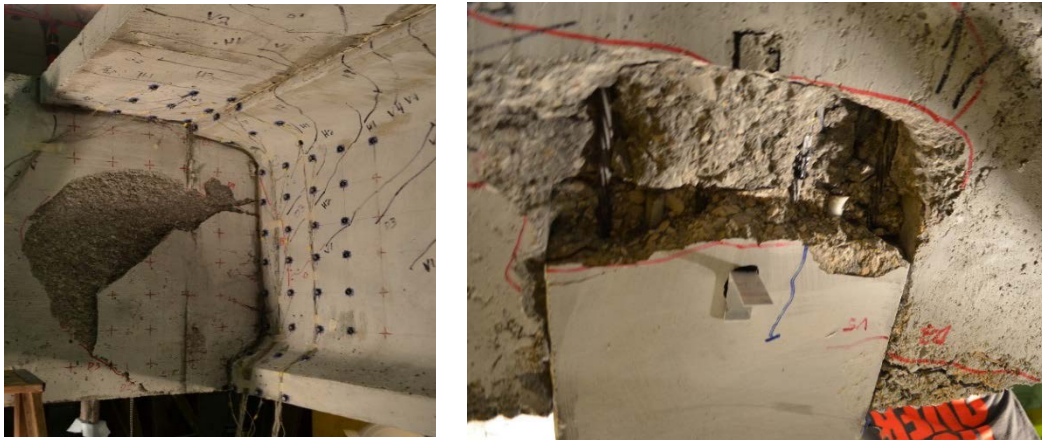


Figure 4.41: Spalling of cap and girder cover concrete

4.6.2.2 Failure Mechanism

During the displacement cycles one of the extended strands fractured which decreased the positive moment capacity of the connection. At the ultimate displacement of +15 in./-7.5 in. two more of the extended strands fractured as shown in Figure 4.42. After strand fracture, the positive moment capacity of the connection greatly decreased and testing of the connection was ended. The final condition of the connection is shown in Figure 4.43.

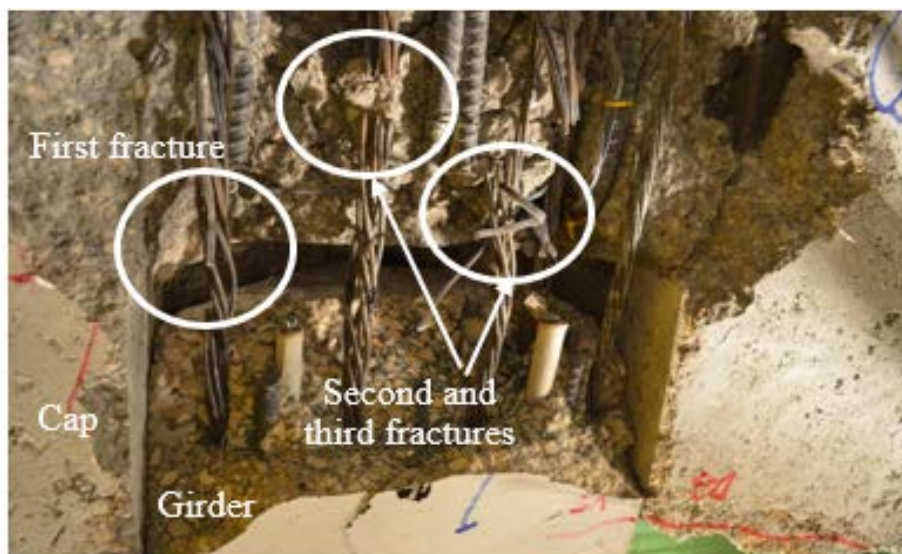


Figure 4.42: Fracture of extended strands



Figure 4.43: Final condition of connection region

4.6.2.3 Connection Interface Performance

The ESBF connection remained elastic for positive and negative moments up to values equivalent to the combined loads of gravity, horizontal seismic corresponding to the column overstrength moment, and vertical acceleration of 0.71g. The connection reached a maximum positive moment of 416 k-ft and a maximum negative moment of -1032 k-ft. The overall moment versus displacement response of the connection is shown in Figure 4.44.

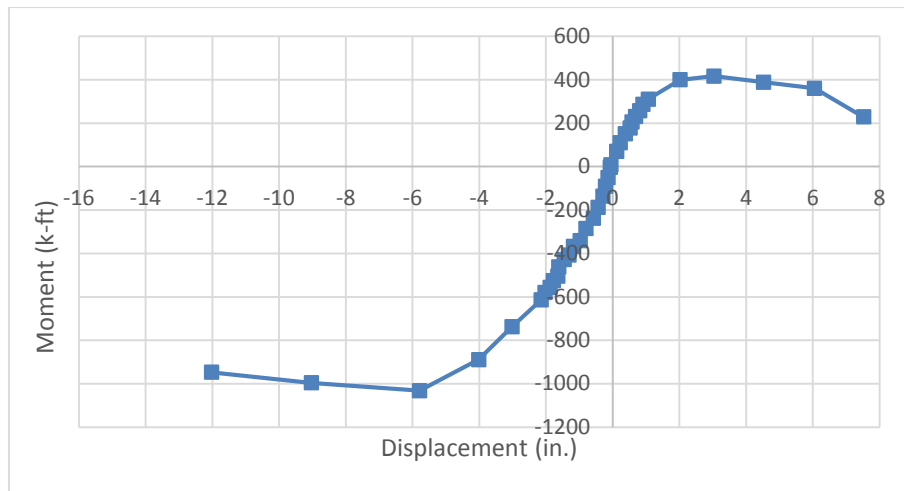


Figure 4.44: Moment vs. black actuator displacement of ESBF connection

The ultimate capacity of the connection in the negative direction was less than originally expected. The yield moment for the deck steel was originally calculated to be -940 k-ft, however, the yield moment of the test was around -615 k-ft. The predicted yield moment of -940 k-ft assumed that all the deck steel yielded simultaneously. The strains recorded in the deck steel during the test indicated that the rebar in the center of the deck reached yield sooner than rebar closer to the edge of the deck as shown in Figure 4.45 where zero position represents the center of the deck. The rebar in the middle of the deck began to exhibit inelastic behavior before yielding of the outer deck steel which caused the connection to behave in an inelastic manner at a lower than predicted moment value of -615 k-ft.

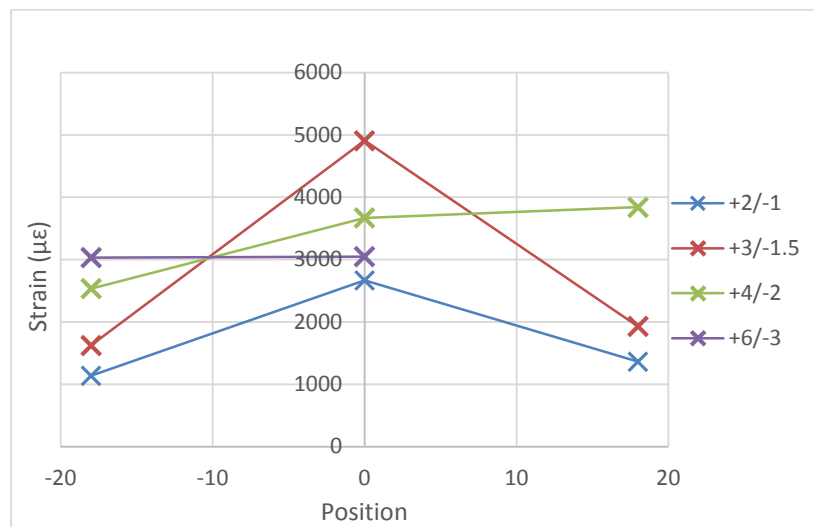


Figure 4.45: Strain profile of deck steel

The connection did continue to gain a considerable amount of strength after the initial yield moment of -615 k-ft and reached the ultimate moment capacity of -1032 k-ft. It is possible that the moment capacity of the connection would have continued to increase beyond -1032 k-ft but was prevented due to the damage at the connection interface. Spalling at the bottom of the girder and cap connection (Figure 4.41) reduced the compressive area and negative moment lever arm at the connection region. The spalling of cover concrete adjacent to the girder interface caused vertical separation between the girder and the deck. The vertical separation prevented the girder and deck from behaving as a fully composite section and this combined with the reduced compressive area of the section to cause a drop in negative moment resistance.

4.6.2.4 Unstressed Strand and Dowel Bar performance

The response of the extended strands and dowel action was examined to further understand the behavior of the connection during positive moments. The positive yield moment of the connection was defined as the moment at which inelastic behavior began and was found to be 286 k-ft. At this moment value, the strain in the extended strands at the connection interface was 3100 $\mu\epsilon$ and the dowel bar strain was 1800 $\mu\epsilon$ as shown in Figure 4.46. These strain values were then converted to stresses and moment resistance using an equivalent stress block approach. It was found at the yielding of the connection that the moment resistance of the strands was 111 k-ft and the moment resistance due to dowel action was 175 k-ft.

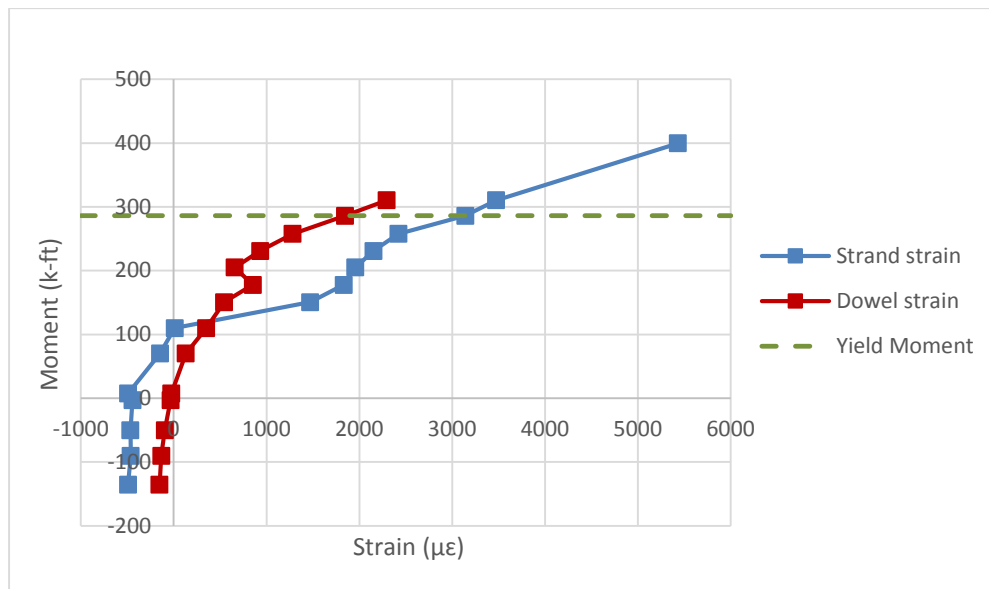


Figure 4.46: Strand and dowel bar strains

Observing the moment resistance provided by each mechanism at the connection yield point, it appears that the concrete friction and dowel bars actively resist the majority of the connection moment (61%). However, Figure 4.46 shows that the extended strands consistently were subject to higher strain values than the dowel bars after the connection moment exceeded 100 k-ft. The dowel action resists a large percentage of the overall moment through friction and concrete adhesion between the end of the girder and the cap beam as well as dowel bar strain. The yield point of the connection is very close to the yield point of the dowel bars. After the connection yields and the connection loads continue to rise, the strain in the strand increases due to the diminishing capacity of the dowel action. To validate this explanation, the calculation process

performed for the yield point was repeated for the moment values listed in Table 4.6. The table shows that concrete friction and dowel action account for an average of 65% of the moment resistance until the dowel bars reach yield stress. Once the dowel bars reach yield, the cover concrete around the dowel bars began to crack and the strain in the strand increased until the ultimate moment value of the connection was reached. Based on strain measured in the extended strands, 70% of the positive moment resistance at the connection was carried by the extended strands at the ultimate load condition.

Table 4.6: Positive moment values of extended strands and dowel action

| Strand Moment (s) (k-ft) | Dowel bar Moment (D) (k-ft) | Concrete Friction Moment (C') (k-ft) | Dowel Action (D+C) (k-ft) | Connection Moment (k-ft) (S+D+C) | Dowel Action Moment Percentage D/(D+C') |
|-----------------------------------|--------------------------------------|---|------------------------------------|--|--|
| 52.1 | 18.3 | 80.4 | 98.6 | 150.8 | 65% |
| 64.9 | 28.7 | 84.1 | 112.8 | 177.7 | 63% |
| 69.3 | 22.1 | 113.6 | 135.7 | 205.1 | 66% |
| 76.3 | 31.3 | 123.3 | 154.6 | 230.8 | 67% |
| 85.8 | 43.1 | 128.9 | 172.0 | 257.7 | 67% |
| 111.3 | 62.1 | 112.8 | 175.0 | 286.3 | 61% |
| 123.1 | 77.2 | 110.11 | 187.3 | 310.4 | 60% |
| 192.4 | 75.0 | 132.3 | 207.3 | 399.8 | 52% |
| 292.4 | 128.6 | -4.11 | 124.53 | 416.9 | 30% |

The ESBF connection reached ultimate condition in the positive direction with a displacement at the black actuator of -3 inches. The girder was then cycled through displacement of -4.5, 6, and -7.5 inches. The strand strain continued to increase and the concrete adjacent to the girders began to spall. At each displacement cycle beyond -3 in. the positive moment capacity of the girder decreased as shown in Figure 4.47. The decrease in moment at the displacement of -4.5 in. occurred due to cracking of the concrete adjacent to the girder around the lower dowel bar as well as the partial fracture of one of the extended strands. At -6 in. of displacement the moment loss was due to the continued loss of concrete adjacent to the girder which caused the moment capacity of the dowel bars and concrete friction to decrease. At a displacement of -7.5 inches a large drop in capacity was caused by the fracture of a second and third strands.

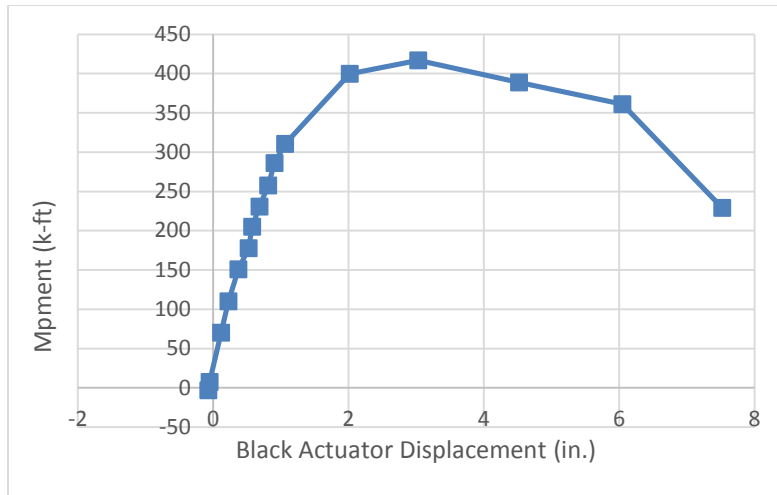


Figure 4.47: Moment decrease in ESBF connection

As noted previously, a large amount of spalling of cap cover concrete occurred adjacent to the girder during positive moment cycles and contributed to a decrease of positive moment capacity at the connection. Stirrups in the cap beam were placed adjacent to the top flange of the girder; however, no stirrups were placed under the top flange as shown in Figure 4.48. Lack of stirrups under the top flange resulted in a six inch gap of unreinforced cover concrete adjacent to the girder web. The dowel bars were located in this region of cover concrete. Movement of the girder and subsequent displacement of the dowel bars caused cracking in the unreinforced region which led to spalling of the cover concrete as shown in Figure 4.43. This problem could be avoided in the field or in future tests by ensuring that the cap stirrups extend all the way under the top flange of the girder and are also adjacent to the girder web as indicated in Figure 4.48.

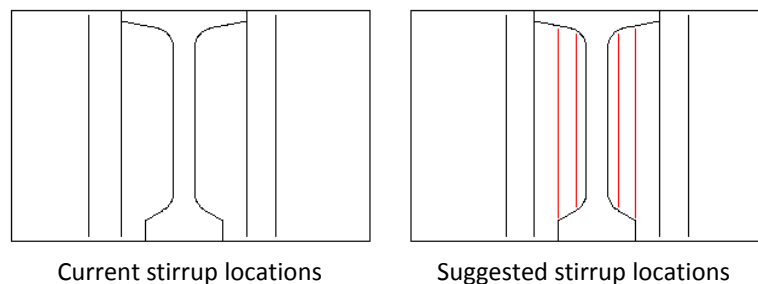


Figure 4.48: Cap stirrup locations

The strain in the extended strands was examined to better understand the transfer of strain along the length of the strand. Strain gages were located at the connection interface, 15 in. from the interface, and 45 in. from the interface. Table 4.7 shows the strain values for each gage along

with the corresponding applied moment. Strain values in the table that are listed as 99999 indicate that the gage was no longer reading values due to overly high strand strains or damage to the gage. The table shows that strain was transferred to the 15 in. gage at relatively low moment values but the 45 in. gage did not experience noticeable strains until the strand approached fracture. The fracture of the strand shows that the development length of 60 in. was sufficient to anchor the 3/8"-diameter strand, and the data in Table 4.7 indicates that an anchorage length of at least 45 in. is needed to prevent slipping of the strand.

Table 4.7: Transfer of strain in extended strands

| Strains ($\mu\epsilon$) | | | Connection Moment (k- ft) |
|---------------------------|--------|--------|---------------------------------|
| Interface | 15 in. | 45 in. | |
| -147 | -66 | 2 | 70.2 |
| 11 | -35 | 2 | 110.1 |
| 1471 | -7 | 3 | 150.8 |
| 1831 | 525 | 5 | 177.7 |
| 1957 | 720 | 22 | 205.1 |
| 2152 | 1123 | 22 | 230.8 |
| 2420 | 1628 | 22 | 257.7 |
| 3141 | 2164 | 22 | 286.3 |
| 2256 | 2873 | 23 | 310.4 |
| 5431 | 5285 | 33 | 399.8 |
| 99999 | 8251 | 198 | 416.9 |
| 99999 | 3900 | 1662 | 388.9 |
| 99999 | 99999 | 99999 | 360.9 |
| Fracture of Strand | | | 229.0 |

4.6.3 ESSP Connection

4.6.3.1 Overall Performance

The ESSP connection was tested in a similar manner to the ESBF connection. To begin the test, the actuators were placed in force control and a gravity load was applied. However, as the first load steps were applied a large amount of cracks began to appear on the deck and girder. The load was slightly increased and even more cracks appear as shown in Figure 4.49. At this point,

the testing was stopped due to the concern that too large of forces were being input into the connection since little to no cracking should have occurred at such a low load level.

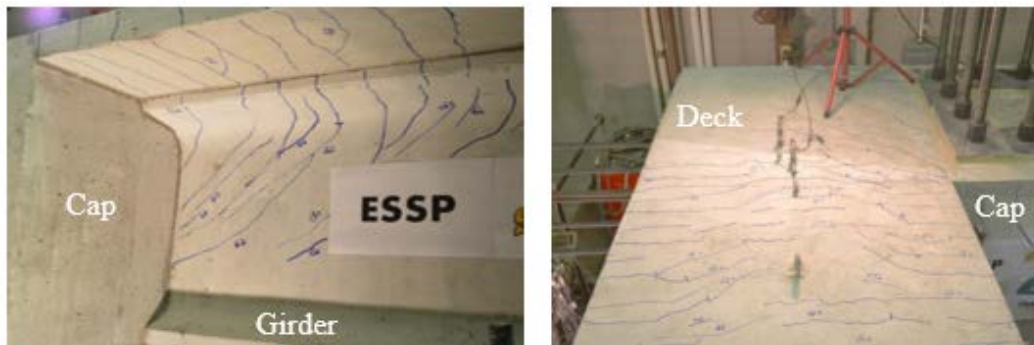


Figure 4.49: Cracking caused by overloading

After checking the loading and test equipment, it was found that the loading pin on the blue actuator was rotated and caused the blue actuator to apply incorrect forces and overload the connection. The overloading was high enough to cause permanent deformation of the test unit including yielding of a small amount of deck steel as well as a displacement near the end of the girder close to 1.0 inch. The extent of the connection damage was not immediately clear but preliminary estimates showed that a 600-700 k-ft negative moment was applied to the connection instead of the gravity moment of -152 k-ft. The loading pin was corrected and the testing resumed. Further details regarding the effects of the overloading will be discussed with the results of the test. When testing resumed, the connection was subject to gravity (G) loads and then gradually increased up to G + horizontal seismic (H). No new cracks were observed in the negative moment direction since the overloading moment exceeded the gravity plus horizontal seismic moment. The connection did not show any cracking in the positive moment direction. The connection moments were then stepped from G+H, to G+H+0.5g vertical acceleration (0.5gV). For negative moments some new girder and deck cracks appeared at 0.5gV. In the positive moment direction a gap started to open between the end of the girder and the cap beam. At 0.5gV the crack was 1/16" wide as shown in Figure 4.50. In both the positive and negative moment directions the behavior of the connection remained elastic.

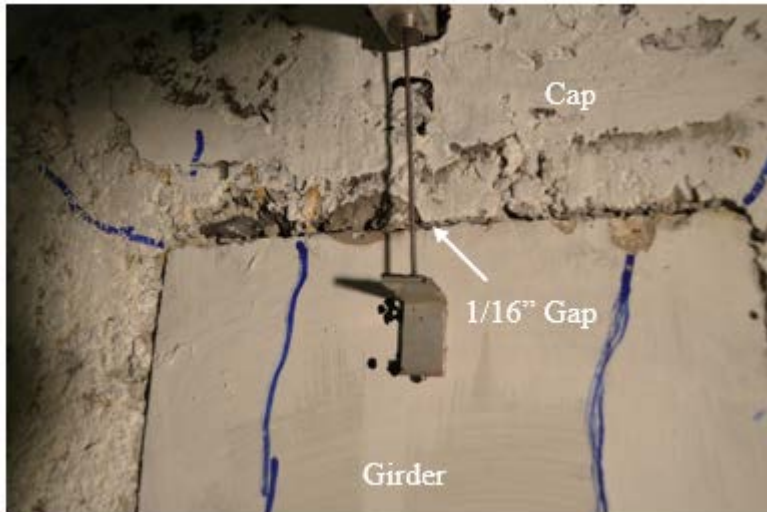


Figure 4.50: Girder to cap gap opening

After reaching 0.5gV, testing stopped temporarily and the cap was post-tensioned to provide adequate torsional capacity for higher moments. Testing continued and the connection was subject to increasing moments up to G+H+1.0g vertical acceleration (1.0gV). As the magnitude of the moments increased in the negative direction, deck cracking continued to increase and extend farther from the connection region. The connection still behaved elastically in this direction without showing any signs of strength loss. In the positive moment direction the gap between the girder and cap continued to increase. At the load step of G+H+0.9g vertical acceleration, the gap between the girder and the cap increased to 5/16 in. and the connection began to soften. Due to the softening, the actuators were switched to displacement control. The ESSP connection was then loaded according to the displacement loading protocol outlined for the ESBF connection.

4.6.3.2 Failure Mechanism

As the displacement cycles progressed, the positive moment caused cracking at the bottom of the girder near the connection region. The cap cover concrete around the girder also continued to spall. The LEDs from the NDI system that were positioned on cap were removed to prevent damage due to spalling. The bottom of the girder began to spall near the connection region, along with the bottom of the cap, which caused a loss of compression area for the girder under negative moment and resulted in the mushrooming of the extended strands as shown in Figure 4.51. The loss of compression area also caused the negative moment capacity to decrease as the lever arm was shortened.



Figure 4.51: Mushrooming of extended strands in ESSP connection

In the positive moment direction one extended strand snapped causing a decrease in moment capacity but the other four strands remained intact. In the last three displacement steps, large amounts of spalling occurred in the cover concrete at the girder interface which fully exposed the dowel bars. The moment capacity in the negative direction continued to decrease and separation between the girder and deck was also observed. The girder was able to reach a final displacement step of +15 in./-7.5 in. but the strength of the connection had already considerably decreased in both the positive and negative moment directions.

4.6.3.3 Connection Interface Performance

The connection remained elastic up to a positive moment capacity corresponding to 0.53g of vertical acceleration and a negative moment capacity corresponding to 0.71g. The maximum capacity of the connection was 286 k-ft in the positive moment direction and -936 k-ft in the negative moment direction. The connection did rotate more than the ESBF connection as a result of softening due to the initial overloading of the connection. The overall behavior of both connections is shown in Figure 4.52.

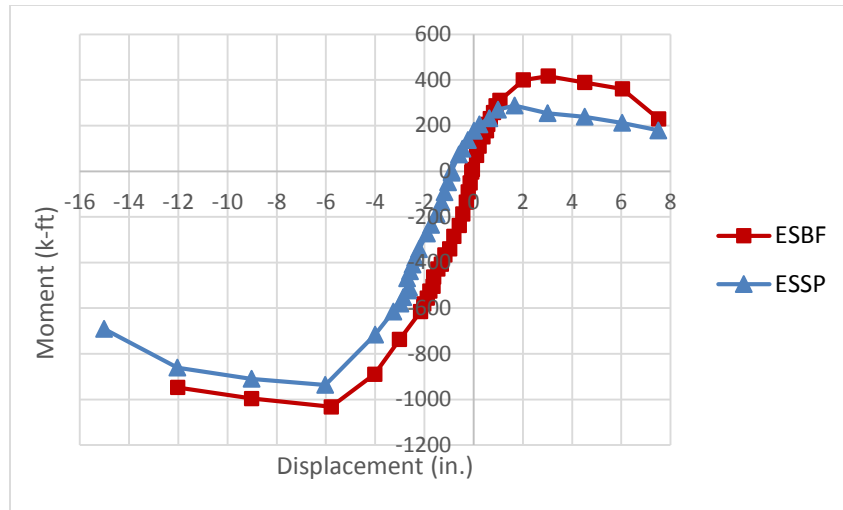


Figure 4.52: Moment vs. black actuator displacement for comparison of ESSP and ESBF connections

The negative moment response of the ESSP connection was very similar to the ESBF connection. The overloading at the beginning of the test resulted in yielding of some of the deck reinforcement and residual strains ranging from 300-900 $\mu\epsilon$ which resulted in a lower overall moment capacity. The connection negative yield moment of -615 k-ft was the same as the ESBF connection but occurred at a larger vertical displacement due to the overloading. The maximum negative moment capacity of the ESSP connection was -936 k-ft.

4.6.3.4 Unstressed Strand and Dowel Bar performance

The positive moment behavior of ESSP connection was very similar to the ESBF connection except for smaller moment capacity at yield and ultimate. The difference in moment between the two connections is most likely due to the overloading of the ESSP connection. Strain data from the ESSP test shows that the overloading caused a permanent downward deflection of the girder. As a result, when testing resumed following the overloading, a strain was present in the dowel bars of approximately 500-600 $\mu\epsilon$. This caused a slight softening of the connection as well as lower overall moment capacity. The lower dowel bar capacity resulted in the bars reaching yield strain at a lower moment value. Similar to the ESBF connection, when the dowel bars reach yield strain, the concrete surrounding the dowel bars began to crack which resulted in a loss of dowel action and an increase in strand strain. The connection behaved similar to the ESBF and as the moment increased, the loss of dowel bar strength continued, and the concrete began to spall which led to the crushing of the girder concrete in the positive moment compression region (Figure 4.53).

Crushing of the girder concrete prevented the strands from being exercised to full capacity and resulted in a lower ultimate positive moment than the ESBF connection.

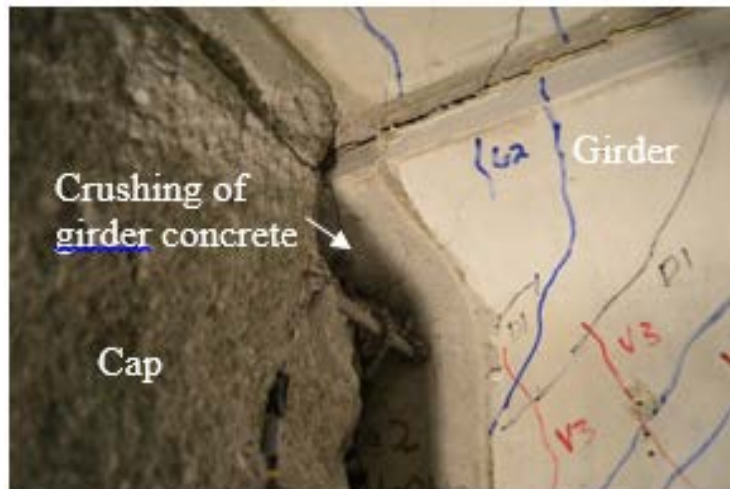


Figure 4.53: Crushing of girder concrete

Even though the ultimate moment capacity of the strands was not developed, strain values of the extended strands and strand ties were compared to validate the transfer of force between the two strand members. It was found that the strand ties did not experience strain values comparable to the extended strands. In fact, the strain values in the strand ties remained constant throughout the test at values ranging from approximately 10-50 $\mu\epsilon$. It is possible that the strain transferred to the cap reinforcement or that the plate and chuck attached to the extended strand was sufficient for anchorage.

Chapter 5. ESMS and ESLS Cap Beam Connections for Bulb Tee Girders

5.1 Prototype Design

The prototype bridge that was used for the ESBF and ESSP connection tests was also used to develop two additional girder-to-cap connections. Use of the same prototype was appropriate since bulb-tee girders were again selected for this portion of the investigation.

5.1.1 Connection Design

5.1.1.1 ESMS Connection

The ESMS (Extended Strand with a Mechanical Splice) connection was designed and tested as the third bulb-tee girder-to-cap connection. The ESMS connection was designed to be an integral connection providing continuity under negative and positive moments between the precast bulb-tee girders and the bridge bent cap. The main differences between the second test unit and this test unit were the connection details and the number of strands extended from the girder to the bent cap. The number of strands was reduced in order to optimize the strand design for the demand expected in the connection. As shown in Figure 5.1, the deck reinforcement was provided over the bent cap and girder connection region as continuous reinforcement for negative moment tension continuity, similar to the previously-tested details. Unstressed strands were extended from the precast girder and spliced with strands extended from the opposite girder using splice chucks. A mechanical device was selected to splice the strands to ensure full strength development of strands and to reduce congestion in the connection region, which was compact in size.

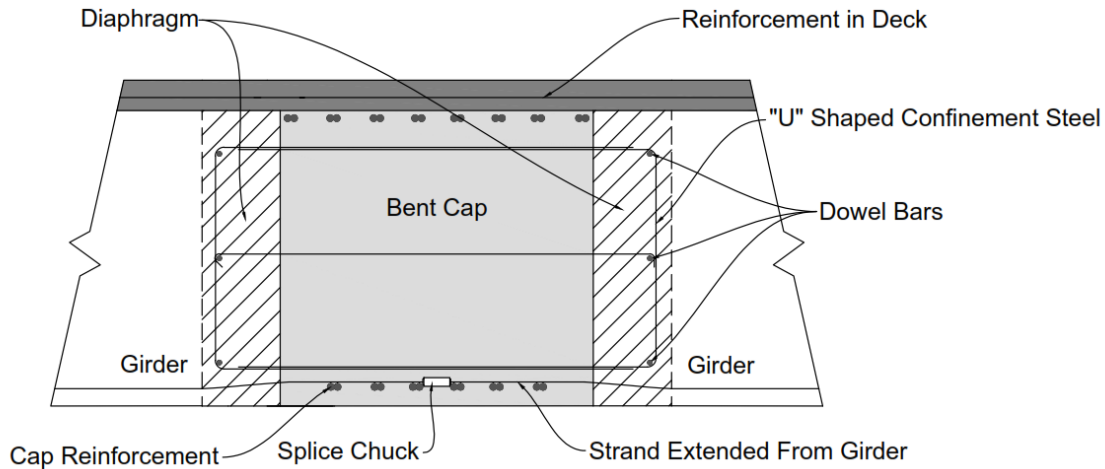


Figure 5.1: ESMS connection schematic

5.1.1.2 ESLS Connection

The last girder to bent cap connection was the ESLS (Extended Strand with a Lap Splice) connection as shown in Figure 5.2. The ESLS connection was also designed to provide continuity such that the precast girder and cast-in-place bent cap formed an integral superstructure. The reinforcement in the deck, which provided negative moment tension continuity, was placed in the same configuration as in the ESMS connection. Unstressed strands extended from the bulb-tee girder were anchored with strand chucks which included bearing plates, barrel anchors, and wedges. The extended strands with strand chucks were then lap spliced with strands extended from the opposite girder. The expected anchorage mechanism for the strands extended from the girder is shown in Figure 5.3. The tension in the strands is resisted by the bearing plate anchorage and the bond stress along strands. In addition, the tension from the girder strands is transferred to the strands extended from opposite girders by struts along the lap splice length.

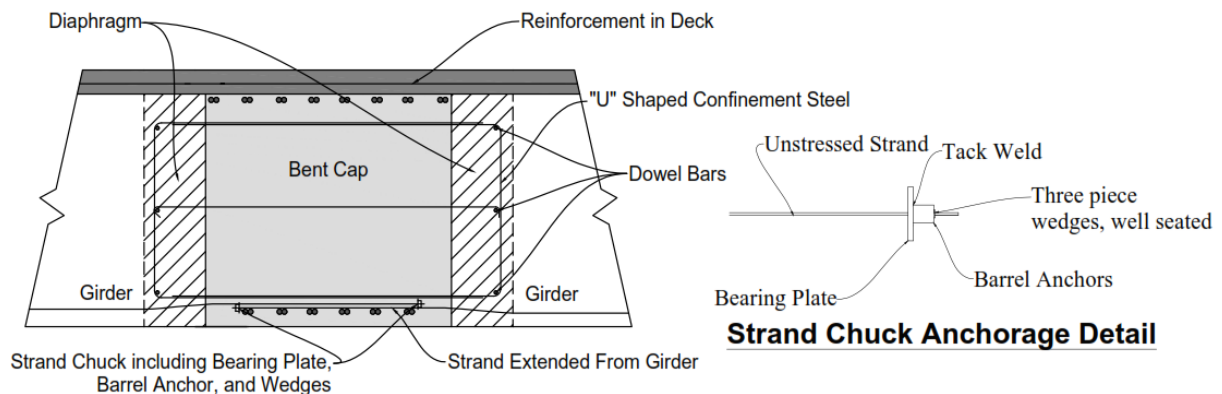


Figure 5.2: ESLS connection schematic

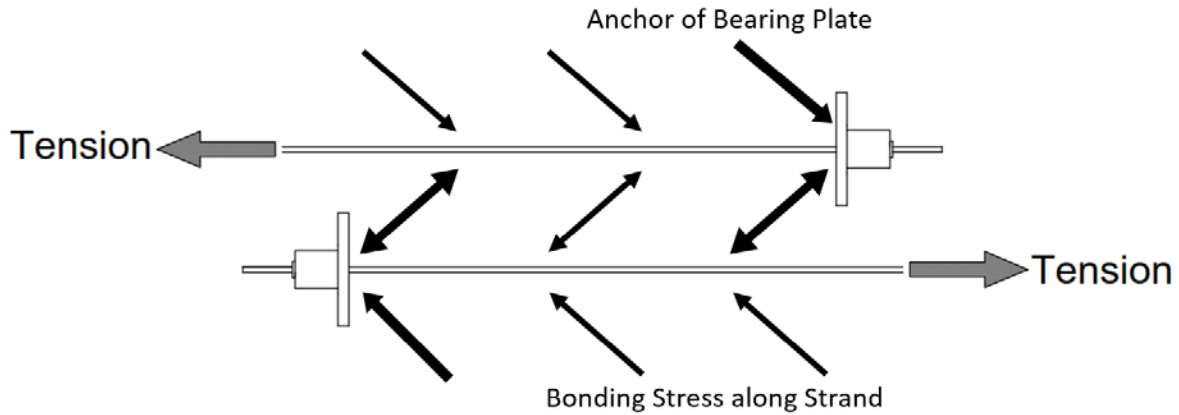


Figure 5.3: Expected anchorage mechanism for strands in the ESLS connection

5.2 ESMS/ESLS Test Unit Design

Following the completion of the second test with the ESBF and ESSP connections the third test unit was constructed with the ESMS and ESLS connections. Based on a comparison with the details used in the ESBF/ESSP test unit, three modifications were made to the ESMS/ESLS test unit. First, only four strands were extended into the cap from the girder as opposed five used in the connection tests with the second unit. The reduction to four strands was based on an effort to optimize the connection reinforcement needed for the target load of $G+H+0.5gV$. This change also recognized the contribution of the dowel action provided in positive moment resistance in the ESMS and ESLS connections. The second modification was the addition of “U” shaped confinement steel in the cap beam next to the sides of the girder as shown in Figure 5.4. The confinement steel replaced the dowel bar crossties used in the ESBF and ESSP connections and provided additional confinement for the concrete surrounding the dowel bars at the girder to cap interface. Finally, BASF M100 micro fiber added at 0.5 lbs. per cubic yard and BASF MAC MATRIX macro fibers added at 3.0 lbs. per cubic yard were added to the concrete mix design for the bent cap, diaphragm, and deck to prevent cracking and spalling from the deck and girder-bent cap interface region observed in the ESBF/ESSP test unit.

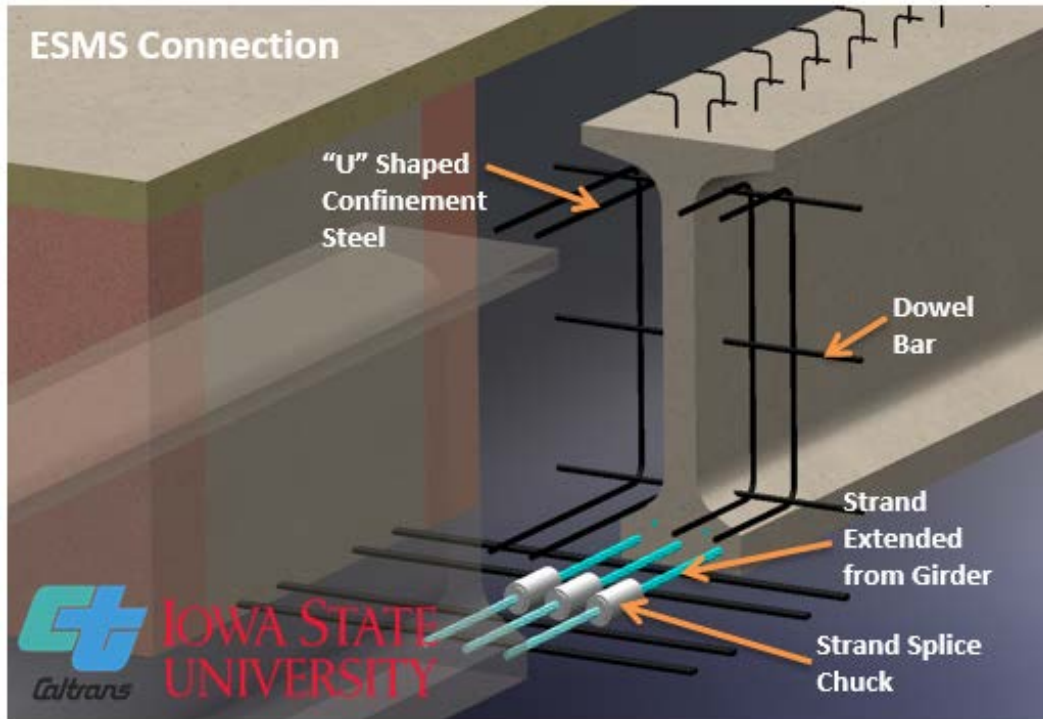


Figure 5.4: Addition of “U”-shaped confinement steel

5.3 ESMS/ESLS Test Unit Construction

5.3.1 Construction Sequence

Construction of the ESMS/ESLS test unit took place in the structural laboratory of Iowa State University. The footing and column were reused from the second test unit. The falsework was placed surrounding the column to support the bent cap throughout the construction process. Two bulb-tee girders cast at Cretex Concrete Products in Iowa Falls, IA were then placed on bent cap falsework and temporary support throughout the construction of the test unit, as shown in Figure 5.5.



Figure 5.5: Place the girder on temporary falsework

The girders arrived at the ISU laboratory with six of the ten girder strands extending 8 ft from each girder. Since only four strands were required to extend into the cap, the strands in the upper row were cut. Before the fabrication of bent cap, the dowel bars were inserted through the web of the girders, and grouted in place as shown in Figure 5.6. The reinforcement cage for the bent cap and diaphragm was tied on the falsework and the unstressed strands were spliced according to each connection details. Mechanical splices with strand chucks were used within the ESMS connection to splice the strands extending from girder with the strands added on the back of the bent cap. The strands on the back of the cap represented the strands that would come from an opposite girder in the prototype structure, as shown in Figure 5.7a. For the ESLS connection, the strands extending from the girder with plates and strand chucks were lap spliced with other strands that also included plates and strand chucks, as shown in Figure 5.7. Again, these additional anchored strands represented the strands that would come from the opposite girders in the prototype structure. The mechanical splice chucks and strand chucks from opposing sides of the cap were staggered in order to avoid congestion within the connection region.

In addition to the girder strands, the ducts for longitudinal cap post-tensioning were also inserted through the bent cap. Similar to the previous test units, the deck formwork was constructed

with bridge hangers, brackets, and plywood, and the deck reinforcement was placed over the girder and formwork, as shown in Figure 5.8. The formwork for the bent cap was then fabricated and set into place. The bent cap and girder concrete with both synthetic micro and macro fibers was then placed in one continuous pour and allowed to cure. The finished test unit is shown in Figure 5.9.



Figure 5.6: Dowel bars inserted through the web of girder



(a) Spliced strands in ESMS detail



(b) Anchored strand lap splices in ESLS detail

Figure 5.7: Spliced strands extended from girders within the ESMS and ESLS connections



Figure 5.8: Reinforcement cage for bent cap and deck reinforcement



Figure 5.9: Third test unit with the ESMS and ESLS connections

5.3.2 Construction Challenges

5.3.2.1 Unraveling of Unstressed Strand

When the precast bulb-tee girders were being fabricated, the sudden release of the prestressing force during the transfer caused a small portion of the strands to unravel, as shown in Figure 5.10. Strain gages were mounted on the unraveled portion of the strand to capture the behavior when the strands were stressed. The effect of unraveling was investigated and is discussed in following section.

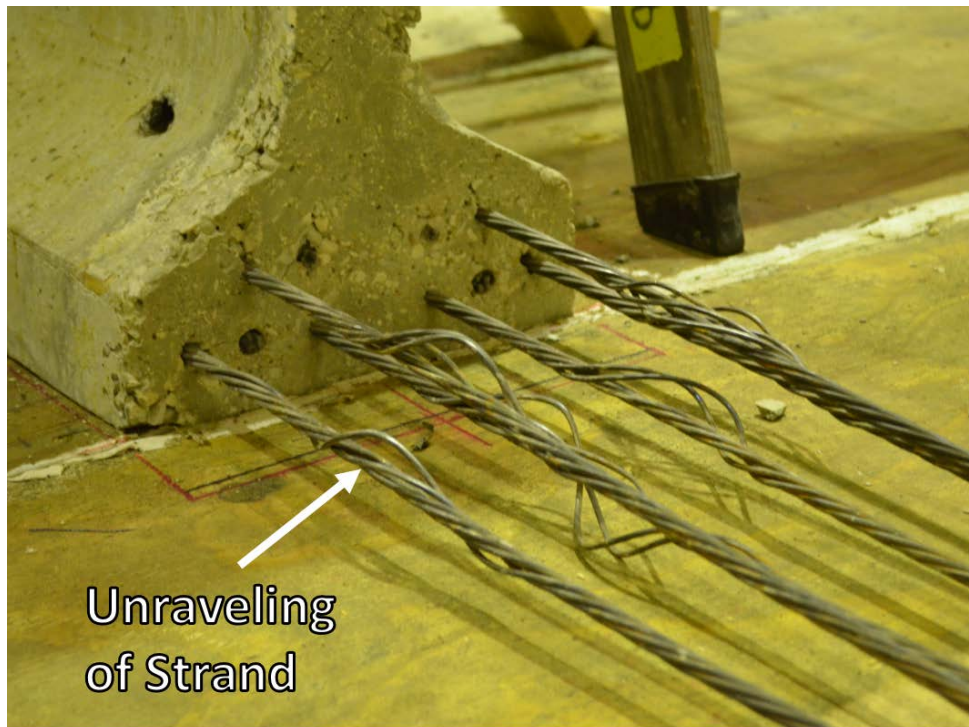


Figure 5.10: Unraveling of portion of unstressed strands

5.3.2.2 Placement of the Bent Cap Concrete

Before the placement of the bent cap and deck concrete, a trial batch of concrete with BASF M100 micro fiber added at 0.5 lbs. per cubic yard and BASF MAC MATRIX macro fibers added at 3.0 lbs. per cubic yard was mixed to determine the effect of fiber on the flowability of concrete. Results showed that the additional synthetic micro and macro fiber significantly reduced the slump of concrete, producing issues with the consolidation of the concrete. The heavily-reinforced bent cap also added to the difficulty of the concrete placement and increased the likelihood of honeycombing in the concrete. In order to minimize the honeycombing, 1/2 in. or smaller aggregate was used in the mix design. Plasticizer and retarding admixtures were also used to

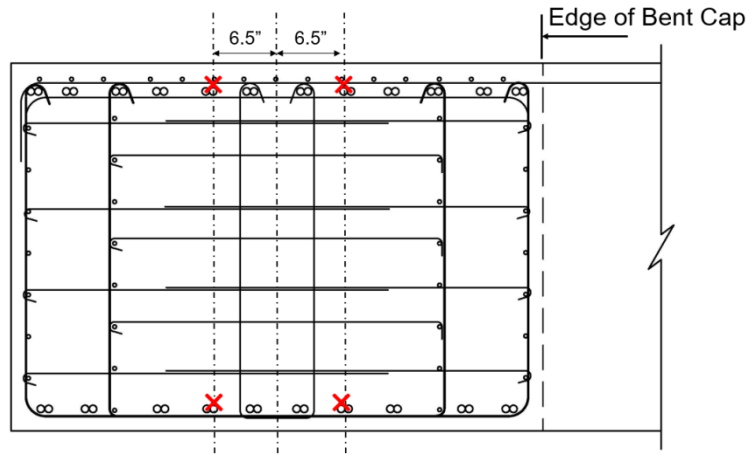
improve the concrete flowability, with the recognition that the compressive strength of concrete can be reduced by the use of admixtures. Strength tests showed that the concrete used in the test unit satisfied the design requirements, despite the use of admixtures.

5.4 Instrumentation

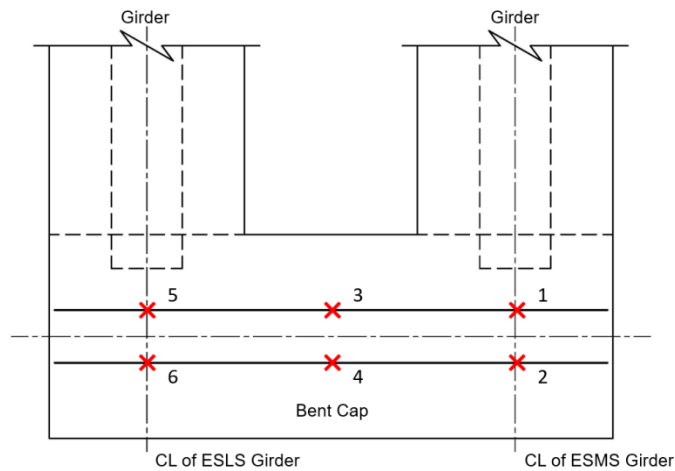
In order to capture the response of specimens during testing, a significant amount of internal and external instrumentation was incorporated in the critical regions of the test unit. Uniaxial steel strain gages were the primary internal sensors, and their locations are given in the following sections. The external instrumentation was the same as that used for the ESBF and ESSP connection tests, and the corresponding details can be found in Section 4.4.3.

5.4.1 Bent Cap

Both top and bottom longitudinal reinforcing bars in the bent cap were instrumented with a total of twelve strain gages. The instrumented reinforcing bars were located at 6.5 in. from the center line of bent cap (Figure 5.11). The strain gages were lined up with the center of bent cap and the center lines of girders as detailed in Figure 5.11. Note that the strain gages were labeled using the following format: BCT(B)# (Bent Cap strain gage at Top/Bottom longitudinal reinforcing bars in Location #). For example, BCTB2 corresponds to bent cap strain gauge at bottom longitudinal reinforcing bar at location 2 noted in Figure 5.11 (b).



(a) Side View

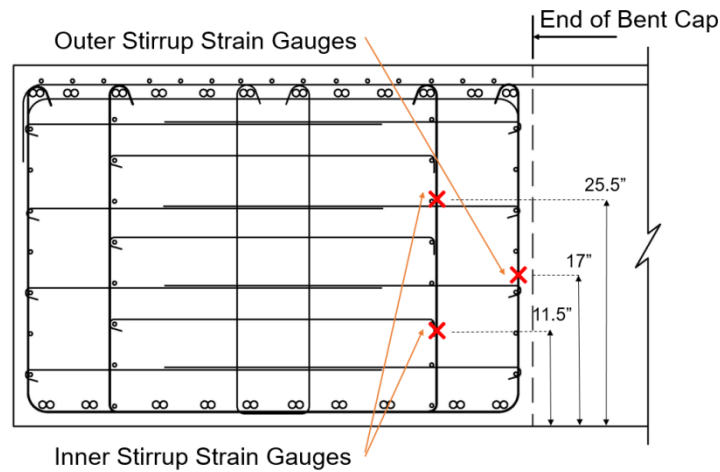


(b) Top View

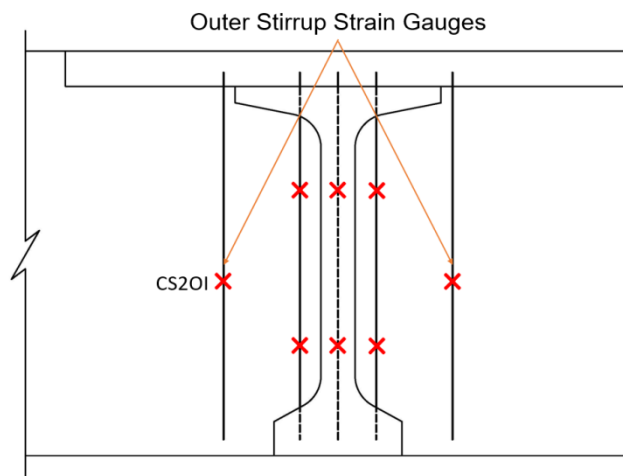
Figure 5.11: Strain gage locations for the bent cap longitudinal reinforcing bars

In addition, both the inner stirrups behind the girder and the outer stirrups next to the girder were instrumented with a total of eight strain gages in each connection. As shown in Figure 5.12, three inner stirrups were instrumented with six strain gages which were located 11.5 in. and 25.5 in. from the base of bent cap. Moreover, two strain gages were mounted on the outer stirrups at locations 17 in. from the base of the cap. For the inner stirrups, the strain gages were labeled as CS#O(C/I)T(B) (Cap Stirrup strain gage for connection 1/2 on Outside/Central/Inside stirrup at Top/Bottom), whereas the strain gages for the outer stirrups were labeled as CS#OO(I) (Cap Stirrup strain gage for connection 1/2 on Outer stirrup at Outside/Inside location). The ESMS connection was referred as Connection 1 and the ESLS connection was referred to as Connection

2. For example, CS2OI corresponded to cap stirrup strain gage for the ESLS connection on outer stirrups at inside location.



(a) Side View



(b) Front View

Figure 5.12: Strain gage location for cap stirrups

5.4.2 Precast Bulb-Tee Girder

As with the ESBF and ESSP connections, one of the ten prestressing strands at the bottom of each precast girder was gaged as identified in Figure 5.13. A total of four strain gauges were placed at 12 in., 24 in., 48 in., and 15 ft from the end of the girder. The strain gauges were installed after the prestressing strands had been tensioned. Consequently, the recorded initial strain readings did not include the initial prestrain and subsequent prestrain losses.

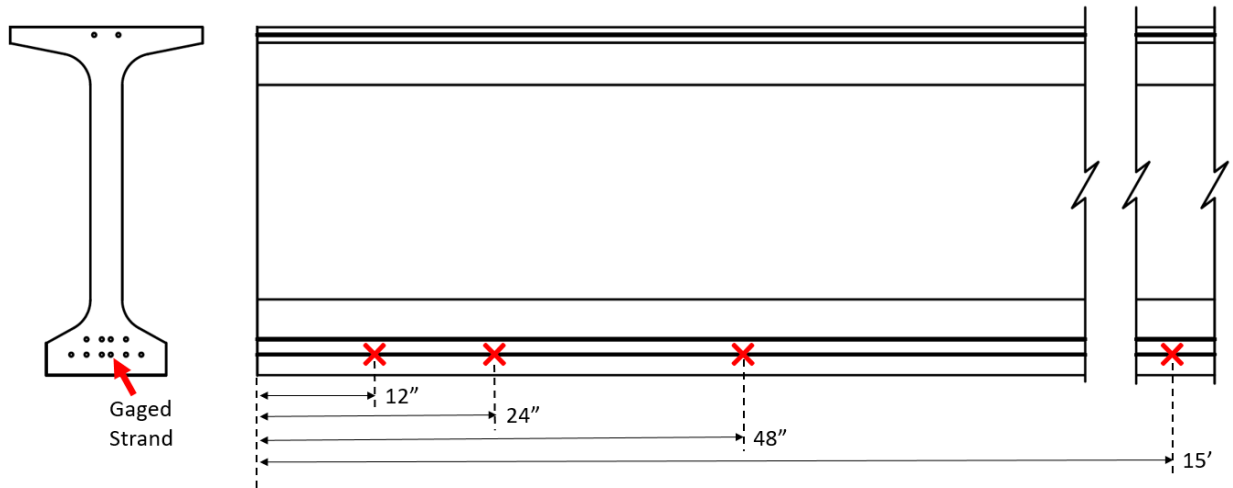


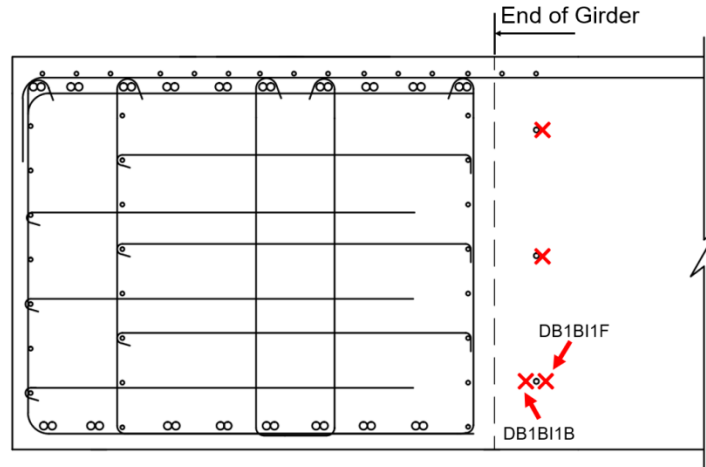
Figure 5.13: Location of strain gages in a prestressed strand of each bulb-tee girder

5.4.3 Precast Bulb-Tee Girder to Bent Cap Connections

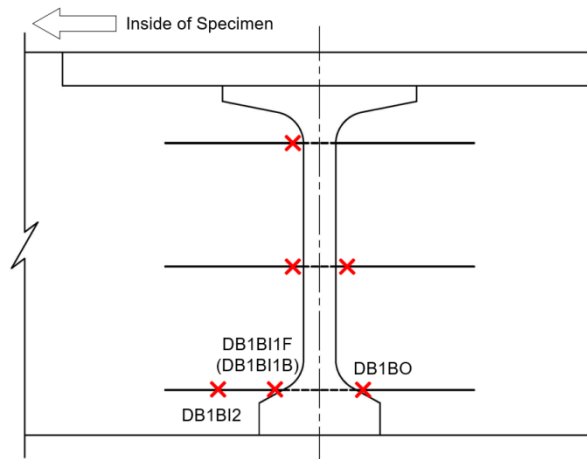
The connections of the precast bulb-tee girders to the bent cap were the most critical regions of the specimens. These regions were instrumented extensively with thirty-four strain gages. The gages were placed on the dowel bars, the “U” shaped confinement steel (dowel confinement), and the strands extended from the girder. The deck reinforcement over the connection region was also instrumented. The following sections describe these gage locations in detail.

5.4.3.1 Dowel Bars

A total of three #4 reinforcing bars with length of 2.5 ft were used as dowel bars through the girders in the third test unit. As shown in Figure 5.14, only one strain gage was placed on the top dowel bar and located 1 in. from the inside face of the precast girder. The middle dowel bar was instrumented with two strain gages on both sides of the precast girder. The bottom dowel bar, being most critical, was instrumented with a total of four strain gages. These gages were placed 1 in. from both inside and outside face of girder, and 6.25 in. from the inside face and were installed on both the front and back of the dowel bar as shown in Figure 5.14b. Similarly, the strain gages on the dowel bars were labeled in a logical format. DB#T(M)I(O) were used to label the strain gages on the top and middle dowel bars (Dowel Bar strain gage for connection 1/2 on Top/Middle dowel bar at Inside/Outside location), and the strain gages on the bottom dowel bar were labeled as shown in Figure 5.14a. For example, DB1MO represented the dowel bar strain gage for the ESMS connection on middle dowel bar at outside location.



(a) Side View



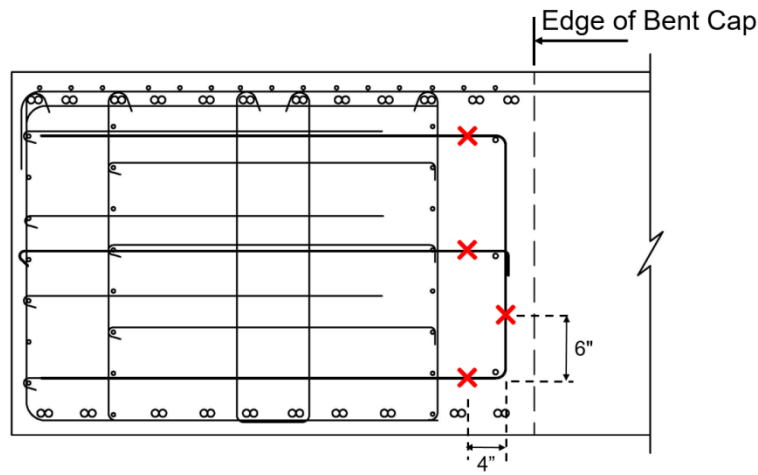
(b) Front View

Figure 5.14: Location of strain gage mounted to the dowel bars

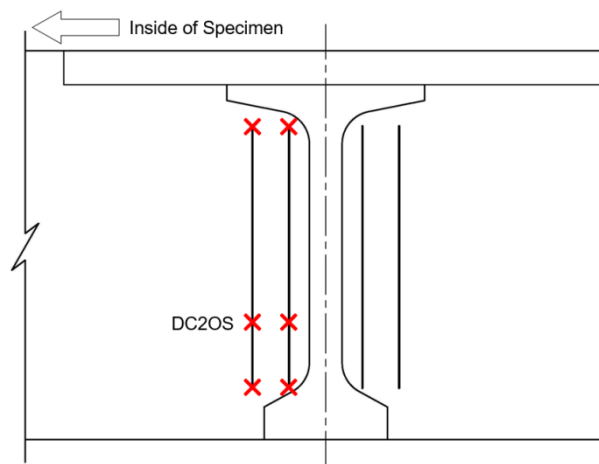
5.4.3.2 "U" Shaped Confinement Steel

As previously noted, "U" shaped confinement steel (dowel confinement) was placed on both sides of the precast girder to reinforce the concrete where the dowel bars were embedded. In order to evaluate the performance of dowel confinement, eight strain gages were installed in the configuration shown in Figure 5.15. The two dowel confinement bars located on the inside of the specimen were also instrumented. For each of them, the strain gages were placed on the horizontal legs of the U-shaped confinement. Additionally, the midpoint between the bottom and middle dowel bar was instrumented with a strain gage. Note that the labels of strain gages were named as DC#I(O)T(M/B/S) (Dowel Confinement strain gage for connection 1/2 on Inner/Outer confinement at the Top/Middle/Bottom/Side location). Accordingly, DC2OS corresponded to the

dowel confinement strain gage for the ESLS connection on the outer confinement at the side location.



(a) Side View



(b) Front View

Figure 5.15: Location of strain gages on the dowel confinement reinforcing bars

5.4.3.3 Strands Extended from Girder

As discussed previously, in the ESMS connection the strands extended from the girder were spliced with the strands on the other side of the bent cap by the splice chucks, whereas for the ESLS connection, the strands were anchored with bearing plates, barrel anchors, and wedges. Several of these strands in both details were instrumented extensively with strain gages as shown in Figure 5.16 and Figure 5.17 for the ESMS connection and the ESLS connection, respectively.

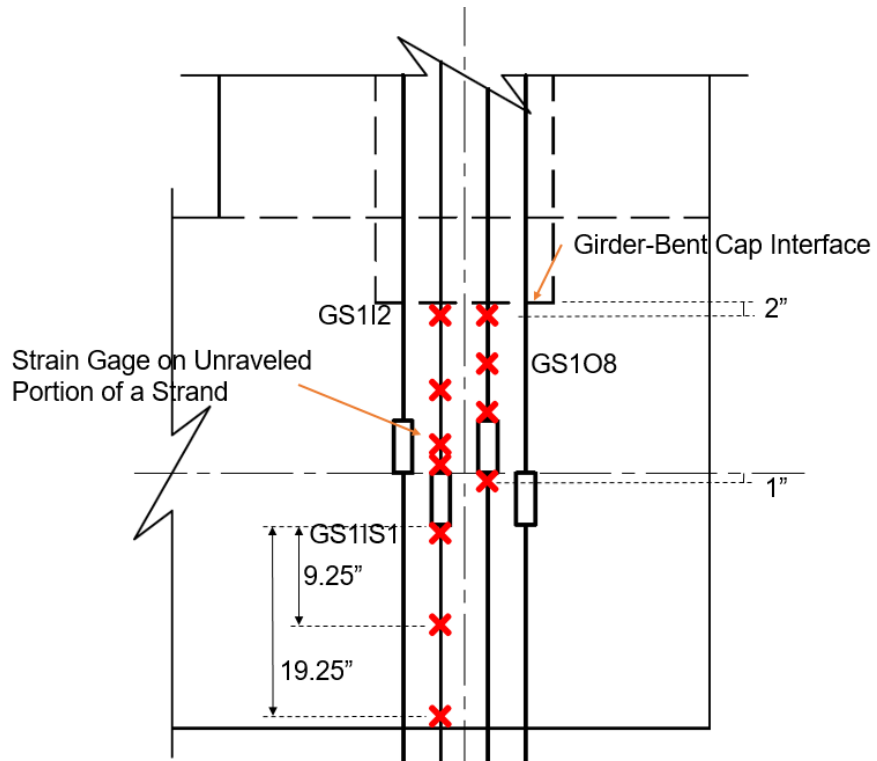


Figure 5.16: Location of strain gages on the strands in the ESMS connection

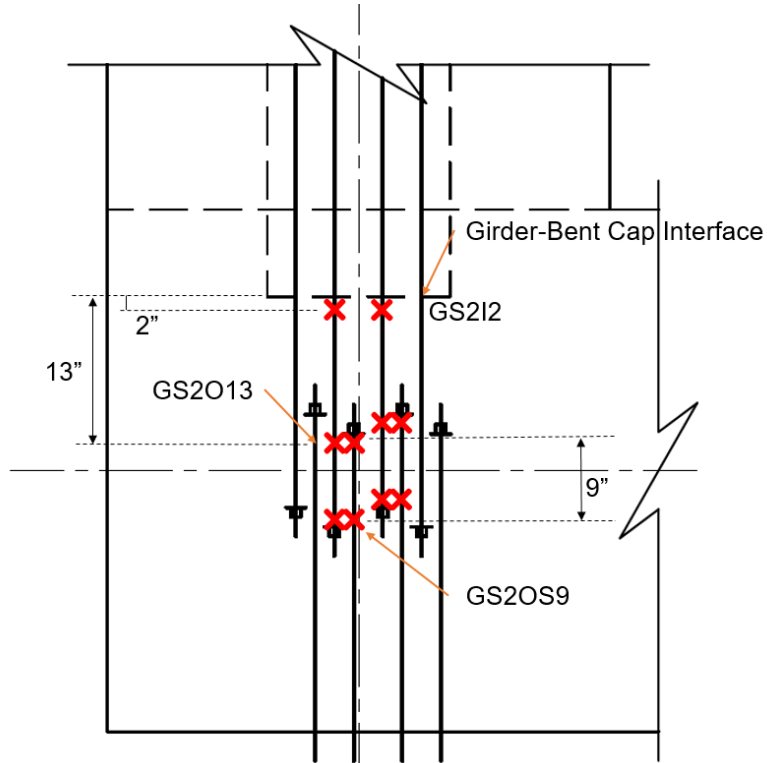


Figure 5.17: Location of strain gages on the strands in the ESLS connection

Two of the four strands extended from the girder were instrumented in the ESMS connection, and the strain gages were placed 2 in. from the girder to cap interface and 1 in. from the ends of splice chuck, and strain gages were also placed at the midpoint between the girder to bent cap interface and splice chuck. Moreover, in order to verify the continuity developed by the spliced strands, two strain gages were installed on the spliced strands at 9.25 in. and 19.25 in. from the end of splice chuck. The unraveled portion of the strand was instrumented with an additional strain gage to investigate the effect of unraveling on the strand behavior as shown in Figure 5.18.

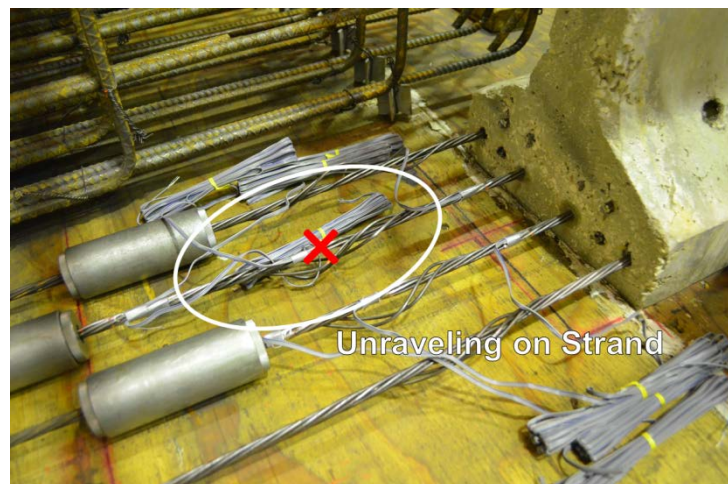


Figure 5.18: Placement of strain gage on unraveled portion of a strand in the ESMS Connection

Two of the four strands extended from girder were also gaged in the ESLS connection. Besides the strain gages located at 2 in. from the girder to cap interface, a total of eight strain gages were placed near the ends of lap spliced region. The strain gages were labeled as GS#I(O)# (Girder Strand strain gage for connection 1/2 on Inside/Outside strand located # in. from the girder to cap interface), or GS#I(O)S# (Girder Strand strain gage for connection 1/2 on Inside/Outside Splicing strand located # in. from the anchorage). For example, GS2O2 corresponded to the girder strand strain gage for the ESLS connection on outside strand located 2 in. from the girder to cap interface.

5.4.3.4 Deck Reinforcement

Similar to the previous connection details, deck reinforcement provided tension continuity for resisting negative moment in the girder-to-cap connection. To monitor this action, a total of nine strain gages were placed as shown in Figure 5.19. The first set of strain gages were lined up

with the girder-to-cap interface, and other two sets of strain gages were placed 18 in. from the first set of gages. The side strain gages were installed on the top longitudinal deck reinforcement at 17 in. in transverse direction from the girder center line. Note that the “center” gages were placed 2 in. from the girder center line. Furthermore, the strain gages were labeled as DR#I(M/O)G(I/C) (Deck Reinforcement strain gage for connection 1/2 on Inside(Middle/Outside) reinforcing bar at Girder side(Interface/Cap beam side). For example, DR1OG identified the deck reinforcement strain gage for the ESMS connection on outside reinforcing bar at girder side.

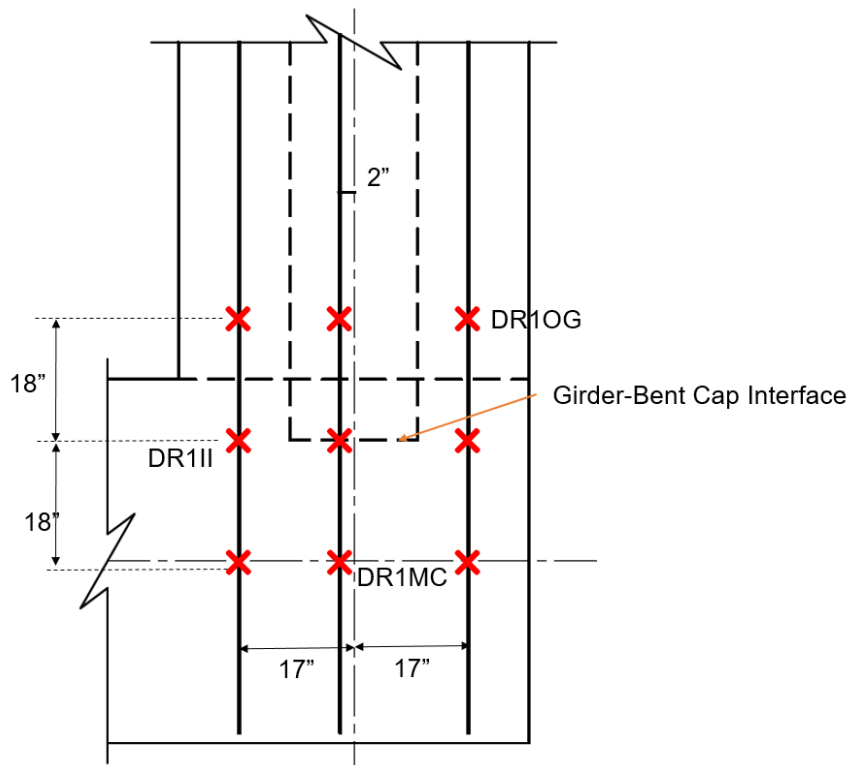


Figure 5.19: Location of strain gages on the deck reinforcement

5.5 Load Protocol

The same loading protocol that was developed for the ESBF/ESSP test unit was incorporated for the ESMS/ESLS test unit. Reusing this protocol was appropriate because both test units were based on the same prototype bridge. The details of this load protocol were presented previously in Section 4.5.

5.6 Experimental Observations and Results

5.6.1 ESMS Connection

5.6.1.1 Overall Performance

Testing of the ESMS connection was conducted from Sep. 25, 2014 to Sep. 26, 2014 in the Iowa State University Structures Laboratory. As with the previous connection tests, the ESMS connection was subjected to combination of gravity, horizontal seismic acceleration, and vertical seismic acceleration. The connection was then subjected to vertical displacement cycles until reaching a failure state. Figure 5.20 shows the connection moment resistance versus vertical displacement measured at the black actuator location 28.5 ft from the girder-to-cap interface. The moment magnitudes corresponding to gravity, horizontal seismic load, and vertical load effects relating to 0.5g, 0.7g, 1.0g, and 1.75g accelerations are also shown in this figure. The connection remained elastic for negative moments up to -914 k-ft, which corresponded to the summation of gravity load, horizontal seismic load, and 1.41g vertical acceleration effects. The connection also remained elastic for positive moment demands up to 159 k-ft, which corresponded to a demand equal to that expected for the combined load due to gravity, horizontal seismic load, and the effects of 0.4g vertical acceleration. Moreover, the ESMS connection reached a maximum negative moment of -1124 k-ft (which is equivalent to a demand beyond 1.75g of vertical acceleration in addition to the gravity and horizontal seismic effects) and a maximum positive moment of 300 k-ft (which is equivalent to a demand representing the gravity load, horizontal seismic load and 0.7g vertical acceleration). Thus, the ESMS connection exhibited moment resistance well beyond the target seismic effects including the 0.5g vertical acceleration. The connection also exhibited considerable ductility in both the negative and positive moment directions.

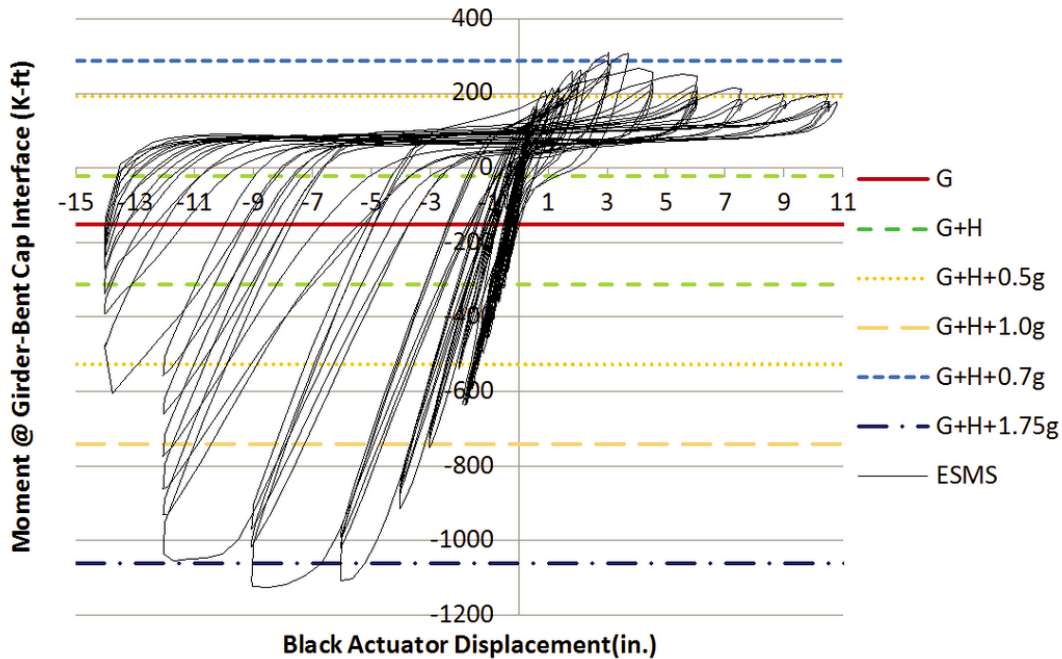


Figure 5.20: The measured moment resistance versus black actuator displacement for the ESMS connection

The negative moment resistance of the connection, as previously noted, relied on the reinforcement in the deck to resist tension while the bottom region of the girder was compressed against the cap beam. A few flexural cracks on the deck were the only observable damage under the target negative moment corresponding to the summation of gravity load, horizontal seismic load and 0.5g vertical acceleration effects. In order to achieve the better understanding of failure mechanism, the load was increased to produce larger negative moment magnitudes. A significant number of cracks in the deck had extended the entire width and penetrated the full depth of the deck during the large displacement cycles as shown in Figure 5.21. The cracks were well distributed over the connection region, and the crack width was relatively small compared to previous connection tests due to the use of macro and micro fibers in concrete. Furthermore, no spalling of concrete was observed on the deck during the entire test. In comparison, the deck concrete spalled in the ESBF and ESSP connections when subjected to large displacement cycles.



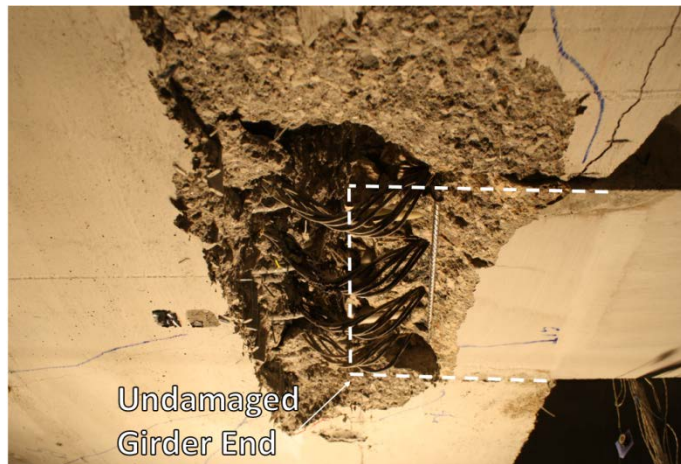
Figure 5.21: Flexural cracks formed on the deck of the ESMS Connection

Under the target seismic effects including 0.5g vertical acceleration, no visual damage was observed on the bent cap and girder. The bottom cover concrete at the end of girder began to visually separate with the girder strands, as shown in Figure 5.22a, when the applied load equivalent to gravity load, horizontal seismic load, and 1.0g vertical acceleration effects was reached. As the test continued, the girder cover concrete spalled off. The bent cap cover concrete behind the girder spalled significantly at -6 in. vertical displacement. Meanwhile, the unstressed strands were compressed, resulting in the mushrooming of strand and the pushing out of the bent cap cover concrete, as shown in Figure 5.22b. The damage at the interface between the bottom of girder and the bent cap continued to grow with the incrementally increased vertical displacement. Eventually the concrete surrounding the bottom region of girder to cap interface crushed and spalled off, resulting in a void between the girder and bent cap as shown in Figure 5.22c.



(a)

(b)

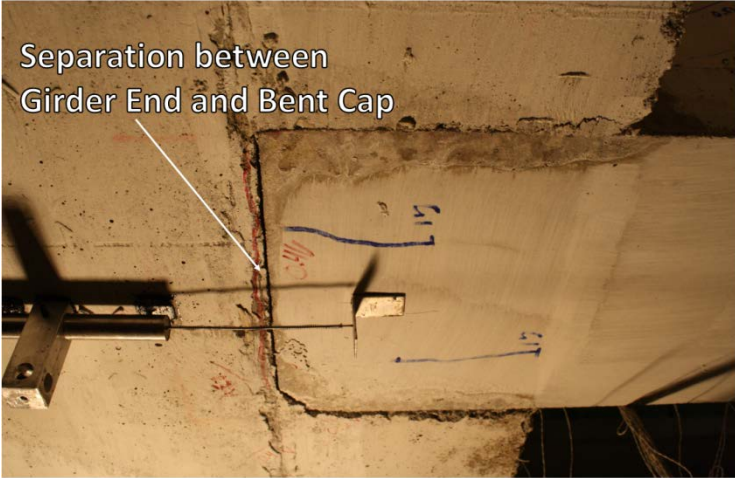


(c)

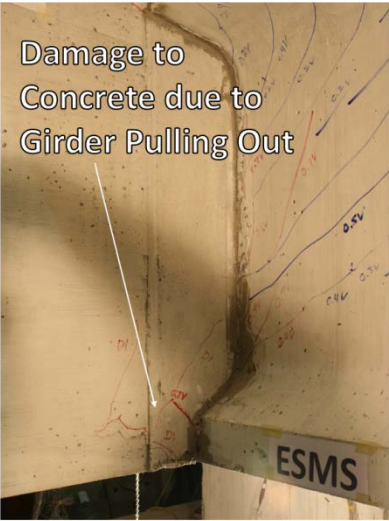
Figure 5.22: (a) Visual separation of girder cover concrete with girder strands; (b) Spalling of concrete at bent cap behind girder; (c) Void formed between the girder and bent cap

For the connection behavior in the positive moment direction, only hairline cracks were observed on the deck and girder up to the positive moments corresponding to gravity, horizontal seismic load, and 0.4g vertical acceleration effects. When the test continued beyond 0.4g vertical acceleration, the bottom of girder and bent cap began to separate at the interface (Figure 5.23a). A 0.1 in. gap between the bottom of the girder and the bent cap was the only damage when the connection was subjected to the target seismic effect. Damage due to the girder pulling out subsequently appeared on the diaphragm next to the girder at the load equivalent to the summation of gravity, horizontal seismic load, and 0.7g vertical acceleration as shown in Figure 5.23b. At 4.5

in. of vertical displacement (measured at the black actuator location 28.5 ft from girder to cap interface) the concrete adjacent to girder on the front diaphragm surface began to spall. As shown in Figure 5.23c, a large portion of the diaphragm next to the girder spalled off and separated from the girder after the vertical displacement reached 7.5 in. The compressed strands at negative moments were stretched and straightened when the positive moments were applied on the connection, but the extended strands did not fracture during the entire test.



(a)



(b)



(c)

Figure 5.23: (a) Separation between girder end and bent cap; (b) Damage to concrete due to girder pulling out on the diaphragm; (c) Diaphragm region where the spalling of concrete was observed

5.6.1.2 *Failure Mechanism*

Under negative moments, the yielding of the deck reinforcement caused the first yield condition for the ESMS connection, and as the vertical displacement increased, the plastic behavior developed simultaneously with concrete crushing and spalling at the bottom of the girder to cap interface. The spalling resulted in a reduced lever arm and therefore reduced the negative moment resistance of the connection starting from a displacement of -9 in. The negative moment behavior will be described in more details in the following section.

Under positive moments, the capacity of the connection was dependent on strands extending from the girder for tension continuity while the deck and top region of the girder compressed against the bent cap. The shear-friction developed by the dowel bars through the web of the girder as well as the adhesion between the embedded girder end and adjacent cap concrete also contributed to positive moment resistance. During the testing, the separation between the bottom of the girder and the bent cap was the first sign of yield for the connection under positive moment loading, but the strength softening did not take place until the damage to the concrete due to the girder pulling out occurred on the diaphragm next to the girder. After the damage to the concrete because of the girder pullout, the positive moment resistance incrementally reduced, as a result of the concrete spalling from the diaphragm adjacent the girder. The strands extended from girder experienced high strains simultaneously with the inelastic behavior of the connection and provided the residual positive moment resistance during the displacement cycles beyond 6 in. vertical displacement.

5.6.1.3 *Connection Interface Performance*

The test unit of the ESMS connection was subjected to a maximum negative vertical displacement of 14 in. and a maximum positive displacement of 10.5 in. at the black actuator location. Both the negative and positive responses showed sufficient moment resistance and considerable connection ductility. Figure 5.24 depicts the measured moment resistance versus rotation response for the negative moment direction. The negative moment resistance of the connection relied on the deck steel to resist tension as the bottom region of the girder was compressed against the bent cap. When the applied moment reached target seismic effects corresponding to the summation of gravity load, horizontal seismic load, and 0.5g vertical acceleration effects, no severe damage was observed at the connection interface, and the connection exhibited elastic response. The connection was then subjected to seismic effects

beyond the target values to investigate the failure mechanism. Figure 5.24 provides the strain data of the deck reinforcement at the interface between the girder and the bent cap. Yielding of the ESMS connection was observed to occur when the strain within the deck reinforcement at the girder-to-cap interface reached the yield value, but distinct overall softening behavior did not take place until the applied moment increased beyond -1101 k-ft.

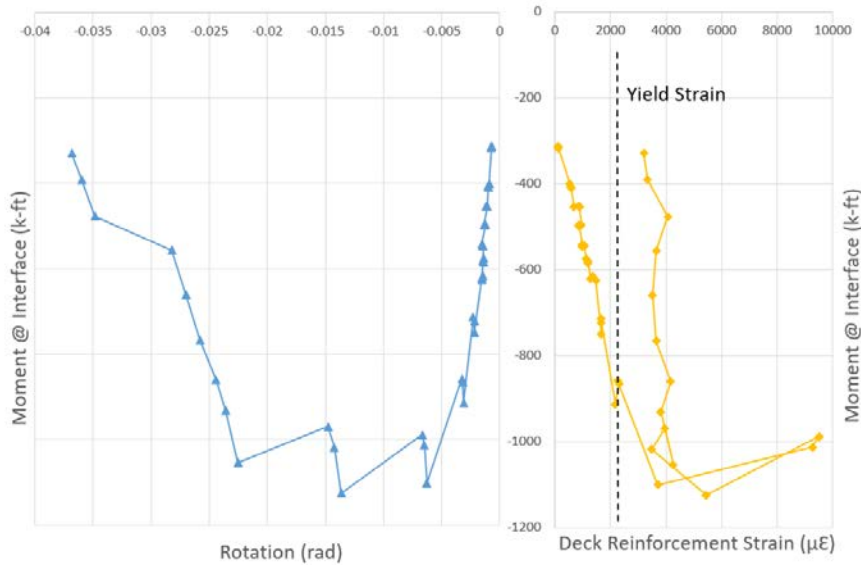


Figure 5.24: Negative moment versus rotation and negative moment versus deck reinforcement strain for the ESMS connection

As the applied moment increased beyond the yield, the deck reinforcement underwent strain hardening, but the strain of the reinforcement remained less than 5500 $\mu\epsilon$ for negative rotations beyond 0.0136 rad. Under negative moment loading, the bottom region of girder end and bent cap behind the girder were compressed. This local compression caused the strands to mushroom out. The expanding diameter of mushroomed strands pushed the cover concrete out at the bottom of the girder between the girder end and the first girder stirrup, thus causing spalling of concrete in this region as shown in Figure 5.25a. However, test data indicated that this spalling did not significantly change the elastic response of the connection. The continued increase of the strand mushrooming eventually caused the cap concrete to spall on the bottom surface, as shown in Figure 5.25b. Consequently, softening of the connection strength occurred, because this significant loss of concrete induced a gap between the girder and bent cap. The gap allowed the girder to rotate more prior to compressing against the bent cap in the negative moment cycles. As the cyclic load continued to be applied, the concrete immediately adjacent to the girder-to-cap interface began to

crush and spall off, as shown in Figure 5.25c. The crushing of concrete allowed the girder to rotate even more and eventually formed a void between the girder end and bent cap, as shown in Figure 5.25d. The void decreased the depth of girder to cap interface and reduced the lever arm for negative moment resistance, which resulted in a significant degradation in negative moment resistance. Comparable interface performance was observed during the earlier tests of the ESSP and ESBF connections.

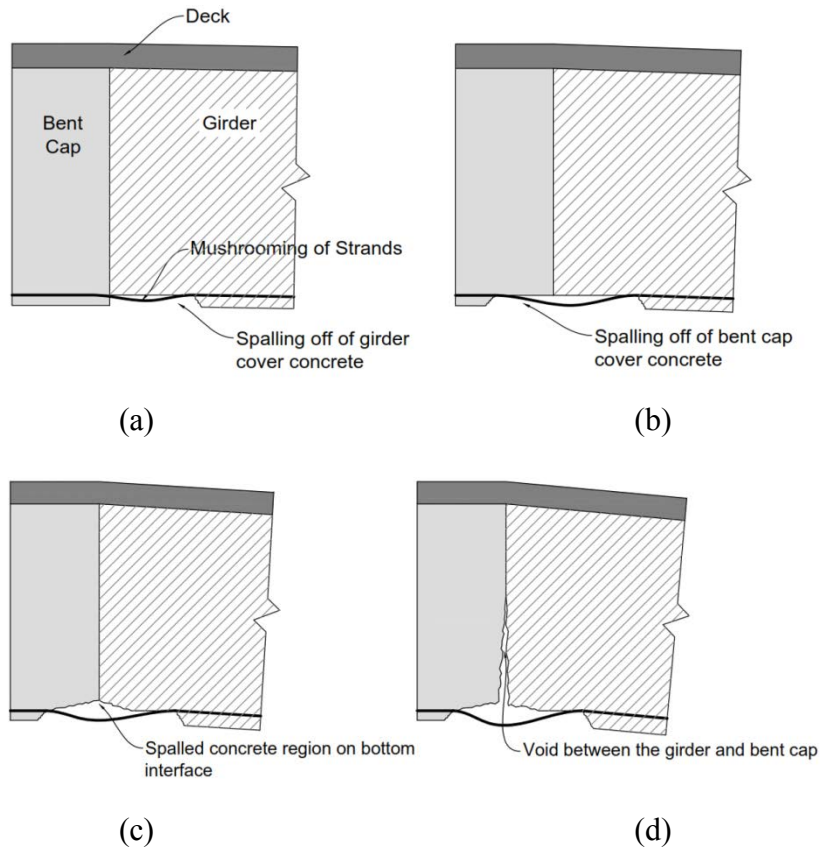


Figure 5.25: Illustration of damage of the girder and bent cap region

The dowel action was complicated and any direct measurement of this behavior was not possible. Therefore, the moment resistance due to dowel action was approximated by subtracting the moment resistance of the strands from the overall connection resistance. A series of pullout tests of strands with different sizes and configurations were performed at ISU to investigate the strain penetration behavior of unstressed strands. The tests provided the strain distribution along the strands as a function of the applied force, which was then used to estimate the strand behavior in the ESMS connection. In Figure 5.26, the moment resistance of the strands is plotted as a function of the connection rotation; the moment resistance provided by the dowel action is also

shown. The data graphed in Figure 5.26 was consistent with previously mentioned test observations. Generally, the connection exhibited an elastic behavior under the applied positive moments corresponding to the target seismic effects including 0.5g vertical acceleration. The yielding of the dowel action was indicated by the separation between the bottom of girder and the bent cap, and caused the yield condition for the connection. Thereafter the increase in overall moment resistance relied on tension in the extended girder strands, which continued to grow with incremental increasing of in connection rotation. The connection reached its ultimate moment capacity close to 0.01 radians which corresponded to a drop in dowel action capacity.

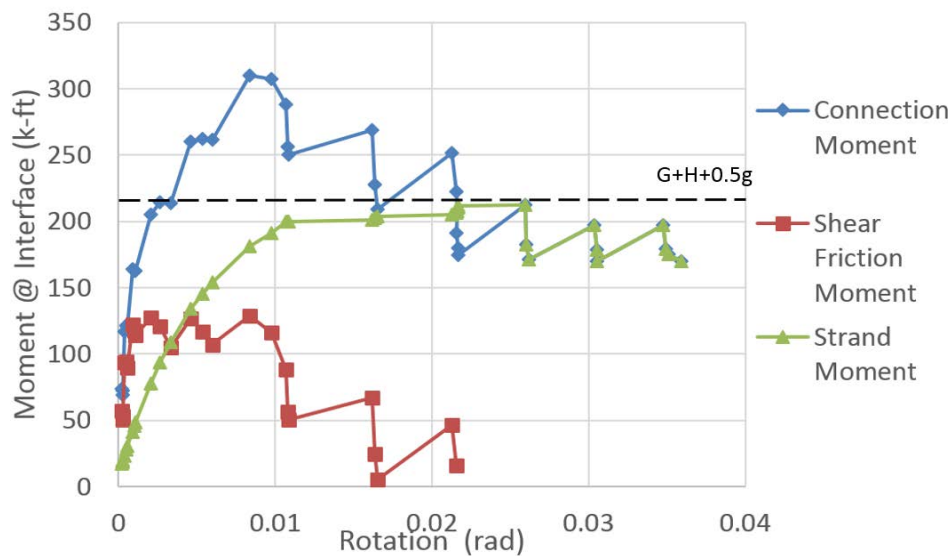


Figure 5.26: Estimating the contribution of the positive moment resistance in the ESMS connection

5.6.1.4 Unstressed Strand and Dowel Bar performance

The performance of unstressed strands and dowel action were critical for the positive moment resistance of the connection. For the unstressed strands, the mushroomed strands under negative moment loading were observed to straighten under positive moment loading, and the tension resistance of strands was not reduced by this behavior. The continuity provided by mechanical splicing of the extended strands was initially assumed to transfer the tension to the opposite girder. However, the test data indicated that the splice chucks provided sufficient anchorage for the unstressed strands and that tension forces were not transferred through the splice chuck to the other side. The unraveled portion of the strands caused by a sudden release of the prestressing force during the transfer, as mentioned previously, did contribute to a drop in tensile

strength of the strands extended from girder. Test data indicated the strands to be only 78% effective in providing tension resistance. To account for this loss of effectiveness, 0.067 in^2 was used as the effective area for a single strand in the ESMS connection.

As loads were applied to the extended strands, strain penetration occurred along the strands causing extension of the strands and a gap opening at the girder-to-cap interface. The unstressed strands used in the ESMS connection exhibited comparable performance with observations from pull-out tests mentioned previously. The pull-out test results indicated that strain distribution can be approximately linearly along the embedded strand length. As the tension force in the strands increased, the strain penetration occurred into both the girder side and bent cap side. When the strain penetration reached the splice chuck, fully anchored behavior was exhibited. The strain distribution along the strand prior to yield is shown in Figure 5.27.

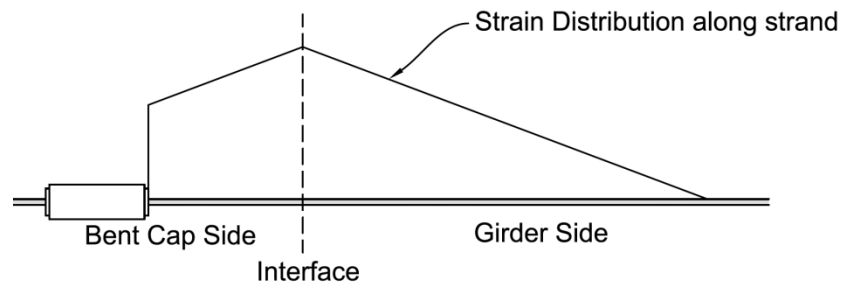


Figure 5.27: Strain distribution along strand

A general illustration of the dowel mechanism may be described as follows: the dowel action was developed between the precast girder and cast-in-place diaphragm surrounding the girder and provided resistance against pullout of the bottom of the girder under positive moment loading. The displacement between the girder and the surrounding diaphragm was resisted by cohesion and aggregate interlock at the interface between the girder and the diaphragm as well as shear-friction resulting from the clamping force developed by the dowel bars crossing the interface. Recalling the moment resistance from dowel action behavior shown in Figure 5.26, the first yield condition appeared when the bottom of girder separated from the bent cap, which indicated that the cohesion and aggregate interlock began to degrade. The shear-friction resulting from the clamping force provided further moment resistance from the dowel action until damage to the concrete due to girder pullout appeared on the front face of diaphragm at the bottom dowel bar location. The damage to the concrete due to girder pullout led to the further spalling of the cap cover concrete. At this point, the shear-friction began to degrade because of the decreased clamping force due to

the loss of bond strength of concrete around the dowel bars, which resulted in a significant reduction of the moment resistance resulting from dowel action.

5.6.2 ESLS Connection

5.6.2.1 Overall Performance

The ESLS connection was tested from Oct. 7, 2014, to Oct. 8, 2014, at Iowa State University. As with the ESMS connection, the ESLS connection was subjected to equivalent loads up to gravity plus horizontal seismic corresponding to the column overstrength moment plus vertical acceleration effects. Vertical displacement cycles of increasing magnitude were then utilized until failure of the connection was reached. Figure 5.28 shows the connection moment resistance versus the vertical displacement measured at the black actuator location (28.5 ft from the girder to cap interface). The moment magnitudes corresponding to gravity, horizontal seismic load, and seismic effects relating to 0.5g, 1.0g, and 1.75g vertical acceleration are shown as well. The connection remained elastic for negative moment up to the yield moment of -800 k-ft which corresponded to G+H+1.14gV. The connection also remained elastic up to a positive moment magnitude of 206 k-ft, which corresponded to G+H+0.5gV. The ESLS connection reached a maximum negative moment of -1158 k-ft (which is equivalent to a demand beyond G+H+1.75gV) and a maximum positive moment of 387 k-ft (which is equivalent to a demand representing G+H+0.95g vertical acceleration). In addition, the connection exhibited significant ductility in both the negative and positive moment directions. Also, an unexpected positive moment as large as 387 k-ft was applied after the G+H+0.5gV load cycle. The performance of connection during the overloading period was monitored and will be illustrated in the following sections.

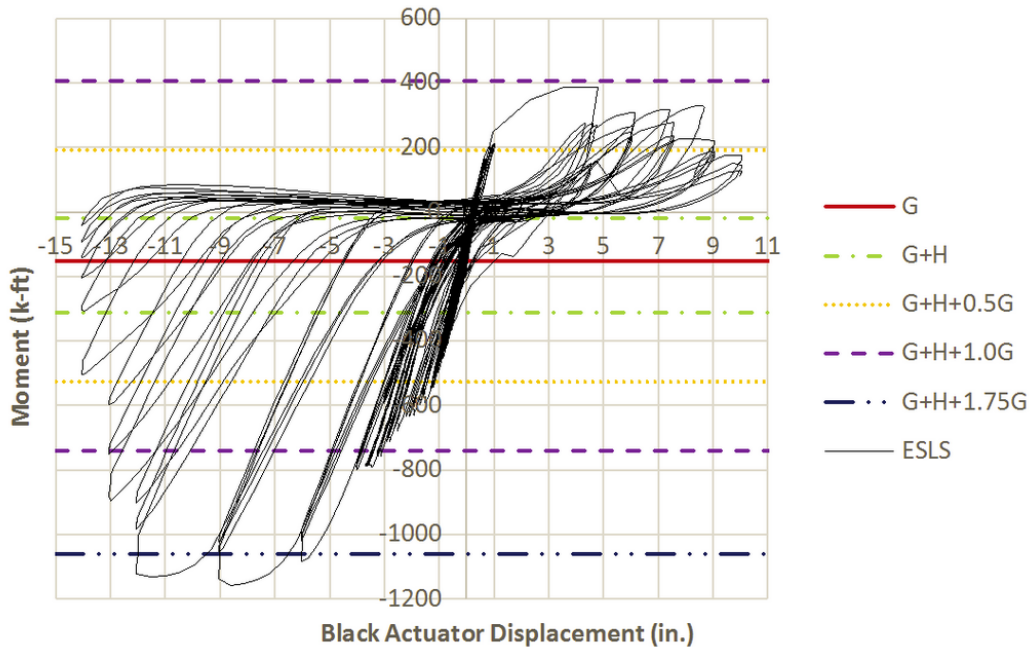


Figure 5.28: The measured moment resistance versus the black actuator displacement for the ESLS connection

The testing observations of the ESLS connection were similar to those noted during the test of the previous connections. When the target seismic effects were applied on the ESLS connection, no severe damage occurred except a few flexural cracks on the deck. Related to connection performance in the negative moment direction, the only cracks that were observed throughout the entirety of the test had limited width and formed on the deck over the connection region, as shown in Figure 5.29. The cover concrete at the bottom of girder end and a portion of the cover concrete on the bent cap spalled off after the overloading process as shown in Figure 5.30a. However, the crushing and spalling off of concrete surrounding the girder to cap interface did not significantly increase until the vertical displacement of black actuator reached -6 in. (Figure 5.30b). Similar to the previous connection tests, the concrete at the girder to cap interface gradually crushed and spalled at higher displacements, eventually forming a void at the bottom region of the girder-to-cap interface as shown in Figure 5.30c.



Figure 5.29 Cracks on Deck of the ESLS Connection

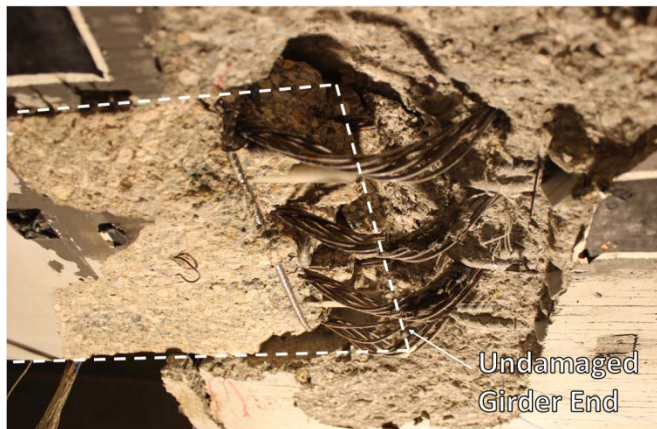
Under the target positive moment due to gravity, horizontal seismic load, and 0.5g vertical acceleration effects, no visual damage was noticed within the ESLS connection. In comparison, the girder end was separated with the bent cap under the same target seismic effects within the test of the ESMS connection. During the process of applying the next load step, one of the actuators shut off, causing a large unexpected positive moment of 387 k-ft to be applied to the connection. The large positive moment caused damage to the concrete due to girder pullout on the diaphragm next to the girder as shown in Figure 5.31a. No further damage was observed in the connection region when the test was resumed to the next step in the loading protocol. As the displacement of black actuator increased to 6 in. within the displacement controlled cycles, the diaphragm next to girder spalled as shown in Figure 5.31b. One of the four strands extended from the girder fractured when the displacement reached 9 in., causing a reduction in moment resistance. When cycled at a displacement of 10 in., another strand fractured as shown in Figure 5.31c, but the rest of strands remained effective through the end of test.



(a)

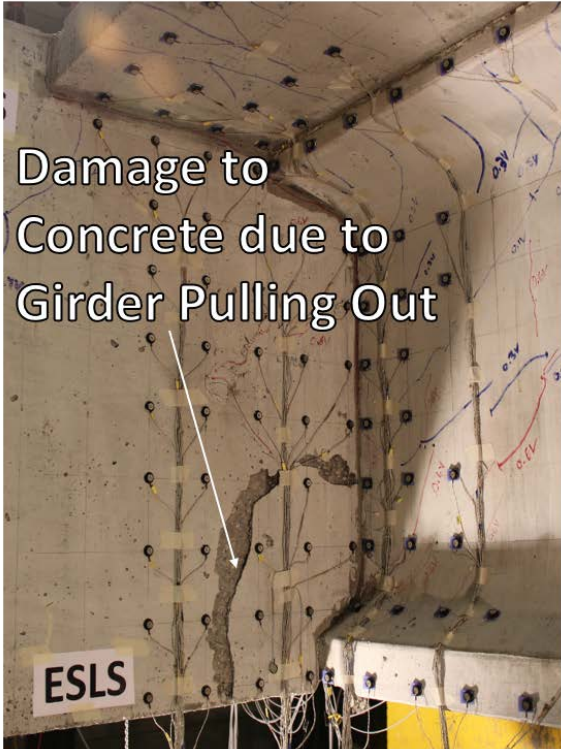


(b)

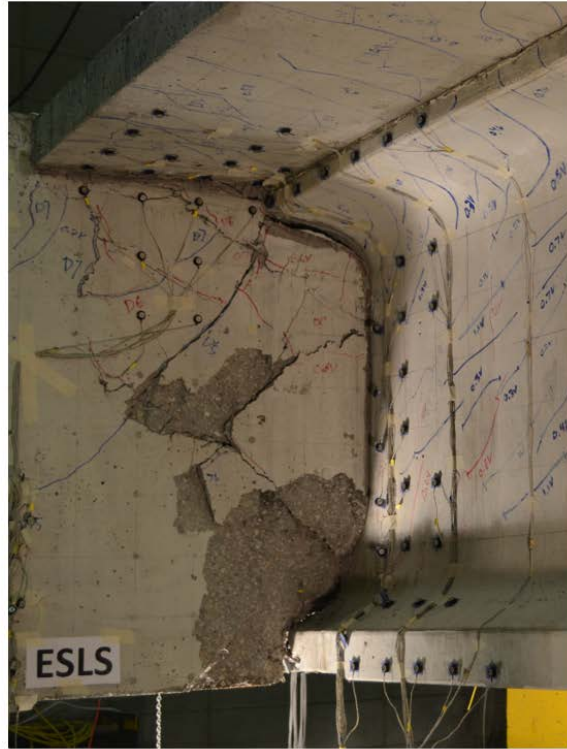


(c)

Figure 5.30: (a) Spalling of cover concrete at girder end; (b) Spalling of concrete at bent cap behind the girder; (c) the void formed between the girder and bent cap



(a)



(b)



(c)

Figure 5.31: (a) Damage to concrete due to girder pulling out on the diaphragm after overloading process; (b) Concrete next to girder spalled off; (c) Fracture of the strands within the ESLS Connection

5.6.2.2 *Failure Mechanism*

The ESLS connection failed in a similar manner to the ESMS connection under negative moment loading. Yielding of the deck reinforcement caused the first yield condition of the connection, and as the moment increased the strength softening took place simultaneously with crushing and spalling of the concrete in the bottom region of the girder-to-cap interface. At high displacement cycles, the concrete at interface experienced significant crushing, falling off and producing a reduction of negative moment resistance.

Under positive moments, the moment resistance of the connection is dependent on strands extended from the girder and the dowel action as same as the previous connections. The yield condition of the test unit connection occurred when the bottom of the girder separated with the bent cap. When the connection reached its ultimate capacity, the damage to the concrete due to girder pullout occurred on the diaphragm next to the girder as the extended girder strands simultaneously experienced high strain magnitudes. The strength reduction of the connection resulted from significant concrete spalling on the diaphragm and eventual strand fracture during the higher displacement cycles.

5.6.2.3 *Connection Interface Performance*

The relative displacement between the bottom of the girder end and the bent cap indicated the amount of concrete crushing and spalling that would occur at the bottom of the girder-to-cap interface. Figure 5.32 depicts the measured relative displacement between the girder and bent cap versus rotation response for the negative moment direction. Strength softening was observed as crushing and spalling of the concrete increased when the interface moment exceeded -630 k-ft due to the damage caused by the overloading. At an applied moment of -1158 k-ft, the significant increase in relative displacement indicated that severe crushing and spalling occurred, resulting in a reduced negative moment lever arm and subsequent strength degradation.

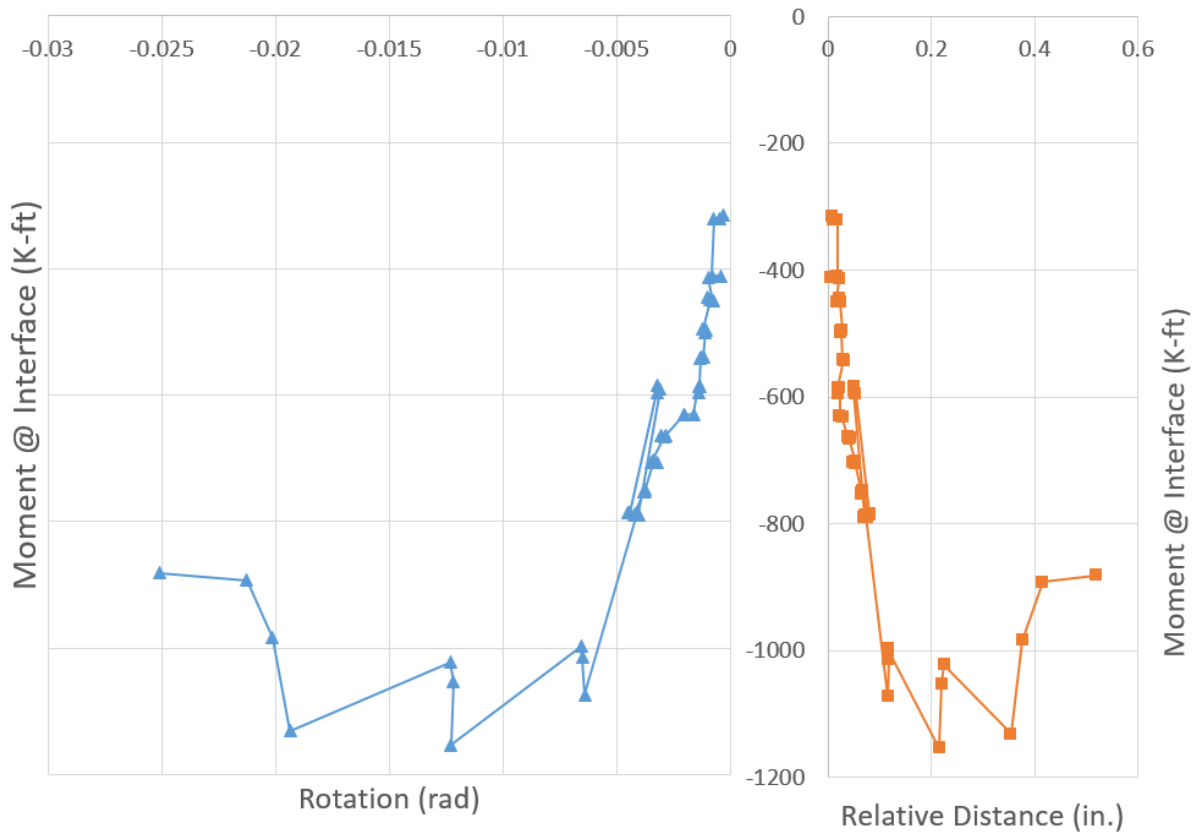


Figure 5.32: Negative moment versus rotation and negative moment versus relative displacement between girder end and bent cap for the ESLS connection

The positive moment at the girder-to-cap interface for the ESLS connection is shown in Figure 5.33, plotted versus the girder rotation. The moment resistance generated by dowel action and the moment capacity produced by the extended girder strands are also shown in Figure 5.33. The behavior of the ESLS connection in the positive moment direction was consistent with the behavior of the ESMS connection. The yield of the dowel action behavior took place simultaneously with the first yield condition of the connection. Subsequently the connection reached its ultimate moment capacity when the unexpected positive moment was applied. Under the ultimate moment, damage to the cap due to girder pullout appeared on the diaphragm adjacent to the girder, indicating a potential loss in dowel action. As the connection was subjected to higher displacement cycles, the positive moment resistance decreased due to continued degradation of the dowel action. Although the moment resistance of the dowel action was reduced, the extended strands remained effective to provide resistance until fracture occurred at a rotation slightly above 0.0268 rad.

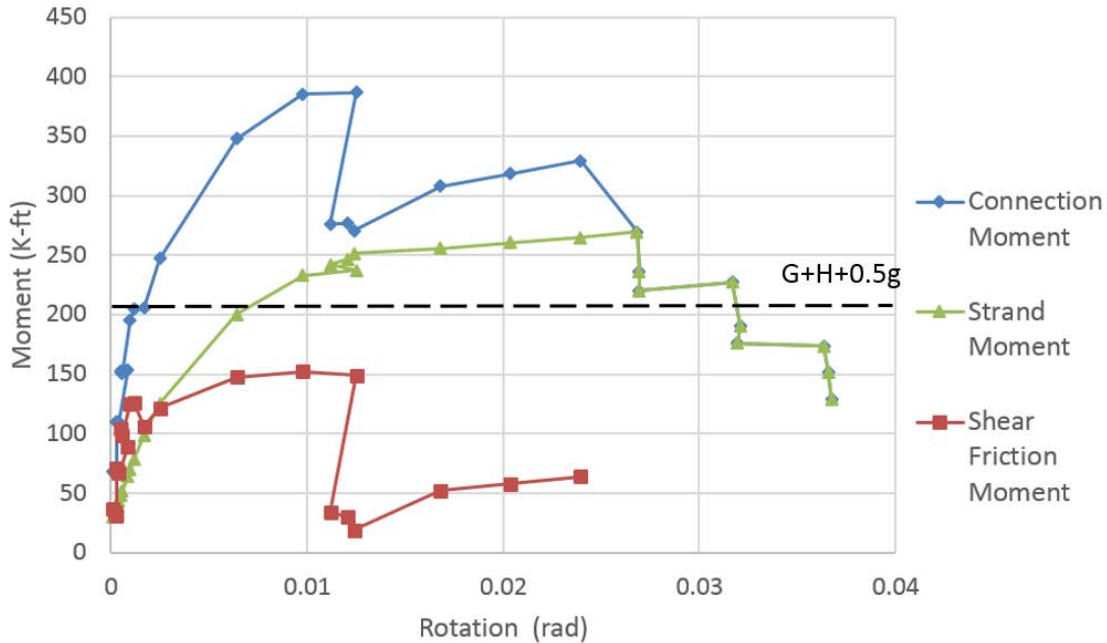


Figure 5.33: Positive moment versus rotation for the ESLS connection

5.6.2.4 Unstressed Strand and Dowel Bar performance

The positive moment resistance of the connection was produced by the extended girder strands, dowel action, and deck compression against the bent cap. The performance of the strands and the dowel bars were critical for connection behavior. The dowel action of the ESLS connection can be characterized in the same manner as the previous connections. The extended strand within the ESLS connection did not transfer the tension force through the lap splice. The strand chucks including bearing plates, barrel anchors, and wedges developed sufficient anchorage to fully develop the strand strength. As the connection was subjected to increasing rotations under positive moment, strand slip occurred at the connection interface resulting in an opening between the girder end and the bent cap. The strain distribution along the strands in the ESLS connection before yielding of the strands is shown in Figure 5.34, demonstrating fully anchored behavior at the strand chuck.

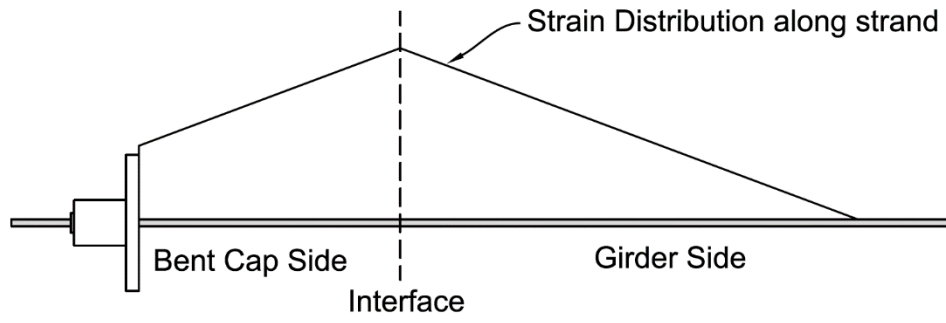


Figure 5.34: Strain distribution along strand in the ESLS connection

Chapter 6. Design Recommendations

To facilitate the implementation of the connection details investigated in this study, recommendations that can be easily adopted in further design practice have been developed. Because of the different load-transfer mechanisms that are involved in the negative and positive moment directions, the recommendations are presented below for each of the two loading directions. Both the I-girder and bulb-tee girder sections implemented in the experimental study were designed to simulate the largest standard I-girder and bulb-tee sections currently detailed and implemented by Caltrans. Because of the shear and moment interaction and the complexity of the load transfer mechanisms in the various connection details, appropriate caution should be exercised when extending the recommendations from this research project to other girder types.

6.1 Negative Moment Resistance

The precast bulb-tee girder to bent cap connection under negative moments may be evaluated using a sectional analysis of the composite girder-deck cross-section that is present at the girder to cap interface. The effect of the dowel bars embedded in the diaphragm is conservatively neglected for the negative moment calculation. For the composite section of the girder-deck assembly, an approximate effective deck width and the corresponding deck reinforcement should be defined as shown in Figure 6.1. The effective deck width may be calculated according to the location (i.e. interior vs. exterior) and current Caltrans design practices. Recommendations on moment distribution by Vander Werff and Sritharan (2015) that included test data from previously completed system tests for Caltrans may also be used for this purpose. Material properties for the deck and girder concrete as well as the steel reinforcement should be assigned according to appropriate Caltrans specifications.

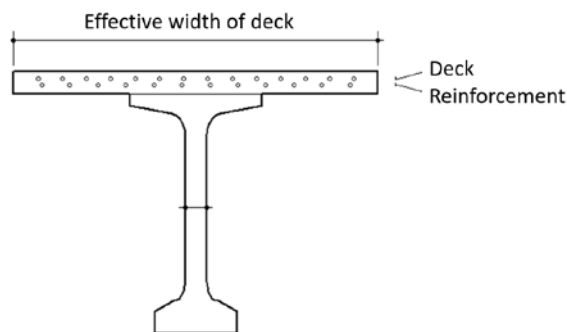
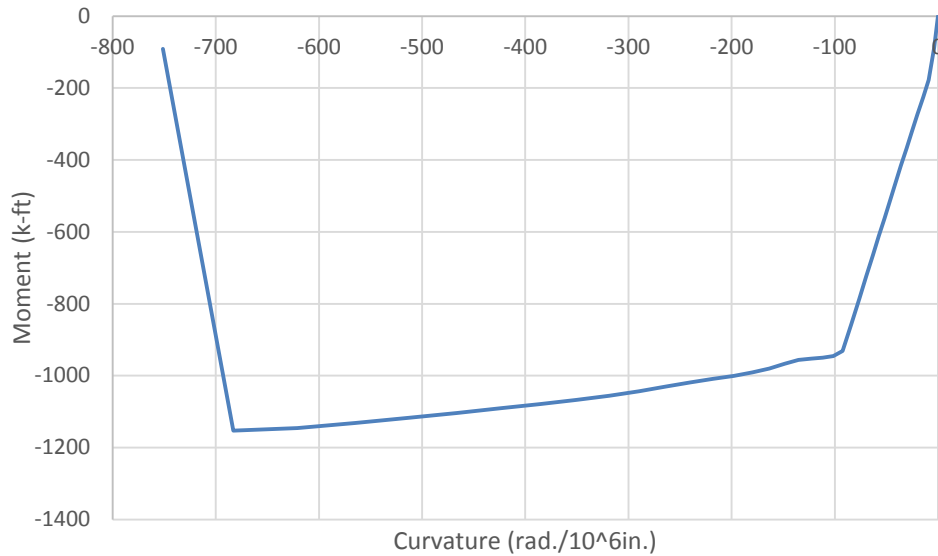
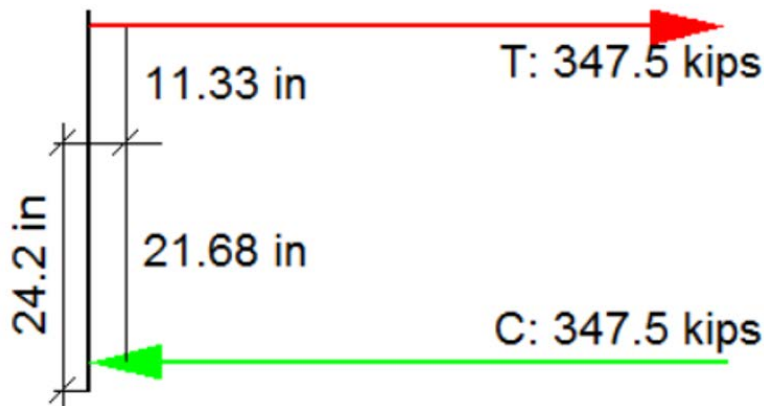


Figure 6.1: Section of the precast bulb-tee girder to bent cap connection in negative moment direction

The sectional analysis for the composite cross-section can be performed and a moment-curvature response showing the idealized yield and ultimate moment resistance of the section can be estimated. The corresponding tension force developed in the deck reinforcement can also be easily calculated (Figure 6.2).



(a) Moment-curvature response of the composite cross-section



(b) Internal forces at idealized yield condition

Figure 6.2: Results of sectional analysis

In addition to the connection moment resistance, the girder rotation corresponding to the applied moment needs to be determined in order to accurately calculate the behavior of the connection. The experimental testing indicated that concrete crushing and spalling at the girder to cap interface contributed to the majority of the rotation under negative moments by inducing the growing relative distance between the bottom of the girder end and the bent cap. Unfortunately,

concrete crushing is a localized failure and thus the corresponding relative distance is difficult to estimate numerically. Hence, an empirical approach was followed. Figure 6.3 shows experimentally measured relative distance, a good indicator of the amount of the crushed concrete, plotted with the compressive stress which is estimated based on the applied negative moment. Within Figure 6.3, the assumptions made were that the compressive stress is uniform at the girder to cap interface and that the area of girder below the neutral axis is compressive area. It is indicated from the test data that the point of relative distance occurs when the girder rotates about the neutral axis (N.A.) according to the corresponding applied connection negative moment. For moment values below the connection yield moment, which corresponds to when the deck reinforcement reaches yield stress, the neutral axis may be assumed to be located at the centroid of the girder (see Figure 6.4(a)). For moments beyond the connection yield moment, the axis of rotation may still be assumed as the girder centroid, but the neutral axis depth ($d_{N.A.}$) should be multiplied by a factor of 0.8 (Figure 6.4(b)) since the lever arm for negative moment resistance increases as the applied moments increase.

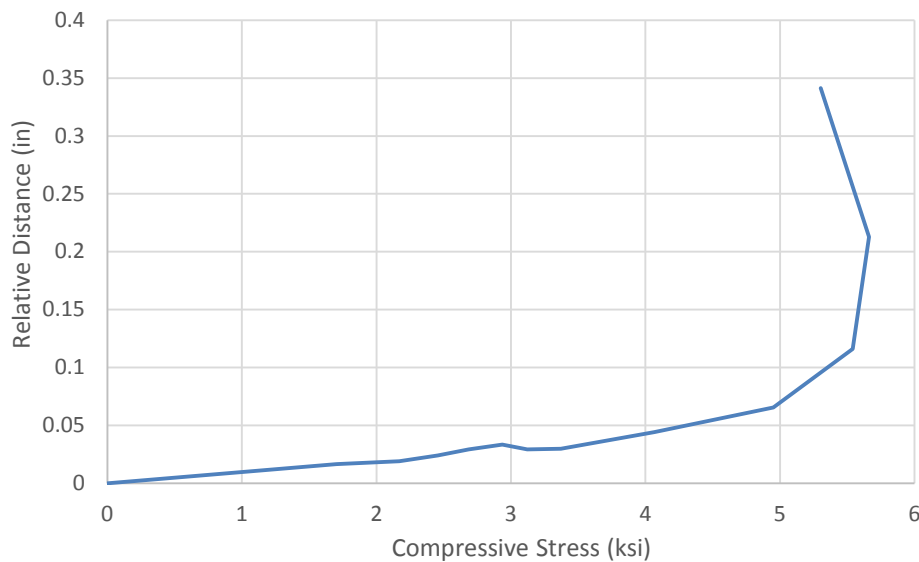


Figure 6.3: Experimental measured relative distance between bulb-tee girder end and bent cap

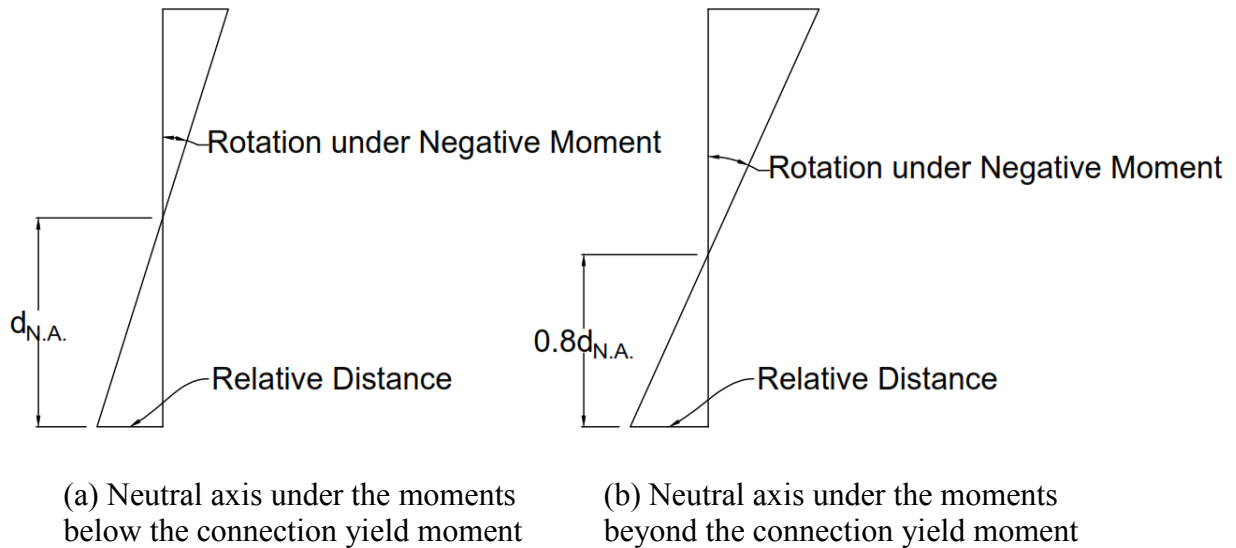


Figure 6.4: Assumed rotation at the girder to bent cap connection under negative moment

For any given moment value, the resultant tension force can be obtained from the sectional analysis and is equivalent to the compression force if there is no axial force on the girder to cap interface. For design purposes, it may be assumed that the compressive stress is uniform within the girder to cap interface region below the neutral axis. Therefore, Figure 6.3 allows a graphical determination of relative distance by using the compressive stress resulting from the equivalent compression force. The girder rotation (θ) can then be calculated using Equation 6.1 or Equation 6.2 depending on if the moment is greater or less than the connection yield moment. Since the rotation of the girder is caused by concrete crushing due to the compressive stress developed under negative moment, it is important to design the deck steel such that the composite section is not compression controlled under the target design demands. If the composite section contains too large an amount of deck reinforcement, a very large tension force will be required in order for the connection to yield. If the tension force becomes too large, the corresponding compressive stress will cause significant crushing and subsequent rotation of girder. In this case, it is possible that the connection will begin to soften before yielding of the deck reinforcement resulting in a compression controlled section.

$$\theta = \frac{\text{Relative Distance}}{d_{N.A.}} \quad (6.1)$$

$$\theta = \frac{\text{Relative Distance}}{0.8d_{N.A.}} \quad (6.2)$$

In summary, by performing the sectional analysis and using Figure 6.3, the moment-rotation behavior of the precast bulb-tee girder to bent cap connection can be determined. In order to verify the accuracy of the proposed method, the procedure was used to determine the behavior of the ESMS and ESLS connections. A comparison of the calculated behavior and the experimental results are shown in Figure 6.5. Overall, the calculated behavior compares well with the experimentally measured response envelopes. This confirms that the proposed analysis model is adequate to determine the behavior of connections with similar geometry and girders with no end block as used in the second and third test units. It is noted that since Figure 6.3 is determined empirically from test data quantifying localized failure, the same assumption may not be used for other girder type or bulb-tee girders with other end details. For full-scale 7 ft – 5/8 in. depth bulb-tee girders with no end block as the girders used in the second and third test units, the recommendations in Figure 6.3 can be scaled as shown in Figure 6.6. For shallow girders, the same correction may be proportion with caution.

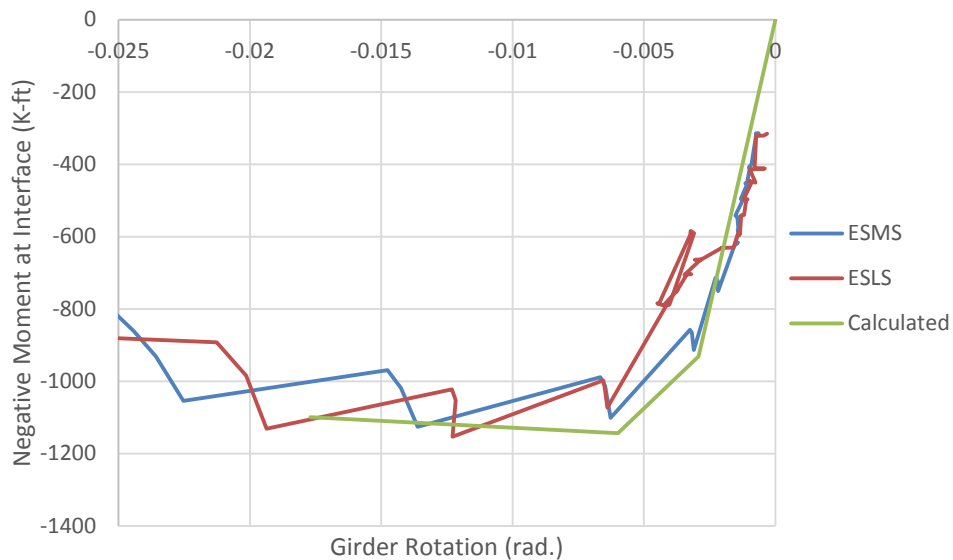


Figure 6.5: Comparison between the calculated and the measured moment-rotation response envelope

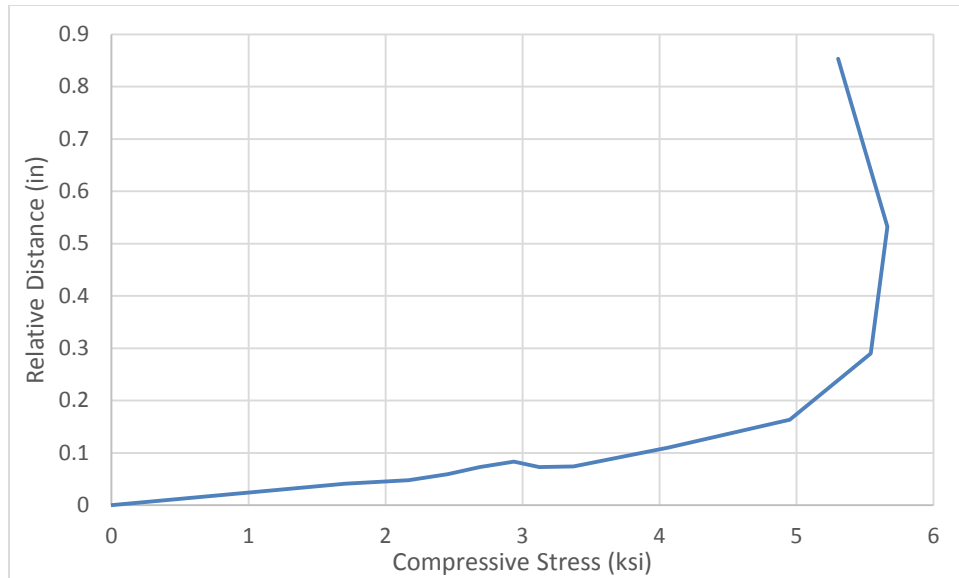


Figure 6.6: Relative distance at the bottom of girder end under negative moment for full-scale 7 ft – 5/8 in. depth bulb-tee girders

6.2 Positive Moment Resistance

For positive moment, the experimental investigations indicate that the dowel bars embedded in the diaphragm and the extended girder strands contribute to resist the applied moments simultaneously. The shear friction behavior developed at the interface between the girder and the surrounding diaphragm concrete provides moment resistance by restraining the pull out of the embedded girder end as shown in Figure 6.7; meanwhile, the extended girder strands anchored into the cap provide tension continuity for additional positive moment resistance. These two mechanisms may be modeled separately and then combined to determine the total moment resistance of the connection. (Note that since the LUSC detail does not use strand to provide a direct tension-transfer mechanism, a slight modification to the analysis is required as discussed in Section 6.2.4.) The following presents the proposed method for qualifying the connection positive moment behavior.

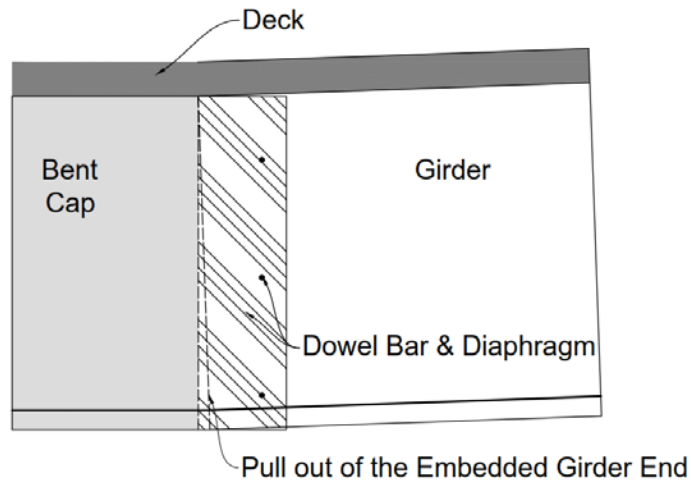


Figure 6.7: An illustration showing pull out of an embedded girder into the diaphragm

6.2.1 Shear Friction

When a precast bulb-tee girder is used in conjunction with a cast-in-place bent cap, the girders are erected on temporary falsework. The dowel bars are then grouted through the girder web, and the diaphragm is cast around the ends of the precast girder. As the girder rotates upward under positive moments, the embedded girder end tends to pull out from the diaphragm activating the shear friction mechanism. Shear friction includes two components: cohesion and friction. The cohesion results from shear transferred through the slip plane and is contributed by aggregates from the diaphragm concrete bearing on the girder and by dowel action (Mattock 1979). The friction component results from the tension force developed in the dowel bars, which in turn causes compression on concrete at the interface. The corresponding shear transfer should be accounted for using an appropriate coefficient of friction. In order to establish an appropriate moment-rotation behavior for the positive moments, the displacement associated with shear friction should be established and can then be used to determine the gap opening at the bottom of girder and bent cap as shown in Figure 6.8.

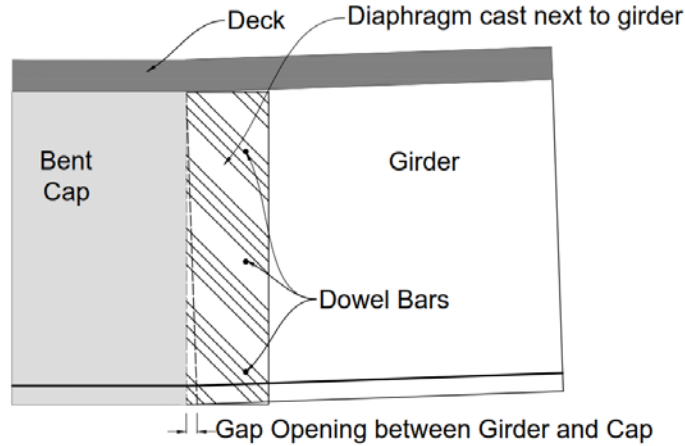


Figure 6.8: Gap opening under positive moments

AASHTO LRFD Bridge Design Specifications (AASHTO, 2012) proposes that the resistance due to shear friction as explained above can be estimated as follows:

$$V_{ni} = cA_{cv} + \mu(A_{vf}f_y + P_c) \quad (6.3)$$

The nominal shear resistance (V_{ni}) used in the design should not be greater than the lesser of:

$$V_{ni} \leq K_1f'_cA_{cv} \quad (6.4)$$

$$V_{ni} \leq K_2A_{cv} \quad (6.5)$$

where,

A_{cv} = area of concrete considered to be engaged in interface shear transfer (in.²);

A_{vf} = area of interface shear reinforcement crossing the shear plane within the area A_{cv} (in.²);

c = cohesion factor;

μ = friction factor;

f_y = yield stress of reinforcement (not to exceed 60 ksi for Grade 60 reinforcement);

P_c = permanent net compressive force normal to the shear plane, which is zero for this study;

f'_c = specified 28-day compressive strength of the lowest strength concrete on either side of the interface (ksi);

K_1 = fraction of concrete strength available to resist interface shear; and

K_2 = limiting interface shear resistance.

According to AASHTO, for concrete placed against a clean concrete surface, free of laitance, but not intentionally roughened as in the case for all girder to diaphragm interfaces in this study:

$$c = 0.075 \text{ ksi};$$

$$\mu = 0.6;$$

$$K_1 = 0.2;$$

$$K_2 = 0.8 \text{ ksi}.$$

In order to estimate the displacement corresponding to shear friction, experimental observations were used in conjunction with models suggested in literature. This resulted in a bi-linear model shown in Figure 6.9, which is similar to that suggested by Harries et al. (2012). This model identified the yield and ultimate shear friction resistance for the shear friction behavior, which is also correspond to visible damage at connection interface. Yielding of the shear friction mechanism usually takes place at displacement values ranging from 0.025 to 0.042 in. for any given interface (Harries et al., 2012). At this yield limit state, a gap would be visible between the bottom of the girder and cap as shown in Figure 6.10. The ultimate shear resistance, approximated to have the same capacity as that at yield, is expected for shear displacement values ranging from 0.25 to 0.3 in. (Kahn & Mitchell, 2002). After the ultimate shear displacement is reached, there is a significant drop in strength due to bond failure between the dowel bars and surrounding concrete. The ultimate shear displacement is characterized by damage to concrete on the diaphragm adjacent to the girder and spalling of concrete around the dowel bars as shown in Figure 6.11 due to the girder pulling out. Based on the results from the experimental tests, 0.025 in. and 0.27 in. were identified as the yield shear friction displacement and the ultimate shear friction displacement, respectively.

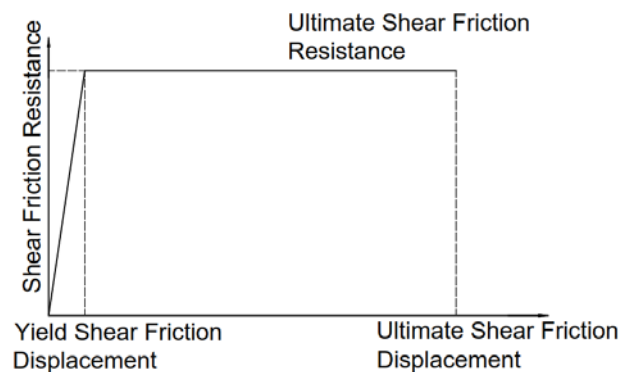


Figure 6.9: Identified shear friction behavior



Figure 6.10: Gap observed between cap beam and bottom of girder

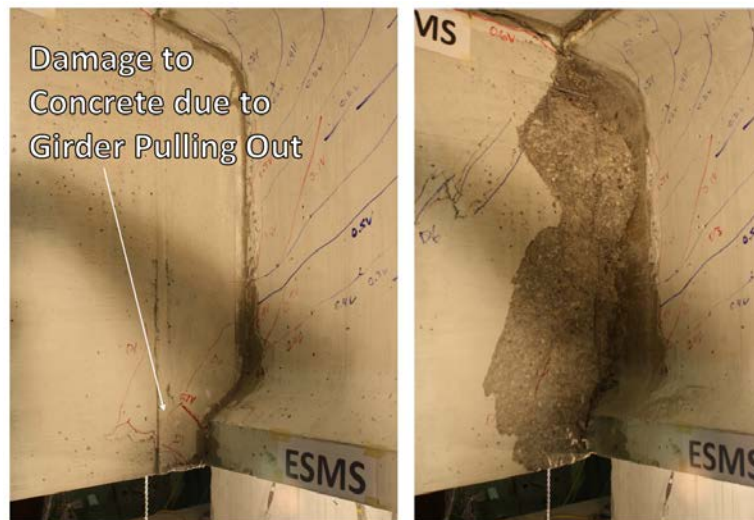


Figure 6.11: Damage to concrete due to girder pulling out on the diaphragm adjacent to the girder

The shear resistance provided by shear friction behavior should be calculated at the location of dowel bars as shown in Figure 6.12 using Equation 6.3. The concept of tributary area is used to define the amount of concrete considered to be engaged for each dowel bar as the force in each bar may be different. However, since the yield shear friction displacement was determined to be a small value (i.e. 0.025 in.), it should be assumed that each dowel bar reaches the ultimate shear resistance simultaneously.

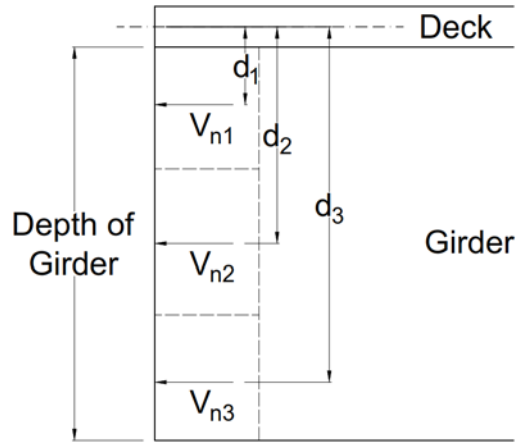


Figure 6.12: Distance to dowel bars for the positive moment resistance developed between the diaphragm and girder

In a similar manner to the calculations in the negative moment direction, the connection is modeled with the assumption that the shear friction displacement results from rotation of the girder at the interface about the neutral axis. The yield shear friction displacement and ultimate shear friction displacement occur at the location of the lowest dowel bar. Based on equivalent stress block calculations, the neutral axis for positive moments is located at the top of the girder as shown in Figure 6.13.

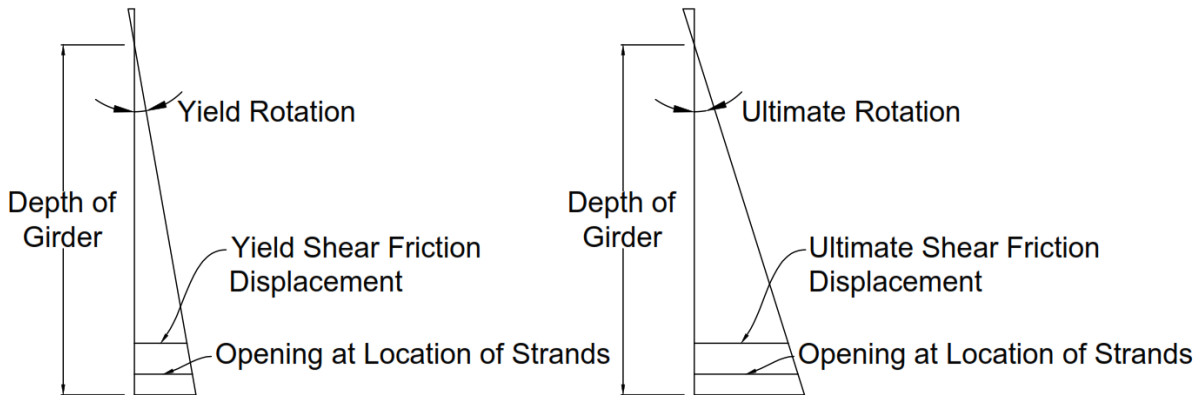


Figure 6.13: Rotation of girder to bent cap connection for positive moment direction

Therefore, the moment resistance developed by shear friction should be taken as:

$$M_{s-f} = \sum d_i V_{ni} \quad (6.6)$$

where,

M_{s-f} = moment resistance of dowel action;

d_i = distance from the middle of deck to the dowel bar; and

V_{ni} = nominal shear resistance of the interface plane.

The interface rotation (θ) should be calculated as:

$$\theta = \frac{\Delta_{LD}}{d_{LD}} \quad (6.7)$$

where,

Δ_{LD} = shear displacement at the location of the lowest dowel bar; and

d_{LD} = distance from neutral axis to location of lowest dowel bar.

6.2.2 Extended Girder Strands

In addition to the shear friction contributing to the moment resistance, the extended girder strands also contribute to the positive moment resistance. The experimental tests indicated that the 90 degree bend, mechanical splice chuck, and anchor chuck with steel plate and lap splice were able to fully anchor the strands. Anchorage of the strands was validated using the strain gauges mounted to them, which confirmed many of the strands experienced strains approaching yield and in some cases fracture under the applied positive moments. However, local strand slip did occur at the connection interface due to the effects of strain penetration and associated debonding. Based on the measured data, the strand behavior was characterized to accurately determine the moment resistance using the corresponding gap opening at the location of strands.

The connection interface is the location where the girder rotation occurs, and is therefore also where the extended strand experiences the highest strain. The strain in the strand decreases in both the girder and cap in proportion to the distance from the interface at a rate that is assumed to be linear as shown in Figure 6.14(a), where the strain shown reflects the change in strain due to the applied positive moments. The length of strand required for the strand strain to reduce to a value of zero is defined as the strain penetration length. If the strain penetration length reaches the strand anchor as shown in Figure 6.14(b), the strain will not penetrate beyond the anchorage point. Instead the strain will increase along the anchorage length (l_a) between the interface and strand anchor with the remaining force taken by the end anchor or go past the end anchor to the opposite side. As mentioned previously, pull-out tests were performed on 3/8 in. and 0.6 in. diameter strands at Iowa State University. Results from the pull-out tests showed that the strain reduction along the length can be approximated to $K = 0.00022$ strain/in. for 3/8 in. strands and 0.0001 strain/in. for 0.6 in. strands. Integration of the strain along the strain penetration length for both the girder and

bent cap is equal to the total strand elongation. Note that the same distribution is assumed for the strand along the girder for simplification, this models the debonding expected for the strands at the girder end. Elongation of the strand results in an opening between the girder and the bent cap at the location of strands. In other words, the area of the total strain distribution diagram (for both the cap and girder) is equal to the gap opening of the interface at the strand location.

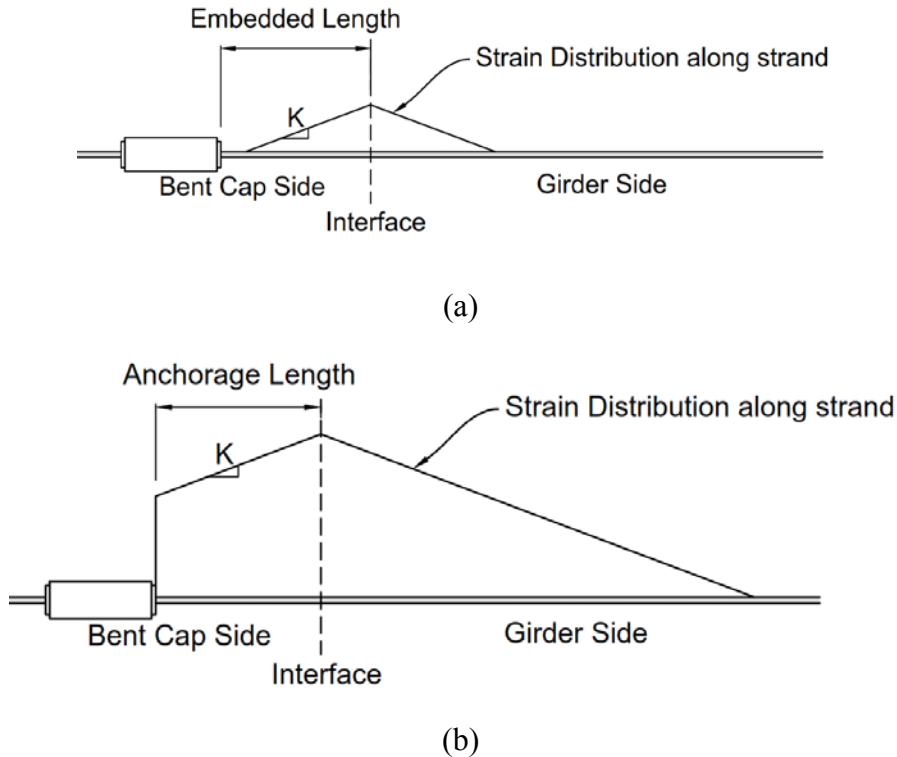


Figure 6.14: Assumed Strain distribution along the strand

Therefore, for a given interface rotation (θ) the gap opening, $\Delta_{opening}$, shall be taken as:

$$\Delta_{opening} = \theta d_s \quad (6.8)$$

where,

θ = rotation calculated from shear friction displacement;

d_s = the depth of strand measured from the neutral axis (neutral axis again assumed to be at the top of the girder).

The strain at interface ($\epsilon_{interface}$) may be estimated using Equation 6.9 if the strain penetration length is less than the anchorage length or Equation 6.10 if the calculated strain penetration length is greater than the anchorage length.

$$\varepsilon_{interface} = \sqrt{\Delta_{opening}k} \quad \text{if } \frac{\varepsilon_{interface}}{k} \leq l_d \quad (6.9)$$

$$\varepsilon_{interface} = \sqrt{2k \sqrt{\frac{\Delta_{opening}}{k} + l_d^2} - kl_d} \quad \text{if } \frac{\varepsilon_{interface}}{k} > l_d \quad (6.10)$$

where,

k = strain distribution factor (strain/in.); and

l_d = anchorage length of the strand embedded in the bent cap (in.).

The stress in the strand can be obtained from the estimated strain using an appropriate stress-strain relationship. It should be noted that an overestimated stress value may be obtained if a constant elastic modulus (i.e. 28,500 ksi) is used when strain exceeds the elastic limit. The moment resistance contribution by the strands can be, thus, taken as:

$$M_s = \sigma_s A'_{ps} N d_{sc} \quad (6.11)$$

where,

σ_s = stress of strand at interface;

A'_{ps} = nominal area of stand;

N = number of strands extended from precast girder; and

d_{sc} = distance from strands to the moment compression force.

The behavior of shear friction associated with the dowel bars and the extended girder strands were modeled independently. However, the overall positive moment connection behavior should be estimated by combining the two mechanisms as the estimated shear displacement at the interface based on experimental data which reflected both mechanisms acting simultaneously. As shown, the contribution of shear friction is calculated first and the resulting rotation can then be used to calculate the additional moment resistance provided by the extended girder strands. The yield condition of the connection should be approximated as the yield point of the shear friction. The ultimate moment capacity of the connection should be designed to occur before the shear friction displacement exceeds the ultimate value of 0.27 in. However, it is recommended that for the estimated positive moment demand, the connection should be designed to remain elastic. The suggested models are to establish the connection characteristics so that its expected performance can be established when the moment demand exceeds anticipated values.

For verification of the proposed design method, the behavior of three of the bulb-tee connections was estimated as shown in Figure 6.15. The ESSP connection was not included due to the reduced connection strength resulting from overloading on the connection during test. The calculated moment-rotation behavior is plotted with the experimental test results in this figure. Overall, the analytical behavior compares well with the experimental measured responses. It is important to note that for the ESBF connection, the ultimate rotation was overestimated; however, it is likely that the connection experienced a lower rotation value due to the absence of the “U” shaped confinement steel that was present in the ESMS and ESLS connections. Without the “U” shaped bars, degradation of bond between the dowel bars and the surrounding concrete will occur at a lower level of rotation due to less concrete confinement.

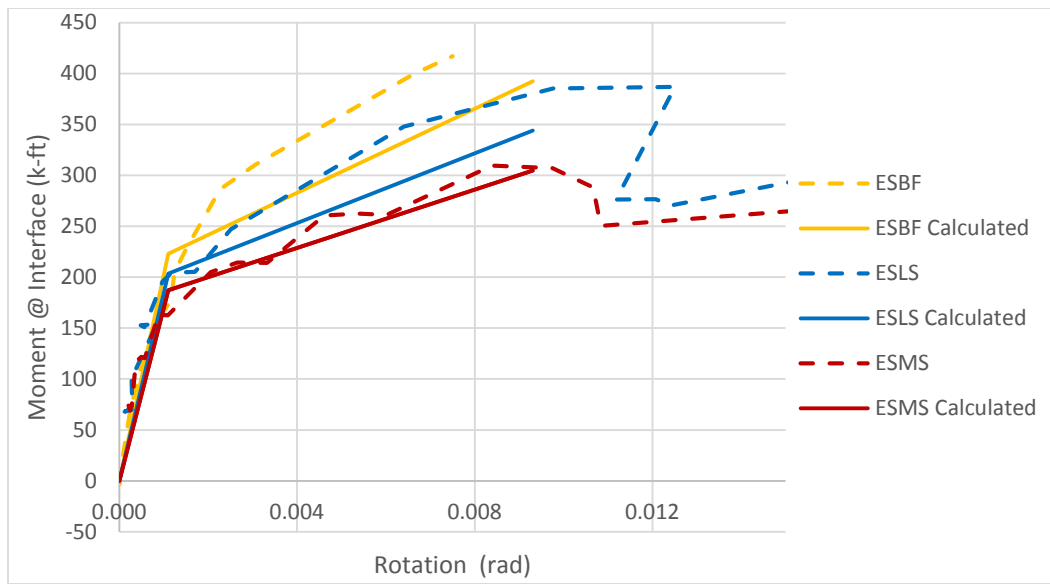


Figure 6.15: Comparison between calculated and the experimental positive moment to rotation response

The calculated and experimental ultimate moment resistance are relatively different for each of the three connections as shown in Figure 6.15. The measured ultimate moment of the ESBF connection was the highest at 416 k-ft followed by the ESLS and ESMS connections at 387 k-ft and 307 k-ft, respectively. The ESBF connection contained five extended strands as opposed to the four in the ESLS and ESMS connections. It is also important to note that the ultimate moment of the ESLS connection developed at a lower connection rotation, which is due to the influence of the overloading of the connection that occurred at a higher displacement rate (see Section 5.6.2). Based on design calculations, one additional strand in the ESBF connection should lead to an additional moment resistance of 55 k-ft. Therefore, the expected ultimate moment for the ESLS

and ESMS connection is 361 k-ft with respect to the measured resistance of ESBF. It is possible that the ESLS connection produced a slightly higher moment due to the high displacement rate associated with an overloading mentioned above. In addition, the unraveled strands reduced the effective-area of the strands to be reduced by 78% in the ESMS connection as discussed in Section 5.6.1. The decrease in effective strand area lead to a moment reduction of 47.5 k-ft. This compares well with the difference between the expected moment of 361 k-ft and the observed moment of 307 k-ft which is 54 k-ft. Therefore, it is concluded that the strength reduction observed for the ESMS connection is due to the unraveled extended strands in the connection, reducing the effective area of the extended strands.

6.2.3 Modified approach for dapped end I-girders

The general approach for the dowel shear friction action, presented in Section 6.2.1, can also be applied to girders with dapped ends when they are used with a cast-in-place or precast inverted-tee bent cap. However, the experimental results from the GUSC and LUSC details revealed that the dap causes a horizontal eccentricity between the dowel bar location and the apparent center of rotation for the connection. Consequently, the lever arm distances shown in Figure 6.12 need to be modified accordingly. For ease of determination, the center of rotation is again assumed to be at the top of the girder. However, a horizontal eccentricity, h , is incorporated along with vertical distances d_1 , d_2 , and d_3 to determine the modified lever arm distances d'_1 , d'_2 , and d'_3 , as shown in Figure 6.16. Based on the experimental results, it is recommended that h be defined as the horizontal distance from the dowel bars to the center of the girder dap. Using this distance for h , the modified distances can be determined. Equation 6.6 can then be used by substituting d' for d . The remainder of the approach presented in Section 6.2.1 can now be carried out with no additional modifications.

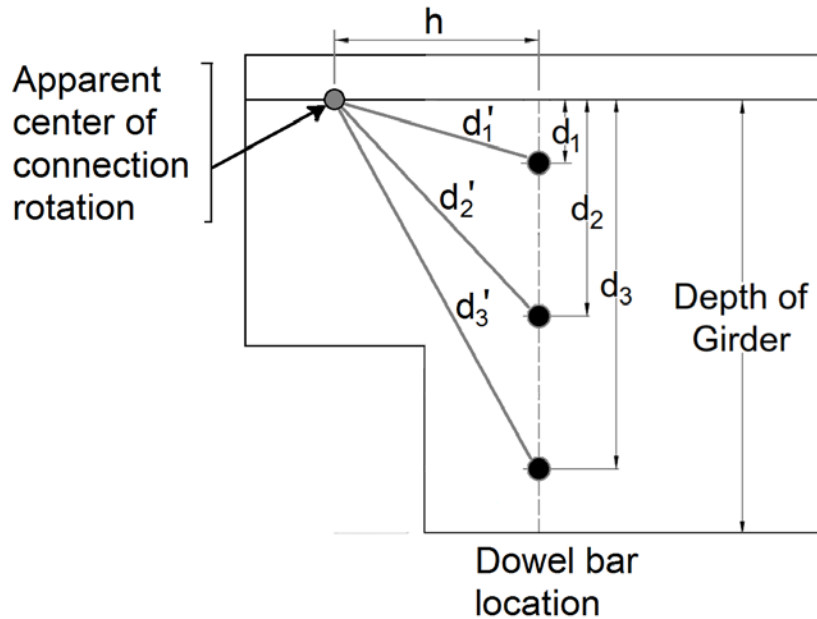


Figure 6.16: Modification to dowel bar distances about the girder rotation point for calculating the positive moment resistance for girder with dapped end

This modified approach for the dowel bar resistance was used along with the approach in Section 6.2.2 for continuous strand contribution to estimate the yield and ultimate positive moment capacities for the GUSC detail. The resulting calculations predicted the yield moment and ultimate moment to be underestimated by about 8 percent and 24 percent, respectively.

6.2.4 Modified approach for dowel bar confinement from looped strands

The approach presented in the previous section can also be appropriate for dapped end girders with dowel bars confined by looped unstressed strands, such as was incorporated in the LUSC detail, provided that slight modifications are incorporated appropriately. Since such a detail does not incorporate any strand that provides a direct tension transfer mechanism for positive moment, the moment capacity from the extended strand such as was calculated in Section 6.2.2 is neglected in this case. The absence of continuous strand also means that the approach presented previously for determining connection yield does not apply here, since the yield was based upon the strand behavior at the interface. Consequently, the capacity of the connection is based entirely on the shear friction in the dowel/strand region, and this calculated capacity is likely somewhere between the overall connection yield capacity and the connection ultimate capacity. Using the modifications for dowel bar distances presented in the previous section and incorporating a shear friction

coefficient $\mu = 0.6$ as with the previous connections, the calculated capacity of the LUSC detail is 466 kip-ft. This capacity is approximately 32% higher than the experimentally-observed connection yield strength and about 16% lower than the experimentally-observed connection ultimate strength.

6.3 Recommended Connection Design Approach

Based on the experimental and analytical findings for each of the ABC details investigated for establishing seismic connections between precast girders and bent caps, the design recommendations are formulated in this section. These recommendations can be used when designing integral bridges with precast I-girders and bulb-tee girders in high seismic regions.

6.3.1 Positive Moment Resistance

The first step in the formulation of these design recommendations is the consideration of the positive moment transfer mechanisms in the different test units. Positive moment resistance for each of the tested ABC connections came from one or both of the following two mechanisms: (1) shear friction; and (2) direct tension transfer through unstressed girder strands. The magnitudes and percentages of contributions of these two mechanisms for each connection at the yield and ultimate limit states are summarized in Table 6.1, where yield limit state was defined by a significant change in rotational stiffness due to the opening of a visible crack at the bottom of the girder to cap interface due to mobilizing the shear friction mechanism. The ultimate limit state corresponded to the maximum moment resistance reached by each connection during the entire experimental test. Since the superstructure is generally designed to remain elastic, as per capacity design principles for bridges, the yield limit state is of primary interest. However, the ultimate limit state was also quantified to allow a designer to estimate the reserve capacity of the connection beyond the yield moment resistance.

Since the strands were not fully engaged at the yield limit state due to the dominant behavior of the shear friction mechanism at small rotations, the strand stresses observed for each connection at the yield and ultimate limit states are also summarized in Table 6.2. The moment contributions are seen to vary for the various connections due to the use of different quantities of strands, improvements to detailing of the connection reinforcement, and the use of fiber concrete in the cap region of one of the test units. For all the test units, the lower bound percentage contribution of the shear friction mechanism is 59.8% of the total positive yield moment, and the corresponding strand

stress is $0.38f_{pu}$. When the shear friction contributed to a higher percentage, the strand stress dropped to $0.22f_{pu}$. At the ultimate limit state, the corresponding values are, respectively, 30%, $0.95f_{pu}$ and $0.72f_{pu}$.

Given that the bridge superstructures are designed to remain elastic at the time of fully developing the plastic hinge at the column top, designing the girder-to-cap connections using the moment contributions at the yield limit state is recommended. The ESLS connection test was optimized to minimize the strand quantities, and thus the measured values from this connection test are considered more representative. Using these values and those in Table 6.1 and Table 6.2, the following approach is recommended for quantifying the required number of strands to resist the positive moment demand: a) the moment resistance provided by the unstressed strand should not be taken as less than 40% of the total positive moment demand due to the gravity effects, column overstrength flexural moment, and vertical acceleration effects, and b) the stress in the strand is recommended to be limited to $0.30f_{pu}$.

For the LUSC detail, a modified approach is required since the looped strands and dowel bars work together to resist the entire moment by the shear friction mechanism and the strands do not provide a direct tension transfer mechanism across the girder-cap interface. In this case, it is important to make sure sufficient quantities of dowel bars and loop strands are provided. The needed reinforcement can be quantified at the yield limit state assuming the following:

- 30% of the moment will be resisted by adhesion and dowel action. The dowel bars can be sized based on shear friction carrying 70% of the total required positive moment demand.
- The required area of dowel bars should not be less than $T/(f_y * \mu)$, where T is the tension force corresponding to positive moment that needs to be resisted by the shear friction component (i.e., 70% total required moment) and μ is the coefficient of friction which should not be higher than 0.6.
- Appropriate amounts of confinement in the form of looped unstressed strands should be placed in the diaphragm on both sides of the girder and also within the girder, as shown in Chapter 7, Figure 7.2. The looped strands in the diaphragm should be anchored into the cap beam. The tested connection, which contained two strands on each side of the girder and four strands within the girder, developed a maximum tension force of 13 kips (52 kips at prototype scale) in a single strand.

Table 6.1: Magnitudes and percentage of positive moment resisted by shear friction and unstressed strand for different connections

| ID | Contribution to Moment Resistance | Magnitudes | | Percentages | |
|-------|-----------------------------------|-------------------|----------------------|-------------------|----------------------|
| | | Yield Limit State | Ultimate Limit State | Yield Limit State | Ultimate Limit State |
| ESBF | Shear friction | 171 k-ft | 125 k-ft | 59.8% | 30.0% |
| | Strand | 115 k-ft | 291 k-ft | 40.2% | 70.0% |
| | Total | 286 k-ft | 416 k-ft | 100.0% | 100.0% |
| ESSP | Shear friction | 109 k-ft | 125 k-ft | 52.9% | 43.4% |
| | Strand | 97 k-ft | 163 k-ft | 47.1% | 56.6% |
| | Total | 206 k-ft | 288 k-ft | 100.0% | 100.0% |
| ESMS | Shear friction | 122 k-ft | 129 k-ft | 74.4% | 41.6% |
| | Strand | 42 k-ft | 181 k-ft | 25.6% | 58.4% |
| | Total | 164 k-ft | 310 k-ft | 100.0% | 100.0% |
| ESLS | Shear friction | 125 k-ft | 152 k-ft | 64.1% | 39.3% |
| | Strand | 70 k-ft | 235 k-ft | 35.9% | 60.7% |
| | Total | 195 k-ft | 387 k-ft | 100.0% | 100.0% |
| GUSC | Shear friction | 309 k-ft | 368 k-ft | 91.0% | 84.4% |
| | Strand | 31 k-ft | 68 k-ft | 9.0% | 15.6% |
| | Total | 340 k-ft | 436 k-ft | 100.0% | 100.0% |
| LUSC* | Shear friction | 400 k-ft | 539 k-ft | N/A | 100.0% |
| | Strand | N/A | N/A | N/A | N/A |
| | Total | 400 k-ft | 539 k-ft | 100% | 100.0% |

* The configuration of the LUSC mechanism is such that its entire moment is resisted by a shear friction mechanism.

Table 6.2: Strand stress corresponding to the yield moment and ultimate moment resistance

| Connection Detail | Stress | | Fraction of strand strength | |
|-------------------|-------------------|----------------------|-----------------------------|----------------------|
| | Yield Limit State | Ultimate Limit State | Yield Limit State | Ultimate Limit State |
| ESBF | 101.5 ksi | 256.8 ksi | $0.38f_{pu}$ | $0.95f_{pu}$ |
| ESSP | 74.24 ksi | 124.3 ksi | $0.27f_{pu}$ | * |
| ESMS | 59.0 ksi | 254.1 ksi | $0.22f_{pu}$ | $0.94f_{pu}$ |
| ESLS | 77.2 ksi | 259.2 ksi | $0.29f_{pu}$ | $0.96f_{pu}$ |
| GUSC | 33.1 ksi | 72.7 ksi | $0.12f_{pu}$ | $0.27f_{pu}$ |

Notes:

1. f_{pu} for the strand used in the experiments was 270 ksi
2. *Due to unexpected overloading of the specimen, this value was not reliably obtained

6.3.2 Selection of Connection Details

The first step in the design of the connection between the precast girders and a cap beam is to choose the appropriate connection concept. Since several different connection details have been examined, a designer can choose the LUSC concept or one of the other connection details that uses a combination of shear friction transfer and direct tension transfer through the unstressed strands. To help with this process, Table 6.3 to Table 6.6 list the advantages and challenges associated with the different connection concepts and detailing options. In consideration of these suggestions and feasible construction options, a designer may select the connection details.

Table 6.3: Choices for positive moment resisting mechanisms

| Mechanism | Advantages | Challenges |
|--|---|---|
| Shear friction mechanism and Direct tension transfer through unstressed strands (the GUSC, ESSP, ESBF, ESMS, and ESLS connections) | <ul style="list-style-type: none"> • Two complementary mechanisms contribute to the moment resistance. • Unstressed strands provide a stable moment resistance at large rotation. | <ul style="list-style-type: none"> • Unstressed strands need to be properly anchored in the bent cap. |
| Shear friction mechanism only (the LUSC connection) | <ul style="list-style-type: none"> • Relatively less reinforcement is required in the connection region. • Configuration allows for easy construction since strands are not placed through the girder-to-cap interface. | <ul style="list-style-type: none"> • The mechanism of shear friction is considerably more complex due to more variables (interface condition, strength of concrete, etc.). • Large diameter headed dowel bars are required. • Additional strands are required within the precast girders. • Only one test has been completed, and the connection reinforcement details are not optimized. |


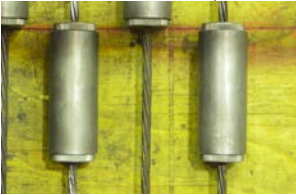
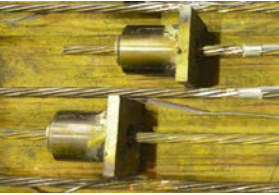
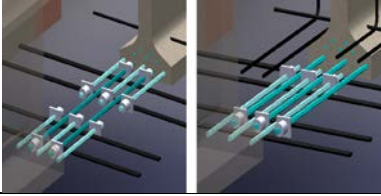
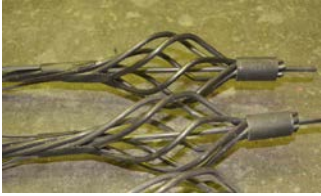
Table 6.4: Bent cap options

| Bent cap | Advantages | Challenges |
|------------------|--|---|
| Inverted-tee cap | <ul style="list-style-type: none"> • The concept is suitable for precast bent cap option. • No falsework is needed to support the precast girders before the continuity connection is cast. • The ledges of the cap minimizes vertical shear slip between the girder and the cap. | <ul style="list-style-type: none"> • The additional reinforcement and construction challenges may arise in the dapped end of girders and ledges of the inverted tee bent cap. • The center of girder rotation is relatively difficult to determine due to the presence of ledges. • A concrete diaphragm is required adjacent to the bent cap. |
| Rectangular cap | <ul style="list-style-type: none"> • The design and constructions are relatively simple. • Girders are embedded within the bent cap without needing a concrete diaphragm. | <ul style="list-style-type: none"> • The falsework is required to support the precast girders. • Girders may separate from the bridge deck if they are subjected to large inelastic rotations. |

Table 6.5: Options for providing unstressed strands

| Strand | Advantages | Challenges |
|--|--|--|
| Extend the pretensioned strands from the precast girder (e.g., ESSP, ESBF, ESMS, and ESLS connections) | <ul style="list-style-type: none"> • Relatively short embedment length to fully develop the strength of strand when embedded with anchorage devices. | <ul style="list-style-type: none"> • The extended girder strands may be damaged during transportation. • Care is needed to prevent the extended strands from unraveling when prestress is released. • Use of precast bent cap may not be easy. |
| Grouted through a corrugated duct in the field (e.g., GUSC connection) | <ul style="list-style-type: none"> • Precast bent caps can be easily implemented. • No extension of strands is required. • Strands are continuous through the cap and | <ul style="list-style-type: none"> • The corrugated ducts need to be placed in the precast girders and bent cap. • A low construction tolerance is required to align the ducts during field assembly. • The interface between the bent cap and girder require fiber-reinforced grout. • Assurance of proper grouting of the duct may be difficult. |

Table 6.6: Options for anchoring strands within the cap

| Anchorage method | Advantages | Challenges |
|---|--|---|
| <p>Free end with 90 degree bend (as used in ESBF connection)</p>  | <ul style="list-style-type: none"> • No anchorage device is required • Easier to route the strands as they can be placed underneath the longitudinal reinforcement of the cap beam | <ul style="list-style-type: none"> • Additional equipment is required if strands are bent in field |
| <p>Mechanical splice chuck (as used in ESMS connection)</p>  | <ul style="list-style-type: none"> • Short embedment length • Installation is relative easy • No significant congestion | <ul style="list-style-type: none"> • Length of splice is longer than that used for the plate anchorage |
| <p>Strand chuck consisting of a bearing plate, a barrel anchor, and wedges (as used in ESSP and ESLS connections)</p>  | <ul style="list-style-type: none"> • Relatively short embedment length is required to fully develop the strength of strand • Extended strands from girders can be anchored by overlapping the strands or using splice strands. Test data, however, confirmed no overlapping is necessary  | <ul style="list-style-type: none"> • Post-tensioning equipment is required to correctly install the strand chuck. |
| <p>Bond head (evaluated using a pull test) and not recommended for use</p>  | <ul style="list-style-type: none"> • No special anchorage elements are required | <ul style="list-style-type: none"> • Need special equipment • Long embedment length required • Benefit of its use with 90 degree bend has not been justified |

6.3.3 Design Procedure

Once the suitable connection details for the girder-to-cap connection are identified, this section suggests how the reinforcement quantities may be established in a way that is consistent with the findings and experimental observations. The girder-to-cap connection should be designed as a capacity protected region and can be designed using any one of the connection details that have been investigated in this report. The connections must be able to resist the connection load resulting from the overstrength forces developed in the column along with the vertical seismic effects without connection damage or inelastic superstructure behavior. For the proposed precast girder-to-cap connections, therefore, the nominal moment strength may be approximated to the yield moment capacity.

In design practice, the aforementioned percentages for moment resistance from shear friction and extended strands at the yield condition of the connections can be used to estimate the required moment capacities resulting from these two mechanisms, and then determine the number of girder strands to be extended and detail the dowel bars and diaphragm as per the illustration in Chapter 6. The design procedure outlining the steps to determine the connection details is given in Table 6.7. The dowel bar and pier diaphragm are recommended to be detailed as per Table 6.8. A design example following the suggested design procedure can be found in Appendix E.

Table 6.7: Suggested design procedure for precast girder-to-cap connection

| | |
|--------|--|
| Step 1 | Determine the required moment demand at precast girder-to-cap connection |
| Step 2 | Estimate the required moment to be resisted by the extended strands |
| Step 3 | Determine the number of strands that should be extended from the girder |
| Step 4 | Design the anchorage details for the extended unstressed girder strands |
| Step 5 | Detail the dowel bars and the diaphragm |

Notes:

- 1) The suggested percentages of nominal positive moment capacity used in Step 2 are 60% and 40%, respectively, for shear friction moment and strand moment.
- 2) The suggested allowable strand stress in Step 3 is $0.30f_{pu}$.

Table 6.8: Suggested details for dowel bars and diaphragm

| | |
|------------------------------|---|
| Size of dowel bars | Not less than #10 Grade 60 reinforcing bar for Bulb Tee and #8 Grade 60 reinforcing bar for I-Girders |
| Number of dowel bars | Not less than 3 |
| Location of dowel bars | The dowels are recommended to be placed within the web of girder to avoid possible conflict with the prestressed girder strands, which are typically placed in the girder flanges. For the case of three dowel bars, the suggested locations are 12.5 in. below the top of the girder, 12.5 in. above the bottom of the girder, and the mid height of the girder. |
| Length of dowel bars | Not less than 6 ft in total length, positioned symmetrically through the girder |
| Thickness of pier diaphragm | The recommended minimum value is 22.5 in. (Exception: For the LUSC detail, use 36 in. from the ledge of the inverted tee cap beam.) |
| “U” shaped confinement steel | #6 Grade 60 reinforcing bar at the maximum spacing of 6 in. |

6.3.4 Detailing Requirements

In addition to designing the appropriate quantities of unstressed strands and dowels bars, it is suggested that the following detailing requirements be met when designing the seismic connections between precast girders and a bent cap.

- Polypropylene fibers as used in the third test unit (i.e., BASF M100 micro fiber added at 0.5 lbs. per cubic yard and BASF MAC MATRIC macro fibers added at 3.0 lbs. per cubic yard) are recommended to be added into the concrete mix to control the cracking in the cap beam and diaphragm.
- When the strands are cut loose from the bulkheads of the stressing bed, the release of prestressing strands may unravel the extended portion, which can be prevented by placing a small diameter pipe around the strands.
- The extended strands must be anchored in the bent cap to provide a reliable tension transfer mechanism to fully develop the strength of the strands. The experimental studies have demonstrated that the following details provide sufficient anchorage:

- Strand with a 90 degree bent
- Straight strand grouted inside a corrugated duct,
- Strand splice chuck, or
- Strand chuck consisting of a bearing plate, a barrel anchor, and wedges.

The suggested embedment lengths for the anchorage details are summarized in Table 6.9 according to a series of pull-out tests conducted at Iowa State University.

Table 6.9: Suggested embedment length for extended strand

| Strand Embedded in Concrete | | |
|---------------------------------|------------------|--|
| Nominal diameter, in. | Anchorage detail | Embedment length |
| 0.375 | 90-degree bend | Greater than 42 in. with 6 in. beyond the bent |
| 0.5 | | Greater than 56 in. with 6 in. pre-bent length |
| 0.6 | Strand Chuck | Greater than 18 in. |
| 0.6 | Bond head | Greater than 22 in. |
| Strand Embedded in Grouted Duct | | |
| Nominal diameter, in. | Anchorage detail | Embedment length, in. |
| 0.375 | Straight | 48 in. |

- Additional diaphragm stirrups (“U” shaped confinement steel) are recommended to be detailed to fit alongside the girder web and between the top and bottom girder flanges to confine the concrete surrounding the dowel bars and prevent spalling on the front face of diaphragm.
- The dowel bars are to be placed through the interface between the side of girder and the surrounding diaphragm to activate the shear friction mechanism providing positive moment resistance. The holes are to be blocked out transversely through the web of precast girder. The dowel bars are recommended to be grouted through the holes in the field to avoid damage or fracture of the dowels during fabrication and transportation.

- To activate the shear friction mechanism, the dowel bars need to be properly anchored into the diaphragm surrounding the end of girder. For the external girder, which typically will have insufficient spacing at the external side of girder, headed bars can be used to fully develop the dowel anchorage despite the reduced embedment length.
- Embedment of a steel angle at the bottom edge of the girder end could prevent spalling of girder cover concrete due to gap opening and closing at the connection interface. A steel angle could also be positioned adjacent to the girder plate in the bent cap to prevent spalling of the cap cover concrete as shown in Figure 6.17.

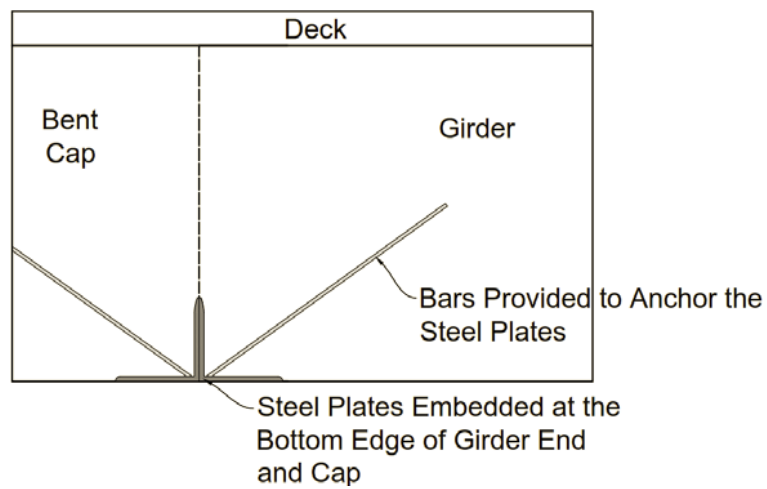


Figure 6.17: Location of steel angles in girder and cap beam

Chapter 7. Conclusions and Benefits

7.1 Overview

The overall goal of the research presented herein was to investigate different cap beam connections for precast girders used for integral bridges. The work included the development of connection details for I-girders and bulb tee girders along with analytical and experimental verifications of the overall moment resistance and shear transfer capability of these details. A previous project had verified the bridge system analytically and experimentally (Snyder et al., 2011). However, limitations of that work prevented full quantification of the girder-to-cap connection details. The connection detail developed in that project was confirmed in this work, and new connection details for I-girders as well as bulb tee girders were investigated.

Previously, Caltrans has been understandably reluctant in incorporating accelerated bridge construction techniques utilizing precast components, based on the poor performance of precast structures in previous earthquakes. The poor performance has occurred primarily because of connection failures between precast components; precast building failures were evident in notable earthquake events such as Loma Prieta in 1989 (Housner and Thiel, 1990) and Northridge in 1994 (SEAOC, 2010).

Integral precast girder connections sufficient for large seismic demands will provide increased opportunity to incorporate ABC methods. A particular detail that provides the opportunity to utilize precast bridge girders is the inverted-tee bent cap. Dapped end I-shaped girders can quickly and easily be placed on a corbel of an inverted-tee cap beam. Previous Caltrans practice for this detail incorporates dowel bars through the girder ends and a cast-in-place diaphragm in the connection region to establish fixity. This detail provides significant negative moment capacity for vertical loads due to the continuity of the deck reinforcement through the connection. However, previous design practice often disregarded the positive moment capacity of the connection, since there were seldom any quantitative elements that provide tension continuity in the bottom half of the girder. The lack of positive moment capacity in the connection eliminates the possibility of designing for a column plastic hinge just below the superstructure. Having a plastic hinge region only at the bottom of the column increases the column moment and results in larger foundation requirements, making the use of precast girders less desirable in seismic regions than the cast-in-place bridge alternatives. Developing a robust girder-to-cap connection will

increase the usefulness of the inverted-tee concept in seismic regions and facilitate the ABC techniques.

Another option for ABC construction that provides the benefits of a fixed superstructure connection is the use of precast girders with no dapped ends and a cast-in-place cap beam. Although falsework is needed to support the cap beam, a fixed connection can be achieved by extending prestressing strands from the girder into the cap beam and incorporating dowel bars through the girder ends. The extended strands and shear friction involving dowel bars provide positive moment resistance to the connection while negative moments are resisted by traditional deck reinforcement placed continuously over the girders and cap beam. The fixed behavior of the connection then allows for the formation of a second plastic hinge at the top of the column, making the precast girder design detail economical and useful for facilitating ABC construction in seismic regions.

An additional limitation of the precast girder-to-cap connections is related to vertical acceleration effects. The current Caltrans Seismic Design Criteria (SDC) stipulates that a static vertical load equal to 25% of the dead load, applied upward and downward, needs to be incorporated for Ordinary Standard bridges where the site peak ground acceleration is 0.6g or greater (Caltrans, 2013). Where this acceleration must be considered, longitudinal side mild reinforcement in the girders must be capable by means of shear friction of resisting 125% of the dead load shear at the cap beam interface. This requirement, which exists to protect against potential shear failures when the bottom of the connection opens up under positive moment loading, has been disadvantageous in utilizing the inverted-tee system, because it is almost impossible to incorporate the mild reinforcement in the precast girders since it causes steel congestion. Verifying the necessity of this requirement would be helpful in understanding the usefulness of the inverted-tee detail in seismic regions.

To examine the suitability of the precast girder systems for accelerated bridge construction in seismic regions, this study has considered several different girder-to-cap connection details for both I-shaped and bulb tee precast girders. The study has utilized analytical work from a previous Caltrans study (Snyder et al., 2011), additional analysis, and several large-scale experimental tests. The study has shown that appropriate connection details can indeed make precast girders designed for accelerated bridge techniques a viable option for integral bridges in high seismic regions, without needing any additional side reinforcement in the girders.

7.2 Summary of Connection Test Results

The tests of the girder-to-cap connection details progressed well. The test setup worked well to verify and quantify the seismic capabilities of the various details considered. While all the details were shown to be viable approaches for providing seismically-adequate integral connections between cap beams and precast concrete girders, the tests did provide insight into advantages and disadvantages of the various approaches. Summaries of the tests of the different details are provided in the following sections.

7.2.1 I-Girder and Inverted-Tee Cap Beam

The first test unit was constructed with the deepest California I-girders and a precast cap beam at 50% scale with the GUSC and LUSC connections. The GUSC connection, shown in Figure 7.1, included continuous deck reinforcement for negative moment tension continuity. In addition, unstressed strands passed through the girder-to-cap interface in the region of the girder bottom flange to provide positive moment tension continuity. Dowel bars oriented transversely and passing through the girder web into the cap beam diaphragm were also incorporated based on the existing Caltrans detail to provide increased shear friction resistance for positive moment resistance. The LUSC connection, shown in Figure 7.2, also utilized deck reinforcement for negative moment resistance; however, it did not include the continuous unstressed strands but rather utilized four dowel bars confined by looped unstressed strands to provide increased shear friction for the positive moment resistance.

GUSC Connection

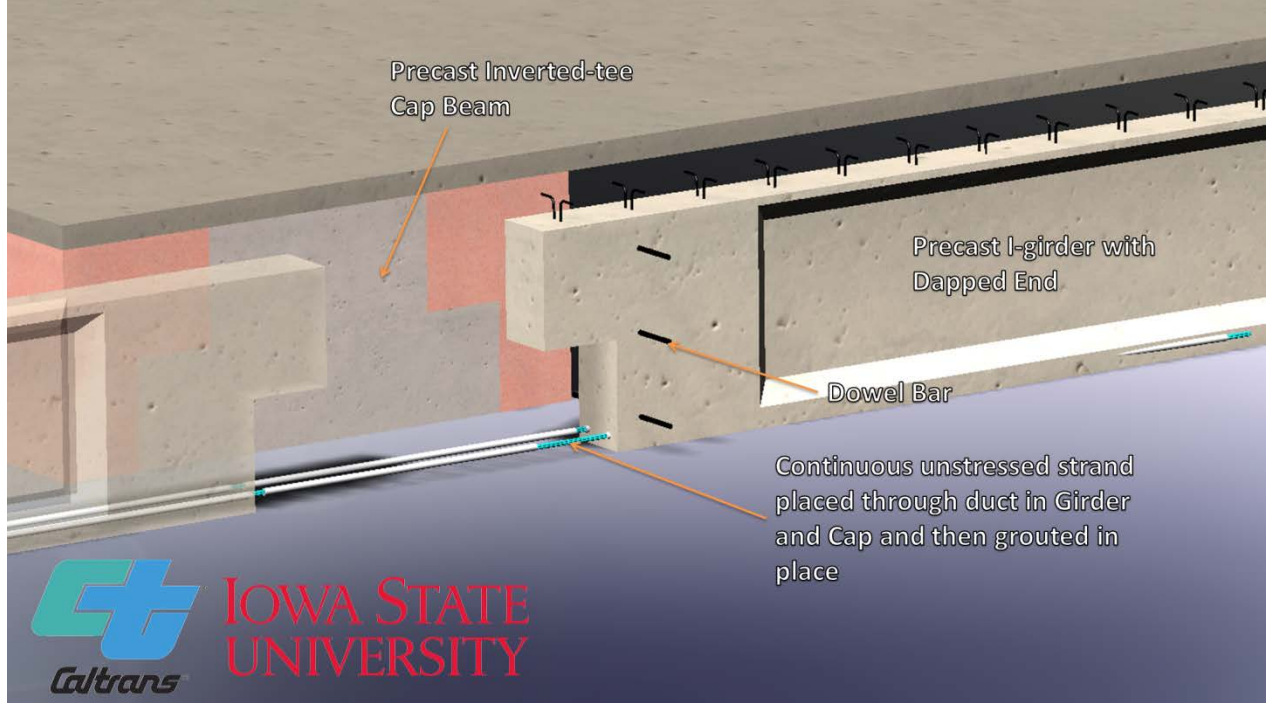


Figure 7.1: GUSC Connection Detail

LUSC Connection

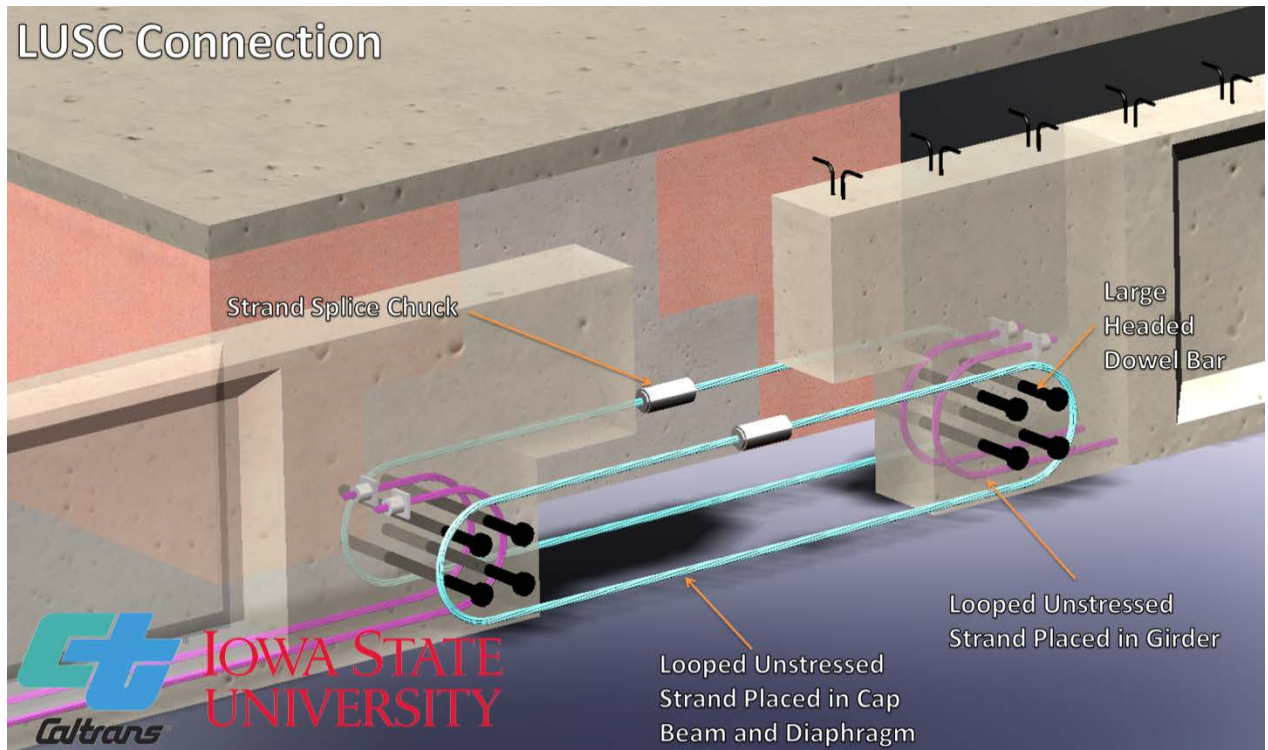


Figure 7.2: LUSC Connection Detail

The construction and experimental tests for both the GUSC and LUSC details progressed smoothly. Both details were shown to be constructible, and both details exhibited successful seismic performance up to load conditions simulating gravity load, large horizontal seismic displacements of the bridge superstructure, and large magnitudes of vertical acceleration, well beyond the design vertical acceleration of 0.25g suggested in Caltrans' SDC (Caltrans, 2013). Specific comparisons of the two details are summarized in the following two sections.

7.2.1.1 GUSC Detail

The GUSC detail remained elastic during testing for positive moment magnitudes considerably higher than the expected girder-to-cap connection moment due to gravity load (G) and column overstrength moment under horizontal seismic acceleration (H). The elastic behavior was also maintained when shear and moment related to 0.5g and 1.0g vertical seismic accelerations were added to the load corresponding to G + H, despite the fact that Caltrans' SDC only suggests 0.25g vertical acceleration as a target. In addition, adequate shear resistance of the connection was verified by exposing the connection to large-magnitude displacements in both the positive and negative moment directions, including the incorporation of shear forces that were much larger than an equivalent prototype structure would be expected to experience under realistic gravity, horizontal, and vertical seismic loads. The connection maintained full shear resistance throughout the duration of the test and showed considerable ductility in maintaining moment capacity up to displacements at least three times as large as the yield displacements in both the positive and negative moment directions.

The unstressed strand detail utilized in the GUSC test verified that sufficient strand anchorage for the girder-to-cap connections can be accomplished while terminating the strand within the girder span. Terminating the strands in the span rather than running the strands continuously through the girder bottom flange, as used in the system test (Snyder et al., 2011), may be desirable to simplify the construction process. Furthermore, despite the use of unstressed strands in the connection, its full tension capacity was successfully developed.

Examination of the data from the GUSC test revealed that the dowel bars and strand in the GUSC detail acted together to resist the positive moment. The combined shear friction and strand mechanism increased the positive moment resistance by about 1.7 over what would be expected from the strand mechanism alone. Hence, retaining the dowel bars in the precast girder connection is recommended.

Overall, the GUSC connection showed fully elastic behavior and only minimal cracking at the load level simulating the $G + H + 0.5g$ vertical acceleration condition, clearly indicating its suitability for capacity design in high seismic regions. Its eventual failure mode was the fracture of one of the unstressed strand pairs in the girder-to-cap interface. This failure occurred in the positive moment loading direction at a load level equivalent to $G + H + 1.4g$ vertical acceleration. Prior to the failure, the connection reached a negative moment load level equivalent to approximately $G + H + 4.0g$ vertical acceleration.

7.2.1.2 LUSC Detail

The LUSC detail produced slightly larger positive and negative moment capacities than the GUSC. Similar to the GUSC, the elastic positive moment capacity was considerably larger than the expected connection moment corresponding to the $G + H$ load condition. Also, elastic behavior was maintained when the connection was subjected to shear and moment corresponding to $G + H + 0.5g$ vertical acceleration and $G + H + 1.0g$ vertical acceleration. As with the GUSC detail, adequate shear resistance of the connection was verified by applying large-magnitude displacements in both the positive and negative moment directions. These loadings included shear forces that were much larger than an equivalent prototype structure would experience under realistic gravity, horizontal, and vertical seismic loads. The connection maintained full shear resistance throughout the duration of the test. It exhibited considerable ductility in maintaining moment capacity up to displacements three to four times as large as the yield displacements in both the positive and negative moment directions.

Overall, the LUSC connection showed fully elastic behavior and only minimal cracking at the load level simulating the $G + H + 0.5g$ vertical acceleration condition, clearly indicating its suitability for capacity design in high seismic regions, similar to the GUSC connection. Its eventual failure mode was the failure of the diaphragm concrete providing anchorage for the dowel bars and looped strands in the connection region. The maximum load levels reached in the LUSC connection were approximately equivalent to $G + H + 1.6g$ vertical acceleration under positive moment loading and $G + H + 4.2g$ vertical acceleration under negative moment loading.

7.2.2 Bulb-Tee Girder and Cast-in-Place Cap Beam

The second and third test units were designed using the deepest bulb-tee girders used in bridge design practice in California. The second unit utilized the ESBF and ESSP connections, while the third unit incorporated the ESMS and ESLS connections. All the connections were successfully constructed and tested at 40% scale. The connections performed well and each connection was able to resist the moment and shear values corresponding to a combined load of $G + H + 0.5g$ vertical acceleration, despite the fact that Caltrans' SDC only recommends use of $0.25g$ vertical acceleration. The moment resistance of each detail showed that bulb-tee girder connections have adequate capacity to resist high seismic forces and can be designed as fixed connections. Additionally, each connection had sufficient shear and moment capacity at vertical acceleration values substantially above $0.25g$, suggesting that the additional longitudinal reinforcement required by Caltrans SDC is unnecessary.

7.2.2.1 ESBF Detail

The ESBF connection, shown in Figure 7.3, incorporated extended strands bent at 90 degrees with a development length of 60 in. for $3/8$ " diameter strand. The connection remained elastic up to $G + H + 0.5g$ vertical acceleration with minimal cracking. The ultimate capacity of the connection corresponded to $G + H + 1.68g$ vertical acceleration in the negative moment direction and $G + H + 1.0g$ vertical acceleration in the positive moment direction. The failure mechanism of the ESBF connection was fracture of the extended strands which validated that for a $3/8$ in diameter bent strand an embedment length of 60 in. was sufficient. When 0.5-in. and 0.6-in strands are used with a minimum concrete compressive strength of 4.5 ksi, the embedment lengths of 78.5 in. and 93 in. may be used respectively.

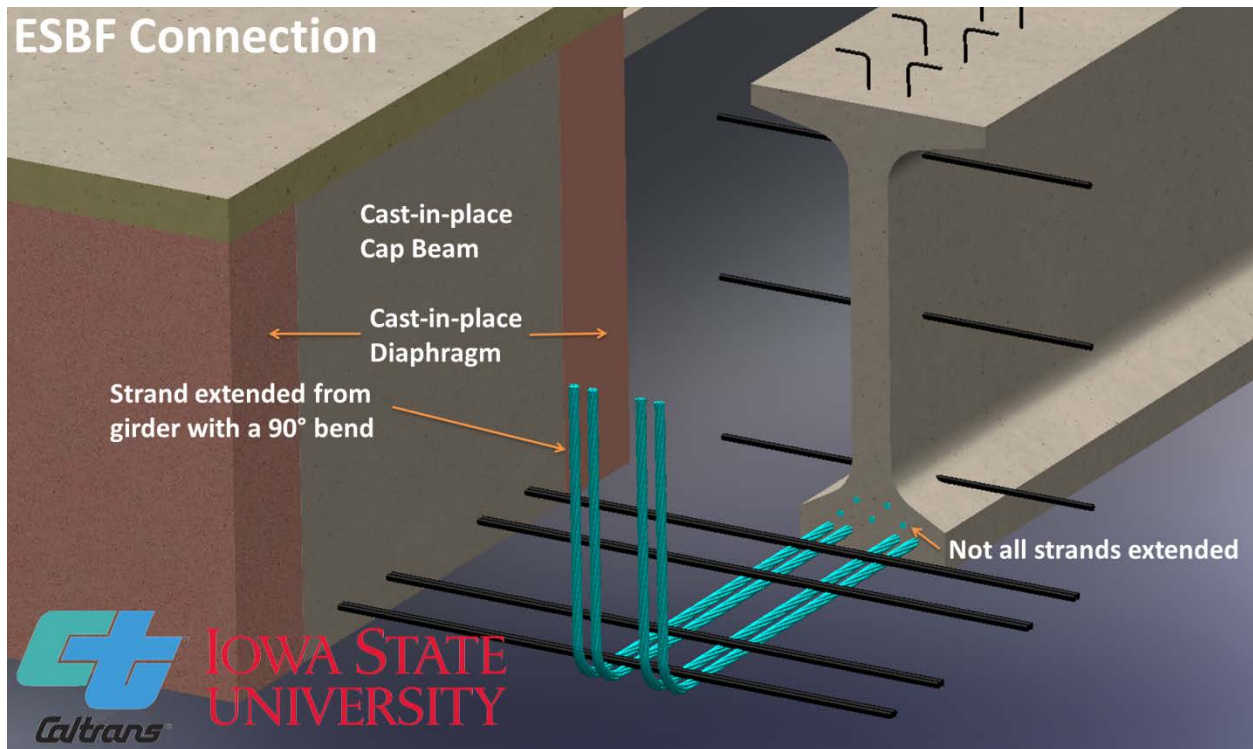


Figure 7.3: ESBF Connection Detail

7.2.2.2 ESSP Detail

The ESSP connection utilized strands anchored with plates and chucks at the end of the extended strands and lap splicing with a similar detail on the extended strands coming from the opposite girder, as shown in Figure 7.4. This connection had slightly less capacity than the ESBF connection. It is thought that the difference in capacity is likely due to the mechanical malfunction at the beginning of the test which resulted in overloading of the connection. At the load level corresponding to $G + H + 0.5g$, the connection remained elastic with minimal cracking. The ultimate capacity of connection in the positive moment direction was $G + H + 0.72g$ vertical acceleration, with a negative moment ultimate capacity of $G + H + 1.46g$. The failure of the connection was due to a combination of two events. First, spalling of the cap beam cover concrete occurred adjacent to the girder due to the absence of cap stirrups under the top flange of the girder. The absence of stirrups in this region resulted in a large volume of unconfined concrete around the dowel bars. The concrete in this region eventually spalled after being damaged due to the girder pulling this concrete out, which exposed the dowel bars and reduced the capacity of the connection. Second, crushing of the lower concrete at the bottom end of the girder occurred, which reduced

the lever arm associated with both positive and negative moment resistance and tension development in the strands and deck steel, respectively.

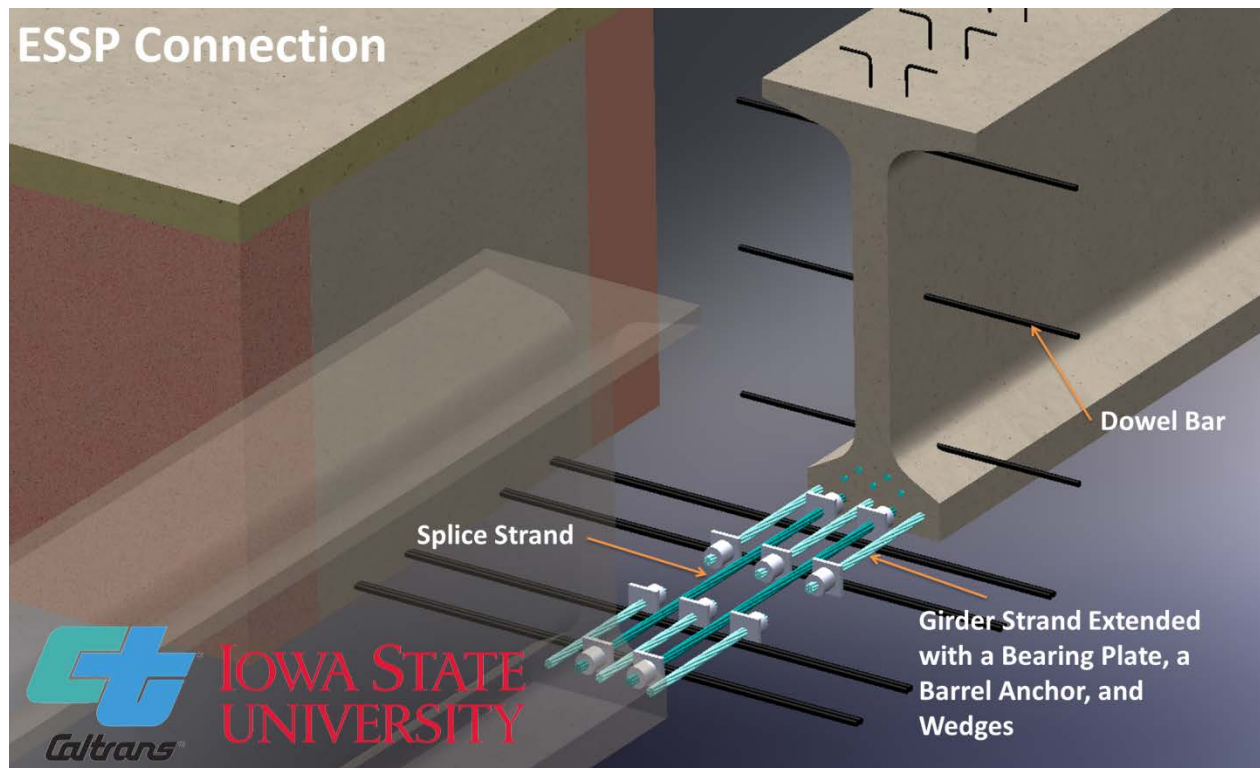


Figure 7.4: ESSP Connection Detail

The behavior of the strand splices was examined throughout the test, and it was observed that the extended strands did not transfer force through the lap splices as was previously purposed but instead experienced very low strains. It appeared that the force in the extended strands was sufficiently anchored by the attached plate and chuck. Therefore, the strand ties which form the splices with the extended strands are not necessary to include in the connection design, as long as the end plate is located 14 in. (test-unit scale) into the cap beam and anchored into the core concrete of the cap beam.

7.2.2.3 ESMS Detail

The ESMS connection, shown in Figure 7.5, was designed with strand splice chucks that connected strands which extended from girders on each side of the cap beam as well as the same dowel bar layout utilized in the ESSP and ESBF connections. The ESMS connection had sufficient capacity to resist shear and moment demands expected for the connections under combined

gravity, horizontal seismic and vertical acceleration effects. Assuming that the maximum design vertical acceleration would not exceed 0.5g, the ESMS connection was designed with optimum connection reinforcement. The ESMS connection reached a maximum positive moment of 300 kip-ft (a load equivalent to $G + H + 0.7g$ vertical acceleration) and a maximum negative moment of -1124 k-ft (equivalent to $G + H + 1.75g$ vertical acceleration). The connection remained elastic with minimal cracking up to the load level corresponding to $G + H +$ vertical accelerations of 0.4g and 1.0g applied in the positive and negative moment directions, respectively.

Overall, the maximum negative moment reached by ESMS connection was slightly higher than the ESBF connection, but the maximum positive moment of the ESMS connection was 100 k-ft lower than the ESBF connection. This reduction resulted from the reduced number of extended girder strands. (Four 3/8 in. diameter strands were used in the ESMS connection, while five 3/8 in. diameter strands were used in the ESBF connection.) The positive moment capacity of the ESMS connection may have been slightly reduced due to unraveling of the extended girder strands which occurred during the fabrication process of the precast girders.

Failure of the ESMS occurred due to spalling of the cap concrete which was caused by rotation of the girder at high displacements beyond $G + H + 0.5g$ vertical acceleration. Under displacements in the negative moment direction, cover concrete spalled at the bottom of the girder to cap interface which resulted in an upward shift of the compressive region and subsequent shortening of the negative moment lever arm. Under positive moments spalling of the cap cover concrete adjacent to the sides of the girder allowed girder pullout and subsequent loss of shear friction moment resistance.

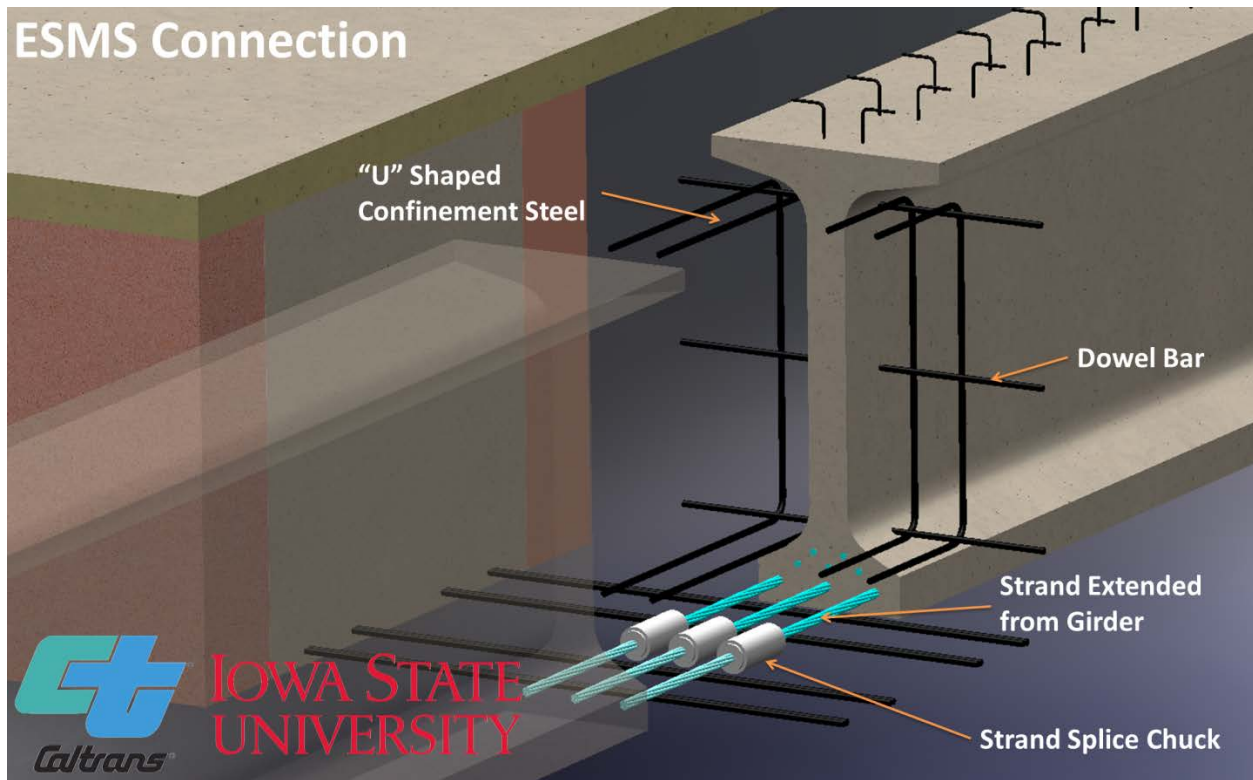


Figure 7.5: ESMS Connection Detail

7.2.2.4 ESLS Detail

The ESLS connection, shown in Figure 7.6, was similar to the ESMS connection except it utilized lap splices for the extended strands to provide positive moment continuity, similarly to the ESSP connection. The ESLS connection performed slightly better than the ESMS connection under positive moment demands and had sufficient capacity to resist the shear and moment demands expected for the connections under combined gravity, horizontal seismic and vertical acceleration effects. This connection reached a maximum positive moment of 387 k-ft (equivalent to $G + H + 0.95g$ vertical acceleration) and a maximum negative moment of -1158 k-ft (equivalent to $G + H + 1.75g$ vertical acceleration). Additionally, the ESLS connection remained elastic with minimal cracking up to the load level corresponding to $G + H + 0.5g$ vertical acceleration. In comparison, the ESLS connection reached the maximum negative capacity values very close to the previously tested ESMS connection, and the maximum positive moment of the ESLS connection was 87 k-ft higher than the ESMS connection. This improvement in positive moment performance may be related to the unraveling of the extended strands in the ESMS connection.

Failure in the ESLS connection occurred in a similar manner to the ESMS connection under high displacements beyond the vertical acceleration capacity of 0.5g. In the negative moment

direction, crushing at the bottom of the girder to cap interface again resulted in a reduced lever arm and drop in connection strength. In the positive moment direction the girder pull out and loss of shear friction resulted in high strains in the extended strands and ultimately led to fracture of the strands.

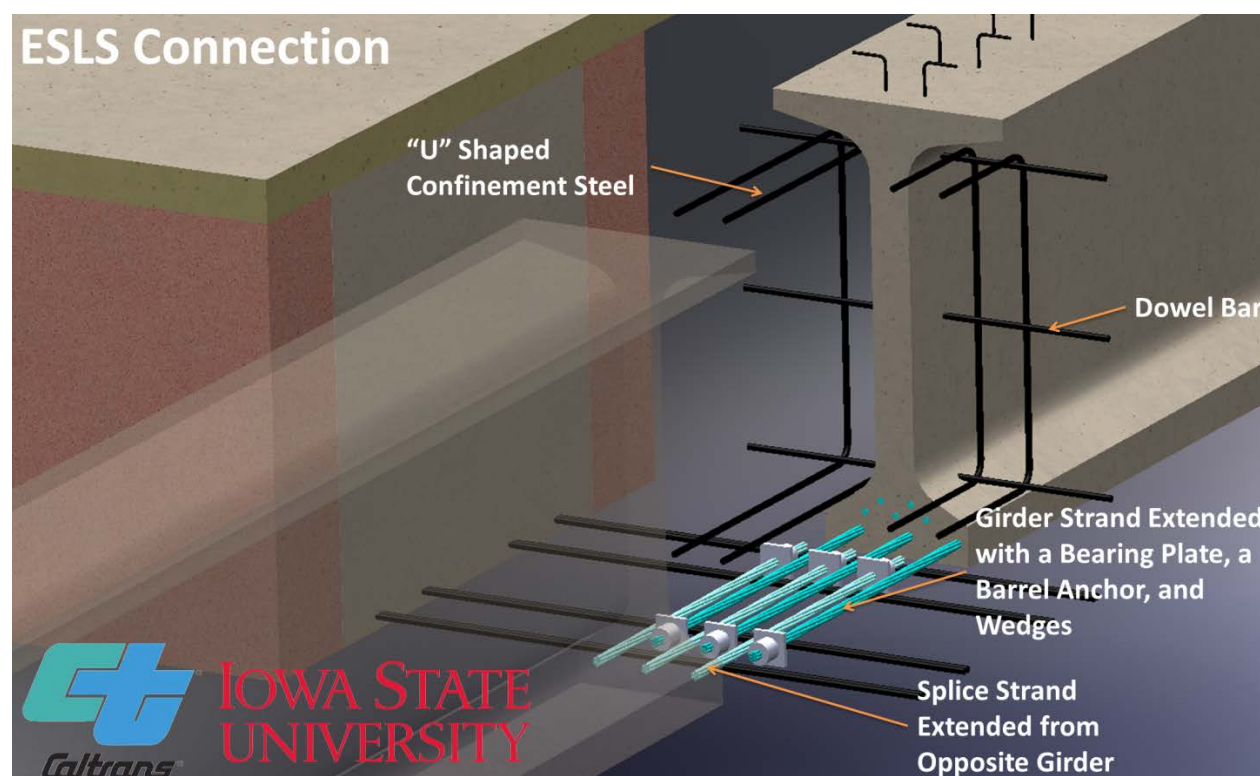


Figure 7.6: ESLS Connection Detail

7.3 Conclusions

In addition to the experimental summary presented for each of the ABC seismic connections between the precast girder and cap beam, the following conclusions can be drawn from the completed study which included complimentary analytical work to understand the response of various connections:

- All the connection details used between precast girder and cap beam performed well experimentally. The details provided strength well in excess of the expected connection shear and moment levels at the column overstrength condition due to horizontal seismic loading. All the details were shown to maintain elastic superstructure behavior at shear and moment levels beyond the maximum moment demand expected during horizontal seismic loading.

- Girder-to-cap connection details were established in this study for both precast I-girders and precast bulb-tee girders. The successful response of the connection details confirmed that the selected details are viable, structurally-sufficient ways to implement both girder types in high seismic regions. Both girder types offer alternatives to incorporating precast concrete girders and accelerated bridge construction techniques in regions that have been reluctant to do so currently because of poor performance of precast connections in past earthquakes.
- When combined with extended strands for the purpose of positive moment resistance, the shear friction mechanism determines the initial stiffness of the connection as well as a large portion of the corresponding moment resistance until a specified shear friction displacement of 0.025 in. is reached at the lowest dowel bar location. Beyond the displacement of 0.025 in., the capacity of the connection is influenced by the number of extended prestressing strands. The connection will continue to gain strength until either the yielding of the strands occur or the ultimate shear displacement of 0.27 in. is reached at the lowest dowel bar location.
- The size and number of dowel bars used in a connection region should be determined at the yield limit state of the connection. The required quantity of unstressed strands may be estimated with considerations to the shear friction as detailed in Section 6.3.
- The number of extended strands used in the connection region should be determined by the design ultimate moment demand of the connection. The shear friction will account for a specified moment capacity but the strength of the connection beyond yield is determined by the number of extended strands.
- If the precast I-girder or bulb-tee girder does not include an end block or dapped end at the girder-to-cap interface, additional cap beam or diaphragm stirrups should be detailed to fit alongside the girder web and in between the top and bottom girder flanges at the connection interface to prevent spalling.
- Macro and micro concrete fibers as used in the third test unit according to recommendations from Caltrans and controlled cracking of the bridge deck under negative moments. However, no additional benefit was found in relation to the prevention of spalling or crushing due to the rotation of the girder under negative moments.

- Since the shear friction generated by the dowel bars in the diaphragm is a critical part of the positive moment transfer mechanism, similar proportions as were utilized in this work are recommended for the dowel bar locations in all the girder-to-cap connections. For the LUSC detail, similar proportions to this work should be maintained for the spacing of the dowel bars inside the looped strand.
- Miscellaneous conclusions related to the construction of these connections include:
 - High strength, precision, fluid, non-shrink grout ($f'_c = 8500$ psi) pumped into the strand ducts provided sufficient anchorage to fully develop the strength of the strand and provide a reliable tension transfer mechanism in the connection.
 - For connection details with grouted strand ducts across the connection interface, the duct must be completely sealed to ensure proper grouting.
 - Engineered wire mesh reinforcement can serve as an acceptable substitute to traditional shear reinforcing bars in precast girders used in integral bridge superstructures. This has been demonstrated with casting of both I-girders and bulb-tee girders.
 - Embedment of a steel angle at the bottom edge of the girder end could prevent spalling of girder cover concrete due to gap opening and closing at the connection interface. A steel angle could also be positioned adjacent to the girder plate in the cap beam to prevent spalling of the cap cover concrete as shown in Figure 7.7.

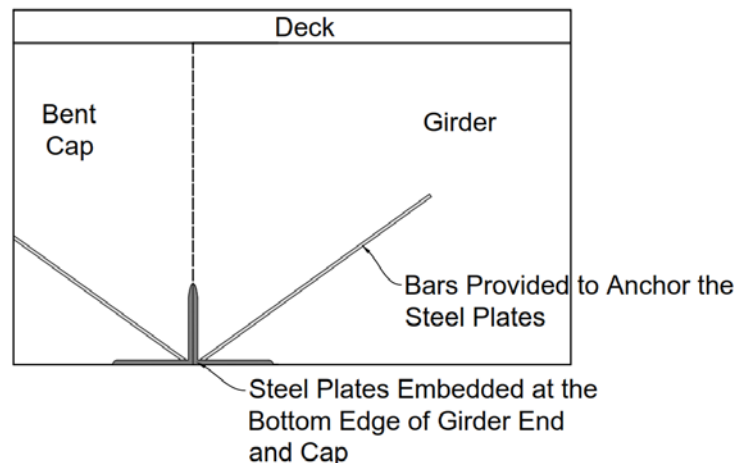


Figure 7.7: Location of steel angles in girder and cap beam

7.4 Benefits of Research Results

The research completed in this report provides several benefits. These benefits range from providing good understanding of the seismic performance of California bridges that are designed with precast girders and an inverted-tee or rectangular bent cap to improving design efficiencies to ensuring safety of precast bridges when subjected to seismic motions. Some of the notable benefits can be summarized as follows:

- Presents multiple options for precast girder-to-cap beam connections in seismic regions such that precast options can be incorporated competitively in comparison to a cast-in-place alternative, thereby promoting ABC in California.
- Provides large-scale experimental validations for all suggested connections, ensuring safe responses of bridges designed with recommended connection details.
- Details the force transfer mechanisms associated with the moment resistance of the connection, which allows connection reinforcement to be quantified while promoting the development of other connection alternatives.
- Validates that the suggested connections can withstand vertical accelerations equivalent to 0.5g in addition to the demand due to gravity and horizontal seismic motions, eliminating the need for placing special reinforcement in the girder as per the current recommendations (SDC Section 7.2.2).
- Presents analysis models that can be used to satisfactorily produce the expected performance of the precast girder-to-cap beam connections.
- Proposes the use of unstressed prestressing strands in connection design, in particular those extended from prestressed girders as it reduces costs and improves construction flexibility.
- Includes recommendations to design positive moment connections between precast girders and cap beams.

References

- AASHTO. (2003). *LRFD bridge design specifications, 3rd Ed.* Washington, D.C.
- AASHTO. (2011). *US 6 Keg Creek Bridge*. Retrieved October 2012, from America's Transportation Awards:
<http://www.americastransportationaward.org/Default.aspx?ContentID=250>
- AASHTO (2012). *LRFD Bridge Design Specifications*. Washigton, DC: American Association of State Highway and Transportation Officials.
- Abrahamson, N. A., and Silva, W. J. (1997). "Empirical Response Spectral Attenuation Relations for Shallow Crustal Earthquakes." *Seismological Research Letters*. 68(1): 94-127.
- Ambraseys, N. N., Simpson, K. A., and Bommer, J. J. (1996). "Prediction of Horizontal Response Spectra in Europe." *Earthquake Engineering and Structural Dynamics*. 25, 371-400.
- Ambraseys, N., and Douglas, J. (2000). "Reappraisal of the effect of vertical ground motions on response," *Engineering Seismology and Earthquake Engineering*, ESEE Report No. 00-4, August 2000.
- Ambraseys, N. N., and Douglas, J. (2003). "Near-field horizontal and vertical earthquake ground motions," *Soil Dynamics and Earthquake Engineering*, 23(1), 1-18.
- ACI Committee 318. (2011). *ACI 318-11: Building Code Requirements for Structural Concrete and Commentary*. Farmington Hills, MI: ACI.
- Bommer, J. J., Akkar, S., and Kale, O. (2011). "A Model for Vertical-to-Horizontl Response Spectral Ratios for Europe and the Middle East." *Bulletin of the Seismological Society of America*, 101(4), pp. 1783-1806, August 2011.
- Boroscheck, R., Soto, P., Leon, R., & Comte, D. (2010). "Preliminary Report No. 4 of National Strong Motion Observation Net." *Chile Earthquake of February, 27, 2010*.
- Caltrans. (2003). *Bridge Design Specifications*. Sacramento, California.

- Caltrans. (2006). *Seismic Design Criteria*. Sacramento, California.
- Caltrans. (2006). *Seismic Design Criteria, v. 1.4*. Sacramento, California.
- Caltrans. (2011). *Bridge Design Practice Manual*. Sacramento, California: Caltrans. Online: <http://www.dot.ca.gov/hq/esc/techpubs/manual/bridgemanuals/bridge-design-practice/bdp.html>. Accessed August 2012.
- Caltans. (2012). *Bridge Design Aids*. Sacramento, California.
- Caltrans. (2013). *Seismic Design Criteria, Version 1.7*. Sacramento, California.
- Caltrans. (2014, June). *Seismic Retrofit Program*. Retrieved December 13, 2014, from California Department of Transportation: About Caltrans: <http://www.dot.ca.gov/hq/paffairs/about/retrofit.htm>
- Chen, W. F. and Lian Duan. (2014). *Bridge Engineering Handbook, Second Edition: Construction and Maintenance*. Boca Raton, Florida: CRC Press.
- Federal Highway Administration. (2006). *Rapid Bridge Construction: How to Get There*. Retrieved October 2012, from 2006 Concrete Bridge Conference Workshop: <http://www.fhwa.dot.gov/bridge/prefab/pbesreport.cfm>
- Federal Highway Administration. (2009, February/March). Accelerated Bridge Construction Picks Up Steam. *Innovator: Accelerating Innovation for the American Driving Experience*, 2(11). Retrieved October 2012, from *Innovator: Accelerating Innovation for the American Driving Experience*, Volume 2, Issue 11, February/March, U.S. Department: <http://www.fhwa.dot.gov/hfl/innovator/pdfs/issue11.pdf>
- Federal Highway Administration. (2010). *Fact Sheet 16 - States Across the Country Implement Accelerated Bridge Construction*. Retrieved October 2012, from Publication No. FHWA-HOP-11-006, U.S. Department of Transportation: <http://www.ops.fhwa.dot.gov/wz/practices/factsheets/factsheet16/index.htm>

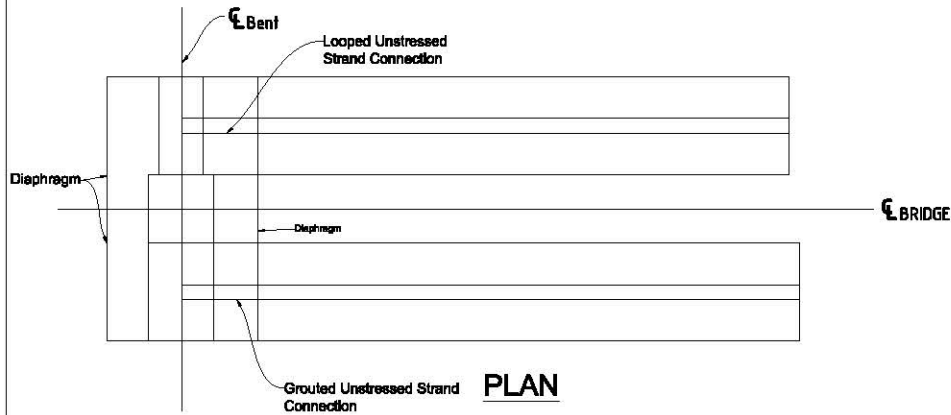
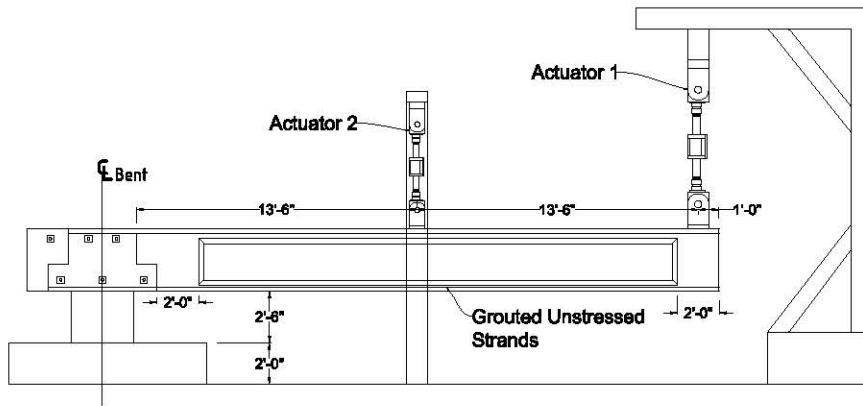
- Federal Highway Administration. (2010, September). *FHWA Bridge Conference Spotlights Opportunities and Successes in Accelerated Bridge Construction*. Retrieved August 2012, from Publication No. FHWA-HRT-10-017, U.S. Department of Transportation: <http://www.fhwa.dot.gov/publications/focus/10sep/01.cfm>
- Federal Highway Administration. (2012). *ABC/PBES Costs*. Retrieved December 2012, from Prefabricated Bridge Elements and Systems, U.S. Department of Transportation: http://www.fhwa.dot.gov/everydaycounts/technology/bridges/pbeswebinartraining/s2_m4.cfm
- Federal Highway Administration. (2009). Connection Details for Prefabricated Bridge Elements and Systems. *Publication No. FHWA-IF-09-010*.
- Florida International University. (2014). *2014 National Accelerated Bridge Construction Conference*. Retrieved December 13, 2014, from Florida International University: <http://2014abc.fiu.edu/>
- Gulerce, Z., and Abrahamson, N. N. (2011). "Site-specific spectra for vertical ground motion," *Earthquake Spectra*, 27(4).
- Harries, K. A., Zeno, G., & Shahrooz, B. (2012). Toward an Improved Understanding of Shear-Friction Behavior. *ACI Structural Journal*, 835-844.
- Hastak, M., Mirmiran, A., Miller, R., Shah, R., & Castrodale, R. (2003). State of Practice for Positive Moment Connections in Prestressed Concrete Girders Made Continuous. *Journal of Bridge Engineering*, 8(5), 267-272.
- Hida, Sue. (2012). "California Department of Transportation's Next Generation Bridges." Report presented at the Fourth Kwang-Hua Forum, Opening Symposium of the Tongji Shaking Table Array, Shanghai, China.
- Holombo, J., Priestley, M. N., & Seible, F. (1998). *Longitudinal Seismic Response of Precast Spliced-Girder Bridges*. San Diego: University of California, San Diego.

- Housner, G. W., & Thiel, C. C. (1990). *Competing Against Time: Report of the Governor's Board of Inquiry on the 1989 Loma Prieta Earthquake*. Earthquake Spectra.
- International Federation of Structural Concrete. (2007). *Seismic Bridge Design and Retrofit - Structural Solutions (Volume 39)*. Lausanne, Switzerland: FIB.
- Iowa Department of Transportation. (2012). *U.S. 6 Bridge over Keg Creek*. Retrieved December 2012, from Iowa Department of Transportation:
<http://www.iowadot.gov/us6KegCreek/projectinfo.html>
- Kahn, L., & Mitchell, A. D. (2002). Shear Friction Tests with High-Strength Concrete. *ACI Structural Journal*, 99(1), 98-103.
- Kalkan, E. and Gulkan, P. (2004). "Empirical attenuation equations for vertical ground motion." *Earthquake Spectra*, 20(3), 853-882.
- Kalkan, E., and Sevilgen, V. (2011). "March 11, 2011 M9.0 Tohoku, Japan Earthquake," *USGS*, Accessed online: <http://nsmpr.wr.usgs.gov/ekalkan/Tohoku/index.html>.
- Kam, Weng Yuen and Stefano Pampanin. (2011). General Building Performance in the Christchurch CBD: a contextual report. Christchurch, New Zealand: University of Canterbury. Online: <http://www.dbh.govt.nz/UserFiles/File/Reports/quake-contextual-report-canterbury-uni.pdf>. Accessed October 2012.
- Khaleghi, B. (2012). Design Memorandum on Extended Strand Continuity Design. Washington: Washington State Department of Transportation.
- Kyaleghi, Bijan. "Washington State Department of Transportation Plan for Accelerated Bridge Construction" (2010). *Transportation Research Record: Journal of the Transportation Research Board*. Volume 2200, pages 3-11.
- Kostem, C. N., & Ragazzo, S. C. (1993). Grillage Analogy for Multigirder Bridges. *Computing in Civil and Building Engineering* (pp. 188-192). American Society of Civil Engineers.

- Marsh, M. L., Wernli, M., Garrett, B. E., Stanton, J. F., Eberhard, M. O., Weinert, M. D. (2011). *NCHRP Report 698: Application of Accelerated Bridge Construction Connections in Moderate-to-High Seismic Regions*. Washington, D. C.: Transportation Research Board.
- Mattock, A. H. (1979). "Design and Behavior of Dapped-End Beams." *PCI Journal*. Volume 24, No. 6. Chicago, Illinois: Prestressed Concrete Institute (PCI).
- Miller, R., Castrodale, R., Mirmiran, A., & Hastak, M. (2004). *NCHRP Report 519: Connection of Simple-Span Precast Concrete Girders for Continuity*. Washington, D.C.: Transportation Research Board.
- Ou, Y. C., M. Chiewanichakorn, A. J. Aref, G. C. Lee (2007). "Seismic Performance of Segmental Precast Unbonded Post-tensioned Concrete Bridge Columns." *Journal of Structural Engineering*, 133(11), 1636-1647. ASCE.
- Ou, Yu-Chen; Ping-Hsiung Wang; Mu-Sen Tsai; Kuo-Chun Chang; George C. Lee (2010). "Large-Scale Experimental Study of Precast Segmental Unbonded Posttensioned Concrete Bridge Columns for Seismic Regions." *ASCE Journal of Structural Engineering*, 136(3), 255-264.
- Papazoglou, A. J., and Elnashai, A. S. (1996). "Analytical and field evidence of the damaging effect of vertical earthquake ground motion," *Earthquake Engineering and Structural Dynamics*, Volume 25, 1109-1137.
- Patty, J., Seible, F., & Uang, C. (2002). *Seismic Response of Integral Bridge Connections*. University of California, San Diego, Structural Engineering. San Diego: University of California, San Diego.
- PEER. (2005). *Northridge Earthquake*. (R. o. California, Producer) Retrieved 2009 from Pacific Earthquake Engineering Research Center: <http://nisee.berkeley.edu/northridge/>
- Priestley, M. N., Seible, F., & Uang, C. (1994). *The Northridge Earthquake of January 17, 1994*. La Jolla: The University of California.

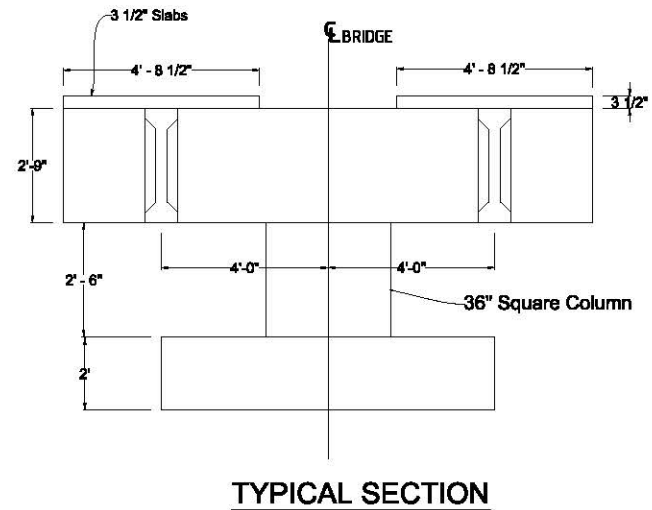
- Priestley, M., Seible, F., & Calvi, G. (1996). *Seismic Design and Retrofit of Bridges*. New York: John Wiley & Sons, Inc.
- Seismology Committee, S. E. (2010). *Seismic Design of Concrete Parking Structure Ramps. Structure*.
- Shoup, L. D. (2011). *The Fix We're In: The State of Our Nation's Bridges*. Washington, D.C.: Transportation for America.
- Snyder, R. (2010). *Seismic performance of an I-girder to inverted-t bent cap bridge connection*. Iowa State University. Ames, Iowa.
- Snyder, R., Vander Werff, J., Thiemann, Z., Sritharan, S., Holombo, J. (2011). *Performance of an I-Girder to Inverted-T Bent Cap Connection, Final Report*. Caltrans and Iowa State University. Sacramento, California and Ames, Iowa.
- Sritharan, S., Bromenschenkel, R., Vander Werff, J., and Peggar, R. (2013) "Two Alternate Connections for Integral Precast Concrete Girder Bridges in Seismic Regions." *Proceedings of the Seventh National Seismic Conference on Bridges and Highways*, Oakland, CA, May 2013.
- Sritharan, S., Vander Werff, J., Abendroth, R., Wassef, W., & Greimann, L. (2005). Seismic Behavior of a Concrete/Steel Integral Bridge Pier System. *Journal of Structural Engineering*, 131(7), 1083-1094.
- Takeda, T., Sozen, M. A., & Nielsen, N. N. (1970). Reinforced Concrete Response to Simulated Earthquakes. *Journal of the Structural Division Proceedings of the American Society of Civil Engineers*, 96(2), ST 12, 2557-2573.
- Tezcan, J., and Cheng, Q. (2012). "A nonparametric characterization of vertical ground motion effects." *Earthquake Engineering and Structural Dynamics*. 41(3): 515-530, March 2012.
- Thiemann, Z. (2010). *Pretest 3-D finite element analysis of the girder-to-cap-beam connection of an inverted-tee cap beam designed for seismic loadings*. Ames, IA: Iowa State University.

- Vander Werff, J., and Sritharan, S. (2015). "Girder Load Distribution for Seismic Design of Integral Bridges." *ASCE Journal of Bridge Engineering*. 20(1), 04014055-1-11.
- Veletzos, M. J. and Restrepo, J. I. (2014) "Equivalent Unbonded Length for Modeling of Multistrand Tendons in Precast Segmental Construction." *ASCE Journal of Bridge Engineering*. 19(1), 101-109.
- Veletzos, M. J., & Restrepo, J. I. (2011). Modeling of jointed connections in segmental bridges. *ASCE Journal of Bridge Engineering*, 16(1), 139-147.
- Yang, J., and Lee, C. M. (2007). "Characteristics of vertical and horizontal ground motions recorded during the Niigata-ken Chuetsu, Japan Earthquake of 23 October 2004," *Engineering Geology*, 94(1-2), 50-64, October 2007.



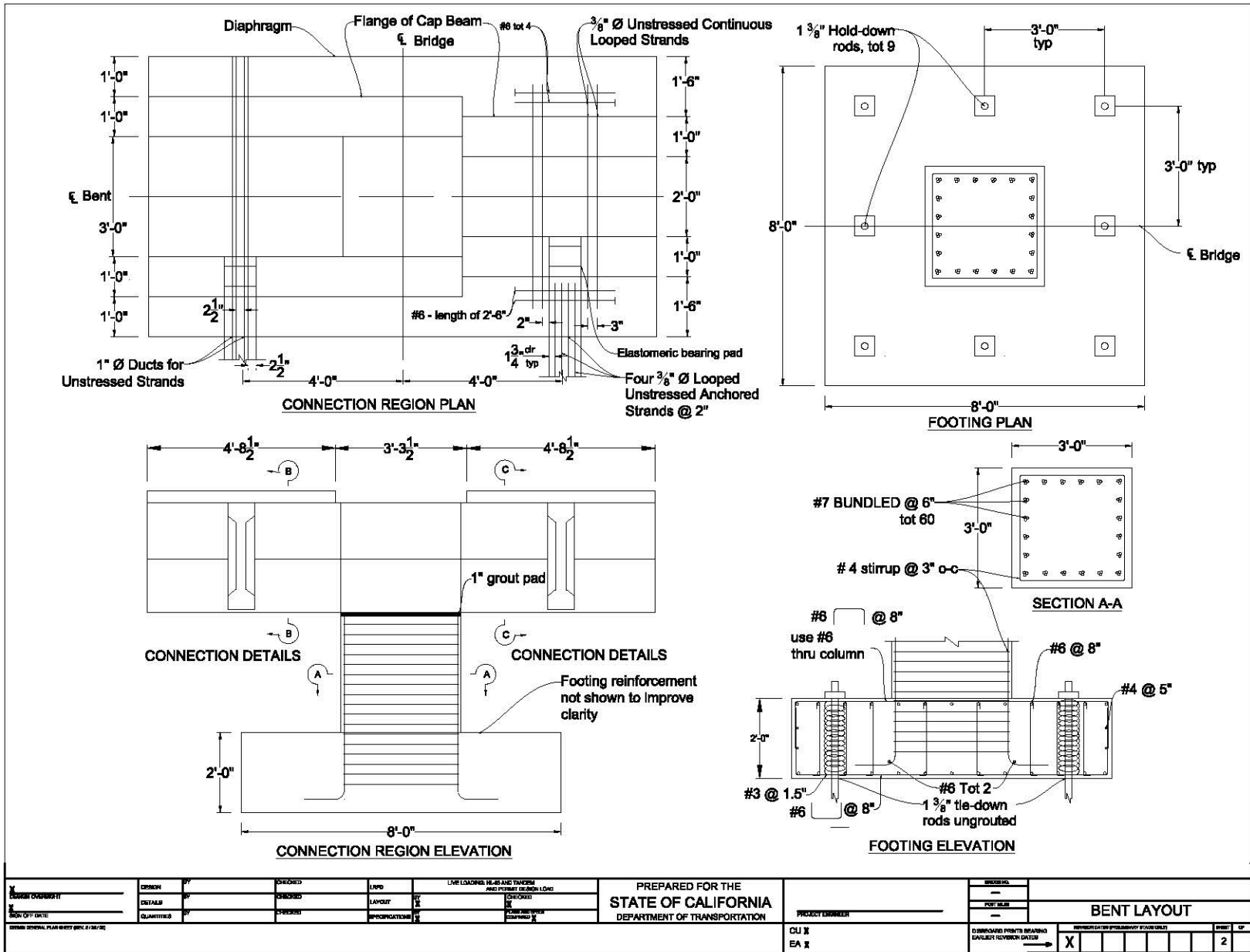
General Notes:

- Concrete Strength (28 days):** 5000 psi
- Steel:** Use A706 Grade 60 reinforcement and 270 ksi low-relaxation strands
- Minimum clearance:** Clearance between parallel reinforcing steel should be one inch or one bar diameter, whichever is greater
- Bent Cap Post-tensioning steel:** Six 1.0" Ø reinforcing bars
- Duct Grout:** High-strength, non-shrink, highly cementitious grout
- Cap-Column Connection Grout:** High-strength, non-shrink, highly cementitious grout with percentage of polypropylene fibers
- Provide (temporary) corrosion protection for stand loops prior to casting diaphragm



APPENDIX A
I-GIRDER TEST UNIT

| | | | | | |
|--|--------------------|---|-------------------------------------|-----------------|------------|
| Seismic Performance of Connections that Facilitate Accelerated Bridge Construction | Test Units 1 and 2 | PREPARED FOR THE STATE OF CALIFORNIA DEPARTMENT OF TRANSPORTATION | Charles Sikorsky PROJECT MANAGER | ISSUED FOR | 09-12-2012 |
| | | | | GENERAL PLAN | |
| CONTRACT #: 66A0411 PROJECT ID: 000001016 | | | DESIGNED BY/DATE | CHECKED BY/DATE | DATE |
| | | | X | | 1 |

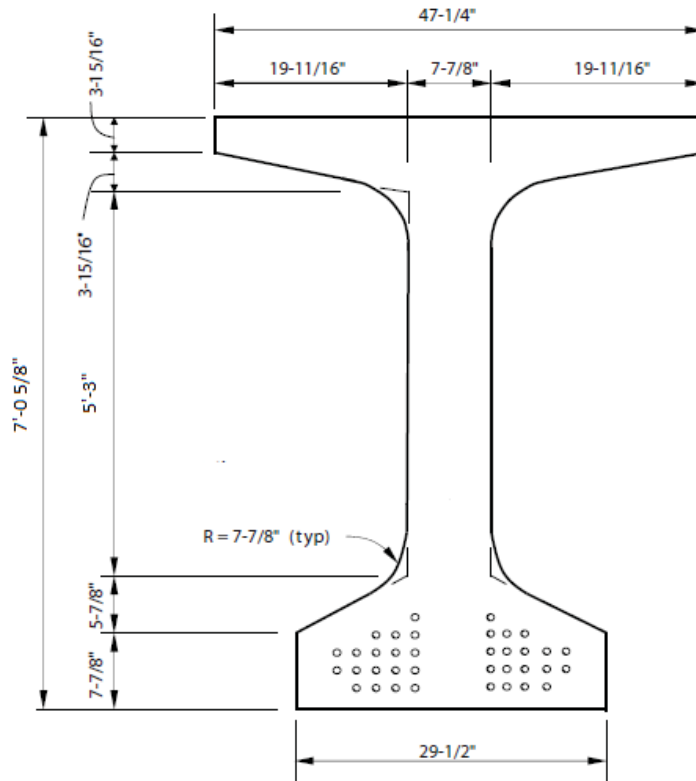


| | | | | | | | | | | | | | | | |
|--|---------|---------|----------|--------|------|---|--|--|----------|-------------------------------------|-----------------------------------|-------------|----|--|---|
| DESIGNER CHECKED DATE | DESIGN | BY | CHECKED | LAYOUT | DATE | LIVE LOADS, WINDS AND TRENDS AND FLOOR FINISH LOAD | PREPARED FOR THE STATE OF CALIFORNIA DEPARTMENT OF TRANSPORTATION | PROJECT NUMBER | DESIGNED | DATE | REVISIONS NO. DATE DESCRIPTION | BENT LAYOUT | | | |
| | DETAILS | BY | CHECKED | LAYOUT | DATE | | | | FOOTING | DATE | | | | | |
| QUANTITIES | BY | CHECKED | APPROVED | | | | | | | | | | | | |
| STANDARD GENERAL PLAN SHEET (SHEET NO. 2) OF 2 | | | | | | | | | | | | | | | |
| CU 2 EA 2 | | | | | | | | DISBURSED WEIGHTS BEARING ENGLISH FEET/INCH UNITS | | REPRESENTATION PROVISIONS FOR UNITS | | DATE | OF | | |
| | | | | | | | | | | X | | | | | 2 |

APPENDIX B
EQUATIONS AND CALCULATIONS

Deck steel equations for bulb-tee prototype:

For calculation purposes the bottom flange of the girder was treated as a rectangular flange with a height of 10.8 inches. The girder deck is 8" thick with the centroid of deck steel located 4" above the top of the girder.



Equation 4.3:

$$M_{neg} = A_s f_y \left(d - \frac{a}{2} \right)$$

M_{neg} = Negative design moment

A_s = Area of steel

f_y = yield strength of steel

d = depth from center of deck steel to bottom of girder

a = depth of compressive block

$$7150 * 12 \frac{\text{in}}{\text{ft}} = A_s * 66 \text{ ksi} * \left(88.625 - \frac{a}{2}\right)$$

$$85800 = A_s * 66 \text{ ksi} * \left(88.625 - \frac{a}{2}\right)$$

$$A_s = \frac{85800}{66 \text{ ksi} * \left(88.625 - \frac{a}{2}\right)}$$

Equation 4.4:

$$A_s f_y = 0.85 f'_c a b_f$$

f'_c = compressive strength of concrete

b_f = width of lower flange

$$A_s * 66 \text{ ksi} = 0.85 * 4 \text{ ksi} * a * 29.5$$

$$A_s * 66 \text{ ksi} = 100.3$$

$$A_s = 1.52a$$

Set Equations 4.3 and 4.4 equal to each other and solve:

$$1.52a = \frac{85800}{66 \text{ ksi} * \left(88.625 - \frac{a}{2}\right)}$$

Solved using online solver:

$$A_s = 15.56 \text{ in.}^2$$

$$a = 10.24 \text{ in}$$

Extended strand equations for bulb-tee prototype:

Centroid of strands is located 4 inches from bottom of girder. The effective girder width was calculated based using the same distribution factor of 0.24 with a total deck width of 34.5 feet.

Derivation of Equation 4.5:

$$M_{tot} = A_s f_{ys} \left(d_s - \frac{a}{2}\right)$$

M_{tot} = total positive moment

f_{ys} = yield strength of strand

A_s = area of prestressing strands

d_s = depth from top of deck to centroid of strands

a = depth of compression block

$$M_{tot} = M_{pos} - M_{DA}$$

M_{pos} = positive design moment

M_{DA} = moment resistance of dowel action

$$A_s = N_s * A_{strand}$$

N_s = number of strands

A_{strand} = area of a single 0.6 in. diameter prestressing strand

$$M_{pos} - M_{DA} = N_s * A_{strand} * f_{ys} * (d_s - \frac{a}{2})$$

$$N_s = (M_{pos} - M_{DA}) / (f_{ys} * A_{strand} * (d_s - \frac{a}{2}))$$

Equation 4.6:

$$a = \frac{A_s f_{ys}}{0.85 * f'_c * b_d}$$

b_d = effective width of deck

$$a = \frac{N_s * A_{strand} * f_{ys}}{0.85 f'_c b_d}$$

$$N_s = \frac{0.85 f'_c b_d * a}{A_{strand} * f_{ys}}$$

Solution of equations:

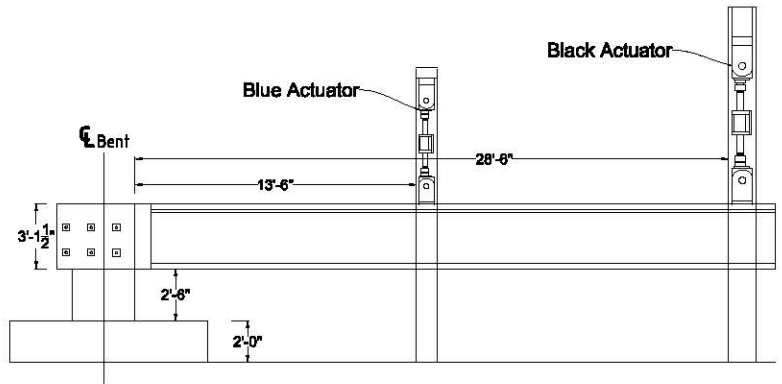
$$\frac{0.85 * 4 \text{ ksi} * 100 \text{ in.} * a}{0.217 * 230} = ((3065 - 1280) * 12 \text{ in./ft}) / (230 \text{ ksi} * 0.217 \text{ in.}^2 * (88.625 - (a/2)))$$

$$6.812a = 21402 / (49.91 * (88.625 - \frac{a}{2}))$$

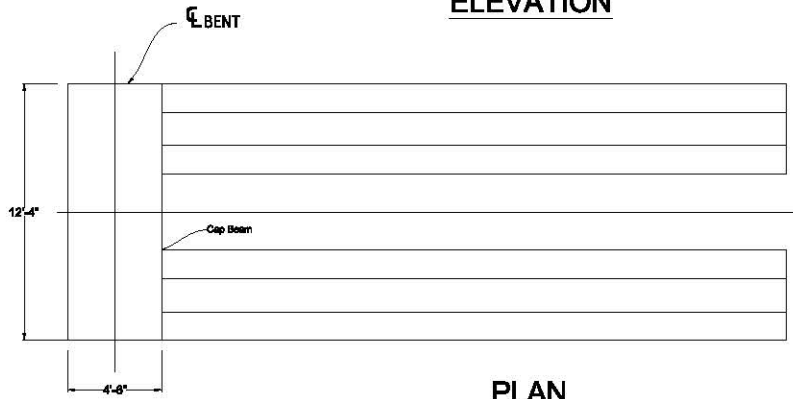
Solved using online solver:

$$a = 0.714$$

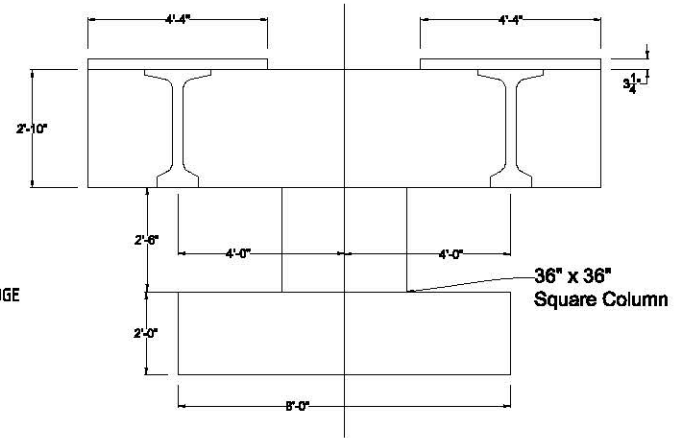
$$N_s = 5 \text{ strands}$$



ELEVATION



PLAN



TYPICAL SECTION

General Notes:

Concrete Strength (28 days): 4000 psi

Steel: Use A706 Grade 60 reinforcement and 270 ksi low-relaxation strands

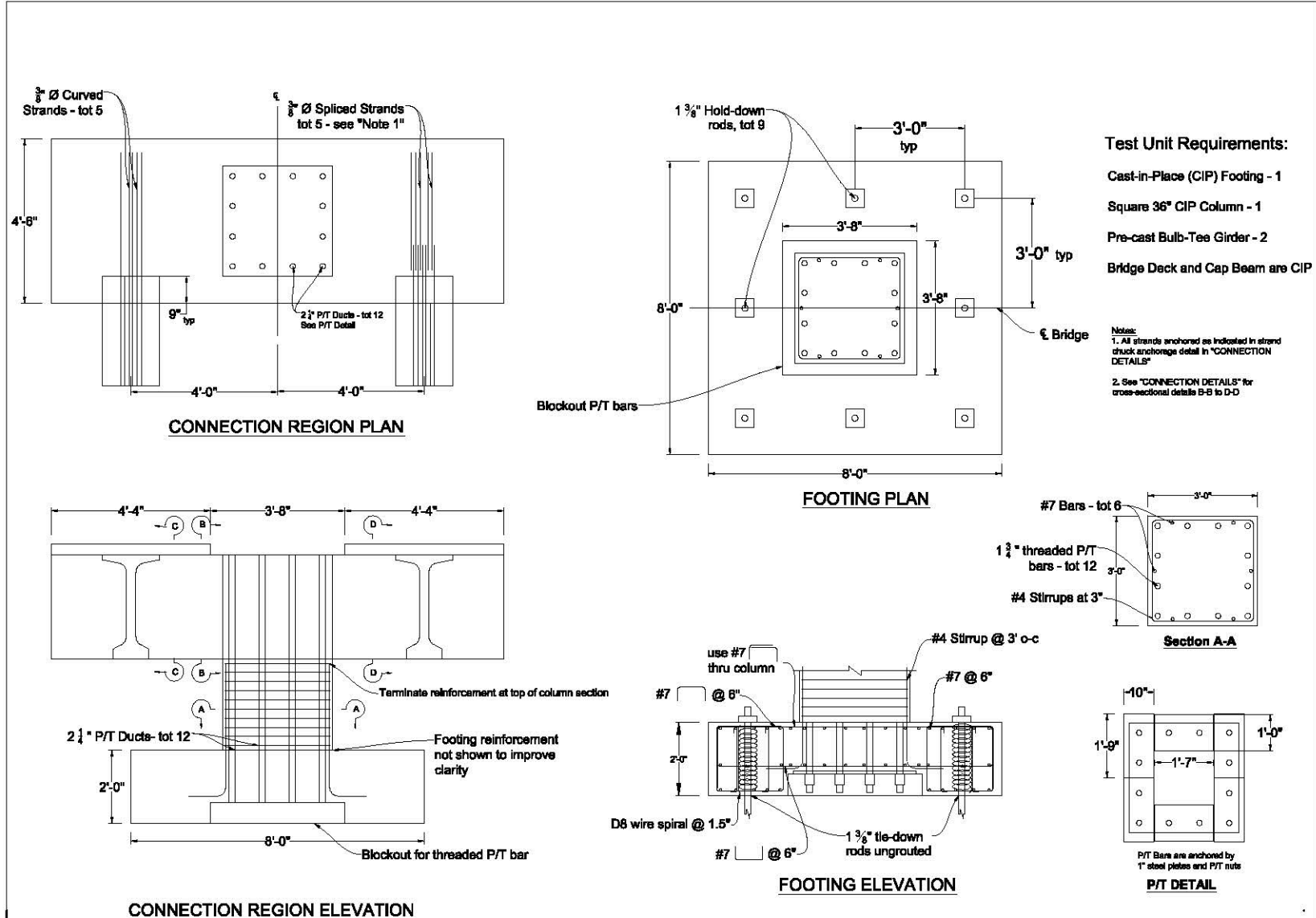
Minimum clearance: Clearance between parallel reinforcing steel should be one inch or one bar diameter, whichever is greater

Bent Cap Post-tensioning steel: Six 1 3/8" \varnothing deformed prestressing bars

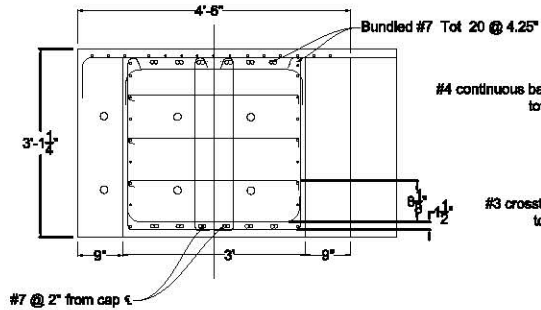
Cap-Column Connection Grout: High-strength, non-shrink, highly cementitious grout with percentage of steel fibers

APPENDIX C
BULB-TEE TEST UNIT

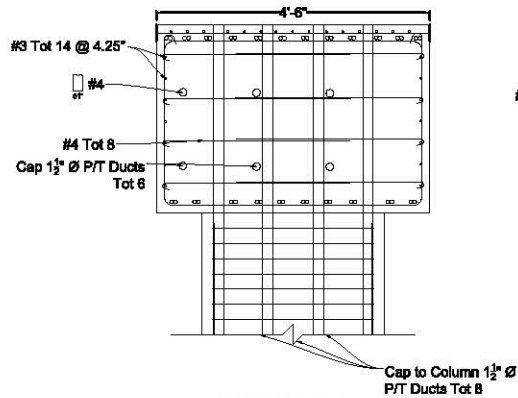
| | | | | | |
|--|---------------------------------|---|---------------------------------------|------------|--------------|
| Seismic Performance of Connections that Facilitate Accelerated Bridge Construction | Test Unit 2 - Connections 3 & 4 | PREPARED FOR THE STATE OF CALIFORNIA DEPARTMENT OF TRANSPORTATION | Charles Sikorsky PROJECT ENGINEER | ISSUED FOR | 01-03-2014 |
| | | | | FOR | GENERAL PLAN |
| CONTRACT #: 65A0411 PROJECT ID: 000001016 | | | DESIGNED WITH BEARING CAPACITY DESIGN | REVISIONS | DATE |
| | | | <input checked="" type="checkbox"/> | | 1 |



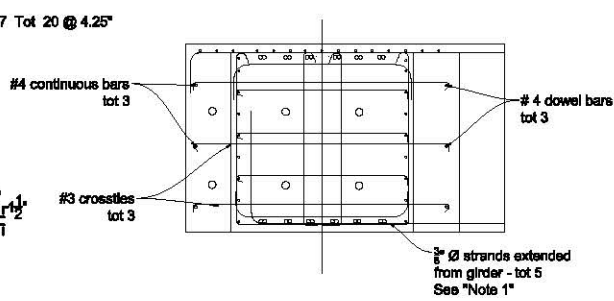
| | | | | |
|--|---------------------------------|--|-------------------------------------|---------------------------------|
| Seismic Performance of Connections that Facilitate Accelerated Bridge Construction | Test Unit 2 - Connections 3 & 4 | PREPARED FOR THE STATE OF CALIFORNIA DEPARTMENT OF TRANSPORTATION | Charles Sikorsky PROJECT MANAGER | DATE: 01-03-2014 |
| | | | | BENT LAYOUT |
| CONTRACT #: 65AD411 PROJECT ID: 0000001016 | | | CHECKED BY: [] APPROVED BY: [] | REVISIONS: [] SHEET: 2 OF 2 |



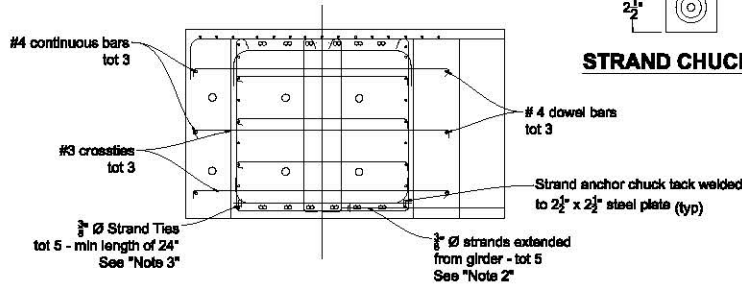
TYPICAL CONNECTION REGION



SECTION B-B

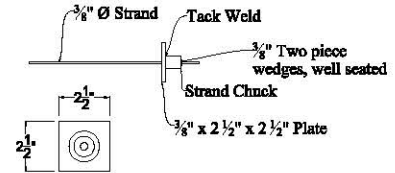


**SECTION C-C
ESBF DETAIL**



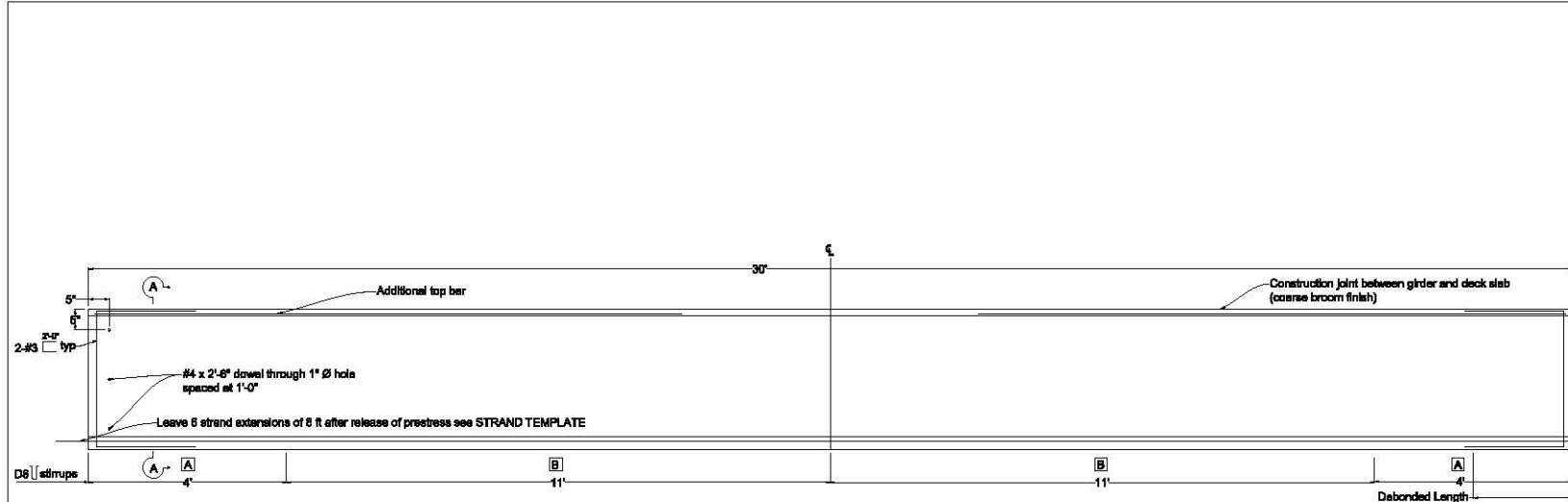
**SECTION D-D
ESSP DETAIL**

- Notes:**
1. For CURVED STRAND DETAIL extension length from girder face must be at least 60"
 2. For SPLICED STRAND DETAIL extension length from girder face must be at least 10"
 3. For SPLICED STRAND DETAIL the strand ties will be placed on the side of and parallel to the strands extending from the girder (same horizontal plane)



STRAND CHUCK ANCHORAGE DETAIL

| | | | | | | | | | | | | | |
|--|---------------------------------|---|--------------------------------------|---|--|------|----|-----|-----|---|--|--|--|
| Seismic Performance of Connections that Facilitate Accelerated Bridge Construction | Test Unit 2 - Connections 3 & 4 | PREPARED FOR THE STATE OF CALIFORNIA DEPARTMENT OF TRANSPORTATION | Charles Sikorsky PROJECT ENGINEER | ISSUED FOR | 01-03-2014 | | | | | | | | |
| | | | | CONNECTION DETAILS | | | | | | | | | |
| CONTRACT #: 65A0411 PROJECT ID: 000001016 | | | | DESIGNED WITH REGARDING ENGINEER REVIEW ONLY | <table border="1"> <tr> <td>DATE</td> <td>BY</td> <td>CHK</td> <td>APP</td> </tr> <tr> <td>X</td> <td></td> <td></td> <td></td> </tr> </table> | DATE | BY | CHK | APP | X | | | |
| DATE | BY | CHK | APP | | | | | | | | | | |
| X | | | | | | | | | | | | | |

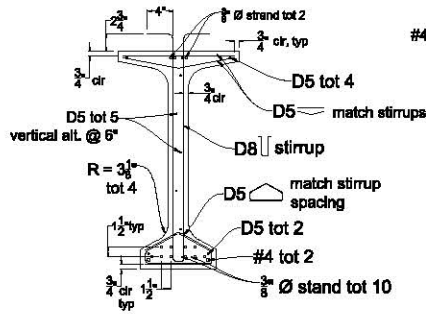


| Location | A | B |
|-----------------|---------|---------|
| Stirrup Spacing | D8 @ 2' | D8 @ 4' |

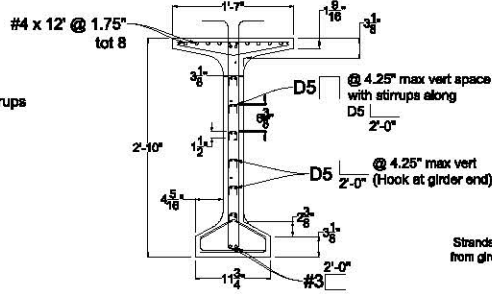
PRESTRESSING NOTES
 Concrete strength: $f_c = 5.5$ ksi at the time of initial stressing
 $f_c = 7.0$ ksi at 28 days
 $P_{jack} = 207$ kips (total jacking force)

GIRDER ELEVATION

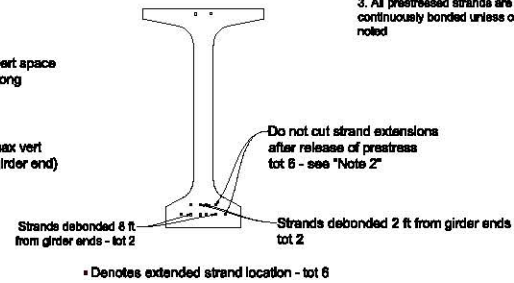
- Notes:**
- Girder ends to be cast such that a level surface is provided at bearing pads
 - After release of prestress, leave 6 ft of strand extending from end of girder with dowel bar holes.
 - All prestressed strands are $\frac{3}{8}$ " Ø and continuously bonded unless otherwise noted



TYPICAL GIRDER SECTION

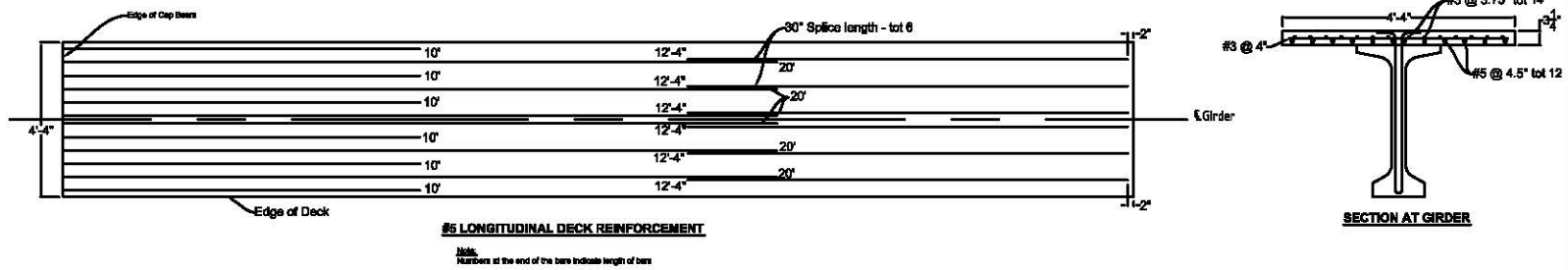


SECTION A-A



STRAND TEMPLATE & DEBONDING PATTERN

| | | | | |
|--|---------------------------------|--|-------------------------------------|----------------------|
| Seismic Performance of Connections that Facilitate Accelerated Bridge Construction | Test Unit 2 - Connections 3 & 4 | PREPARED FOR THE STATE OF CALIFORNIA DEPARTMENT OF TRANSPORTATION | Charles Sikorsky PROJECT MANAGER | DATE: 01-03-2014 |
| | | | | GIRDER LAYOUT |
| CONTRACT #: 65AD411 PROJECT ID: 0000001016 | | | CHECKED BY: [] REVIEWED BY: [] | SHEET 4 OF 4 |



| | | | | | | | | | | | | | | | |
|---|---------------------------------|---|--|--|--|-----------|------|----|------|-------|---|--|--|--|--|
| Seismic Performance of Connections that Facilitate Accelerated Bridge Construction | Test Unit 2 - Connections 3 & 4 | PREPARED FOR THE STATE OF CALIFORNIA DEPARTMENT OF TRANSPORTATION | Charles Sikorsky PROJECT MANAGER | ISSUED FOR | 01-03-2014 | | | | | | | | | | |
| | | | | FOR | DECK DETAILS | | | | | | | | | | |
| | | | CONTRACT #: 65A0411 PROJECT ID: 000001016 | DESIGNED WITH BEARING ENGLISH REVISION DATE | <table border="1"> <tr> <td>REVISIONS</td> <td>DATE</td> <td>BY</td> <td>CHKD</td> <td>APP'D</td> </tr> <tr> <td>X</td> <td></td> <td></td> <td></td> <td></td> </tr> </table> | REVISIONS | DATE | BY | CHKD | APP'D | X | | | | |
| REVISIONS | DATE | BY | CHKD | APP'D | | | | | | | | | | | |
| X | | | | | | | | | | | | | | | |

APPENDIX D
 BULB-TEE TEST UNIT LOADING PROTOCOL
 Force Controlled Cycles

| | Blue Actuator (kips) | Black Actuator (kips) | Moment (k-ft) | Shear (kips) |
|----------------------------|----------------------|-----------------------|---------------|--------------|
| Gravity (G) | 7.9 | -8.2 | -37.7 | 10.7 |
| | 25.7 | -15.3 | -75.7 | 21.4 |
| | 43.3 | -22.3 | -113.8 | 32 |
| | 61.1 | -29.4 | -151.7 | 42.7 |
| G±0.25H | 60.9 | -27.9 | -191.8 | 44 |
| | 61.2 | -30.6 | -118.9 | 41.6 |
| | 60.9 | -27.9 | -191.8 | 44 |
| | 61.2 | -30.6 | -118.9 | 41.6 |
| | 60.9 | -27.9 | -191.8 | 44 |
| | 61.2 | -30.6 | -118.9 | 41.6 |
| G±0.5H | 60.8 | -26.4 | -233.2 | 45.4 |
| | 61.3 | -31.8 | -86 | 40.5 |
| | 60.8 | -26.4 | -233.2 | 45.4 |
| | 61.3 | -31.8 | -86 | 40.5 |
| | 60.8 | -26.4 | -233.2 | 45.4 |
| | 61.3 | -31.8 | -86 | 40.5 |
| G±0.75H | 60.6 | -24.9 | -273.2 | 46.7 |
| | 61.4 | -33 | -53.2 | 39.4 |
| | 60.6 | -24.9 | -273.2 | 46.7 |
| | 61.4 | -33 | -53.2 | 39.4 |
| | 60.6 | -24.9 | -273.2 | 46.7 |
| | 61.4 | -33 | -53.2 | 39.4 |
| G ± Horizontal Seismic (H) | 60.6 | -23.5 | -313.1 | 48.1 |
| | 61.5 | -34.2 | -20.3 | 38.3 |
| | 60.6 | -23.5 | -313.1 | 48.1 |
| | 61.5 | -34.2 | -20.3 | 38.3 |
| | 60.6 | -23.5 | -313.1 | 48.1 |
| | 61.5 | -34.2 | -20.3 | 38.3 |
| G±H±0.1G | 65.7 | -24.4 | -356.3 | 52.3 |
| | 56.2 | -33.2 | 22.7 | 34 |
| | 65.7 | -24.4 | -356.3 | 52.3 |
| | 56.2 | -33.2 | 22.7 | 34 |
| | 65.7 | -24.4 | -356.3 | 52.3 |
| | 56.2 | -33.2 | 22.7 | 34 |

| | Blue Actuator (kips) | Black Actuator (kips) | Moment (k-ft) | Shear (kips) |
|----------|----------------------|-----------------------|---------------|--------------|
| G±H±0.2G | 71.1 | -25.4 | -400.7 | 56.7 |
| | 51.1 | -32.2 | 63.1 | 29.9 |
| | 71.1 | -25.4 | -400.7 | 56.7 |
| | 51.1 | -32.2 | 63.1 | 29.9 |
| | 71.1 | -25.4 | -400.7 | 56.7 |
| | 51.1 | -32.2 | 63.1 | 29.9 |
| G±H±0.3G | 76.4 | -26.5 | -440.9 | 60.9 |
| | 45.7 | -31.2 | 107.5 | 25.5 |
| | 76.4 | -26.5 | -440.9 | 60.9 |
| | 45.7 | -31.2 | 107.5 | 25.5 |
| | 76.4 | -26.5 | -440.9 | 60.9 |
| | 45.7 | -31.2 | 107.5 | 25.5 |
| G±H±0.4G | 81.7 | -27.5 | -484 | 65.2 |
| | 40.4 | 30.2 | 150.5 | 21.2 |
| | 81.7 | -27.5 | -484 | 65.2 |
| | 40.4 | 30.2 | 150.5 | 21.2 |
| | 81.7 | -27.5 | -484 | 65.2 |
| | 40.4 | 30.2 | 150.5 | 21.2 |
| G±H±0.5G | 86.8 | -28.4 | -527.2 | 69.4 |
| | 35.3 | -29.3 | 193.7 | 17 |
| | 86.8 | -28.4 | -527.2 | 69.4 |
| | 35.3 | -29.3 | 193.7 | 17 |
| | 86.8 | -28.4 | -527.2 | 69.4 |
| | 35.3 | -29.3 | 193.7 | 17 |

Post-tensioning of Cap Beam

| | | | | |
|----------|------|-------|--------|------|
| G±H±0.6G | 92.2 | -29.4 | -571.6 | 73.8 |
| | 30 | -28.2 | 233.9 | 12.8 |
| | 92.2 | -29.4 | -571.6 | 73.8 |
| | 30 | -28.2 | 233.9 | 12.8 |
| | 92.2 | -29.4 | -571.6 | 73.8 |
| | 30 | -28.2 | 233.9 | 12.8 |
| G±H±0.7G | 97.5 | -30.5 | -611.8 | 78 |
| | 24.6 | -27.2 | 278.3 | 8.4 |
| | 97.5 | -30.5 | -611.8 | 78 |
| | 24.6 | -27.2 | 278.3 | 8.4 |
| | 97.5 | -30.5 | -611.8 | 78 |
| | 24.6 | -27.2 | 278.3 | 8.4 |

| | Blue Actuator (kips) | Black Actuator (kips) | Moment (k-ft) | Shear (kips) |
|------------------------------|-------------------------|-----------------------------|------------------|-----------------|
| G±H-0.8G | 102.6 | -31.4 | -655 | 82.2 |
| | -2 | -5 | 4.7 | 4 |
| | 102.6 | -31.4 | -655 | 82.2 |
| | -2 | -5 | 4.7 | 4 |
| | 102.6 | -31.4 | -655 | 82.2 |
| | -2 | -5 | 4.7 | 4 |
| G±H-0.9G | 107.9 | -32.4 | -698 | 86.5 |
| | -2 | -5 | 4.7 | 4 |
| | 107.9 | -32.4 | -698 | 86.5 |
| | -2 | -5 | 4.7 | 4 |
| | 107.9 | -32.4 | -698 | 86.5 |
| | -2 | -5 | 4.7 | 4 |
| G±H-1.0G | 113.3 | -33.4 | -742.4 | 90.9 |
| | -2 | -5 | 4.7 | 4 |
| | 113.3 | -33.4 | -742.4 | 90.9 |
| | -2 | -5 | 4.7 | 4 |
| | 113.3 | -33.4 | -742.4 | 90.9 |
| | -2 | -5 | 4.7 | 4 |
| G±H-1.1G | 118.4 | -34.4 | -782.8 | 95 |
| | -2 | -5 | 4.7 | 4 |
| | 118.4 | -34.4 | -782.8 | 95 |
| | -2 | -5 | 4.7 | 4 |
| | 118.4 | -34.4 | -782.8 | 95 |
| | -2 | -5 | 4.7 | 4 |
| End of Force Controlled Test | | | | |

Displacement Controlled Cycles

| | Blue Actuator (K) | Black Actuator (in.) |
|----------|-------------------|----------------------|
| | 20 | -1 |
| | -10 | 0.5 |
| | 30 | -1.5 |
| | -15 | -0.75 |
| D -2/1 | 40 | -2 |
| | -22 | 1 |
| | 40 | -2 |
| | -22 | 1 |
| | 40 | -2 |
| | -22 | 1 |
| D -3/1.5 | 40 | -3 |
| | -22 | 1.5 |
| | 40 | -3 |
| | -22 | 1.5 |
| | 40 | -3 |
| | -22 | 1.5 |
| D -4/2 | 40 | -4 |
| | -22 | 2 |
| | 40 | -4 |
| | -22 | 2 |
| | 40 | -4 |
| | -22 | 2 |
| D -6/3 | 40 | -6 |
| | -22 | 3 |
| | 40 | -6 |
| | -22 | 3 |
| | 40 | -6 |
| | -22 | 3 |
| D -9/4.5 | 40 | -9 |
| | -22 | 4.5 |
| | 40 | -9 |
| | -22 | 4.5 |
| | 40 | -9 |
| | -22 | 4.5 |

| | Blue Actuator (K) | Black Acuator (in.) |
|---------------|-------------------|---------------------|
| D -12/6 A | 40 | -12 |
| | -22 | 6 |
| | 40 | -12 |
| | -22 | 6 |
| | 40 | -12 |
| | -22 | 6 |
| D -12/6 B | 50 | -12 |
| | -22 | 6 |
| | 60 | -12 |
| | -22 | 6 |
| | 70 | -12 |
| | -22 | 6 |
| D - 14/7.5 | 70 | -14 |
| | -22 | 7.5 |
| | 70 | -14 |
| | -22 | 7.5 |
| | 70 | -14 |
| | -22 | 7.5 |
| D -14/9 | -22 | 9 |
| | 70 | -14 |
| | -22 | 9 |
| | 70 | -14 |
| | -22 | 9 |
| D - 14/10 | -22 | 10 |
| | 70 | -14 |
| | -22 | 10 |
| | 70 | -14 |
| | -22 | 10 |
| | 70 | -14 |
| End of Test | | |

APPENDIX E
DESIGN EXAMPLE

Suggested design procedure for precast girder-to-cap connection

| | |
|--------|---|
| Step 1 | Determine required moment demand at precast girder-to-cap connection |
| Step 2 | Estimate the required moment capacities resulting from the extended strands |
| Step 3 | Determine the number of strand extended from girder |
| Step 4 | Design the anchorage details for the extended unstressed girder strands |
| Step 5 | Detail the dowel bars and the diaphragm |

Notes:

- 1) The suggested percentages of nominal positive moment capacity used in Step 2 are 60% and 40%, respectively, for shear fiction moment and strand moment.
- 2) The suggested allowable strand stress in Step 3 is $0.30f_{pu}$.

Step 1 - Determine required moment demand at precast girder-to-cap connection

For this example, the precast girder-to-cap connection is located at Bent 3 within a typical 4-span pretensioned prestressed concrete beam bridge as shown in Figure 1. The largest bulb-tee girders currently used in the state of California (CA BT85) are chosen for the bridge. The analysis results show that the required positive moment demand for a single girder-to-cap connection is 3065 kip-ft. This demand is determined from considering gravity loads, overstrength forces developed in the column from horizontal seismic acceleration, and 0.5g vertical seismic acceleration.

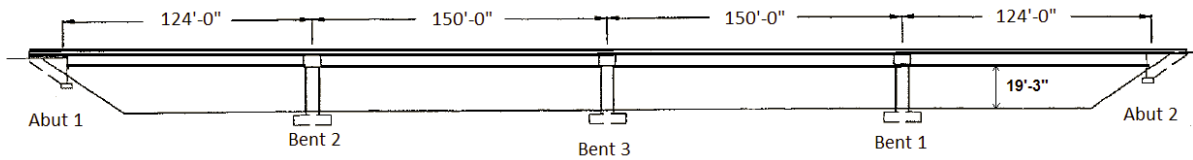


Figure E1: Elevation of the designed bridge

For all capacity-protected members, the resistance factor shall be taken as 1.0 for bending (Caltrans, SDC). Therefore, the nominal moment capacity (M_n) for designed connection shall not be lesser than 3065 k-ft.

Step 2 – Estimate the required moment capacities resulting from the extended strands

The magnitudes of moment resistance generated by shear friction and extended unstressed girder strands are calculated based on the distribution of total positive moment resistance. According to the experimental test results, percentages of the nominal positive moment capacity are suggested as 60% corresponding to the shear friction moment and 40% corresponding to the strand moment, resulting in a conservative design.

The required moment capacity resulting from the strand (M_s) is:

$$M_s = 0.4M_n = 0.4 \times 3065 = 1226 \text{ k-ft.}$$

Step 3 – Determine the number of strand extended from girder

As per the discussion in Chapter 6, the neutral axis for positive moment in the connection is located at the top of the girder, and the concrete compressive stress is equivalent to a compression force located at the middle of the deck. The moment resistance contribution by the strands can thus be taken as:

$$M_s = \sigma_s A'_{ps} N d_{sc}$$

where,

σ_s = stress of the strand at the interface;

A'_{ps} = nominal area of the stand;

N = number of strands extended from the precast girder; and

d_{sc} = distance from the center of gravity of the strands to the moment compression force.

For design practice, the stress of the strand at the connection interface should be limited to $0.3f_{pu}$, which is 81 ksi for Grade 270 strands.

For this example, the depth of the CA BT85 girder is 7'-0 5/8" (84.625"), and the depth of the deck is 8 in. It is assumed that the center of gravity of the extended girder strands is located at 8" above the bottom of girder. Hence, the distance from the strand to the moment compression force (d_{sc}) is:

$$d_{sc} = 84.625 - 8 + \frac{8}{2} = 80.625"$$

Since 0.6-in. diameter strands are used in this example, the nominal area of the strand, A'_{ps} , is 0.216 in.² The number of strands required to be extended from the girder, therefore, is:

$$N = \frac{M_s}{\sigma_s A'_{ps} d_{sc}} = \frac{1380 \times 12}{81 \times 0.216 \times 80.625} = 10.4$$

Hence, for this example, a total of eleven 0.6-in.-diameter strands need to be extended from the girder and anchored in the cap.

Step 4 - Design the anchorage details for the extended unstressed girder strands

To minimize the congestion in the connection region, a short embedment length is preferred. Pull-out tests demonstrated that the strand chuck consisting of a bearing plate, a barrel anchor, and wedges resulted in the shortest embedment length, 18 in., to fully develop the strength of the 0.6-in. diameter strands. In addition, the strand chucks are recommended to be placed in a staggered pattern to reduce the congestion caused by chucks. Therefore, in this example, the 18 strands shall be extended into cap at least 18" with the staggered strand chucks as shown in Figure 2. The details of the strand chuck anchoring the 0.6-in. diameter strand are shown in Figure 3.

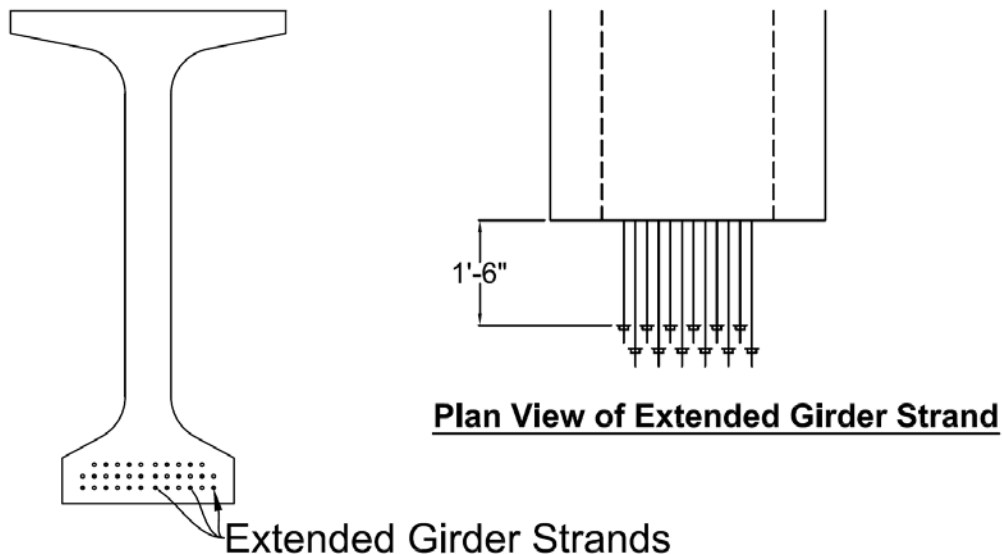


Figure E2: Extended girder strand details

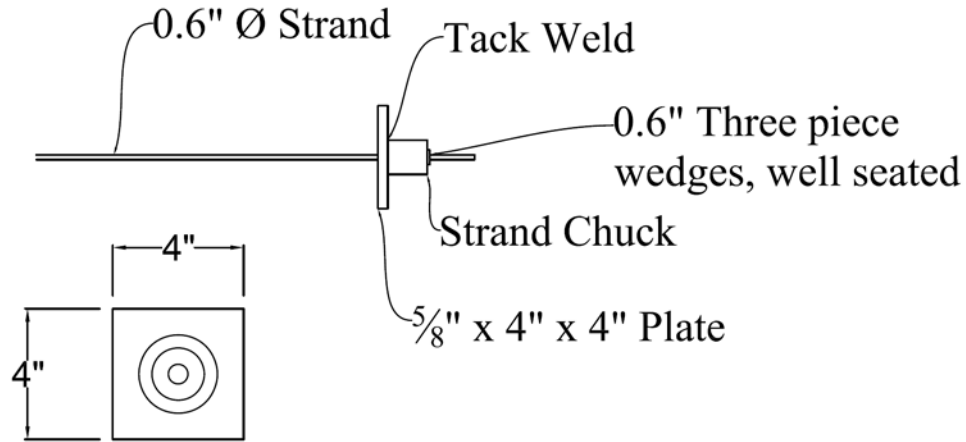


Figure E3: Strand chuck details

Step 5 - Detail the dowel bars and the diaphragm

Three #10 Grade 60 reinforcing bars are selected as the dowels in this example. The dowel bars are located as per the suggested location in Table 6.8. The minimum dowel bar length of 6.5 ft is used to reduce the congestion of reinforcement in the connection region. The thickness of the pier diaphragm used in this example is selected as 24-in. Therefore, the dowel bars and diaphragm are detailed as shown in Figure 4.

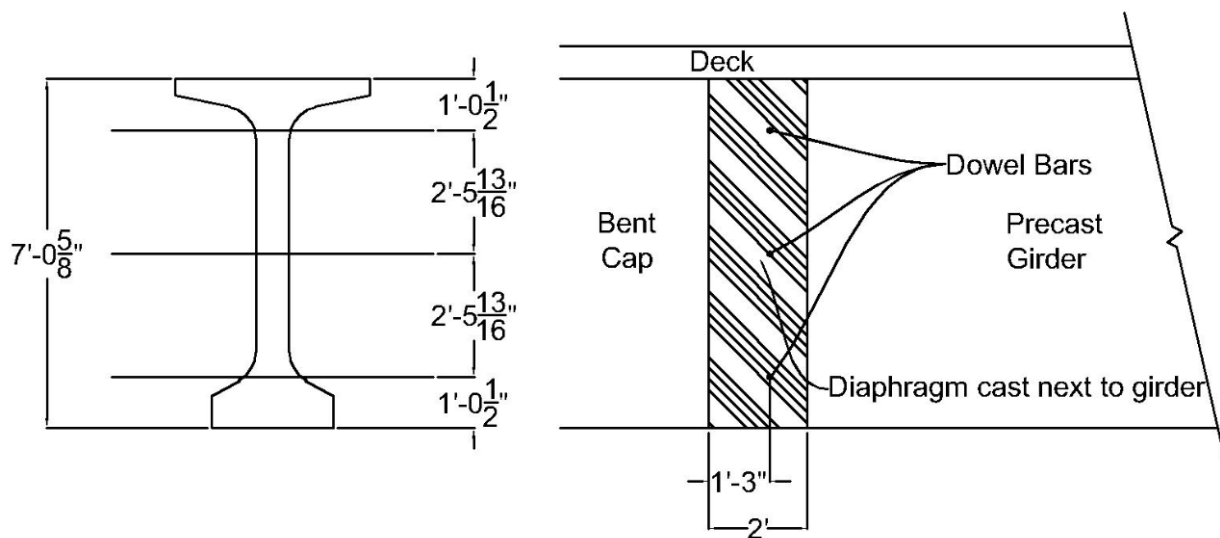


Figure E4: Dowel bars and pier diaphragm details

In addition, diaphragm stirrups (U-shaped confinement steel) shall be added to fit alongside the girder web and between the top and bottom girder flanges to confine the concrete surrounding the dowel bars. The size of U-shaped confinement steel is suggested to be #6, and the spacing for the additional stirrups is suggested to be not lesser than 6 in. For this example, the length of the U-shaped confinement steel leg is determined as 4 ft to fully confine the diaphragm concrete surrounding the dowels. The dowel bars details are illustrated in Figure 5.

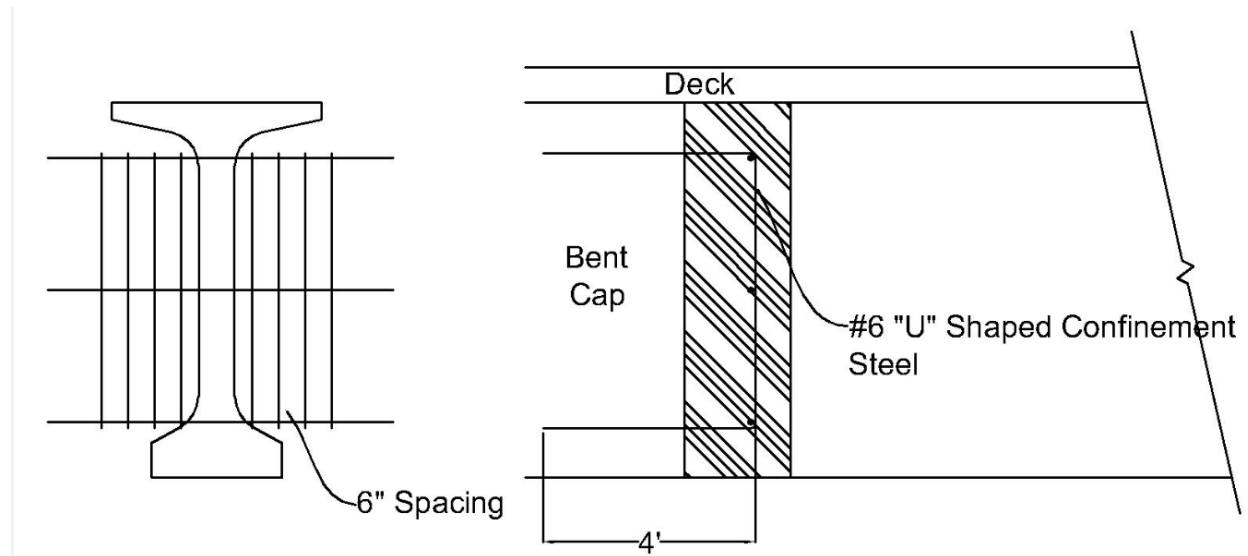


Figure E5: U-shaped confinement steel details

